VNiVERSiDAD Ð SALAMANCA

CAMPUS DE EXCELENCIA INTERNACIONAL

Departamento de Ingeniería Cartográfica y del Terreno

Tesis Doctoral

Mención Internacional

ANÁLISIS Y MONITORIZACIÓN DE MATERIALES DE CONSTRUCCIÓN SOSTENIBLES A TRAVÉS DE TÉCNICAS ÓPTICAS DE CAMPO COMPLETO

Jorge López Rebollo

2024

Institución:

Universidad de Salamanca

Escuela Politécnica Superior de Ávila

Departamento de Ingeniería Cartográfica y del Terreno

Programa de doctorado:

Geotecnologías Aplicadas a la Construcción, Energía e Industria

Línea de investigación:

Integración de Técnicas No Destructivas en Ingeniería Civil

Análisis y monitorización de materiales de construcción sostenibles a través de técnicas ópticas de campo completo

- Tesis Doctoral con Mención Internacional -

2024

Autor:

Jorge López Rebollo

Directores:

Dr. Diego González Aguilera

Dr. Luis Javier Sánchez Aparicio

Informe de los directores de Tesis

La presente Tesis Doctoral con mención internacional, titulada "*Análisis y monitorización de materiales de construcción sostenibles a través de técnicas ópticas de campo completo*", presentada por D. Jorge López Rebollo, queda integrada en la línea de investigación *Análisis de materiales y soluciones industriales a través de correlación digital de imágenes y termografía activa* del grupo de investigación, afiliado a la Universidad de Salamanca, TIDOP (https://tidop.usal.es/).

Fruto de la actividad investigadora desarrollada por el doctorando, durante el periodo de elaboración de la Tesis Doctoral, diversos trabajos científicos han sido publicados en revistas internacionales de prestigio. Complementario a ello, se ha de reseñar el desarrollo de una patente nacional (en proceso de concesión, P202230901), bajo el título de "*Sistema de caracterización de objetos a partir de su reconstrucción en 360 grados mediante generación de imágenes*", que aúna la metodología de correlación digital de imágenes 3D desarrollada y empleada en parte de las publicaciones desarrolladas. Asimismo, hay que reseñar la estancia internacional de 3 meses que ha realizado el doctorando en la Universidad de Cuenca (Ecuador) en el marco de su Tesis Doctoral. El objetivo principal de la estancia se ha centrado en el análisis de materiales de base tierra empleando técnicas de caracterización mecánica como la correlación digital de imágenes.

En lo referente a las publicaciones mostradas en el presente documento, y a fin de corroborar la validez y robustez de los trabajos científicos desarrollados, los artículos científicos fruto de dichos trabajos fueron publicados en 5 revistas científicas impacto, algunas de ellas con un alto factor de impacto y posicionadas en primer cuartil, Q1. Éstas, por orden de publicación, se distribuyen del siguiente modo:

1. El artículo científico: *Improvement of mechanical properties of compressed earth blocks with stabilising additives for self-build of sustainable housing.* Publicado en la revista *Buildings,* indexada en el Journal Citation Report y emplazada en el segundo cuartil, Q2, de las categorías: *Construction & Building Technology; Engineering Civil.* Ocupando la posición 23, en factor de impacto, de las 68 revistas indexadas. DOI: https://doi.org/10.3390/buildings14030664.

2. El artículo científico: *Compression and strain predictive models in non-structural recycled concretes made from construction and demolition wastes.* Publicada en la revista *Materials.* Dicha revista, indexada en el primer cuartil, Q1, de la categoría Metellurgy and Metellurgical Engineering, ocupando la posición 17 de 80 revistas. DOI: https://doi.org/10.3390/ma14123177.

3. El artículo científico: *Monitoring the thermal contribution of certain mortar additives as a way to optimize the energy performance of buildings.* Publicada en la revista científica Sustainable Energy Technologies and Assessments, indexada y emplazada en el primer cuartil, Q1, de la categoría *Energy and Fuels* ocupando la posición 28 de 119 revistas, en términos de impacto. DOI: https://doi.org/10.1016/j.seta.2023.103268.

4. El artículo científico: *Experimental study on the thermal properties of pigmented mortars for use in energy efficiency applications.* Publicada en la revista científica *Cleaner Production*, indexada y emplazada en el primer cuartil, Q1, de la categoría *Enviromental*

Sciences ocupando la posición 8 de 55 revistas, en términos de impacto. DOI: https://doi.org/10.1016/j.jclepro.2022.135280.

5. El artículo científico: *Enhancing thermal efficiency in water storage tanks using pigmented recycled concrete.* Publicada en la revista *Materials.* Dicha revista, indexada en el segundo cuartil, Q2, de la categoría Metellurgy and Metellurgical Engineering, ocupando la posición 20 de 79 revistas. DOI: https://doi.org/10.3390/ma17051008.

A tenor de los requerimientos para la presentación de la Tesis Doctoral por compendio de artículos establecidos por la Universidad de Salamanca (https://posgrado.usal.es/TESIS%20NUEVA%202012/Formato_Tesis_compendio.pdf), se considera que los artículos principales, así como los méritos adicionales de la misma, se ajustan de modo óptimo a dichas necesidades, quedando así validadas las metodologías, resultados y conclusiones presentadas en este documento.

Los resultados arrojados durante la elaboración de la Tesis Doctoral han permitido avanzar en la integración de técnicas de correlación digital de imágenes y termografía activa sobre nuevos materiales de construcción para mejorar sus propiedades mecánicas y térmicas, permitiendo una construcción más sostenible y energéticamente más eficiente.

La Tesis Doctoral concluye con el correspondiente apartado de Conclusiones en el que de forma precisa y concreta se especifican las principales aportaciones realizadas de tal manera que puedan ser objeto de crítica y de proyección hacia el desarrollo de futuros trabajos integrados en líneas de investigación.

Lo que firman, a todo los efectos oportunos, en Ávila, a 17 de Abril de 2024.

Dr. Diego González Aguilera

Dr. Luis Javier Sánchez Aparicio

Listado de artículos publicados

La presente Tesis Doctoral está constituida por un compendio de cinco artículos científicos, publicados en revistas internacionales de alto impacto indexadas en el Journal Citation Report (JCR). A continuación, se enumeran estas publicaciones:

1. **Improvement of mechanical properties of compressed earth blocks with stabilising additives for self-build of sustainable housing**

Jorge López-Rebollo[1], Xavier Cárdenas-Haro[2,3], Juan Parra-Vargas[2], Kevin Narváez-Berrezueta[2] and Julver Pino[3]

[1] Department of Cartographic and Land Engineering. University of Salamanca, Higher Polytechnic School of Ávila, Hornos Caleros, 50, 05003, Ávila (Spain)
[2] Facultad de Arquitectura y Urbanismo, Virtual Tech, Universidad de Cuenca, Av. 12 de Abril s/n y Av. Loja, 010201 Cuenca (Ecuador)
[3] Facultad de Ingeniería, Departamento de Ingeniería Civil, Universidad de Cuenca, Av. 12 de Abril s/n y Av. Loja, 010201 Cuenca (Ecuador)

2. **Compression and strain predictive models in non-structural recycled concretes made from construction and demolition wastes**

Evelio Teijón-López-Zuazo[1], Jorge López-Rebollo[2], Luis Javier Sánchez-Aparicio[3], Roberto Garcia-Martín[4] and Diego Gonzalez-Aguilera[2]

[1] Department of Construction and Agronomy, University of Salamanca, Higher Polytechnic School of Zamora, Campus Viriato, Avenida Requejo, 33, 49022, Zamora (Spain)
[2] Department of Cartographic and Land Engineering. University of Salamanca, Higher Polytechnic School of Ávila, Hornos Caleros, 50, 05003, Ávila (Spain)
[3] Department of Construction and Technology in Architecture (DCTA), Escuela Técnica Superior de Arquitectura de Madrid (ETSAM), Universidad Politécnica de Madrid, Av. Juan de Herrera 4, 28040, Madrid (Spain)
[4] Department of Mechanical Engineering, University of Salamanca, Higher Polytechnic School of Zamora, Campus Viriato, Avenida Requejo, 33, 49022, Zamora (Spain)

3. **Monitoring the thermal contribution of certain mortar additives as a way to optimize the energy performance of buildings**

Jorge López-Rebollo[1], Natalia Nuño Villanueva[1], Ignacio Martín Nieto[1], Cristina Sáez Blázquez[1], Susana Del Pozo[1], Diego González-Aguilera[1]

[1] Department of Cartographic and Land Engineering. University of Salamanca, Higher Polytechnic School of Ávila, Hornos Caleros, 50, 05003, Ávila (Spain)

4. **Experimental study on the thermal properties of pigmented mortars for use in energy efficiency applications**

Jorge López-Rebollo[1], Susana Del Pozo[1], Ignacio Martín Nieto[1], Cristina Sáez Blázquez[1,2], Diego González-Aguilera[1]

[1] Department of Cartographic and Land Engineering. University of Salamanca, Higher Polytechnic School of Ávila, Hornos Caleros, 50, 05003, Ávila (Spain)
[2] Department of Electric, System and Automatic Engineering, Universidad de León, León, Spain

5. **Enhancing thermal efficiency in water storage tanks using pigmented recycled concrete**

Jorge López-Rebollo[1], Ignacio Martín Nieto[1], Cristina Sáez Blázquez[1], Susana Del Pozo[1], Diego González-Aguilera[1]

[1] Department of Cartographic and Land Engineering. University of Salamanca, Higher Polytechnic School of Ávila, Hornos Caleros, 50, 05003, Ávila (Spain)

Resumen

La industria de la construcción ha sido considerada históricamente una de las mayores consumidoras de recursos naturales y generadoras de residuos, por lo que existe la necesidad de reducir el impacto ambiental asociado a este sector. Abordar esta cuestión supone un reto integral, desde la fase de fabricación de nuevos materiales de construcción más sostenibles hasta la fase funcional donde sus capacidades se alineen con los conceptos de sostenibilidad y eficiencia energética. En este contexto, la utilización de materiales reciclados y la mejora de sus propiedades mecánicas y térmicas mediante la incorporación de aditivos son aspectos clave para avanzar hacia una construcción más sostenible y energéticamente más eficiente.

A pesar de que la ingeniería civil y de materiales disponen de múltiples herramientas y técnicas para el diseño de infraestructuras, generalmente se emplean metodologías asociadas a materiales convencionales. Sin embargo, los nuevos materiales presentan composiciones y comportamientos diversos, lo que provoca que los métodos tradicionales no siempre arrojen buenos resultados. En este sentido, para avanzar en el conocimiento de los nuevos materiales de construcción, es fundamental contar con técnicas de caracterización avanzadas que permitan evaluar y validar sus propiedades de manera precisa y detallada.

Con el fin de fomentar la incorporación de nuevos materiales sostenibles en el sector de la construcción y mejorar su competitividad, la presente Tesis Doctoral pone el foco en la integración de nuevas técnicas avanzadas para el análisis y caracterización de nuevos materiales que contribuyan a la construcción sostenible. Para ello, se propone el empleo de dos técnicas ópticas de campo completo basadas en imagen: la correlación digital de imágenes y la termografía infrarroja, para la caracterización mecánica y para la evaluación térmica, respectivamente. Estos avances tienen el potencial de promover prácticas más sostenibles en la industria de la construcción y contribuir al desarrollo de nuevos materiales para alcanzar un futuro más resiliente y eficiente desde el punto de vista energético y medioambiental.

Inicialmente, el trabajo se centra en la caracterización mecánica y la mejora de sus propiedades. Para ello, se plantea en primer lugar el empleo de materias primas básicas como la tierra para fabricar elementos como los bloques de tierra comprimida. Estos sistemas constructivos son ampliamente utilizados por su elevada versatilidad y a pesar de su menor rigidez y resistencia, los resultados demuestran que son una solución muy interesante desde el punto de vista de la sostenibilidad. A continuación, en busca de materiales con mayor capacidad mecánica se propone la sustitución de áridos naturales por áridos reciclados en la fabricación de hormigones. La mejora de las propiedades mecánicas de estos materiales de construcción es caracterizada mediante la técnica óptica de correlación digital de imágenes, empleada en su enfoque bidimensional para la evaluación de paneles de tierra comprimida en primer lugar y en su enfoque tridimensional para el análisis de probetas cilíndricas de hormigón reciclado en segundo lugar.

En paralelo al desarrollo mecánico, se investiga la mejora térmica de los materiales de construcción. En primera instancia se aborda a través de la incorporación de residuos como aditivos para la modificación de su conductividad térmica. Posteriormente, se busca una mejora desde el punto de vista de la absorción de radiación solar empleando pigmentos inorgánicos como aditivos. Esta optimización térmica es validada utilizando la técnica óptica de termografía infrarroja, empleando un simulador solar para replicar la exposición al sol de los materiales.

Finalmente, se propone un estudio integral que combina los avances mecánicos y térmicos en un material multifuncional. Este enfoque aborda el desafío de integrar los avances obtenidos en los estudios anteriores con el objetivo de validar su aplicabilidad en un contexto práctico y aplicado tanto al sector de la ingeniería civil como al sector industrial. Para ello, se propone la fabricación de depósitos acumuladores de calor para el aumento de la temperatura del agua almacenada, que posteriormente pueda ser empleada en procesos industriales donde se requiere agua caliente o a nivel doméstico como agua caliente sanitaria. Los resultados demuestran que el hormigón sostenible, fabricado con áridos reciclados a partir de rechazos de prefabricados de hormigón y con aditivos pigmentados, puede utilizarse con éxito para fabricar elementos con capacidades estructurales y térmicas como son los depósitos de agua acumuladores de calor. Estos resultados representan un avance significativo en la búsqueda de soluciones innovadoras para la construcción sostenible.

Abstract

The construction industry has historically been considered one of the largest consumers of natural resources and a significant generator of waste, highlighting the challenge of reducing the environmental impact associated with this sector. Addressing this issue is a comprehensive challenge, ranging from the production phase of more sustainable construction materials to the functional phase where their performance is aligned with sustainability and energy efficiency concepts. In this context, the use of recycled materials and the improvement of their mechanical and thermal properties through the incorporation of additives are key aspects in moving towards more sustainable and energy efficient construction.

Although civil and materials engineering have a wide range of tools and techniques for infrastructure design, methods associated with conventional materials are generally used. Nevertheless, new materials have different compositions and behaviours, so that traditional methods do not always give satisfactory results. Therefore, advancing the understanding of new construction materials requires advanced characterisation techniques that allow for accurate and detailed evaluation and validation of their properties.

To promote the incorporation of new sustainable materials into the construction sector and increase its competitiveness, this Doctoral Thesis focuses on the integration of new advanced techniques for the analysis and characterisation of materials contributing to sustainable construction. To achieve this, the use of two full-field optical techniques based on imaging is proposed: digital image correlation for mechanical characterisation and infrared thermography for thermal evaluation. These advances have the potential to promote more sustainable practices in the construction industry and contribute to the development of new materials for a more resilient and energy efficient future, both from an environmental and energy perspective.

Initially, work focuses on mechanical characterisation and improvement of properties. This involves using basic raw materials such as earth to produce elements such as compressed earth blocks. Despite their lower stiffness and strength, these construction systems are widely used due to their high versatility and are proving to be an interesting solution from a sustainability point of view. Furthermore, in the search for materials with higher mechanical capacity, the substitution of natural aggregates with recycled aggregates in concrete production is proposed. The improvement in the mechanical properties of these construction materials is characterised using the digital image correlation technique, first in its two-dimensional approach for the evaluation of compressed earth blocks, and then in its three-dimensional approach for the analysis of recycled concrete cylindrical specimens.

Simultaneously with mechanical development, thermal improvement of construction materials is investigated. Initially, this is approached through the incorporation of waste as additives to modify their thermal conductivity. Subsequently, an improvement in terms

of solar radiation absorption is pursued using inorganic pigments as additives. This thermal optimisation is validated using infrared thermography and a solar simulator to replicate the exposure of materials to sunlight.

Finally, a comprehensive study combining mechanical and thermal advances in a multifunctional material is proposed. This approach addresses the challenge of integrating the advances made in previous studies to validate their applicability in a practical and applied context, both in civil and industrial sectors. To achieve this, it is proposed to manufacture thermal storage tanks to increase the temperature of the stored water, which can then be used in industrial processes requiring hot water, or domestically for sanitary hot water. The results show that sustainable concrete, made with recycled aggregates from rejected concrete prefabricates and pigmented additives, can be successfully used to manufacture elements with structural and thermal capacities such as thermal storage water tanks. These results represent a significant step forward in the search for innovative solutions for sustainable construction.

ÍNDICE

CAPÍTULO IV

HORMIGÓN RECICLADO ESTRUCTURAL CON CAPACIDAD TÉRMICA101

CAPÍTULO V

APÉNDICES

ÍNDICE DE FIGURAS

CAPÍTULO I
INTRODUCCIÓN

1.1.   Introducción

El sector de la construcción es considerado el mayor consumidor de recursos naturales no renovables y es también un importante generador de residuos [1]. Aunque las materias primas utilizadas en el proceso de fabricación son recursos abundantes, su elevada explotación y los costes derivados de su extracción suponen un problema que puede provocar la escasez de este tipo de material a medio y largo plazo en muchos países donde su producción es muy elevada [2]. Junto al elevado consumo de recursos, la construcción también es considerada una industria "sucia" debido a la elevada generación de residuos (**Figura 1**) y las emisiones generadas durante la producción de los materiales. En este contexto, es necesaria una gestión eficaz que permita reducir tanto la cantidad de recursos consumidos como la cantidad de residuos generados tal y como se establece en las metas del "Objetivo 12: Producción y consumo responsables", de los ODS (Objetivos de Desarrollo Sostenible) establecidos por la ONU (Organización de las Naciones Unidas). Para lograr estos avances, es necesario aprovechar el potencial de estos recursos como materia secundaria de acuerdo con los conceptos de desarrollo sostenible y economía circular.
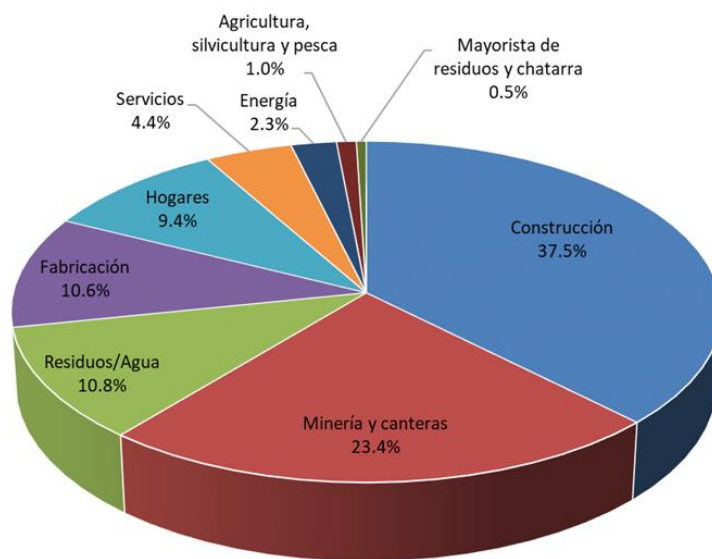
Figura 1: Generación de residuos por actividades económicas en Europa, 2020. (Fuente: Eurostat [3]).

En la búsqueda de soluciones sostenibles desde el punto de vista medioambiental, la incorporación de áridos o aditivos reciclados supone una oportunidad para reducir la cantidad de residuos a la par que el consumo de recursos naturales. Con ello se pueden mejorar distintas propiedades mecánicas, estructurales o térmicas de la mezcla base preservando sus atributos fundamentales. Dado que se trata de nuevas soluciones con composiciones y comportamientos diferentes a los materiales convencionales, es fundamental conocer sus potenciales y sus limitaciones para determinar su idoneidad a la hora de su fabricación y uso. Además, un análisis exhaustivo de estas propiedades es indispensable para mejorar los diseños y optimizar el comportamiento de las infraestructuras construidas con estos nuevos materiales sostenibles.

La caracterización mecánica de los materiales de construcción generalmente se realiza a través de técnicas tradicionales de monitorización que se basan en métodos de contacto como LVDTs (del inglés "Linear Variable Differential Transformers") o las galgas extensiométricas [4] (**Figura 2**). Estas técnicas sólo proporcionan información local, y sus resultados pueden estar influidos por errores en la colocación o patrones de agrietamiento, que pueden hacer que sensores como las galgas extensiométricas se desprendan y dejen de captar datos [5]. Para superar estos inconvenientes, se han desarrollado métodos ópticos de campo completo sin contacto entre los que destaca la correlación digital de imágenes (DIC, del inglés "Digital Image Correlation") [6]. Esta técnica permite analizar desplazamientos y deformaciones de campo completo mediante la adquisición de imágenes.
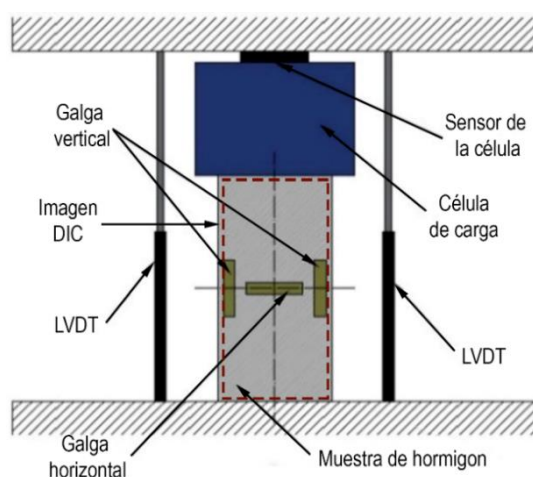
Figura 2: Caracterización mecánica con galga extensiométrica, LVDT y DIC. (Imagen adaptada de [4]).

La mejora de las propiedades térmicas de los morteros se ha enfocado tradicionalmente desde el punto de vista de la conductividad térmica [7]. Sin embargo, los materiales de construcción generalmente se encuentran expuestos al sol, por lo que resulta interesante investigar su comportamiento térmico desde el punto de vista de sus propiedades reflectivas como revestimientos [8]. En este sentido, la termografía infrarroja activa [9], aplicada mediante simulador solar permite monitorizar el comportamiento de los materiales debido a la alteración de la difusividad térmica y el flujo de calor causado por su composición [10] a través de la medición de la temperatura superficial con imágenes térmicas.

En un intento por mejorar la competitividad de los materiales de construcción, la optimización mecánica y térmica de los nuevos materiales permite construir infraestructuras bajo los principios de sostenibilidad y eficiencia energética. En particular, la técnica de caracterización avanzada DIC permite evaluar el comportamiento mecánico de hormigones fabricados con áridos reciclados para cumplir su función estructural. Por su parte, el avance térmico es evaluado a través de la combinación de termografía infrarroja y la simulación solar, lo que permite dotar a estos materiales de una función energética. La fusión de ambos avances se traduce en la posibilidad de aplicar elementos constructivos que beneficien al sector de la ingeniería civil e industrial a través de una construcción con materiales más sostenibles que mejoren el rendimiento térmico.

Materiales de construcción

En el contexto actual de cambio climático y agotamiento de recursos naturales, el estudio de materiales sostenibles ha emergido como una prioridad en el sector de la construcción y edificación. El elevado consumo de recursos se justifica por la gran demanda de hormigón del sector, que es el material artificial más utilizado en el mundo [11]. Por su parte, la arquitectura de tierra es el sistema constructivo natural más empleado, y se estima que un tercio de la población mundial vive en edificios construidos mediante este material [12]. A pesar de que las materias primas empleadas en la construcción son muy abundantes, se trata de recursos no renovables, por lo que su elevado aprovechamiento y los costes derivados de su extracción suponen un problema que puede ocasionar escasez a medio-largo plazo en muchos países donde su producción es muy alta [2]. Además, hay determinadas regiones en las que la extracción de materias primas no es viable debido a su baja disponibilidad, la falta de medios o la dificultad de transporte y acceso [13].

La búsqueda de materiales alternativos que sean respetuosos con el medio ambiente, económicamente viables y eficientes en términos de recursos, se ha convertido en un objetivo fundamental para reducir la huella de carbono asociada a la industria de la construcción, la cual es responsable de hasta el 8% de las emisiones mundiales de CO_2 [14]. En consecuencia, el aprovechamiento de las materias primas locales y la reutilización de residuos se han destacado como opciones prometedoras que cumplen con los criterios de sostenibilidad y circularidad para alcanzar una producción más responsable y desarrollar infraestructuras sostenibles de acuerdo con los ODS.

El fomento del empleo de materiales que aprovechen los recursos locales permite ahorrar tiempo, costes y emisiones asociadas a su transporte. En este contexto, los materiales fabricados a partir de tierra se presentan como una alternativa para la autoconstrucción, aprovechando los recursos locales y siendo una solución respetuosa con el medioambiente [15]. A pesar de su menor capacidad mecánica, son materiales adecuados para muros de carga, cerramientos o sustitución de otros materiales convencionales como los ladrillos [16]. Además, se trata de una solución más sostenible en términos de ahorro energético y emisión de CO_2, puesto que su fabricación requiere el 1% de energía respecto al hormigón convencional [17]. La construcción con estos materiales permite que aquellas regiones que no disponen de recursos convencionales como el acero o cemento puedan autoabastecerse y acceder a la construcción, reduciendo la dependencia de importaciones y disminuyendo los costos asociados al transporte de materiales. Esto facilita la autoconstrucción en regiones de bajos recursos económicos, fomentando el empoderamiento de las comunidades y contribuyendo al desarrollo local sostenible.

Junto con la explotación de materias primas propias, la economía circular se presenta como un enfoque fundamental en la construcción sostenible, donde los residuos se convierten en recursos y se minimiza la extracción de materias primas. En este contexto, los residuos de construcción y demolición (RCD) en la Unión Europea ascienden a 800

millones de toneladas al año, lo que supone más de un 30% de la totalidad de residuos generados [18]. Incluyendo los residuos generados en las minas y canteras para actividades extractivas como la obtención de áridos, los residuos suponen aproximadamente dos tercios de la totalidad de residuos, situándose esta cifra incluso cercana al 90% en algunos países (**Figura 3**). El reciclaje de residuos en la construcción y su incorporación nuevamente en el ciclo de fabricación de materiales como el hormigón cobra especial relevancia, ya que permite reducir la demanda de nuevos materiales y disminuir la cantidad de desechos enviados a vertederos, con el consecuente impacto negativo que esto supone en términos visuales, paisajísticos y ecológicos. De hecho, las directrices europeas establecen la necesidad de reciclar al menos un 70% de los RCD [19]. Sin embargo, las normativas nacionales establecen limitaciones en cuanto a la utilización de estos RCD en la fabricación de hormigones [20], por lo que la tendencia en los estudios más recientes se centra en la posibilidad de mejorar el rendimiento de estos materiales para avanzar hacia una sustitución total de los áridos naturales por áridos reciclados.
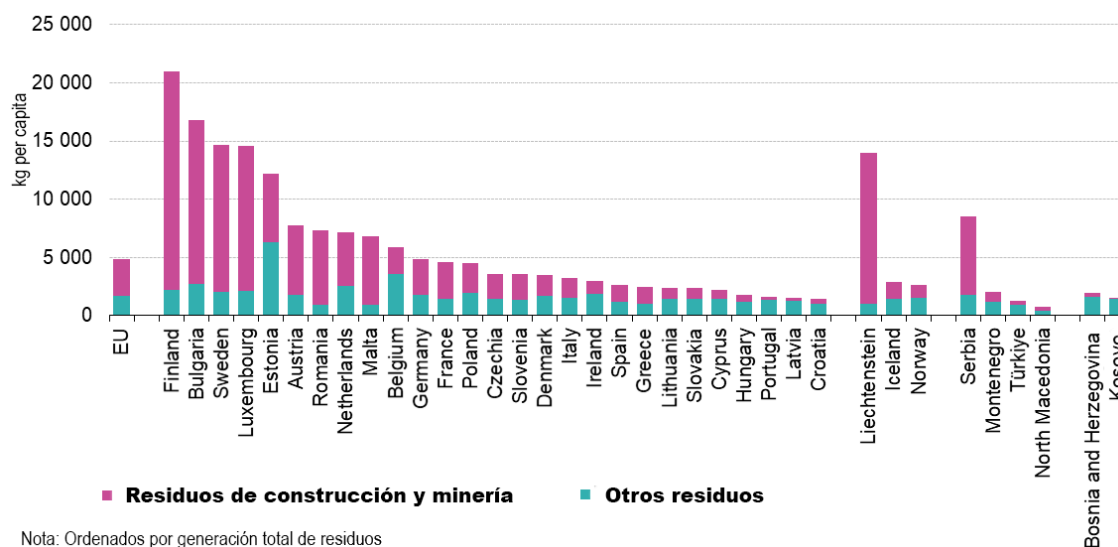
Figura 3: Generación de residuos per cápita por países en Europa, 2023. (Fuente: Eurostat [3]).

Estos materiales se posicionan como elementos claves en la promoción de un desarrollo urbano sostenible y una construcción más responsable. Sin embargo, la alteración de la composición original de los materiales de construcción provoca cambios en sus propiedades y su comportamiento. Estas modificaciones generalmente se traducen en una mayor variabilidad, heterogeneidad e incertidumbre, lo que genera la necesidad de realizar análisis exhaustivos a través de herramientas que permitan un conocimiento más profundo de estos materiales, con el fin de mejorar su rendimiento. Esto incluye estudiar sus principales propiedades, entre las que se encuentran las características mecánicas, térmicas, acústicas, la resistencia al fuego, la durabilidad, la permeabilidad, etc. En términos de construcción y sostenibilidad, las propiedades mecánicas y térmicas son las más relevantes para estos materiales. Por un lado, el conocimiento de las propiedades mecánicas es fundamental para diseñar y construir estructuras seguras que puedan soportar las cargas esperadas durante su vida útil y evitar posibles fallos

estructurales [21]. Por su parte, conocer las propiedades térmicas es esencial para diseñar infraestructuras energéticamente eficientes, minimizando las pérdidas o ganancias de calor, reduciendo los consumos energéticos en el caso de edificaciones e industrias [22].

En función del uso al que se destinen los materiales de construcción, los requerimientos mecánicos pueden variar. Para la construcción de muros y paredes se requieren resistencias a compresión bajas, por lo que los materiales de tierra representan una solución adecuada desde el punto de vista mecánico y sostenible, ya que pueden alcanzar resistencias superiores a los 2 MPa [23]. Para usos constructivos en los que se requiera una mayor resistencia pero no tengan carácter estructural, como pavimentos o soleras, los hormigones reciclados fabricados a partir de RCD son una alternativa a hormigones convencionales, ya que permiten alcanzar resistencias entre 10 y 25 MPa [24]. En el caso de que los requerimientos mecánicos sean mayores, es posible obtener hormigones estructurales empleando RCD que procedan de elementos con mayor calidad, como puede ser el caso de los rechazos de elementos prefabricados [25].

En cualquier caso, los materiales basados en tierra presentan comportamientos mecánicos muy diferentes, ya sea por el empleo de estabilizantes para mejorar las propiedades de la tierra como materia prima principal [26] o por la composición, selección y tratamiento de los áridos reciclados a partir de RCD [27]. Este alto grado de heterogeneidad provoca que, a la hora de realizar ensayos de caracterización mecánica, se obtengan diferentes resultados en función de las condiciones de medida y la zona en la que se ubiquen los sensores de medición. Por ello, el empleo de técnicas ópticas de campo completo basadas en imagen, como DIC, se presenta como una técnica adecuada para analizar y caracterizar el comportamiento global de este material [5].

Por otra parte, en la búsqueda de soluciones energéticamente más eficientes, la mejora de la capacidad térmica de los materiales de construcción supone un reto desde el punto de vista de la eficiencia energética de las infraestructuras [28]. Por un lado, dotar a los materiales de una mayor capacidad de aislamiento permite mitigar el efecto de isla de calor urbana [29] que altera la estabilidad de estas áreas, además de mejorar el confort térmico del interior de los edificios. Sin embargo, en determinados escenarios climáticos, aumentar la absorción de calor y la capacidad de almacenamiento de energía de los materiales puede suponer una ventaja energética con ahorros significativos en los sistemas de calefacción [30].

Ya sea en la función de aislamiento o de acumulación de calor, otorgar estas capacidades a los materiales de construcción implica la adición de aditivos capaces de alterar su comportamiento térmico preservando sus propiedades mecánicas. En este sentido, los principales desarrollos de la Comunidad Científica se han enfocado en la incorporación de aditivos para modificar las propiedades desde el punto de vista de la conductividad térmica [7]. En particular, la adición de residuos o materiales reciclados empleados de manera convencional en la industria de la construcción supone una oportunidad para reducir estos residuos a la par que se obtiene una mejora de la eficiencia energética. En este sentido, residuos de la minería como yesos cristalizados u otros

desechos generados en la industria de la construcción como las fibras de poliéster se presentan como soluciones adecuadas para alterar la conductividad térmica.

No obstante, resulta también interesante analizar el comportamiento térmico de estos materiales desde el punto de vista de la absorción de radiación solar, especialmente para el de aprovechamiento de dicha energía. En este sentido, los pigmentos inorgánicos han demostrado su capacidad no sólo para mejorar las propiedades térmicas de otros materiales de construcción como el asfalto [31], sino también de preservar las propiedades mecánicas en el hormigón [32], siendo un compuesto respetuoso con el medioambiente. La inclusión de estos aditivos pigmentados permite mejorar el rendimiento térmico y optimizar el consumo energético, especialmente en aplicaciones y sectores que requieren de fuentes de calor externas. Sin embargo, la incorporación de aditivos provoca comportamientos heterogéneos que requieren nuevamente el empleo de técnicas de monitorización térmica adecuadas. En este sentido, la termografía infrarroja se presenta como una técnica no destructiva adecuada para analizar el comportamiento térmico de campo completo y considerar todos los factores que influyen en su rendimiento, como pueden ser los puentes térmicos o efectos de borde.

Una de las aplicaciones con un mayor consumo energético tanto a nivel doméstico como a nivel industrial son los procesos térmicos para el empleo de agua caliente. Tanto el agua caliente sanitaria empleada en las viviendas como el agua empleada en la mayoría de las industrias alimenticias requieren de un calentamiento previo para elevar su temperatura. En muchos de estos casos, el agua se almacena en grandes depósitos fabricados de hormigón previo a los tratamientos, ya sea en las estaciones de tratamiento de agua potable o en tanques industriales. La fabricación de estos elementos con materiales de construcción sostenibles que garanticen su capacidad estructural junto con la mejora de su rendimiento término supone una ventaja desde un punto de vista tanto económico como medioambiental. Por un lado, el empleo de hormigones reciclados permite una reducción en cuanto a las materias primas empleadas en la construcción y los residuos generados a la par que una reducción en las emisiones de CO_2 asociadas a la producción de este material. Por otro lado, la mejora de las propiedades térmicas del material garantiza un aumento de la temperatura del agua de estos depósitos provocado por la mayor absorción de radiación solar, lo que supone un ahorro energético en cuanto a la menor cantidad de energía requerida para el calentamiento de agua, e igualmente una reducción en las emisiones de CO_2 asociadas a las fuentes de energía empleadas de manera convencional para producir este calentamiento.

Correlación digital de imágenes

El diseño mecánico de infraestructuras requiere información precisa sobre las propiedades mecánicas de los materiales de construcción, obtenida mediante experimentos donde muestras de estos materiales se someten a diferentes tipos de solicitación, como compresión, tensión o flexión. El enfoque tradicional implica el uso de técnicas de contacto, como LVDTs, extensómetros y galgas extensiométricas, que colocadas en la probeta registran deformaciones y desplazamientos locales. Sin embargo, estas técnicas están influenciadas por parámetros externos como la temperatura y requieren correcciones, además de un proceso complejo de instalación y calibración que puede afectar la precisión de las mediciones [33]. La preparación de la superficie y la manipulación de los sensores también son aspectos críticos, aumentando la complejidad y los costes de los ensayos.

Además, estas técnicas proporcionan mediciones puntuales y pueden alterar el comportamiento del material debido a su carácter invasivo. Como alternativa, se han desarrollado técnicas de no contacto como la interferometría de Moiré [34], el sistema de velocimetría por análisis de imágenes de partículas [35], la fotoelasticidad [36] y la DIC [37]. Esta última se destaca por su capacidad para obtener mediciones globales, especialmente en rangos de elevada deformación y fisuración [38], como es el caso de los materiales de construcción como el hormigón. Además, al basarse en el procesamiento de imágenes, presenta ventajas como la flexibilidad experimental, la resolución ajustable y la disponibilidad de software de código abierto. Estas virtudes aumentan su competitividad frente a otras técnicas convencionales u ópticas para la caracterización y el diseño mecánico de materiales de construcción, situándola además como una solución más accesible y económica.

La DIC es una técnica óptica que emplea métodos de seguimiento y registro de imágenes para realizar mediciones de forma, desplazamiento y deformación de campo completo [6]. Esta técnica utiliza imágenes digitales adquiridas en diferentes estados de carga y realiza un análisis de correlación de las mismas mediante algoritmos de fotogrametría y visión computacional basados en la intensidad de la escala de grises. A partir de la coincidencia entre las imágenes, es posible cuantificar el desplazamiento y las deformaciones de campo completo, lo que permite caracterizar el comportamiento y la respuesta global de los materiales. Esta técnica puede aplicarse a una amplia gama de materiales en el sector de la construcción, incluyendo materiales tradicionales como el acero [39] o la madera [40], materiales compuestos con comportamiento heterogéneo [41] o materiales cementosos reforzados [42]. Además, su flexibilidad experimental permite realizar análisis desde escalas nanométricas [43] hasta kilométricas [44].

A pesar de que la DIC comenzó en la década de 1980 [45], su auge se originó a principios del siglo XXI, impulsado por avances en algoritmos, hardware y la popularidad de la técnica en la Comunidad Científica [46]. Los principales avances recientes se centran en la mejora de la precisión, eficiencia y robustez de los algoritmos, así como en

la introducción de sistemas de imagen que corrigen errores y permiten mediciones tridimensionales.

Inicialmente desarrollada para mediciones en dos dimensiones (2D-DIC), la técnica evolucionó hacia enfoques tridimensionales (3D-DIC), que permiten mediciones fuera del plano y amplían su aplicabilidad a objetos con curvatura [47]. Esto se logra mediante la incorporación de dos o más cámaras al sistema de adquisición de imágenes, lo que permite la correlación y reconstrucción de la superficie analizada. Las principales diferencias entre 2D-DIC y 3D-DIC (**Tabla 1**) resaltan la capacidad tridimensional del último, haciéndola más adecuada para ensayos en probetas no planas, aunque requiere de una mayor preparación y desarrollo de la técnica.

Tabla 1: Enfoque 2D-DIC vs 3D-DIC.

Enfoque		**2D-DIC**	**3D-DIC**
Sistema de imagen	**Equipamiento**	1 cámara	2 o más cámaras
	Posicionamiento	Perpendicular al plano	Ángulo estéreo
Calibración	**Interna**	Recomendada	Obligatoria
	Externa	No	Obligatoria
Imágenes	**Adquisición**	Individuales	Pares sincronizados
	Correlación	2D	2D + reconstrucción
Desplazamientos y deformaciones	**Dimensiones**	*X, Y*	*X, Y, Z*

La aplicación de la técnica DIC, a través de ambos enfoques, requiere de la utilización de un patrón moteado o speckle que proporcione variaciones de intensidad aleatorias en la superficie de las muestras. En este sentido, la técnica del aerosol permite crear patrones speckle con un tamaño de punto milimétrico o submilimétrico sobre la superficie de las muestras [6]. El procedimiento para obtener este patrón requiere, en primer lugar, la aplicación de una pintura blanca sobre la superficie del material. A continuación, mediante un aerosol, se generan los puntos negros (speckle) de manera aleatoria sobre la superficie blanca. Por último, con el fin de asegurar la calidad del parámetro, se procede a su evaluación según el parámetro de Mean Intensity Gradient [48], que permite cuantificar el contraste de los moteados negros respecto al fondo blanco.

Enfoque de la correlación digital de imágenes bidimensional (2D-DIC)

La caracterización de materiales con superficies planas puede llevarse a cabo con el enfoque 2D-DIC, donde una única cámara es necesaria y no se requiere una rigurosa calibración para aplicar los algoritmos de correlación. En este caso, la calibración interna de la cámara se emplea únicamente para corregir la distorsión de lente. Para ello, se puede aplicar el algoritmo fotogramétrico de calibración basado en ajuste de haces (BA, del inglés "Bundle Adjustment") [49], que emplea un modelo de distorsión radial y tangencial no lineal reemplazando las coordenadas idealizadas por las coordenadas corregidas. Este método necesita un conjunto de imágenes (alrededor de 50 [50]) de un panel de calibración del tipo "tablero de ajedrez", de manera que diferentes posiciones y orientaciones del panel sean capturadas en todo el campo de vista de la cámara (FoV , del inglés "Field of View"). El algoritmo minimiza los errores generales de reproyección de las esquinas de los cuadrados (puntos de control) extraídos del objetivo de calibración de tablero de ajedrez para calcular los parámetros físicos de distorsión radial y tangencial, así como los parámetros geométricos de calibración (i.e., focal y punto principal).

Tras la calibración, el método 2D-DIC divide la imagen en subconjuntos de píxeles denominados subsets que se comparan entre imágenes consecutivas, evaluando el grado de similitud entre el subconjunto de referencia y los subconjuntos deformados. Para ello se emplea el criterio de correlación basado en áreas, ZNCC (del inglés "Zero mean Normalized Cross-Correlation") [51], el cual es invariante a los cambios de escala y desplazamiento de la intensidad del subconjunto deformado al sustraer los valores medios de intensidad. El índice de correlación, C_{ZNCC}, indica una buena coincidencia cuando está cerca de 0. Durante este proceso, para evaluar los desplazamientos entre los centroides de los subconjuntos, son asumidos los grados de libertad que se muestran en la **Figura 4**. Para alcanzar una mayor precisión subpíxel, la técnica 2D-DIC emplea estrategias de refinamiento que combinan interpolaciones b-spline [52] junto al método de Composición Inversa de Gauss-Newton (IC-GN, del inglés "Inverse Compositional Gauss-Newton") [53].
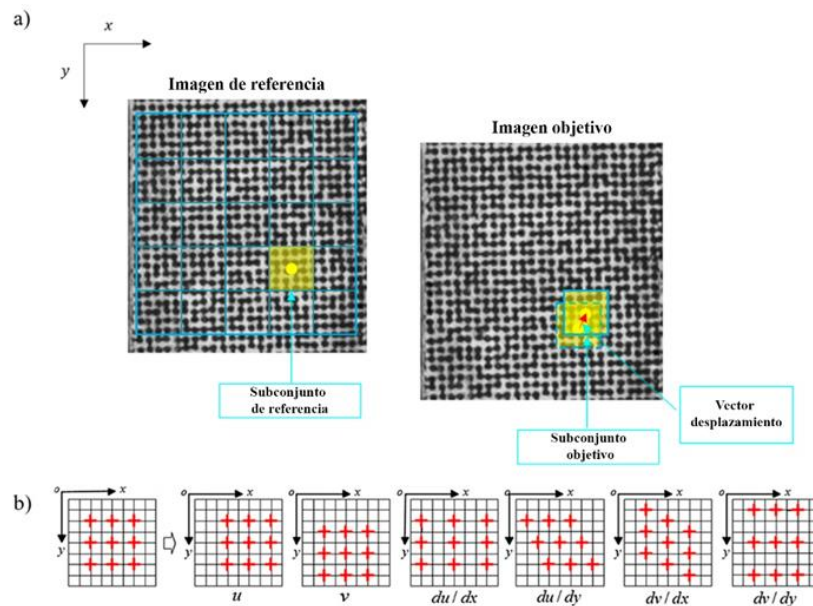
Figura 4: *Algoritmo 2D-DIC: a) Evaluación del desplazamiento generado por un subconjunto; b) Grados de libertad asumidos durante el análisis de los desplazamientos. u y v representa la translación del subconjunto en las direcciones x e y. du/dy y dv/dx representan la deformación cortante del subconjunto en las direcciones x e y. (Imagen adaptada de [41]).*

Esta estrategia se aplica sobre toda la región de interés (ROI, del inglés "Region Of Interest") a través del algoritmo de correlación digital de imágenes guiado por fiabilidad (RG-DIC, del inglés "Reliability-Guided Digital Image Correlation") [54] con el objetivo de minimizar la propagación del error así como optimizar el tiempo de computación. Este método parte de un punto inicial o semilla y procesa el resto de subconjuntos siguiendo un algoritmo que permite la minimización de los errores C_{LS} (del inglés "Least Square correlation error").

Enfoque de la correlación digital de imágenes tridimensional (3D-DIC)

La principal diferencia entre el enfoque bidimensional y tridimensional radica en el uso de dos o más cámaras con un ángulo estero [55] para estimar los desplazamientos fuera del plano principal de la cámara. Para resolver la orientación de las cámaras, se emplea una estrategia fotogramétrica que combina el algoritmo BA empleado para la calibración interna, igual que en el enfoque 2D-DIC, con el algoritmo de orientación externa y reconstrucción 3D basado en la transformación lineal directa (DLT, del inglés "Direct Linear Transformation") [56].

Una vez corregida la distorsión de la lente a través del algoritmo BA, el algoritmo DLT, en una primera fase (fase de cálculo), permite relacionar las coordenadas de la imagen y las coordenadas del objeto para resolver la orientación externa de la cámara. Este algoritmo permite representar mediante una solución lineal de 11 parámetros matemáticos (l_1-l_{11}) el modelo no lineal de 6 parámetros geométricos correspondientes a la posición espacial (X_S, Y_S, Z_S) y angular (Rx, Ry, Rz) de la cámara. Dado que cada punto permite obtener dos ecuaciones (resultantes de la linealización de la condición de colinealidad) [57], el sistema de 11 parámetros se puede resolver conociendo al menos seis puntos de control. En este caso, se emplea un objeto de calibración no plano en el que existen puntos de control con sus coordenadas 3D conocidas. Además, el algoritmo DLT, en una segunda fase (fase de transformación), permite obtener las coordenadas 3D de un punto concreto utilizando las coordenadas 2D de ese punto en al menos dos imágenes.

Para obtener la posición y desplazamiento tridimensional de los puntos de cada imagen, se emplea un proceso de registro de imagen que utiliza los algoritmos DIC descritos para el enfoque bidimensional. Sin embargo, mientras que en el enfoque 2D-DIC las imágenes son rastreadas de manera individual, en el enfoque 3D-DIC la correlación es realizada entre la imagen izquierda y derecha, así como entre la imagen de referencia y sus correspondientes deformadas (**Figura 5**).
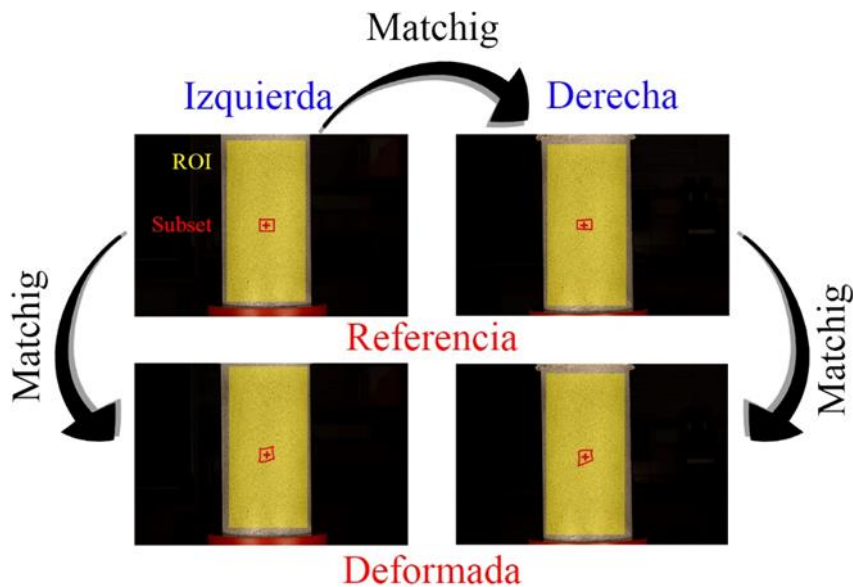
Figura 5: Registro de imágenes en el enfoque 3D-DIC. (Imagen adaptada de [58]).

Una vez realizado el proceso de correlación, es posible realizar la reconstrucción tridimensional de los puntos correspondientes, obteniendo así una nube de puntos asociada a los centroides de cada subconjunto de la ROI (fase de transformación). Para ello, se utilizan los parámetros DLT obtenidos en el proceso de orientación previo (fase de cálculo) junto con las coordenadas de la imagen de los puntos obtenidos del DIC. De esta forma, las coordenadas reales de cada uno de los puntos se pueden calcular siguiendo la fase de transformación de la DLT apoyada por una estrategia de mínimos cuadrados, en la medida en la que puede tener redundancias (i.e., cada par estéreo generará para cada punto 4 ecuaciones para resolver las 3 incógnitas X, Y, Z del punto). El empleo de un objeto de calibración con coordenadas 3D conocidas para la orientación externa permite que las coordenadas X, Y, Z se puedan obtener en un sistema de coordenadas global para todas las cámaras.

Una vez se han obtenido las coordenadas tridimensionales de los puntos homólogos para toda la ROI, éstas son utilizadas para calcular los desplazamientos. De esta forma, es posible obtener un campo completo de desplazamientos para cada uno de los pares estereoscópicos o conjuntos de imágenes.

Termografía infrarroja activa

En el actual contexto de búsqueda de soluciones para mitigar el cambio climático y promover la eficiencia energética en la industria de la construcción, es fundamental la caracterización térmica de los nuevos materiales empleados con el fin de optimizar su rendimiento. Tradicionalmente esta caracterización se ha enfocado en el análisis de propiedades como la conductividad térmica [59] para evaluar la capacidad de aislamiento térmico. Sin embargo, bien sea para analizar esta capacidad de aislamiento o para mejorar su desempeño en términos de almacenamiento de calor, la exposición de los materiales a condiciones solares es fundamental cuando durante su vida funcional estos materiales van a estar expuestos a condiciones ambientales externas.

Para monitorizar este comportamiento térmico generalmente se emplean técnicas de medición convencionales como los termopares o los pirómetros de contacto. Sin embargo, estas técnicas presentan algunos inconvenientes, ya que se trata de técnicas que proporcionan mediciones puntuales de temperatura en un único punto de la superficie del material y además pueden requerir tiempo para ser colocados y obtener lecturas precisas, dificultando las mediciones en tiempo real y de manera continua. En este sentido, el empleo de técnicas de caracterización avanzada como la termografía infrarroja (IRT, del inglés "InfraRed Thermography") [60] cobra especial relevancia para obtener una visión más completa y detallada del comportamiento térmico de los materiales. Se trata de una técnica no destructiva que permite la captura de imágenes térmicas que muestran la distribución completa de la temperatura en un área determinada de manera remota y sin contacto físico, facilitando además el monitoreo constante de la temperatura [61].

En la actualidad, la termografía infrarroja ha ganado una gran importancia en una amplia gama de aplicaciones, desde el mantenimiento predictivo en la industria [62] hasta la monitorización en la construcción [63]. Su versatilidad y capacidad para proporcionar información sobre la temperatura superficial y la distribución térmica interna la convierten en una herramienta valiosa para evaluar el rendimiento de materiales de construcción con el fin de alcanzar una mayor eficiencia térmica y energética en las infraestructuras.

Esta técnica se basa en el principio de que todos los objetos emiten radiación en función de su temperatura. La radiación infrarroja es una forma de radiación electromagnética que todos los objetos con temperatura por encima del cero absoluto emiten. Esta radiación es invisible al ojo humano, pero puede ser detectada por dispositivos sensibles a las longitudes de onda en el rango infrarrojo. La diferencia en la composición de los materiales provoca cambios en su flujo de calor, lo que permite que alcancen diferentes temperaturas y su emisión de radiación sea distinta, permitiendo así a los sistemas de termografía detectar comportamientos dispares entre estos materiales [10]. El funcionamiento de un sistema de IRT comienza con la captura de la radiación infrarroja emitida por la superficie del objeto de interés (**Figura 6**). Este proceso se realiza mediante una cámara termográfica equipada con un sensor sensible a las longitudes de

onda infrarrojas. Estos sensores convierten la radiación infrarroja en señales eléctricas, que luego son procesadas y convertidas en datos digitales por el sistema de la cámara.
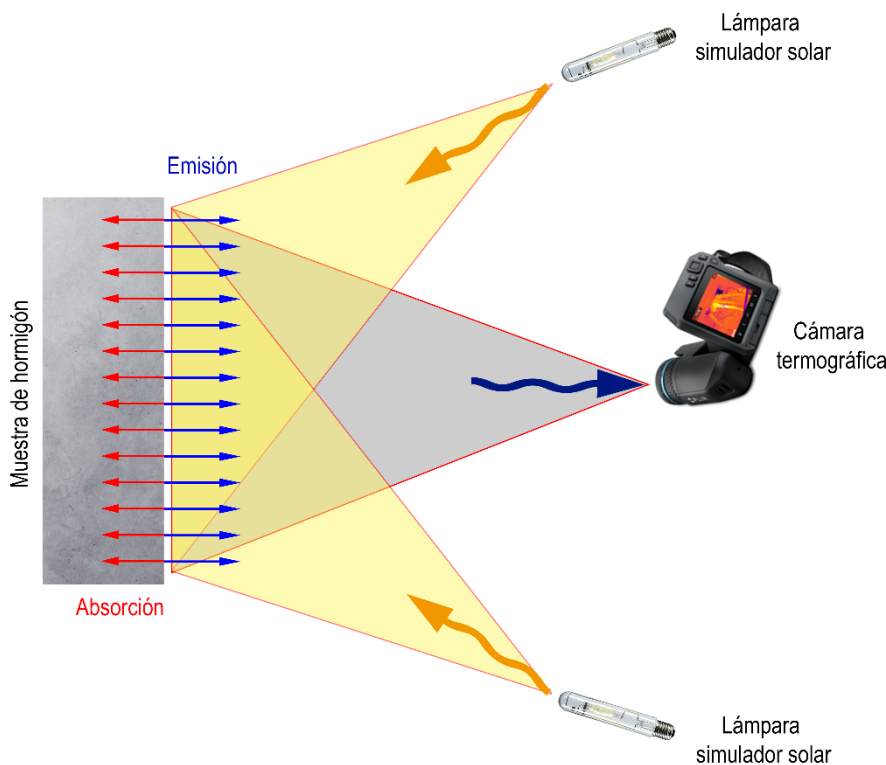
Figura 6: Diagrama de monitorización mediante termografía infrarroja activa empleando lámparas de simulador solar y cámara termográfica. (Fuente: Elaboración propia).

La capacidad de obtención de medidas de temperatura superficial de la IRT puede ser combinada con la aplicación de calor controlado sobre un objeto o superficie para evaluar su rendimiento térmico (termografía activa). Mientras que la termografía pasiva no requiere de una fuente de calor externa y detecta la radiación térmica natural emitida por el objeto, la termografía activa emplea fuentes de calor externas controladas para provocar cambios de temperatura. En este sentido, existe una amplia gama de métodos de excitación como la termografía pulsada, step heating y lock-in [64], lo que permite aplicar esta técnica para múltiples propósitos.

En particular, tal y como se ha comentado anteriormente, resulta interesante conocer el comportamiento térmico de los materiales de construcción sometidos a condiciones solares para determinar su capacidad tanto de aislamiento como de acumulación de calor. En este sentido, los simuladores solares son dispositivos capaces de simular de forma aproximada, mediante luz artificial, la luz del sol [65]. Esto permite simular las condiciones ambientales reales, reproduciendo la radiación solar, a las que pueden exponerse los materiales de construcción. Además, estos dispositivos permiten realizar ensayos y simulaciones en laboratorio bajo condiciones ambientales controladas. Gracias a ello, es posible planificar y programar pruebas diseñadas ad-hoc, además de garantizar la reproducibilidad y repetitividad de los ensayos realizados.

Los simuladores solares integran lámparas que emiten luz artificial que simula las características espectrales y la intensidad de la radiación solar. Entre los tipos de lámparas más empleadas para estos dispositivos de simulación se pueden mencionar los siguientes [66]: las lámparas de xenón, utilizadas en simuladores solares de alta gama; las lámparas de halogenuro metálicos, que ofrecen una buena eficiencia energética y capacidad para simular el espectro solar; las lámparas de tungsteno-halógeno, que ofrecen gran estabilidad lumínica; y las lámparas de arco de carbono, que se emplean en simuladores solares para aplicaciones industriales por los requerimientos de una alta potencia lumínica.

El iluminante más ampliamente empleado como referencia es el D65, que representa la luz diurna media [67]. No obstante, para aplicaciones menos restrictivas en términos de precisión colorimétrica, es posible utilizar fuentes de luz convencionales que no sean estándar como las mencionadas lámparas de halogenuro metálico. En estos casos, es necesario realizar mediciones que permitan llevar a cabo la caracterización lumínica de la luz emitida para evaluar y describir sus propiedades y comportamiento [68]. Las propiedades más relevantes para caracterizar una fuente de luz incluyen su distribución de potencia espectral, (SPD del inglés "Spectral Power Distribution"), temperatura de color correlacionada (CCT, del inglés "Color Correlated Temperature"), iluminancia, y blanco de referencia [69].

Los simuladores solares se emplean habitualmente para realizar pruebas de rendimiento de sistemas solares térmicos y fotovoltaicos en el ámbito de las energías renovables. Sin embargo, su capacidad de simular la radiación solar puede ser utilizada para otros fines relacionados con el ámbito industrial y de la construcción [70]. En este contexto, el empleo de simuladores solares combinado con sistemas de monitorización de temperatura permite realizar estudios sobre el comportamiento térmico de los materiales frente al ciclo sinusoidal de la temperatura diaria.

1.2. Hipótesis de trabajo

De acuerdo con lo expuesto anteriormente, los residuos de la construcción pueden emplearse como materia prima secundaria en la fabricación de nuevos materiales de construcción. Esto permite llevar a cabo una gestión eficaz para reducir tanto la cantidad de recursos consumidos como la de residuos generados, para alcanzar una producción más responsable y desarrollar infraestructuras más sostenibles conforme a los ODS. A su vez, la incorporación de aditivos permite mejorar tanto las propiedades mecánicas como térmicas de estos nuevos materiales permitiendo su empleo en una edificación y construcción más sostenible.

Por otra parte, se ha mostrado la existencia de nuevas técnicas de caracterización tanto mecánica como térmica validadas en materiales de diferente composición y comportamiento. Tanto la correlación digital de imágenes, para obtener desplazamientos y deformaciones, como la termografía infrarroja, para obtener temperaturas, son técnicas que permiten sustituir otras metodologías convencionales. Además, se trata de técnicas sin contacto, no invasivas, no destructivas y de campo completo.

La línea de investigación seguida en la presente Tesis Doctoral plantea la siguiente hipótesis principal:

HP: Las nuevas técnicas de campo completo pueden ser integradas en el sector de la construcción para la mejora de las propiedades mecánicas y térmicas de nuevos materiales sostenibles.

Para avanzar en esta cuestión, se establecen las siguientes hipótesis de trabajo:

H1: La sustitución de áridos naturales por áridos reciclados o la incorporación de aditivos permiten obtener materiales de construcción más sostenibles con capacidades mecánicas adecuadas.

H2: La correlación digital de imágenes es una técnica sin contacto que puede ser empleada para medir desplazamientos y deformaciones de campo completo y obtener las propiedades mecánicas de nuevos materiales de construcción.

H3: La incorporación de aditivos permite mejorar las propiedades térmicas de los materiales de construcción para su uso más eficiente y sostenible.

H4: La aplicación de condiciones ambientales simuladas mediante luz artificial puede ser empleada para replicar el comportamiento de los nuevos materiales ante la luz natural del sol.

H5: La termografía infrarroja es una técnica que puede ser combinada con simuladores solares para monitorizar y evaluar el rendimiento térmico de nuevos materiales de construcción en toda su superficie.

1.3. Objetivos

A partir de las hipótesis de trabajo definidas anteriormente, se plantea el objetivo principal de la presente Tesis Doctoral:

OP: Avanzar en el desarrollo e integración de técnicas ópticas de campo completo como la correlación digital de imágenes y la termografía, para el análisis y caracterización de nuevos materiales que contribuyan a una construcción más sostenible y energéticamente más eficiente.

A su vez, cumplir con dicho objetivo principal implica la necesidad de abordar los siguientes desafíos definidos como objetivos específicos:

OE1: Desarrollar nuevos materiales con propiedades mecánicas aptas para su empleo en la construcción bajo los principios de economía circular y sostenibilidad.

OE2: Implementar la técnica de correlación digital de imágenes en sus enfoques bidimensional y tridimensional para obtener desplazamientos y deformaciones de campo completo tanto en muestras planas como en muestras con curvatura.

OE3: Diseñar y fabricar un prototipo para realizar ensayos de caracterización mecánica en materiales a partir de DIC y reconstrucción tridimensional.

OE4: Explotar los datos proporcionados por la técnica DIC para obtener funciones de densidad probabilística de los principales parámetros mecánicos que permitan realizar análisis exhaustivos del comportamiento espacial de los nuevos materiales.

OE5: Desarrollar nuevos materiales con propiedades térmicas mejoradas para su empleo en la construcción bajo los principios de sostenibilidad y eficiencia energética.

OE6: Diseñar, fabricar y caracterizar un simulador solar low-cost para realizar ensayos de caracterización térmica de materiales.

OE7: Implementar la técnica de termografía infrarroja activa para analizar el comportamiento térmico de nuevos materiales de construcción sometidos a excitación bajo condiciones solares simuladas.

OE8: Integrar los avances mecánicos y térmicos bajo un mismo material y validar su aplicabilidad en un prototipo con aplicación industrial.

1.4.   Estructura de la Tesis Doctoral

La presente Tesis Doctoral se ha desarrollado en la modalidad de "compendio de artículos" de acuerdo con la normativa específica de la Universidad de Salamanca. Se han considerado cinco artículos científicos, todos ellos publicados en revistas internacionales de alto impacto indexadas en el Journal Citation Reports (JCR).

La Tesis Doctoral se ha dividido en cinco capítulos de acuerdo a la estructura que se muestra en la **Figura 7**. Tras este primer capítulo de Introducción, los capítulos II, III y IV se corresponden con los trabajos publicados, abordando los objetivos y las hipótesis de trabajo planteadas. Por último, el capítulo V recoge las principales Conclusiones y Trabajos Futuros.
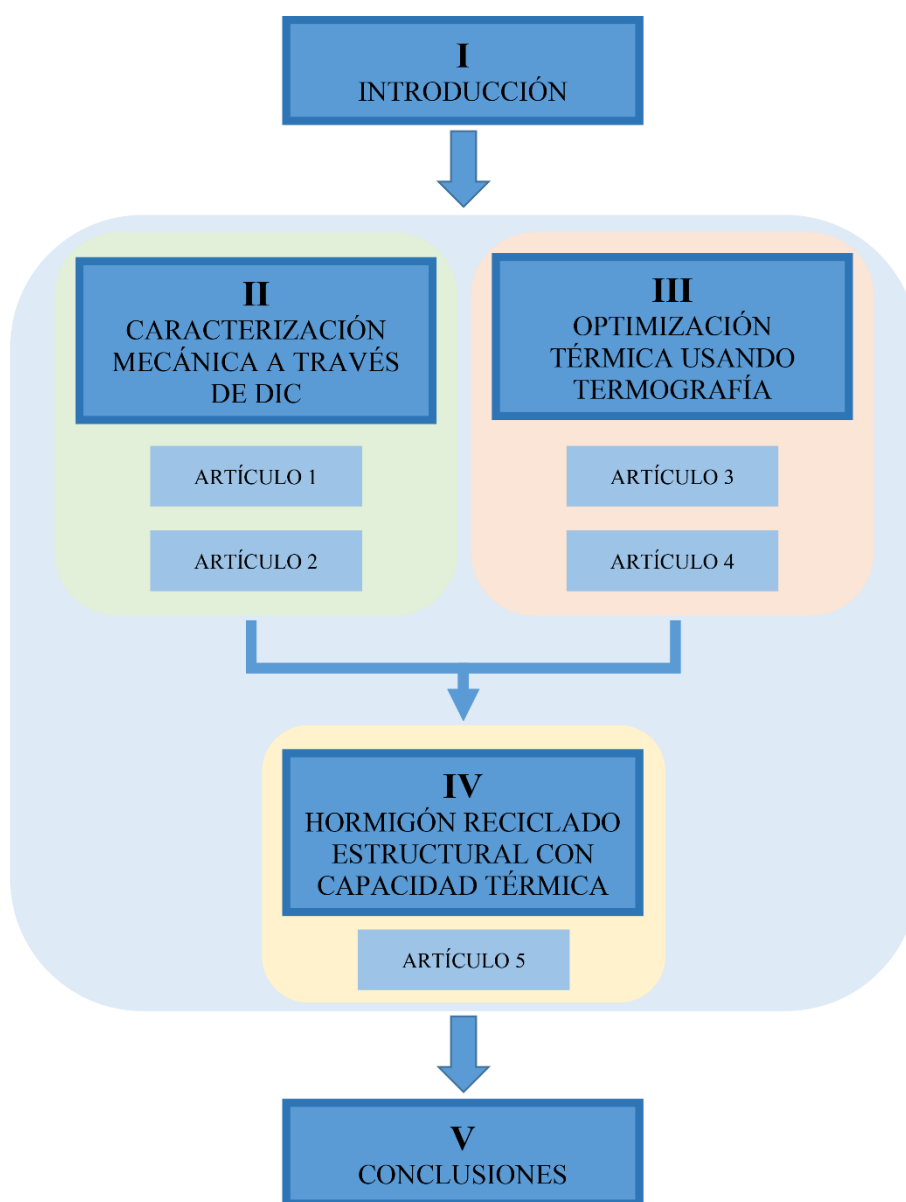
Figura 7: Estructura y capítulos de la Tesis Doctoral.

A continuación, se detallan los capítulos incluidos en la Tesis Doctoral y la relación existente entre cada uno de ellos:

Capítulo I. Introducción

El primer capítulo introductorio describe la motivación de la línea de investigación seguida a lo largo de la Tesis Doctoral y la relación existente entre los diferentes artículos científicos de impacto publicados. En primer lugar, se establecen las bases sobre los materiales de construcción y el enfoque de sostenibilidad desde el punto de vista de sus propiedades mecánicas y térmicas. A continuación, se analizan las técnicas empleadas para el análisis y caracterización de estos materiales como son la correlación digital de imágenes y la termografía infrarroja. Por último, se plantean tanto las hipótesis de trabajo como los objetivos de la investigación y la relación entre los distintos artículos científicos.

Capítulo II. Caracterización mecánica a través de correlación digital de imágenes

El segundo capítulo se centra en el análisis de las propiedades mecánicas de los materiales de construcción. Dentro de este capítulo se plantean dos trabajos científicos en los que se emplean diferentes materiales de construcción que siguen una línea evolutiva en cuanto a su capacidad. En primera instancia, se analizan materiales básicos de menor capacidad mecánica conformados por tierra como principal materia prima (Epígrafe 2.1). En segundo lugar (Epígrafe 2.2), se da el salto a materiales cementosos como el hormigón tratando de lograr un material sostenible con la inclusión de áridos reciclados.

Además del enfoque mecánico de los materiales, los trabajos de este capítulo tienen como nexo común la técnica empleada para su caracterización: la correlación digital de imágenes. En el primero de los trabajos se opta por un enfoque bidimensional para estudiar muestras planas. El segundo trabajo va un paso más allá con la técnica DIC, optando por un enfoque tridimensional para analizar muestras cilíndricas que presentan curvatura en su superficie.

Capítulo III. Optimización térmica usando termografía activa

El tercer capítulo aborda la mejora de las propiedades térmicas de los materiales de construcción. Se incluyen dos estudios en los que se trabaja con morteros de cemento manteniendo el principio de sostenibilidad, para lo cual se incorporan aditivos de diferente procedencia, en todos los casos respetuosos con el medioambiente. El primer trabajo (Epígrafe 3.1) se centra en mejorar las propiedades térmicas desde el punto de vista de la conductividad térmica, alterada mediante la incorporación de residuos o materiales reciclados empleados en la construcción. El segundo trabajo (Epígrafe 3.2) trata de potenciar la capacidad térmica de los materiales desde el punto de vista de la absorción de radiación solar, incluyendo como aditivos pigmentos colorantes.

Para llevar a cabo la optimización de las propiedades térmicas, en ambos estudios se utiliza la técnica de termografía infrarroja activa. Se emplea un simulador solar para el calentamiento de los materiales que permite replicar las condiciones ambientales de la exposición al sol. Los cambios de temperatura son monitorizados con cámara termográfica con el fin de evaluar el comportamiento térmico de estos materiales.

Capítulo IV. Hormigón reciclado estructural con capacidad térmica

El cuarto capítulo fusiona el conocimiento adquirido en los capítulos II y III para desarrollar un material con capacidad mejorada, tanto mecánica como térmica, gracias a las técnicas empleadas anteriormente. En este trabajo (Epígrafe 4.1) se modifica la procedencia de los áridos reciclados para lograr un hormigón con carácter estructural a partir de las mejoras mecánicas planteadas y se combina con la inclusión de pigmentos colorantes para la mejora de sus propiedades térmicas. La técnica DIC para la monitorización mecánica y la termografía infrarroja para la monitorización térmica, ambas de campo completo, son combinadas para desarrollar un depósito de agua con hormigón reciclado pigmentado como material de construcción y cuya función principal es la acumulación de calor.

Capítulo V. Conclusiones y trabajos futuros

El último capítulo expone las principales conclusiones obtenidas tras el desarrollo de la Tesis Doctoral, discutiendo los resultados obtenidos y su aplicabilidad al sector de la ingeniería civil e industrial. Por último, se exponen los trabajos futuros y las nuevas líneas de investigación surgidas a partir de los trabajos desarrollados.

Apéndice I. Indexación y factor de impacto de las revistas

Este apéndice muestra la información relevante de las revistas científicas en las que se han publicado los artículos que conforman la Tesis Doctoral. Se incluyen diferentes métricas para evaluar el impacto y relevancia de cada una de las revistas.

Apéndice II. Patente

Este apéndice incluye la patente solicitada para el prototipo para la caracterización mecánica de materiales a partir de DIC y reconstrucción tridimensional, desarrollado durante la elaboración de la Tesis Doctoral.

CAPÍTULO II

CARACTERIZACIÓN MECÁNICA A TRAVÉS DE CORRELACIÓN DIGITAL DE IMÁGENES

2.1. Materiales de construcción a partir de materias primas básicas: bloques de tierra comprimida

En esta primera parte del capítulo II se incluye el artículo "*Improvement of mechanical properties of compressed earth blocks with stabilising additives for self-build of sustainable housing*", publicado en la revista *Buildings*.

Resumen

Las tecnologías de construcción con materiales de tierra se utilizan cada vez más para promover un modelo de construcción natural y sostenible aprovechando los recursos naturales locales. Además, su empleo permite promover la autoconstrucción de viviendas sostenibles para que zonas con recursos limitados y difícil acceso a materiales convencionales puedan aprovechar el potencial de los materiales de tierra. En este sentido, el **objetivo** de este trabajo es investigar el uso de diferentes tipos de aditivos estabilizantes en bloques de tierra comprimida (BTC) para mejorar sus propiedades mecánicas, aprovechando así los recursos locales y naturales que generan menor contaminación y residuos. A su vez, y con el objetivo de caracterizar mecánicamente y evaluar el comportamiento de las soluciones propuestas, se plantea la aplicación de la técnicas macro-fotogramétricas de campo completo para medir las deformaciones.

La **metodología** seguida consistió en la caracterización de bloques de tierra comprimida fabricados de acuerdo a cuatro tipologías: (i) a base de tierra y agua; (ii) con fibras naturales; (iii) con aditivos cementosos; y (iv) con aditivos de otro origen. Como materia prima se analizaron tierras extraídas de diferentes lugares de Ecuador, que fueron sometidas a ensayos empíricos y pruebas de laboratorio para determinar su idoneidad. Se diseñó y fabricó equipamiento ad-hoc consistente en un cilindro cernidor para la tierra y una prensa hidráulica para la que los usuarios finales puedan elaborar sus propios bloques de tierra comprimida con el fin de fomentar la autoconstrucción.

Los BTCs fueron caracterizados mecánicamente mediante ensayos de compresión para determinar su adecuación a las normativas de la región. Una vez determinadas las tipologías más interesantes desde el punto de vista estructural y de la sostenibilidad, las muestras correspondientes se sometieron a ensayos más exhaustivos para analizar las deformaciones y los mecanismos de rotura. Para ello se empleó la técnica de correlación digital de imágenes (DIC) en su enfoque bidimensional, que permite obtener los desplazamientos y deformaciones en todos los puntos de la superficie de los paneles.

Por último y con el fin de comparar la viabilidad de las soluciones propuestas, se llevó a cabo un estudio económico. Se consideraron los costes de material, equipamiento y

mano de obra para evaluar el coste total de cada tipo de panel y compararlo con los sistemas de construcción convencionales.

Los **resultados** mostraron como solución más adecuada desde el punto de vista estructural los BTCs estabilizados con cemento. En concreto, aquellos con un porcentaje de cemento superior al 15% superan la resistencia a compresión de 2MPa requerida por la normativa. El análisis de deformaciones mostró que presentan una deformación última similar a la del hormigón, produciéndose en la mayoría de los casos en el entorno de las zonas de contacto. Desde el punto de vista de la sostenibilidad, la solución más interesante es la estabilizada con fibras de carrizo. A pesar de que su resistencia no alcanza el mínimo requerido, puede ser interesante para otras aplicaciones en arquitectura con menor solicitación como particiones o tabiques. Además, su mayor capacidad de deformación resulta también interesante para aplicaciones sísmicas. Por último, el análisis económico demostró que los BTCs son una solución económicamente adecuada, ya que permite un ahorro considerable en los costes unitarios por m^2. Además, son considerados un material más limpio gracias al ahorro de costes y a la menor contaminación en su transporte al utilizar materiales locales.

Las principales **conclusiones** del trabajo resaltan la idoneidad de los bloques de tierra comprimida como una solución adecuada en el sector de la construcción para aprovechar los recursos locales y contribuir a la mejora medioambiental, promoviendo la sostenibilidad y la autoconstrucción en zonas con recursos limitados. Se ha mostrado la correlación digital de imágenes como una técnica idónea para analizar los desplazamientos y las deformaciones de campo completo, lo que ha permitido determinar el modo de fisuración y obtener la deformación última en el instante anterior al fallo.

Improvement of Mechanical Properties of Compressed Earth Blocks with Stabilising Additives for Self-Build of Sustainable Housing

Jorge López-Rebollo [1,*], Xavier Cárdenas-Haro [2,3], Juan Pablo Parra-Vargas [2], Kevin Narváez-Berrezueta [2] and Julver Pino [3]

1. Department of Cartographic and Land Engineering, Higher Polytechnic School of Ávila, University of Salamanca, Hornos Caleros, 50, 05003 Ávila, Spain
2. Facultad de Arquitectura y Urbanismo, Virtual Tech, Universidad de Cuenca, Av. 12 de Abril s/n y Av. Loja, Cuenca 010201, Ecuador
3. Facultad de Ingeniería, Departamento de Ingeniería Civil, Universidad de Cuenca, Av. 12 de Abril s/n y Av. Loja, Cuenca 010201, Ecuador
* Correspondence: jorge_lopez@usal.es

Abstract: Earth building technologies are increasingly being used to promote a natural and sustainable construction model and to empower self-building in resource-limited areas. This work focuses on investigating the use of different types of stabilising additives in compressed earth blocks (CEBs). To this end, empirical studies and laboratory analyses of earth samples taken from different sites in Ecuador were combined. Once the most suitable earth for use as a building material was determined, four types of CEBs were produced using equipment designed ad hoc to encourage self-building: earth-based, fibre additives, cementitious additives, and additives of other origin. The panels were characterised by means of compression tests to analyse their mechanical behaviour, obtaining the most promising results for the additivated samples with the highest percentage of cement and for the sample containing ground reeds, with a compressive strength of 3.3 MPa and 0.7 MPa, respectively. These samples were then subjected to more extensive tests using digital image correlation to analyse their full field strains and cracks, where the samples stabilised with cement showed a more homogeneous and consistent behaviour. Finally, an economic and comparative study with conventional construction systems was carried out to demonstrate the feasibility of using the proposed earth materials for cleaner and more economical buildings, mainly due to cost savings and lower pollution in terms of transport when using local resources.

Keywords: sustainable construction; earthen architecture; compressed earth block; earthen materials; mechanical properties; digital image correlation

1. Introduction

The materials used for building and construction are abundant but non-renewable resources, so their availability is not unlimited worldwide. In fact, high exploitation and its associated costs can lead to shortages in the medium and long term in countries with very high production [1]. Together with the high consumption of resources, the production of this type of material, such as concrete, is responsible for up to 8% of world CO_2 emissions [2], so it is necessary to establish construction systems related to the concepts of sustainability and circular economy. On the other hand, there are certain regions in which the extraction of raw materials, such as aggregates, is not feasible due to their availability or the available means [3]. In this context, earth construction is seen as an alternative to the use of other materials such as concrete, taking advantage of its potential as a local material and reducing waste generation according to the concepts of economy and sustainable development [4].

The use of these earthen building technologies is so widespread that it is estimated that approximately one-third of the world's population lives in earthen buildings [5]. It is a

type of construction that was widely used until the beginning of the twentieth century and that regained popularity at the end of the 1970s after the energy crisis in Europe [6], so it is essential to find the tools to improve its potential and continue its use in the 21st century.

There are different earth construction techniques, such as adobe, rammed earth, rammed earth blocks or compressed earth blocks (CEBs). Among them, CEBs are very versatile elements obtained from wet earth compression that can be used in load-bearing walls, enclosures, heat-accumulating walls or as a replacement for conventional bricks [7]. The production of these types of earthen materials requires only 1% of the energy used to produce the same volume of conventional concrete [8], which means a considerable saving in energy and CO_2 emissions. In addition, the savings in time, cost and pollution caused by their transportation make CEBs more environmentally friendly than other building materials [4].

There are different standards around the world that deal with the manufacture of these materials [9]. The most internationally recognised standards are the New Zealand standard [10,11], the American Society for Testing and Materials (ASTM) [12] or the Spanish UNE [13]. Nevertheless, to this day, there is no standardisation or accurate knowledge of these types of materials [14]. Differences in composition due to the local nature of these materials result in heterogeneous properties and behaviour [15], making global standardisation difficult.

Despite the fact that by increasing pressures, adequate strengths can be achieved for CEBs [16], in order to improve the mechanical performance of CEBs, the research trend is moving towards the introduction of stabilisers for the manufacture of stabilised compressed earth blocks (SCEBs) [17], also known as soil cement blocks or soil–cement bricks [18]. The most commonly used stabilisers are Portland cement, lime or asphalt emulsion [4]. In addition, other additives can be added to improve their properties. For example, natural fibres improve thermal properties [19]; oils, fats or waxes allow waterproofing [20]; and biopolymers improve cohesion so that they improve both the strength and durability of the soil [21]. Nevertheless, the efficiency of these types of stabilisers is related to the earth's composition, so it is necessary to carry out in-depth analyses and studies to verify the viability of these materials [22].

Furthermore, the incorporation of these types of additives entails an alteration of their mechanical properties, causing the material to behave differently. In this sense, composite materials with the incorporation of fibres or other additives usually present a high degree of heterogeneity [23]. Additionally, the failure of the material significantly depends on how and where the fracture occurs. This means that strains, especially the so-called peak strain prior to fracture, can differ greatly depending on the measurement area.

Generally, conventional mechanical characterisation techniques use devices such as extensometers, LVDT or strain gauges, which have a local nature and require direct contact with the material. In this sense, earth-derived materials generally present problems due to the disaggregation of the material when it begins to deform, even before failure [24]. Measurement with these devices is conditional on the absence of cracks and disaggregation of the material, as this would prevent further data collection. In contrast to this type of technique, other full-field techniques have emerged that allow monitoring of the complete behaviour without the need for contact with the material [25,26]. One of the most widely used techniques for the analysis of full-field displacements and strains is digital image correlation (DIC). This is a technique that allows analysis of the complete surface of the material using images of the sample acquired while it is subjected to load tests [27]. This technique can be used for flat specimens in its two-dimensional approach and for specimens with greater curvature through its three-dimensional approach [28]. In particular, the 2D approach employed in this study has been used to obtain the strains and to monitor damage progression [29] in works on materials with similar heterogeneous behaviour, including earth-derived aggregates such as sustainable concretes [30] and cementitious materials that incorporate fibres [31]. Nevertheless, it is a novel technique in the field of earthen materials, and there are few studies of its application due to the sample preparation requirements,

although it has proved to be a promising technique for obtaining full-field strains and cracks [32]. Perić Fekete et al. studied the failure mechanisms of rammed earth walls under seismic behaviour using the DIC technique [33]. Nabouch et al. also used DIC to record the evolution of cracks in rammed earth walls [34]. In this way, the peak strain can be measured more accurately, and parameters representative of the real behaviour of the material can be obtained, as it is possible to analyse the strains over the entire surface, including the rupture zone and remote areas.

Consequently, this work aims to advance knowledge concerning the introduction of stabilising additives of different natures in CEBs made with earth from different locations in Ecuador. The aim is to move towards a more sustainable building model, where conventional materials such as concrete and steel can be replaced by these earthen materials with improved mechanical properties, which make use of local and natural resources and generate less pollution and waste. This study seeks to promote the self-build of sustainable housing so that areas with limited resources and difficult access to conventional materials can realise the potential of earthen materials. Empirical tests will be combined with laboratory tests to characterise these types of earth, which will allow the selection of the most adequate option for the manufacture of CEBs. Subsequently, mechanical characterisation tests will determine the feasibility of SCEBs in the manufacturing, transport and construction processes. Finally, these tests will be complemented with DIC analysis to monitor and evaluate its behaviour. In addition, an economic study comparing the production costs of the additive-enhanced CEB solution with other conventional construction techniques is proposed to promote earthen architecture.

Following this introduction, Section 2 describes the materials and techniques used for this research. In Section 3, the experimental results of the physical and mechanical tests are shown and a discussion of these results is included. Section 4 provides an economic analysis of the feasibility of the products studied. Finally, in Section 5, the main conclusions on the suitability of introducing these materials in the construction industry are drawn and future research directions are discussed.

2. Materials and Methods

This work focuses on the fabrication and characterisation of compressed earth blocks with different additives for stabilisation. First, earth samples from different locations are selected and characterised through the use of empirical and laboratory physical tests. Then, the production of CEBs is carried out using the selected earth samples. For their manufacture, different additives were selected in order to achieve stabilisation while considering both economic and environmental aspects. These blocks were mechanically characterised by means of compression tests to check whether they could be used as building elements in accordance with the standards. Finally, an economic analysis was carried out to compare the unit cost of the manufactured blocks with other conventional construction techniques and materials. Figure 1 shows a schematic diagram of the workflow followed.

2.1. Earth Materials

Initially, different types of earth were selected and analysed to determine the best option for the manufacture of the compressed earth blocks. In order to achieve greater variability in the samples and to analyse earth of different provenance, it was decided to select samples from four different locations, although all of them were located in the province of Azuay, Ecuador. The location was determined based on the availability of extractable material and the existence of construction material factories in the vicinity. In addition, different colours of earth were taken into account to widen the spectrum of selection and experimentation. The location and coordinates of the individual samples are shown in Table 1.
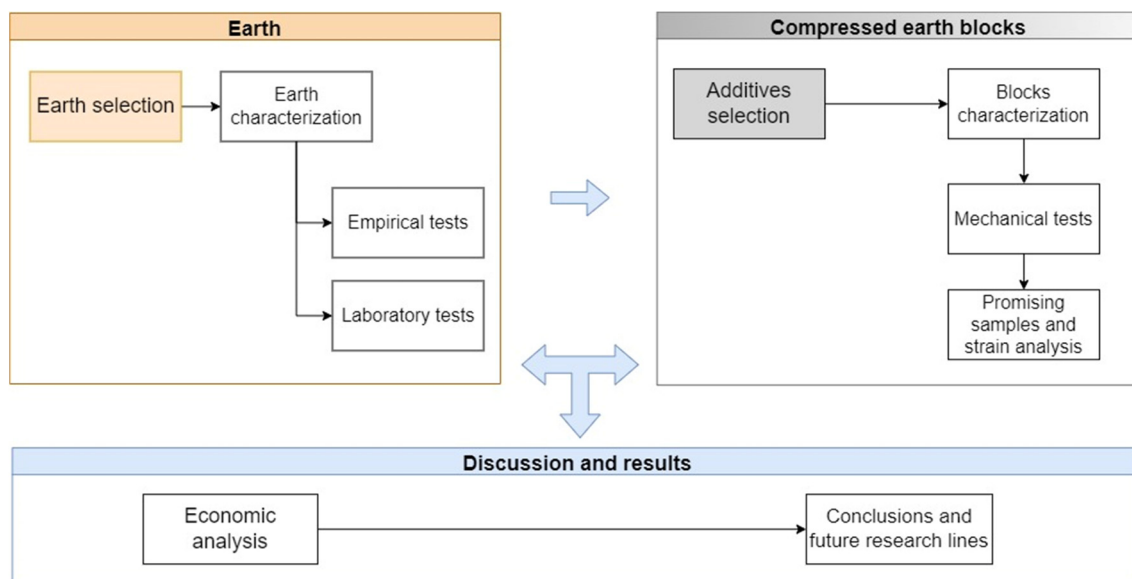
Figure 1. Workflow diagram.

Table 1. Location and coordinates of selected earth samples.

Nomenclature	City	Zone	Latitude	Longitude
E_CC	Cuenca	Challuabamba	−2.859099	−78.921227
E_CM	Cuenca	Monay	−2.916045	−78.973492
E_CN	Cuenca	Nulti	−2.866469	−78.923978
E_PD	Pucará	Deuta	−3.321508	−79.395789

2.2. Earth Characterisation

The selected earth samples were analysed and subjected to different types of tests. Since there are no specific standards for this type of materials and for all the tests in the country where the samples were taken, standards from nearby countries such as Colombia, Peru or the USA were also used.

On the one hand, empirical tests allow us to gain generic knowledge of the samples and to understand some of their properties, such as humidity or the presence of sand, silt and clay [35]. Among these tests, the following can be highlighted according to the Peruvian standard E.080 [36]:

- The odour test allows for the identification of organic matter or humus.
- The bite test allows for the differentiation of the predominance of clay in the stickiest samples.
- The washing test identifies whether the sample is sandy, silty or clayey, depending on the need to use less or more water to remove debris and dirt.
- The cut test consists of cutting the sample and determining whether clay is predominant when seen as shiny or silts if the cut is opaque.
- The ball test consists of dropping a ball on a flat surface and determining its composition so that the sample contains more clay if it does not flatten and crack and less if it breaks up.
- The consistency test requires moulding the sample into an earthworm shape, thus identifying the appropriate moisture content to form a 3 mm earthworm shape. This sample is then shaped into a ball to be dried for 48 h. If the ball is easy to break, it will have a low clay content, whereas if it is more consistent, it will have a higher clay content. If it is not possible to form the ball, it is identified as a sandy sample.

On the other hand, laboratory tests allow the composition and properties of the earth to be determined more accurately.

- Granulometric analysis allows the earth to be classified into gravel, sand, silt and clay according to the particle size that passes through each of the sieves [37].
- The plasticity test allows us to know the plastic limit. Thanks to this test, it is also possible to obtain properties such as the plasticity index, tenacity, liquidity and consistency [38].
- The compaction test or the standard Proctor test allows for the determination of the moisture–density ratio of the compacted material [39].

2.3. Compressed Earth Blocks

Once the study of the earth was carried out, the CEBs were manufactured using the selected solution as the raw material. The panels were designed to be used in the Sandino construction system, so the proposed dimensions were 30 cm × 45 cm × 7 cm, which are the height, width and thickness dimensions, respectively.

The CEB manufacturing process consists of three main phases: (i) drying and sifting of the material, (ii) dosing and compacting of the material, and (iii) the curing and drying of the CEBs.

Initially, 4 m³ of earth was collected, spread and dried for seven days to facilitate sifting, as a maximum particle size of 4.8 and 5 mm is required, according to Brazilian and Colombian regulations, respectively. To facilitate the sifting process, as well as the large-scale implementation of the manufacturing methodology in isolated communities with low resources, a sifting cylinder was designed (Figure 2). The cylinder is 30 cm in diameter and 1 m long and is made of a perforated metal mesh with 5 mm holes. A gate is incorporated in the central section through which the material can be fed into the tank and the larger particles can be discharged. This cylinder performs the simultaneous function of crushing and sifting using a rotating mechanism with a speed of 40 rpm.

Figure 2. Sifting cylinder manufactured for the crushing and sifting of the earth.

Following the same criteria mentioned above, a hydraulic press (Figure 3) was designed for the manufacture of the CEBs, consisting of steel profiles with a capacity of 50 tonnes, which is equivalent to a pressure of 1.82 MPa, considering the surface area of the panels.

Figure 3. Hydraulic press manufactured for pressing compressed earth blocks.

The dosages used for the manufacture of the stabilised CEBs (Figure 4) can be grouped into four main groups (Table 2): (i) reference, consisting only of earth and water; (ii) fibres, using the base bio-fibres as additive and natural white glue paste to facilitate adhesion; (iii) cementing agents, in this case the cement acting as a stabiliser; and (iv) others, using additives such as asphalt emulsion. Based on the analysis of the earth samples, E_CM earth was used for the manufacture of all samples except for sample PR_01, where E_CN earth was chosen. Taking into account the Proctor optimum for the selected earth, a water content of 20% was used for the cementitious samples as they have a higher water loss during the curing process, and a lower water content of 15% was used for the rest of the samples.

Figure 4. Storage and curing of the manufactured compressed earth blocks.

Table 2. Dosages and additives used for the manufacture of stabilised compressed earth blocks.

Nomenclature	Water %	Additive
PR_01	15	-
PR_02	15	-
PF_01	15	5% glue + 5% sawdust
PF_02	15	5% glue + 5% cabuya
PF_03	15	5% glue + 5% ground reed
PF_04	15	5% glue + 5% skeleton reed
PF_05	15	5% glue + 5% totora
PC_01	20	20% lime
PC_02	20	5% cement
PC_03	20	10% cement
PC_04	20	15% cement
PC_05	20	20% cement
PC_06	20	25% cement
PO_01	15	7% asphalt emulsion

2.4. Mechanical Characterisation of Compressed Earth Blocks

The compressed earth blocks manufactured were evaluated by means of compression tests according to guideline NTC 5324 [40], which classifies CEB into three types according to their compressive strength: CEB 20 for a strength of 2 MPa, CEB 40 for 4 MPa and CEB 60 for 6 MPa.

To carry out these tests, an electromechanical test machine, Concrete 2000X by Shimadzu (Kyoto, Japan), was used. The machine was equipped with a UH-X type control measuring unit and a load cell of 2000 kN. For the compression tests, steel profiles were used as compression devices with a 4 mm triplex sheet to homogenise the surfaces in contact. The test was set up at a constant displacement rate of 0.02 mm/s according to guideline NTC 5324 [40].

The compression tests were complemented by strain analysis. For this purpose, the digital image correlation technique [27] was used in a two-dimensional approach. This technique allows displacements and strains to be obtained during tests by acquiring images under different loading states. The images in each state are compared with an initial image without strain in order to obtain the displacement and strain of the sample.

The fundamentals of the DIC technique are based on the comparison of consecutive images by selecting a Region of Interest (ROI), which is divided into subsets [27]. These subsets are compared using the zero mean normalised cross-correlation criterion (ZNCC) [41]. Interpolations and optimisation algorithms are then applied to archive sub-pixel accuracy [42] for full-field displacements and strains. To facilitate this process, the sample must first be prepared by applying a pattern known as a speckle to its surface. This pattern consists of a distinct, unique, non-periodic and stable grayscale spot [43]. In this case, a matte white elastic primer was first applied to generate a greater contrast to the black speckle and to avoid the appearance of shiny spots on the surface. Random mottling was then generated using a matte black spray. Finally, the quality of the pattern was evaluated by means of the indicator known as the mean intensity gradient (MIG) [44]. A MIG value greater than 30 was obtained for all samples, and a coverage factor close to 50%, so that the quality of the pattern can be considered adequate [45].

The equipment used for the tests (Figure 5) consisted of a prototype similar to the one developed by García-Martín et al. [46], although the hardware and sensors were upgraded in order to achieve maximum accuracy. In this study, a high-resolution Manta G-917 1″ Monochrome CCD camera equipped with a 50 mm macro-prime lens was used for image

capture. Additionally, a neutral LED light was used to improve illumination and allow for shorter exposure times. The camera shots were synchronised with the load data collected by the test machine using a microcontroller, which allowed the capture parameters to be set.
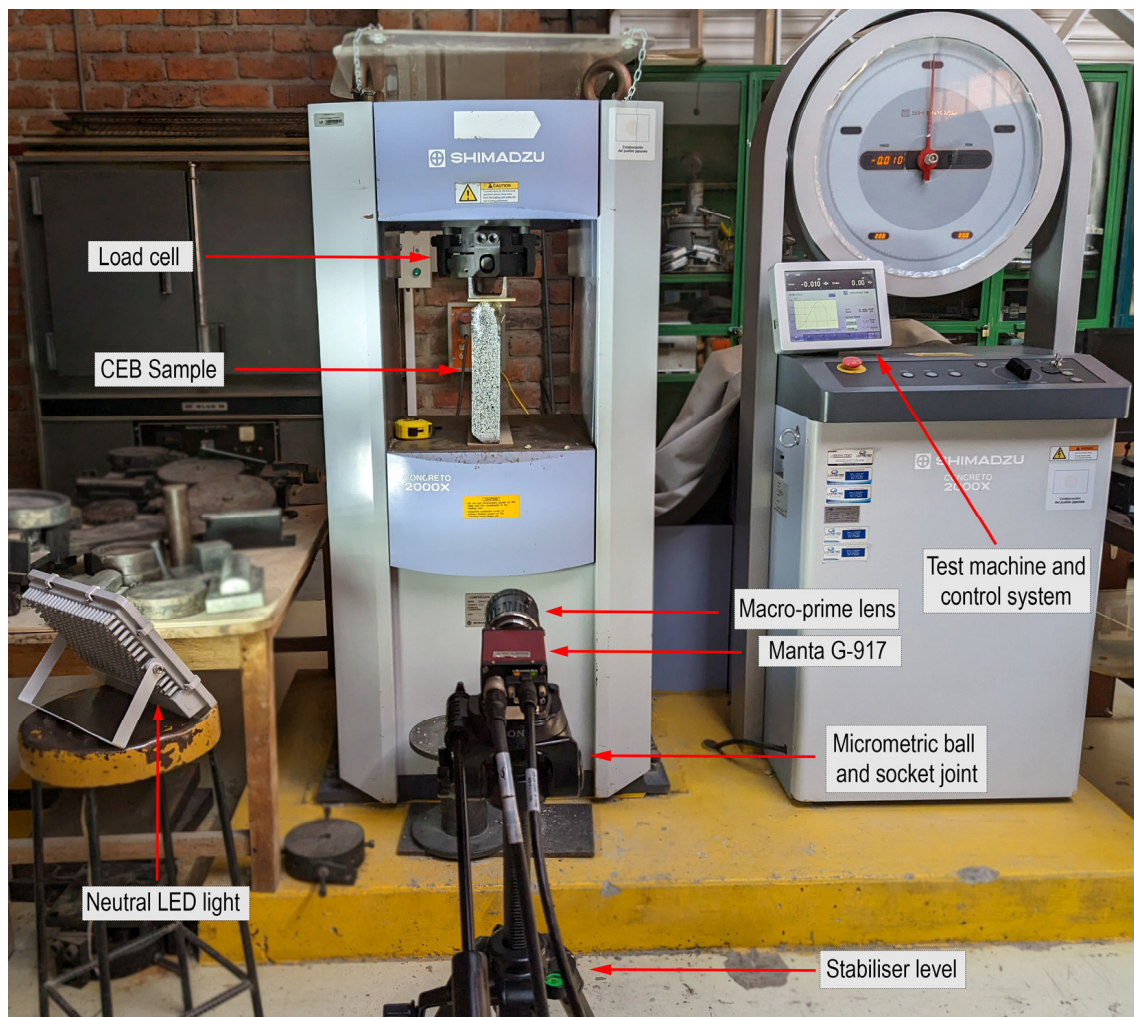
Figure 5. Equipment and setup for compression testing using digital image correlation.

Taking into account the slenderness of the sample, it was decided that DIC analysis would be performed on one side to check for significant lateral displacement. To ensure the perpendicularity of the camera and guarantee the 2D-DIC approach, a micrometric ball and socket joint was used. Given the dimensions of the sample, the camera was placed 1.5 m from the specimen, which allowed a GSD of 0.1 mm/px to be obtained. Artificial illumination allowed for a lens aperture of f8 to be set, thus ensuring an adequate balance for the depth of field. Considering that the displacement speed to which the test was subjected was low, the images were acquired at 1 FPS with a shutter speed of 1/100 s, capturing the first image before starting the test to obtain the reference image.

3. Experimental Results and Discussion

3.1. Earth Properties

3.1.1. Empirical Results

The empirical tests described in Section 2.2 were carried out. For this purpose, a small representative quantity was selected from each of the earth samples. A total of six tests were carried out for each of them, obtaining the results shown in Table 3 according to the criteria described above.

Table 3. Results of empirical tests.

Test	E_CC	E_CM	E_CN	E_PD
Odour	Low level of organic matter	Low level of organic matter	Low level of organic matter	Low level of organic matter
Bite	Sandy with clay	Sandy with clay	High level of clay	Sandy with low clay
Washing	High level of silt	Sandy with low level of clay	High level of clay	Silty-sandy
Cut	Medium level of clay	High level of silt	High level of clay	Medium level of clay as well as silt
Ball	High level of clay	Acceptable level of clay	High level of clay	Acceptable level of clay
Consistency	High level of clay	High level of clay	High level of clay	High level of clay

First, the empirical tests show that the level of organic matter is low for all samples. In terms of composition, the results are not very conclusive as the tests give different results for the same samples. The earth seems to show a higher or lower clay level depending on the water concentration and the mixing time, so the accuracy of these tests is not very high. The empirical tests had a low accuracy in terms of clay content, and some of the tests showed a predominance of sands or silts. In any case, the cracking after drying is very slight, indicating a low presence of expansive clay that could cause volume changes and problems in the curing of the CEBs. Therefore, they are tests that allow for a first impression of the samples in situ without the need to go to the laboratory. In this case, the results of these tests were combined with the laboratory tests to observe the correlation between them and to obtain the composition more precisely in order to select the most suitable sample.

3.1.2. Laboratory Results

The samples were subjected to laboratory tests to determine their granulometric composition, plastic behaviour and compaction. The results of these tests are shown in Figure 6.
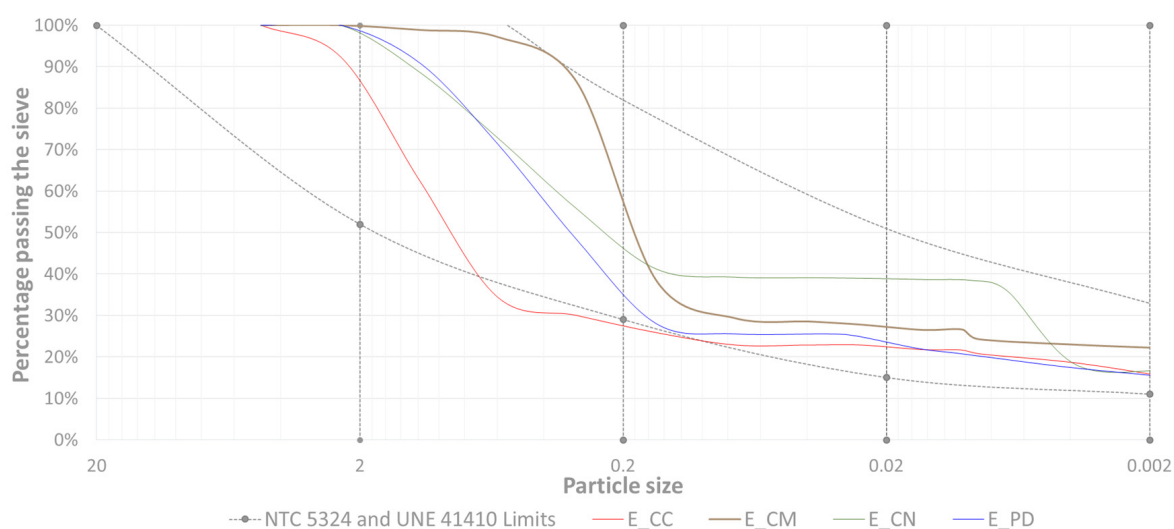
Figure 6. Granulometric curves of the samples analysed and their fit within the limits established by the regulations.

The particle size ranges shown in Figure 6 are those established by the Colombian standard NTC 5324 [40] and the Spanish standard UNE 41410 [13]. Samples E_CM, E_CN and E_PD fit in all particle sizes. Nevertheless, sample E_CC does exceed the established limits, especially in the range of the sands. Although this first test would allow this sample to be discarded, it was also subjected to other tests in order to compare it with the other samples.
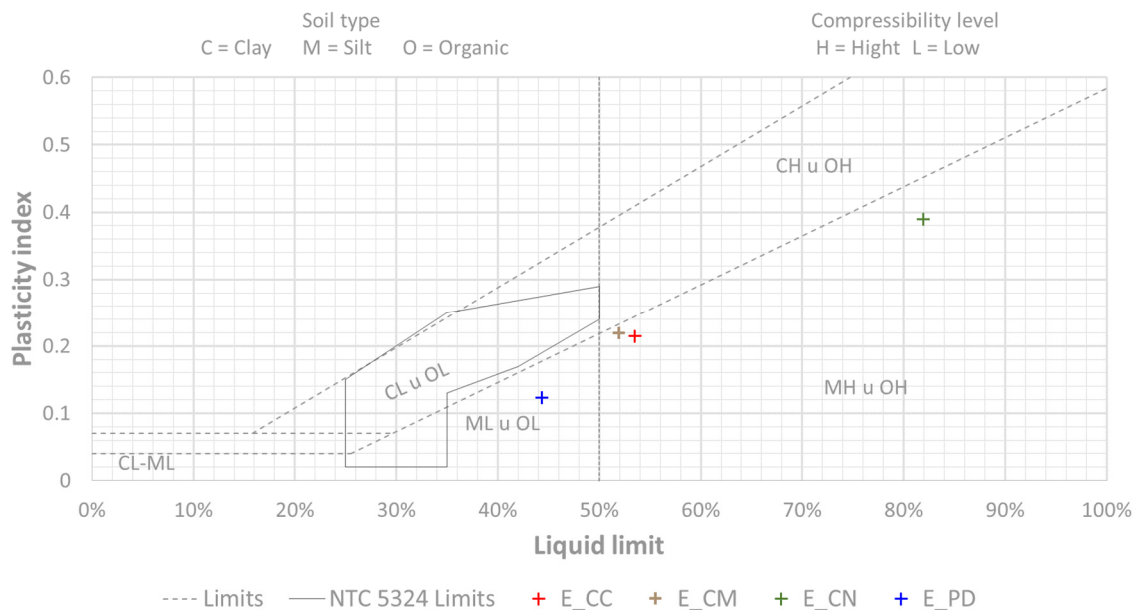
Following the same standards, Figure 7 shows the plasticity ranges for the selection of earths, as well as the results for each of the samples. In this case, none of them is within the normative spectrum, so it is not possible to select or discard any of them. Nevertheless, it can be mentioned that sample E_CM is the closest to the limits.

Figure 7. Diagram of the plasticity test and its fit within the limits established by the regulations.

Finally, the Proctor test allows for the evaluation of the appropriate amount of water to reach higher densities of the material with the same exerted pressure. As shown in Figure 8, sample E_PD fails to reach its maximum compaction limit due to the implication of adding a high percentage of water for this purpose; therefore, it was decided to discard this sample. On the other hand, samples E_CC, E_CM and E_CN find their compaction limit with moisture percentages lower than 30%. Among them, the one with the highest compaction, with even less water, is E_CM. This sample has a dry volumetric weight higher than 1.70 gr/cm^3 at the optimum point, while the value of the other samples is between 1.30 and 1.40 gr/cm^3. Furthermore, once the optimum point has been reached, sample E_CM loses density when the moisture content increases while the other samples remain constant. This makes it possible to determine the right amount of water to obtain higher densities at the same pressure, which is associated with higher block strength. The results of this last test agree with the greater approximation to the limits of the plasticity test of this sample, so it is reaffirmed as the best of the samples. Thus, sample E_CM is the one selected as the base earth for the manufacture of the CEBs.

3.2. Compressed Earth Blocks Properties

3.2.1. Mechanical Results

A total of 42 samples were manufactured, 3 of which were for each of the proposed dosages. The samples were cured for 7 days before being subjected to mechanical characterisation tests. In order to avoid water loss, the cement and lime samples were hydrated during the 7 days of curing, while those with fibres were only protected from the sun as required by the standards. The results of the compression tests, as well as their statistical parameters, are shown in Table 4.
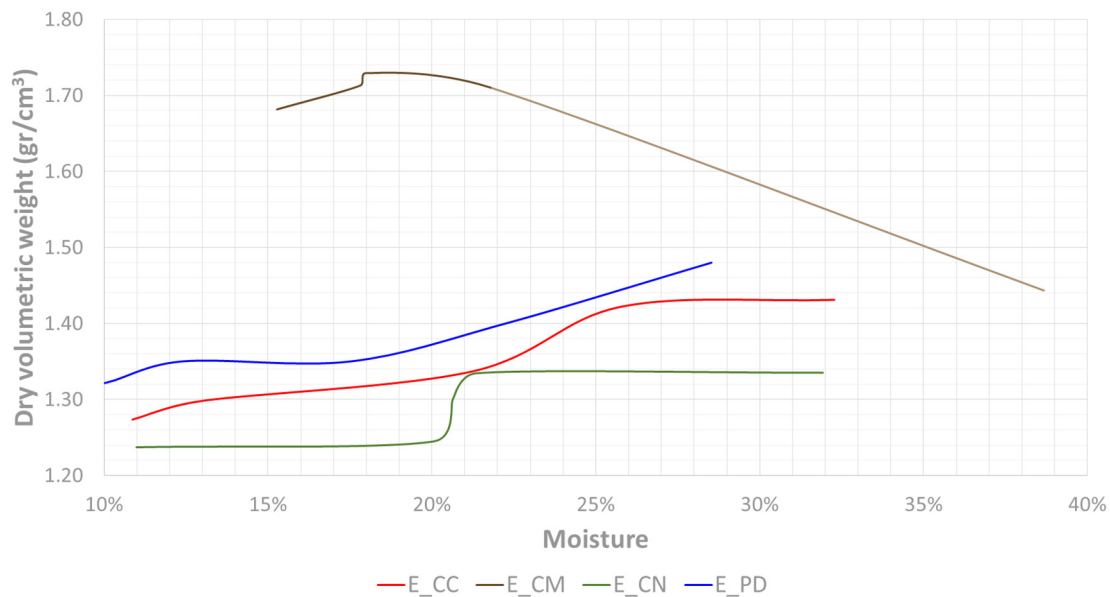
Figure 8. Density and moisture curves obtained from the Proctor test.

Table 4. Results of the compression test for CEB.

Nomenclature	Mean (MPa)	Lower Bound (MPa)	Upper Bound (MPa)	CoV (%)
PR_01	-	-	-	-
PR_02	-	-	-	-
PF_01	0.19	0.18	0.19	3.43
PF_02	0.27	0.15	0.41	48.8
PF_03	0.65	0.41	0.94	40.9
PF_04	-	-	-	-
PF_05	0.07	0.07	0.08	9.8
PC_01	0.36	0.30	0.45	20.7
PC_02	0.75	0.49	1.02	35.5
PC_03	1.61	1.41	1.78	11.7
PC_04	2.02	1.90	2.10	5.3
PC_05	2.43	1.63	3.98	42.4
PC_06	3.28	2.84	3.59	12.5
PO_01	-	-	-	-

The dehumidification process was easy in terms of PR dosages. Nevertheless, this type of specimen did not tolerate transport and placement. The samples cracked and disintegrated before loading and could not be tested.

The panels that incorporated bio-fibres (PFs) as additives were able to withstand the procedures well and could be tested, except for sample PF_04, which showed increased disintegration and broke before the application of the load. In general, the introduction of these fibres improved the stability of the panels and increased compressive strength, helping to control cracking during the drying process. Nevertheless, the strengths obtained are not sufficient to meet the minimum requirements of 2 MPa for the CEB 20 category established by the Colombian standard NTC 5324 [40].

Panels incorporating lime performed similarly to those made with fibres, although they had a very high porosity, and the strength was also not sufficient to comply with the standard.

The cement-stabilised panels performed the best. It can be seen that the higher percentage of cement added leads to an increase in strength. Despite the fact that demoulding was more difficult, the panels were much more stable and resistant to both transport and the testing process. Although all samples showed a higher compressive strength than the rest of the panels, only those with a percentage of cement equal to or higher than 15% (15%, 20% and 25%) complied with the minimum strength determined by the standards.

Finally, the panels tested with asphalt emulsion additives did not yield mechanical results. The difficulties encountered during demoulding led to lower-quality panels, which broke during transport.

In general, the behaviour of the samples that could not be tested is associated with low pressure during the manufacturing process. The lack of compaction means that when the panels are demoulded, they begin to disintegrate and cannot be subjected to compression. In addition, it should be noted that the coefficient of variation (CoV) for some of the samples was quite high. This highlights the high variability and heterogeneity of these types of materials, especially when additives are added to modify their behaviour.

3.2.2. Characterisation of the Final Solution

Although the samples showed different behaviours and not all were in accordance with the standards, it was decided to select the samples with the highest potential for further analysis. The best-performing sample corresponding to the dosage used in PC_06 was selected to represent the cementitious panels. The sample corresponding to the dosage used in PF_03 was selected to represent the panels with natural fibres, given their greater potential in terms of achieving more sustainable construction.

Three new panels for each of the dosages were subjected to more comprehensive compression tests. A 2D-DIC approach using the open source software Ncorr v1.2.2 [42] was used to obtain the displacements and strains (Figure 9a). In this process, a subset size of 20×20 pixels and an overlap of 65%, with a step of seven pixels, was used. Subsequently, a post-processing toolbox (Ncorr Post CSTool) was used. This tool allowed for virtual extensometers to be placed in the different areas of the specimen to analyse their behaviour and spatial influence (Figure 9b).

Due to the variability observed in the results shown above, in this case, the test with the most out-of-average behaviour was discarded. This decision was taken to ensure that the strain measurements were representative since, in some of the tests, disaggregation causes the failure mode to be inappropriate. Therefore, a full analysis of two samples of each dosage was carried out.

A total of nine virtual extensometers were placed on the surface of the specimens at three different heights to investigate the areas of greatest strain and the mode of failure. Three were placed in the central third, as required by the regulations. Three others of equal length were placed in the upper half, and three others in the lower half. The last two groups were placed in order to study the influence of the application of the load and to see the area where the greatest strain occurs. Regarding the distribution of each group, the extensometers were spaced 15 mm apart from each other. Two of them were placed in the area where the load is directly applied, while the third was placed in the outermost area where the load is not directly applied.

Maximum longitudinal strains in the state of loading before failure were extracted for each of the virtual extensometers. To analyse the heterogeneity and spatial distribution of the strains, the results were segregated into different groups, as shown in Table 5, corresponding to PF_03, and Table 6, corresponding to PC_06. On the one hand, the strain in the load zone was analysed, including the extensometers placed at the upper, middle and lower parts. On the other hand, the strain in the area where the load is not directly applied was analysed.

Regarding the results for PF_03, the previously mentioned high heterogeneity for the compression tests can be seen. In all cases, the CoV is slightly above 30%. The mean value for the peak strain in the loading area was 5.4‰, with the highest values in the lower area,

although there is not much difference with respect to the rest. The mean value for the peak strain in the out-of-load area was 1.5‰, which, as expected, is significantly lower. This solution has lower strength and higher strain than the best cement-stabilised solution. Nevertheless, the values obtained can be considered acceptable for applications where a high structural character is not required, such as thin walls or partitions. In addition, the higher strain capacity of this material may be of interest for seismic applications.

Regarding the results for PC_06, despite presenting heterogeneity, it is lower than the previous case, with a CoV value below 25%. The peak strain in the out-of-load area was similar, with a value of 1.3‰. Nevertheless, for the peak strain in the loaded area, different values were obtained with respect to the previous case. In this case, the mean value was 3.0‰, with the highest values being found in the upper zone. The presence of cement as an additive causes the strains to be lower in this case. When comparing the behaviour of cement-stabilised BECs with other conventional materials such as concrete, the range of strains is very close, with values close to 2‰ being considered acceptable in most cases.
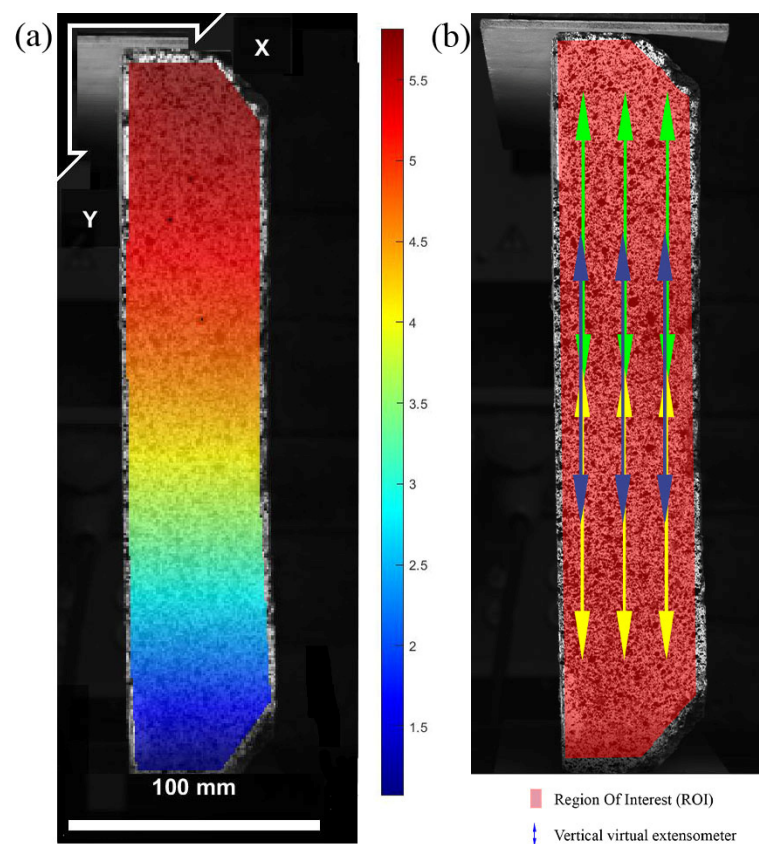
Figure 9. Results obtained during 2D-DIC analysis. (**a**) Vertical displacement before failure for PC_06; (**b**) extraction of the maximum longitudinal strain by means of the virtual extensometer.

Table 5. Results of the peak strain analysis for PF_03.

Strain Area	Mean (mm/mm)	Lower Bound (mm/mm)	Upper Bound (mm/mm)	CoV (%)
Load area	0.0054	0.0033	0.0081	30.4
Upper	0.0052	0.0033	0.0074	32.2
Middle	0.0055	0.0040	0.0072	32.3
Lower	0.0055	0.0035	0.0081	35.7
Out-of-load	0.0015	0.0010	0.0024	33.9

Table 6. Results of the peak strain analysis for PC_06.

Strain Area	Mean (mm/mm)	Lower Bound (mm/mm)	Upper Bound (mm/mm)	CoV (%)
Load area	0.0030	0.0022	0.0046	23.1
Upper	0.0035	0.0029	0.0046	22.8
Middle	0.0030	0.0023	0.0035	17.3
Lower	0.0025	0.0022	0.0032	18.9
Out-of-load	0.0013	0.0010	0.0017	21.4

In both cases and for all specimens, the peak strain value occurs at the edges. According to the results and the full field strain map obtained from DIC, it can be determined that this is the zone where the specimens begin to crack. Fracture begins in these areas, close to the contact with the compression plates, and the material begins to disintegrate until failure, while the core of the specimen remains more stable. This behaviour is typical of earthen materials and is one of the reasons why it is difficult to determine their behaviour using conventional techniques, so the DIC approach used made it possible to obtain the maximum strains in this zone.

4. Economic Analysis

To investigate the efficiency and costs of the proposed panels, an economic study of the different proposed solutions was carried out. Although only the PC_04, PC_05 and PC_06 panels complied with the standards in terms of mechanical properties, the study was carried out for all the samples. In this way, the influence on the costs of each of the additives can be verified. Furthermore, although the panels with fibre additives did not achieve good mechanical results, their incorporation did lead to an improvement, and these panels may have significant potential to be stabilised. This work can be a starting point for future research by improving and increasing some parameters, such as pressure, during the pressing process.

First of all, the costs of equipment were considered. Considering that the equipment was designed for self-manufacture, the cost was relatively low. In addition, the equipment was considered to be amortised over two years of work so that it could be used for the construction of community-level housing. The estimated cost was EUR 0.60 per CEB, considering the sifting cylinder, press and auxiliary material, such as wheelbarrows or shovels.

The labour cost to produce the panels was then considered. Although the solution is focused on self-manufacturing, the cost associated with the labour required was considered, taking into account the experience gained during laboratory manufacture. The estimated cost in this case was EUR 1.31 per CEB, considering the need for a worker and an assistant.

Finally, the material costs were considered. In this respect, water and additives were taken into account because it was considered that the earth is obtained at the same place of manufacture at no cost. In this case, the costs vary considerably for each of the panels, mainly due to the difference in additives.

Taking into account the costs mentioned above, the unit price for each of the panels is shown in Table 7.

Panels that complied with the standard had a cost of EUR 2.50 for PC_04, EUR 2.69 for PC_05 and EUR 2.88 for PC_06. In this case, the 5% increase in cement leads to a 0.19 EUR increase. Since the PC_04 panel was the most economical, a comparison was made with other conventional house enclosure systems in Ecuador. For this purpose, the price per square metre of this solution was compared with conventional brick, masonry block and adobe (Table 8). It should be noted that the prices have been calculated according to the average costs for the year 2023 indicated by the Construction Chamber of Ecuador, so the production cost of the panels should be taken as a guideline. In this sense, in
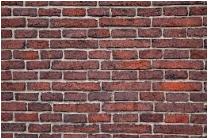
order to facilitate the comparison with other house enclosure systems, the ratio has been incorporated using the proposed solution as a reference.

Table 7. Unit price (EUR) for each panel considering equipment, labour and material costs.

Nomenclature	Equipment	Labour	Materials	Total
PR_01	0.60	1.31	0.01	1.92
PR_02	0.60	1.31	0.01	1.92
PF_01	0.60	1.31	2.74	4.65
PF_02	0.60	1.31	2.74	4.65
PF_03	0.60	1.31	2.74	4.65
PF_04	0.60	1.31	2.74	4.65
PF_05	0.60	1.31	2.74	4.65
PC_01	0.60	1.31	1.90	3.81
PC_02	0.60	1.31	0.21	2.12
PC_03	0.60	1.31	0.40	2.31
PC_04	0.60	1.31	0.59	2.50
PC_05	0.60	1.31	0.78	2.69
PC_06	0.60	1.31	0.97	2.88
PO_01	0.60	1.31	1.97	3.88

Table 8. Comparative of costs per square metre of house enclosure systems.

Material	PC_04	Brick	Masonry Block	Adobe
Image				
Price (EUR/m^2)	7.75	15.06	10.21	10.72
Ratio	1	1.94	1.32	1.38

When compared to conventional and more commonly used building materials, such as bricks, the proposed solution proves to be the most economical at half the cost. In the case of other earthen materials with similar properties, such as adobe, this solution is almost 30% cheaper. This shows that improving the properties of CEBs with this type of additive makes it possible to obtain an interesting solution from a construction, environmental and economic point of view.

5. Conclusions

This research has sought to influence basic construction materials, especially those mainly made of earth, such as compressed earth blocks. CEBs are an appropriate solution that takes advantage of local resources and contributes to environmental improvement, promoting sustainability within the self-building ecosystem in areas with limited resources. For this purpose, ad hoc equipment was manufactured to analyse types of earth from four different locations in Ecuador and to produce and characterise CEBs with stabilising additives.

- Firstly, empirical and laboratory tests were performed on the types of earth. Based on the results of the granulometry, plasticity and Proctor tests, E_CM earth from the Monay region, whose physical properties best met the standards, was selected.

- Subsequently, CEBs were made with this earth, adding additives of natural origin (bio-fibres) and others that are generally used in construction (lime or cement). Despite the fact that the pressure was not very high, the proposed methodology made it possible to manufacture and test panels of different compositions.
- The manufactured panels were mechanically characterised, obtaining the best results for the cement-stabilised panels. The addition of cement improved the compressive strength. The samples with 5% and 10% cement were the only ones that did not reach the minimum resistance of 2 MPa determined by the regulations. The samples with 15% cement reached a strength of 2.02 MPa. Subsequently, increasing the cement content to 20% improved the strength by 20%. Finally, the 25% cement reached the highest compressive strength, 35% higher than the previous ones. This solution is the most suitable from a structural engineering point of view.
- Among the rest of the non-cement samples, the one with the best results was sample PF_03, composed of 5% glue and 5% ground reed. This solution is the most interesting from an ecological point of view as it uses natural and environmentally friendly additives. This solution is interesting for architectural applications with lower load requirements, such as partitions or thin walls, and for consideration in seismic studies due to its high elongation capacity.
- Based on these results, it was decided to carry out a detailed analysis of these two samples using the digital image correlation technique. The DIC technique made it possible to analyse the displacements and strains in the full field to determine the mode of cracking, obtaining the ultimate strain at the instant prior to failure. Peak strain analysis determined a more homogeneous behaviour for the cement-stabilised samples (PF_06), with a peak strain value of 3.0‰ for a maximum load of 3.3 MPa, while for the samples stabilised with bio-fibres (PF_03), the peak strain was higher, with a value of 5.4‰ for a maximum load of 0.7 MPa.
- Finally, economic analysis was carried out to study the feasibility of manufacturing the panels and their use in housing construction. This analysis showed that CEB is an economically suitable solution, as it allows considerable savings in unit costs per m^2 of panel. The cost of a house with the Sandino construction system and this type of panel is 32% lower than the cost of using masonry blocks, 38% lower than using adobe and 94% lower than using conventional bricks.

For both of the panels that comply with the regulations and those that incorporate bio-fibres, the work yielded promising results for the earthen architecture sector, which encourages the continuation of this line of research. In particular, bio-fibre-stabilised panels are interesting from a sustainability point of view, which positions earthen materials as a strong candidate for architecture and construction in the 21st century, where better use of resources is required to support the principles of a circular economy and cleaner construction. The main challenge is to achieve a strength equal to or greater than that of cement-stabilised panels. In such a case, the high cement content could be replaced by cleaner stabilisers, such as lime. Future work will focus on improving and increasing some parameters, such as pressure, during the pressing process to ensure the stabilisation and compaction of the panels. In addition, the use of other additives to stabilise the panels and improve the compressive strength will be investigated. Finally, it is intended to investigate the behaviour of different types of earth in depth, considering the variability of behaviour due to the geographical component, so that the manufacture of CEBs can be adapted to the origin of the earth.

Author Contributions: Conceptualization, J.L.-R. and X.C.-H.; methodology, J.L.-R.; formal analysis, J.L.-R., J.P.P.-V. and K.N.-B.; investigation, J.L.-R., J.P.P.-V. and K.N.-B.; writing—original draft preparation, J.L.-R.; writing—review and editing, J.L.-R., X.C.-H., J.P.P.-V., K.N.-B. and J.P.; supervision, X.C.-H. and J.P.; funding acquisition, X.C.-H. All authors have read and agreed to the published version of the manuscript.

References

1. Peduzzi, P. Sand, rarer than one thinks. *Environ. Dev.* **2014**, *11*, 208–218.
2. de Brito, J.; Kurda, R. The past and future of sustainable concrete: A critical review and new strategies on cement-based materials. *J. Clean. Prod.* **2021**, *281*, 123558. [CrossRef]
3. Herrmann, C.J.; Zappettini, E.O. *Recursos Minerales, Minería y Medio Ambiente*; SEGEMAR: Buenos Aires, Argentina, 2014.
4. Deboucha, S.; Hashim, R. A review on bricks and stabilized compressed earth blocks. *Sci. Res. Essays* **2011**, *6*, 499–506.
5. Costa, C.; Cerqueira, Â.; Rocha, F.; Velosa, A. The sustainability of adobe construction: Past to future. *Int. J. Archit. Herit.* **2019**, *13*, 639–647. [CrossRef]
6. Font, F.; Hidalgo, P. La tapia en España. Técnicas actuales y ejemplos. *Inf. Constr.* **2011**, *63*, 21–34. [CrossRef]
7. Rigassi, V. *Compressed Earth Blocks: Manual of Production*; GATE/BASIN: Eschborn, Germany, 1985.
8. Etzion, Y.; Saller, M. Earth construction—A review of needs and methods. *Archit. Sci. Rev.* **1987**, *30*, 43–48. [CrossRef]
9. Cid, J.; Mazarrón, F.R.; Cañas, I. Las normativas de construcción con tierra en el mundo. *Inf. Constr.* **2011**, *63*, 159–169. [CrossRef]
10. *NZS 4297*; Engineering Design of Earth Buildings. Standards New Zealand: Wellington, New Zealand, 1998.
11. *NZS 4298*; Materials and Workmanship for Earth Buildings. Standards New Zealand: Wellington, New Zealand, 1998; Volume 569, p. 570.
12. *ASTM E2392*; Standard Guide for Design of Earthen Wall Building Systems. ASTM: West Conshohocken, PA, USA, 2010.
13. *UNE 41410*; Bloques de Tierra Comprimida para Muros y Tabiques. Definiciones, Especificaciones y Métodos de Ensayo. AENOR: Madrid, Spain, 2008.
14. Sturm, T.; Ramos, L.F.; Lourenço, P.B. Characterization of dry-stack interlocking compressed earth blocks. *Mater. Struct.* **2015**, *48*, 3059–3074. [CrossRef]
15. McGregor, F.; Heath, A.; Fodde, E.; Shea, A. Conditions affecting the moisture buffering measurement performed on compressed earth blocks. *Build. Environ.* **2014**, *75*, 11–18. [CrossRef]
16. Galíndez, F. Bloques de tierra comprimida (BTC) sin adición de cemento. *Segur. Medio Ambiente* **2007**, *115*, 63–73.
17. Cid-Falceto, J.; Mazarrón, F.R.; Cañas, I. Assessment of compressed earth blocks made in Spain: International durability tests. *Constr. Build. Mater.* **2012**, *37*, 738–745. [CrossRef]
18. *IS 13827*; Improving Earthquake Resistance of Earthen Buildings—Guidelines. Bureau of Indian Standards: Delhi, India, 1993.
19. Gatti, F. *Arquitectura y Construcción en Tierra: Estudio Comparativo de las Técnicas Contemporáneas en Tierra*; Polytechnic University of Catalonia: Barcelona, Spain, 2012.
20. Ribeiro, T.; Oliveira, D.V.; Bracci, S. The use of contact sponge method to measure water absorption in earthen heritage treated with water repellents. *Int. J. Archit. Herit.* **2022**, *16*, 85–96. [CrossRef]
21. Vissac, A.; Bourgès, A.; Gandreau, D.; Anger, R.; Fontaine, L. *Argiles & Biopolymères-Les Stabilisants Naturaels Pour la Construction en Terre*; CRATerre Éditions: Villefontaine, France, 2017.
22. Losini, A.E.; Grillet, A.C.; Bellotto, M.; Woloszyn, M.; Dotelli, G. Natural additives and biopolymers for raw earth construction stabilization—A review. *Constr. Build. Mater.* **2021**, *304*, 124507. [CrossRef]
23. Teixeira, E.R.; Machado, G.; Junior, A.D.P.; Guarnier, C.; Fernandes, J.; Silva, S.M.; Mateus, R. Mechanical and thermal performance characterisation of compressed earth blocks. *Energies* **2020**, *13*, 2978. [CrossRef]
24. Borri, A.; Corradi, M.; De Maria, A. The failure of masonry walls by disaggregation and the masonry quality index. *Heritage* **2020**, *3*, 1162–1198. [CrossRef]
25. Sánchez-Aparicio, L.J.; Villarino, A.; García-Gago, J.; González-Aguilera, D. Photogrammetric, geometrical, and numerical strategies to evaluate initial and current conditions in historical constructions: A test case in the church of San Lorenzo (Zamora, Spain). *Remote Sens.* **2016**, *8*, 60. [CrossRef]
26. Callaway, P.; Gilbert, M.; Smith, C.C. Influence of Backfill on the Capacity of Masonry Arch Bridges. *Proc. Inst. Civ. Eng.-Bridge Eng.* **2012**, *165*, 147–157. [CrossRef]
27. Sutton, M.A.; Orteu, J.J.; Schreier, H.X. *Image Correlation for Shape, Motion and Deformation Measurements: Basic Concepts, Theory and Applications*; Springer Science & Business Media: Berlin/Heidelberg, Germany, 2009.
28. Pisonero, J.; López-Rebollo, J.; García-Martín, R.; Rodríguez-Martín, M.; Sánchez-Aparicio, L.J.; Muñoz-Nieto, A.; González-Aguilera, D. A comparative study of 2D and 3D digital image correlation approaches for the characterization and numerical analysis of composite materials. *IEEE Access* **2021**, *9*, 160675–160687. [CrossRef]
29. Khan, R.M.A.; Shafighfard, T.; Ali, H.Q.; Mieloszyk, M.; Yildiz, M. Strength prediction and experimental damage investigations of plain woven CFRPs with interacting holes using multi-instrument measurements. *Polym. Compos.* **2023**, *44*, 3594–3609. [CrossRef]

30. Teijón-López-Zuazo, E.; López-Rebollo, J.; Sánchez-Aparicio, L.J.; Garcia-Martín, R.; Gonzalez-Aguilera, D. Compression and strain predictive models in non-structural recycled concretes made from construction and demolition wastes. *Materials* **2021**, *14*, 3177. [CrossRef]

31. María, R.-M.; Paula, V.-L.; Jaime, F.-G.; Jorge, L.R. Improvement of tensile properties of carbon fibre-reinforced cementitious matrix composites with coated textile and enhanced mortars. *Constr. Build. Mater.* **2023**, *369*, 130552. [CrossRef]

32. Stazi, F.; Serpilli, M.; Chiappini, G.; Pergolini, M.; Fratalocchi, E.; Lenci, S. Experimental study of the mechanical behaviour of a new extruded earth block masonry. *Constr. Build. Mater.* **2020**, *244*, 118368. [CrossRef]

33. Perić Fekete, A.; Kraus, I.; Grubišić, M.; Dokšanović, T. In-plane seismic performance of rammed earth walls: An eastern Croatia reconnaissance based study. *Bull. Earthq. Eng.* **2023**, *22*, 1359–1385. [CrossRef]

34. El Nabouch, R.; Bui, Q.-B.; Plé, O.; Perrotin, P. Rammed earth under horizontal loadings: Proposition of limit states. *Constr. Build. Mater.* **2019**, *220*, 238–244. [CrossRef]

35. Minke, G. *Manual de Construcción en Tierra: La Tierra Como Material de Construcción y su Aplicación en la Arquitectura Actual*; Nordan Comunidad: Montevideo, Uruguay, 2001.

36. *E. 080*; Diseño y Construcción Con Tierra Reforzada. Ministerio de Vivienda, Construcción y Saneamiento: Lima, Perú, 2017.

37. *ASTM D422-63*; Standard Test Method for Particle-Size Analysis of Soils. ASTM: West Conshohocken, PA, USA, 2007.

38. *INEN 692*; Mecánica de Suelos. Determinación del Límite Plástico. INEM: Quito, Ecuador, 1982.

39. *ASTM D698*; Standard Test Methods for Laboratory Compaction Characteristics of Soil Using Standard Effort. ASTM: West Conshohocken, PA, USA, 2000.

40. *NTC 5324*; Ground Blocks Cement for Walls and Divisions. Definitions. Specifications. Test Methods. Conditions of Delivery. ICONTEC: Bogotá, Colombia, 2004.

41. Pan, B.; Qian, K.; Xie, H.; Asundi, A. Two-dimensional digital image correlation for in-plane displacement and strain measurement: A review. *Meas. Sci. Technol.* **2009**, *20*, 062001. [CrossRef]

42. Blaber, J.; Adair, B.; Antoniou, A. Ncorr: Open-source 2D digital image correlation matlab software. *Exp. Mech.* **2015**, *55*, 1105–1122. [CrossRef]

43. Dong, Y.L.; Pan, B. A review of speckle pattern fabrication and assessment for digital image correlation. *Exp. Mech.* **2017**, *57*, 1161–1181. [CrossRef]

44. Pan, B.; Lu, Z.; Xie, H. Mean intensity gradient: An effective global parameter for quality assessment of the speckle patterns used in digital image correlation. *Opt. Lasers Eng.* **2010**, *48*, 469–477. [CrossRef]

45. Lecompte, D.; Sol, H.; Vantomme, J.; Habraken, A. Analysis of Speckle Patterns for Deformation Measurements by Digital Image Correlation. In *Speckle06: Speckles, from Grains to Flowers*; SPIE: Bellingham, WA, USA, 2006; Volume 6341, pp. 80–85.

46. Garcia-Martin, R.; López-Rebollo, J.; Sánchez-Aparicio, L.J.; Fueyo, J.G.; Pisonero, J.; Gonzalez-Aguilera, D. Digital image correlation and reliability-based methods for the design and repair of pressure pipes through composite solutions. *Constr. Build. Mater.* **2020**, *248*, 118625. [CrossRef]

2.2. Materiales de construcción a partir de residuos de construcción y demolición: hormigones reciclados

En esta segunda parte del capítulo II se incluye el artículo "*Compression and strain predictive models in non-structural recycled concretes made from construction and demolition wastes*", publicado en la revista *Materials*.

Resumen

La industria de la construcción es considerada el mayor consumidor de recursos no renovables, produciendo además una elevada cantidad de residuos. Con el fin de potenciar la sostenibilidad y el concepto de economía circular en el sector de la construcción, se propone la sustitución de áridos naturales por residuos de construcción y demolición en la fabricación de hormigón. Esta incorporación de áridos reciclados provoca un comportamiento muy heterogéneo en los hormigones reciclados. En este sentido, el **objetivo** de este trabajo es predecir el comportamiento mecánico de hormigones fabricados con residuos de construcción y demolición. A su vez, y con el objetivo de caracterizar este comportamiento mecánico, se plantea como una meta la aplicación de la técnicas macro-fotogramétricas de campo completo para obtener las deformaciones.

La **metodología** seguida consistió en la caracterización de hormigones fabricados con diferente tipología de árido para establecer modelos de predicción de su comportamiento. Se emplearon áridos procedentes de residuos de construcción y demolición de dos tipologías: (i) residuos cerámicos y (ii) residuos de hormigón. Estos áridos fueron caracterizados mediante ensayos granulométricos, físicos y químicos para determinar su adecuación a la normativa de fabricación de hormigón.

Los hormigones elaborados con estos áridos reciclados fueron caracterizados mediante ensayos de compresión empleando probetas cilíndricas. Para caracterizar las deformaciones se empleó la técnica de correlación digital de imágenes (DIC) en su enfoque tridimensional. Para ello se empleó un prototipo conformado por dos cámaras, las cuales se calibraron a través de algoritmos fotogramétricos de ajuste de haces (BA) y transformación lineal directa (DLT), para posteriormente aplicar los algoritmos de correlación y obtener los desplazamientos y deformaciones en todos los puntos de la superficie curva de las probetas.

A partir de las características de fabricación del hormigón y su caracterización mecánica, se llevó a cabo una estrategia de modelado predictivo basada en regresión lineal múltiple (MLR) para obtener la resistencia a compresión y la deformación última. Por último, se llevó a cabo un análisis de sensibilidad a través de los índices de Sobol con

el fin de determinar la influencia de cada una de las variables consideradas en los modelos predictivos.

Los **resultados** mostraron la capacidad de los modelos propuestos para predecir la resistencia a compresión de manera precisa para ambos tipos de hormigón reciclado. El modelo presentó como variable de entrada más influyente el ratio agua-cemento, seguida de la edad de curado del hormigón. Por otro lado, el modelo para determinar la deformación última arrojó una precisión adecuada para los hormigones fabricados con áridos con residuos cerámicos, mientras que para los fabricados con residuos de hormigón presentó menores coeficientes de correlación debido a la mayor dispersión de los datos obtenidos en los ensayos experimentales. En ambos casos, la variable más influyente fue la resistencia a compresión del hormigón, seguida de la edad de curado y por último la relación agua-cemento.

Las principales **conclusiones** del trabajo resaltan la idoneidad del enfoque 3D-DIC para obtener de manera precisa las deformaciones últimas del hormigón por su elevada heterogeneidad espacial. Gracias a esta técnica, se han podido desarrollar modelos predictivos para obtener la resistencia mecánica y deformación última en función de variables de entrada como la edad de curado, la relación agua-cemento y la composición de los áridos.

Por último, el enfoque estocástico adoptado en base a la gran cantidad de datos proporcionados por las técnicas de campo completo ha permitido llevar a cabo análisis de sensibilidad para comprender y mejorar el funcionamiento de los modelos. Estas técnicas basadas en confiabilidad se presentan como la mejor opción para diseñar y optimizar materiales con un comportamiento heterogéneo como es el caso de los hormigones reciclados.

Article

Compression and Strain Predictive Models in Non-Structural Recycled Concretes Made from Construction and Demolition Wastes

Evelio Teijón-López-Zuazo [1] , Jorge López-Rebollo [2,*] , Luis Javier Sánchez-Aparicio [3] , Roberto Garcia-Martín [4] and Diego Gonzalez-Aguilera [2]

1   Department of Construction and Agronomy, Campus Viriato, Higher Polytechnic School of Zamora, University of Salamanca, Avenida Requejo, 33, 49022 Zamora, Spain; eteijon@usal.es
2   Department of Cartographic and Land Engineering, Higher Polytechnic School of Ávila, University of Salamanca, Hornos Caleros, 50, 05003 Ávila, Spain; daguilera@usal.es
3   Department of Construction and Technology in Architecture (DCTA), Escuela Técnica Superior de Arquitectura de Madrid (ETSAM), Universidad Politécnica de Madrid, Av. Juan de Herrera 4, 28040 Madrid, Spain; lj.sanchez@upm.es
4   Department of Mechanical Engineering, Campus Viriato, Higher Polytechnic School of Zamora, University of Salamanca, Avenida Requejo, 33, 49022 Zamora, Spain; toles@usal.es
*   Correspondence: jorge_lopez@usal.es; Tel.: +34-920-353-500 (ext. 3820)

Abstract: This work aims to investigate different predictive models for estimating the unconfined compressive strength and the maximum peak strain of non-structural recycled concretes made up by ceramic and concrete wastes. The extensive experimental campaign carried out during this research includes granulometric analysis, physical and chemical analysis, and compression tests along with the use of the 3D digital image correlation as a method to estimate the maximum peak strain. The results obtained show that it is possible to accurately estimate the unconfined compressive strength for both types of concretes, as well as the maximum peak strain of concretes made up by ceramic waste. The peak strain for mixtures with concrete waste shows lower correlation values.

Academic Editor: Paul Lambert

Publisher's Note: MDPI stays neutral with regard to jurisdictional claims in published maps and institutional affiliations.

1. Introduction

The construction industry is considered the largest consumer of non-renewable natural resources and it is also an important generator of waste [1]. The high consumption of resources is justified by the high demand for concrete in the sector, which is the most widely used artificial material in the world [2]. Although the raw materials and natural aggregates used for manufacture are abundant resources, their high exploitation and costs derived from their extraction entail a problem that can cause the shortage of this type of material in the medium to long term in many countries where its production is very high [3]. Construction is also considered a "dirty" industry due to the high generation of waste [4], both in its extraction phase and in the demolition of elements that have concluded their useful life. Most of these wastes are deposited in landfills, with the consequent negative visual, landscape and ecological impact that this entails. In this context, effective management is necessary in order to reduce both the amount of resources consumed and the amount of waste generated, taking advantage of its potential as secondary material in accordance with the concepts of sustainable development and circular economy.

One of the main solutions that stimulate the reuse of construction and demolition waste (CDW) is its use in the manufacture of concrete. However, the main problem in the use of this type of aggregate is focused on the high absorption capacity due to the presence of ceramic material and mortar adhered to the surface of the aggregates [5,6], especially in

the fine ones [7]. This issue reduces the mechanical performance of the resulting concretes. In this sense, the standards on recycled materials, such as the Spanish EHE [8], are quite demanding both in their physical and chemical properties, hindering the use of these materials for the manufacture of structural concrete due to the high requirements in waste treatment [9]. Consequently, it is necessary to establish alternative applications in which the concrete resulting from the use of recycled aggregates does not require high mechanical performance, that is, non-structural concrete (NSC). Multiple studies have been focused on analysing the applicability of this type of concrete, among which are paving blocks [10], kerbstones [11], blocks [12,13] or even prefabricated urban furniture pieces [14].

These new concrete solutions made with recycled aggregates have very different behaviours and one of the main variables that most affects performance is the percentage of replacement of natural aggregates. In this sense, numerous studies have analysed the behaviour according to different mix proportions [11,15,16], suggesting a lower compressive strength for higher percentages of replacement of the natural aggregate, as well as greater strain and a lower modulus of elasticity. However, other studies suggest that the mechanical performance of recycled concrete is similar to that made with natural aggregates, even superior in terms of its compressive strength [17] or tensile performance [18,19].

When the execution of these type of concretes is carried out, it is essential to have tools that allow us to predict their behaviour considering the different mix proportions and curing ages (i.e., hardening curves). However, the high variability of mix proportions based on the substitution of recycled aggregates and their typologies with the consequent diversity of results, increases the difficulty of establishing strength prediction models occuring in conventional concretes [20,21]. Moreover, prediction models that incorporate variables, such as the substitution of natural aggregates for recycled aggregates [22,23], provide a useful design tool and promote the application of sustainable concretes.

Together with the strength values, it is often very useful to know the maximum strain associated with concretes. In this sense, Eurocode 2 [24] provides an expression that allows us to determine the peak strain as a function of the characteristic strength of concrete and that can be used to predict the strain based on the strengths estimated from the curves of hardening. This expression has been adjusted by González-Fonteboa et al. [25] for different substitution percentages of coarse recycled aggregates, but does not take into account the total substitution of coarse and fine aggregates.

The use of CDW as a substitution for aggregates increases the heterogeneity of concrete solutions, showing very different behaviours, if adequate selection and treatment of waste is not carried out [26]. In this sense, the methods generally used to analyse the stress-strain curves and the maximum strain of recycled concrete adapt locally since they are based on point measurements of virtual extensometers [25,27,28]. In practice, concrete failure occurs promptly when the material reaches its maximum strength at the point a fracture begins. This means that the strain, prior to the concrete failure, can be very different if measurements close to the cracks are considered or, on the contrary, the values are taken in very distant areas.

In order to cope with the limitation previously shown, various full-field optical methods have been developed, among which, Digital Image Correlation (DIC) stands out. This method allows us to obtain a full field of displacements and strains through the use of correspondence procedures based on correlations and numerical differentiation algorithms [29]. Thanks to this, DIC has been widely used for the analysis and characterization of various heterogeneous materials, such as wood [30], composites [31] and concrete [32]. In this last field, there are studies that cover both the measurement of strains [33] and the analysis of cracks [34,35], and even the characterization of the influence of aggregate size on drying contractions [36]. The variability of the technique allows carrying out analysis in the plane of cubic specimens using 2D-DIC [34,35] and analysis in non-flat specimens using 3D-DIC [33,36,37], taking into account the variations outside the main plane.

Considering the heterogeneous nature of these materials and the variability of their behaviour, it is worth highlighting the importance of carrying out the DIC approach to

analyse the spatial distribution of the displacements and strains suffered throughout the specimen. The 3D-DIC approach allows us to obtain a large amount of data that facilitates statistical analysis and the estimation of properties [32]. In this way, the peak strain can be studied over a large surface of the specimen, thus analysing the failure zone and determining the peak strain more precisely as compared to other specific measurements that may be far from the actual behaviour of the material. As a result of this technique, it is possible to establish a more precise model to predict strains based on the maximum strength of concretes made with recycled aggregates.

As a consequence, this paper aims to progress understanding in the mechanical characterization of non-structural concretes manufactured with construction and demolition waste through generating predictive models of compressive strength and peak strain. For this, the tests of mechanical characterization of concrete with different mix proportions and curing ages will be integrated together with the 3D-DIC approach for the analysis of the strains suffered during the breaking tests. Within the Materials and Methods section, we describe the materials used in the mixture as well as the experimental and numerical strategies adopted. In Section 3, we show the experimental results obtained by the combination of DIC and the mechanical characterization tests. Then, in Section 4, predictive models are defined and discussed. Finally, in the Conclusion (Section 5), we summarize the findings and discuss future studies.

2. Materials and Methods

2.1. Materials and Mix Proportions

Structural concretes are designed for structures and elements for building or for public works, usually designed for compressive stresses of 25 MPa at 28 days [8]. It is made up by of natural siliceous aggregates, Portland cement and chemical additives such as fluidizers. Within the scope of this study, we focus on evaluating the use of wastes from crushing of this type of concrete in selective demolitions processed at the CDW treatment plant in Calvarrasa de Abajo (Salamanca, Spain) as recycled aggregates for the manufacture of non-structural concrete. More specifically, this study evaluates two potential types of recycled concrete for non-structural applications (borders and sidewalks): (i) a concrete coming from Construction and Demolition Waste from Recycled Concrete (CDWRCon) and; (ii) a concrete made up by the Construction and Demolition Waste from Recycled Ceramic (CDWRCer). In both cases, cement, water and additive were mixed.

On the one hand, CDWRCon is obtained from concrete, cement mortar and prefabricated concrete parts, including untreated aggregates and natural stone aggregates treated with hydraulic binders and other fractions (content < 0.1%) of floating material, cohesive materials (clay and soil), metals (ferrous and non-ferrous), wood, gypsum and non-floating plastics and rubber. Meanwhile CDWRCer is obtained from concrete, including concrete products, cement mortar, prefabricated concrete parts and ceramic materials, showing a continuous granulometry with concrete and ceramic material aggregates. The CDWRCer components are the same as CDWRCon with the addition of other materials as parts of clay (bricks and tiles), calcium silicate masonry, non-floating aerated concrete and glass.

According to the categories established in the UNE-EN 13242 standard [38], the CDWRCon aggregates are classified as Rc_{80}, Rcu_{90}, Rb_{10-}, Ra_{10-}, X_{1-}, FL_{5-} and the CDWRCer aggregates are classified as Rc_{40}, Rcu_{50}, Rb_{50-}, Rg_{2-}, FL_{5-} (Table 1) (Figure 1), where:

Rc = Concrete and mortar (natural aggregates with cement mortar attached).
Ru = Unbound aggregates (natural aggregates without cement mortar attached).
Rb = Ceramics (bricks, tiles, stoneware and sanitary ware).
Ra = Asphalt.
Rg = Glass.
FL = Floating materials.
X = Other impurities (wood, paper, metals, plastic, etc.).

Table 1. Proportions of the different aggregates.

Components	CDWRCon		CDWRCer	
	Contents (%)	Categories	Contents (%)	Categories
Rc	82.5	Rc_{80}	42.4	$Rc_{Declared}$
$Rc + Ru$	90.7	Rcu_{90}	55.0	Rcu_{50}
Rb	0.8	Rb_{10-}	39.6	Rb_{50-}
Ra	8.3	Ra_{10-}	-	-
Rg	-	-	0.1	Rg_{2-}
X	0.1	X_{1-}	5.2	-
FL	≤ 0.1	FL_{5-}	≤ 0.1	FL_{5-}
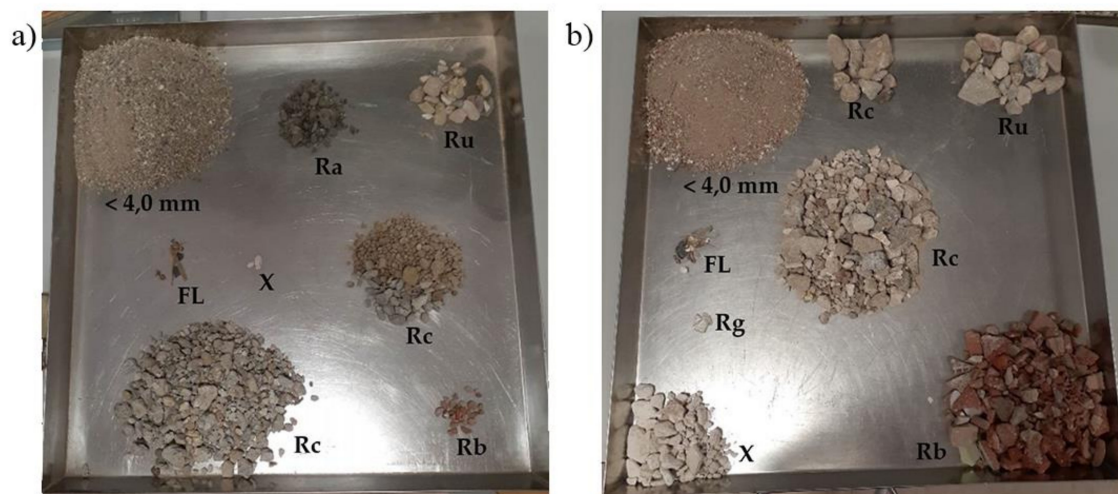
Figure 1. Visual appearance of the aggregates: (**a**) CDWRCon and (**b**) CDWRCer components.

It is noteworthy that the UNE-EN 13242 [38] standard establishes a maximum of 1% for class X, which includes cohesive materials (clay and soil), metals (ferrous and non-ferrous), wood, gypsum, non-floating plastics and rubber. The CDWRCer has an amount of gypsum that represents 5.2% in the general classification of the components, not corresponding to the class established by the standard for this type of material. The gypsum is prejudicial to concrete due to its composition of sulphate and, therefore, it is necessary to consider a sulphate resistant cement.

Table 2 shows the particle size distribution. In CDWRCon, values of uniformity coefficient, $Cu = 75.0$, and curvature coefficient, $Cc = 2.1$, were obtained. The high value of the uniformity coefficient shows the high size variation obtained in the unclassified crushing. The curvature coefficient, $1.0 \leq Cc \leq 3.0$, defines the CDWRCon and the CDWRCer as well-graded and with a low compressibility, a high compactness and correspondingly suitable for use on construction sites.

Table 2. Aggregate type and particle size distribution characteristics of the CDWRCon and CDWRCer.

Material	D_{10} (mm)	D_{30} (mm)	D_{50} (mm)	D_{60} (mm)	C_u	C_c	% Fines	% Sand Size	% (4.75–9.5) mm	% (9.5–40.0) mm
CDWRCon	0.08	1.0	2.5	6.0	75.0	2.1	11.1	56.1	1.2	32.0
CDWRCer	0.08	1.2	7.0	11.0	137.5	1.6	10.4	43.5	12.9	38.6

Additionally, a granulometric study was carried out. In this case it was compared the granulometric curves of both concretes (CDWRCon and CDWRCer) with respect to the Bolomey dosing (reference curve) in accordance to the standard UNE EN 933-1 [39]. This reference curve, which is considered as an improvement of the Fuller law, is adequate for

mass concrete (i.e., non-structural concrete), where the resistance is not the determining characteristic.

The results of this comparison are shown in Figure 2. It is worth mentioning that the granulometric curve of the CDWRCon concrete includes the cement used as an aggregate (20% of the total volume of aggregates). The Bolomey curve was estimated by considering a wet mix macadam with the following proportions [40]: (i) ±2% for the 0.063 mm; and (ii) ±6% for the rest. As this research aims to investigate the manufacture of a sustainable concrete, promoting the use of recycled aggregates replacing natural aggregates in concrete, the continuous granulometry obtained in the crushing of the CDWs has been used in the production of the concrete. Thus, better particle size adjustments have been avoided by classifying it into different fractions, as this would be a commercial disadvantage for its implementation in practice. In the CDWRCon the biggest deviations are in the 20 mm sieve with 13.6% above and 14.7% on the 2.5 mm sieve. There is a little standard error of 2.5% below the medium curve. This curve has the typical form of crushing siliceous aggregates, with a deficit of intermediate sizes in the sand fraction, between the #5–2.5 mm sieves. Even with the logical limitations associated with the heterogeneity of the recycled aggregates, the theoretical dosage curve was close to the bottom of the sieve stack for sizes larger than 6 mm in the case of CDWRCon, while the smaller sizes are above the average stack. It can be seen how the areas between the medium spindle and the particle size curve of the CDWRCon are partially compensated, below the medium spindle in the larger sieves and above in the smaller ones (Figure 2).

Figure 2. CDWRCon versus Bolomey granulometric curves.

Identically, the granulometric curves of the CDWRCer and Bolomey dosing are shown in Figure 3. In this case, the biggest deviations are in the 10 mm sieve with 18.9% above and 9.0% on the 0.08 mm sieve. There is a small standard error of 3.1% above the medium curve. Even with the logical limitations associated with the heterogeneity of the recycled aggregates, the theoretical dosage curve was close to the bottom of the sieve stack for sizes larger than 2.5 mm in the case of CDWRCon, while the smaller sizes are above the average stack. It can be seen how the areas between the medium spindle and the particle size curve of the CDWRCon are partially compensated, below the medium spindle in the larger sieves and above in the smaller ones.
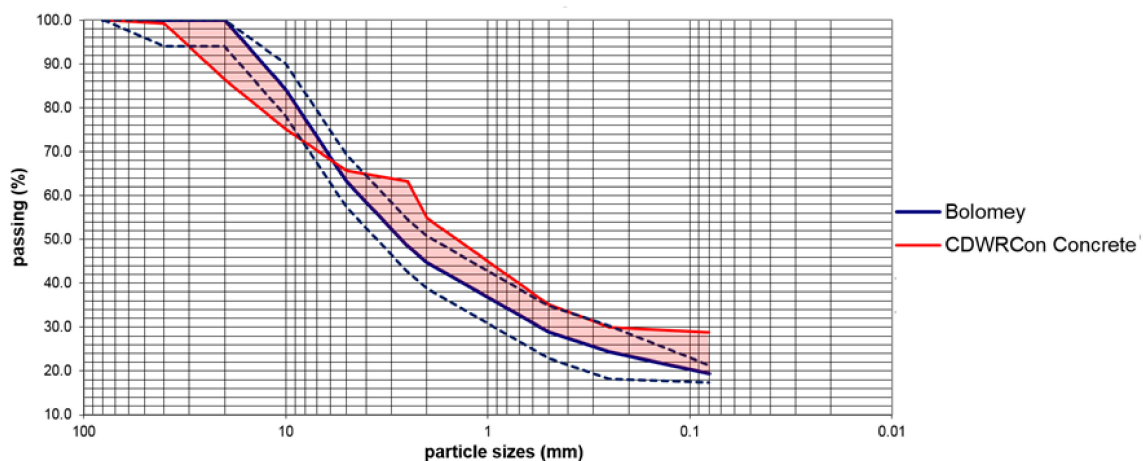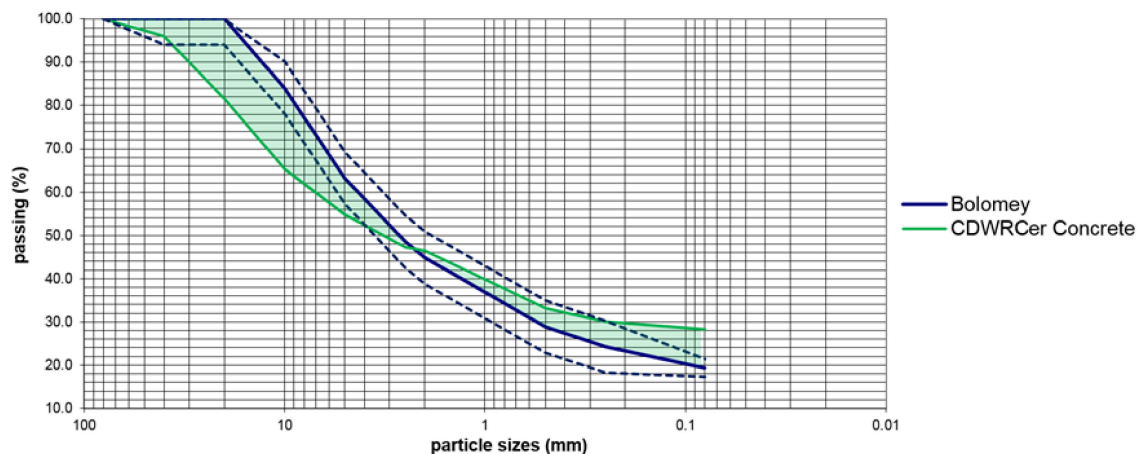
Figure 3. CDWRCer versus Bolomey granulometric curves.

From the results obtained it is possible to conclude that both groups have the right proportions of sand and gravel to make the necessary concrete for non-structural applications. Table 3 shows the main physical and chemical parameters of CDWRCon and CDWRCer.

Table 3. Physical and chemical parameters for CDWRCon and CDWRCer.

Material	SE_4	LA	OM	SS	WA_c (%)	WA_f (%)
CDWRCon	55.9	43.0	0.14	1.1	6.2	4.0
CDWRCer	45.3	52.0	-	-	10.7	4.3

where:

SE_4 = Sand Equivalent, UNE-EN 933-8 [41].
LA = Los Angeles coefficient, UNE-EN 1097-2 [42].
AM = Methylene blue (UNE EN 933-9) [43].
OM = Organic Matter content, UNE 103204 [44].
SS = Soluble Salt content, UNE 103205 [45].
WA_f = Water Absorption Fine aggregate, UNE-EN 1097-6 [46].
WA_c = Water Absorption Coarse aggregate, UNE-EN 1097-6 [46].
SO_3 = acid soluble sulphate content, UNE-EN 1744-1 [47].
S = sulfur compounds total content, UNE-EN 1744-1 [47].
m_{lpc} = light contaminant content, UNE-EN 1744-1 [47].
Humus = light organic contaminant in humus content, UNE-EN 1744-1 [47].

The quality of the fines, expressed as SE_4 sand equivalent, gives a value of 55.9 in CDWRCon. This value is lower than the common values of natural aggregates. The sand equivalent for CDWRCer is even lower than the CDWRCon with a value of 45.3. This difference is motivated by the existence of parts of clays (bricks and tiles), as well as calcium silicate masonry elements that reduce the sand lecture and SE_4 value. Since non-structural recycled concretes (NSRC) are not subjected to any specific exposure class, the aggregates shall be accepted if satisfy the requirement AM $\leq$ 0.3 f/100.

Fragmentation resistance offers an LA coefficient of 43.0 for CDWRCon. The resistance to fragmentation in CDWRCer, with LA = 52.0, is lower than CDWRCon. This difference is motivated by the presence of bricks, tiles and calcium silicate masonry. So, the coarse aggregates have an abrasion resistance between 40 and 55, being possible to make non-structural concrete with a minimum characteristic strength of 15 N/mm^2.

The organic matter test provided a 0.14% value in CDWRCon. The content of soluble salts dissolved in distilled water for CDWRCon was 1.1%. The CDW has a high-water absorption coefficient, higher than natural aggregates. In the CDWRCon, the high absorption was associated with the porosity of the concrete. The water absorption coefficients

are bigger in CDWRCer. In the coarse fraction, the absorption coefficient was 6.2% for CDWRCon and 10.7% for CDWRCer. This difference is associated with the absorption of clay materials, bricks and tiles. The fine fractions have absorption coefficients similar for both materials.

According to UNE-EN 13242 standard [38], the CDWRCon corresponds to the $AS_{0.8}$ class of acid soluble sulphate. The CDWRCer presents a greater content of these parameters, relating to the declared classes ($AS_{Declared}$ and $S_{Declared}$), with a content of 2.1 and 1.2 to acid soluble sulphate and of sulphur compounds, respectively.

The blinder used for manufacturing the concrete was a cement type BL II/B-LL 42,5 R. This cement has the following components: (i) a Clinker content comprised between 65–79%; (ii) a Limestone content of 21–35%; (iii) a Chloride content: ≤0.10; (iv) a Sulphate content: ≤4.0; and (v) a soluble toilet chromium VI content ≤ 0.0002%. It has a beginning setting of: ≥60 min and an end setting of: ≤720 min. The expansion is less than 10 mm. Resistance at 2 days: ≥20 MPa and resistance at 28 days in the interval $42.5 \le R \le 62.5$ MPa. As an additional feature looking for the best termination, a white cement has been chosen, with a whiteness content ≥85%.

2.2. Mechanical Characterization of the Concrete: The 3D Digital Image Correlation Method

This section shows the 3D digital image correlation (3D DIC) strategy used for obtaining a full field of displacements in the different concrete samples tested. Figure 4 shows the methodology followed.

2.2.1. Data Acquisition Prototype and Specimen Preparation

The concrete solutions were evaluated by means of compression tests according to guideline UNE-EN 12390-3 [48]. In order to carry out these tests, an electromechanical test machine Servosis ME-405/50/5 (Servosis, Madrid, Spain) was used with a load cell of 500 kN and the corresponding compression plates.

In order to capture the displacements and strains suffered by the concrete solutions during compression tests, a 3D-DIC approach was used. The acquisition of these images was carried out using a low-cost 3D-DIC prototype similar to the developed by Garcia-Martin et al. [49] (Figure 5). This prototype is made up of (Table 4) (Figure 5): (i) two high resolution cameras Canon EOS 700D equipped with a 60 mm prime macro-lens; (ii) a programmable logic controller (PLC); and (iii) two neutral LED lights.

The synchronization of both cameras was carried out by means of a PLC that allowed us the programming of simultaneous shots. Furthermore, it was connected to a Quantum data acquisition platform (Figure 5b,c), allowing for the association the images to be captured with the load applied by the press.

The application of the DIC approach requires the presence of a speckle pattern that provides random intensity variations on the surface of the samples. In this sense, the aerosol technique allows us to create speckle patterns with millimetre or submillimetre spot size on the surface of the specimens [29]. The procedure to obtain this pattern consists of the following steps: (i) application of a white paint on the surface of the specimen; (ii) creation of black dots over the white surface by means of a spray; and (iii) quality evaluation according to the Mean Intensity Gradient (MIG) parameter [50].
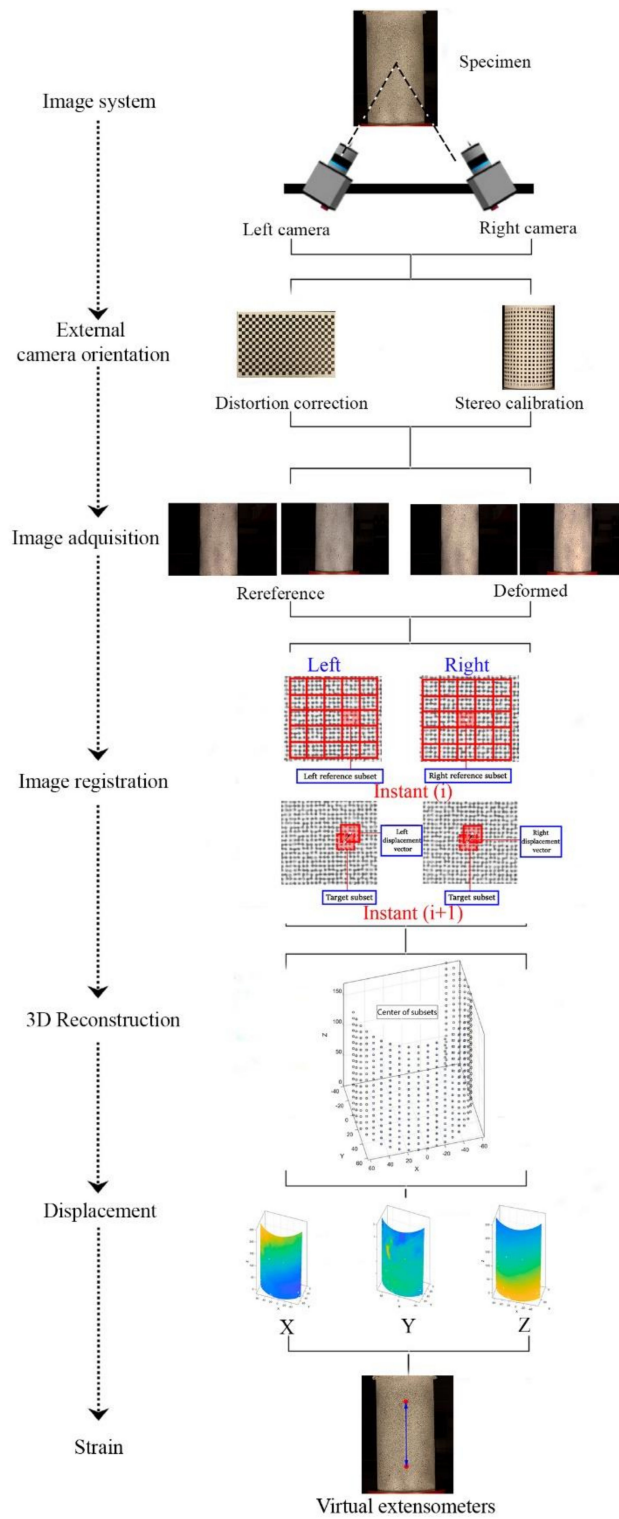
Figure 4. Graphical representation of the 3D-DIC approach.
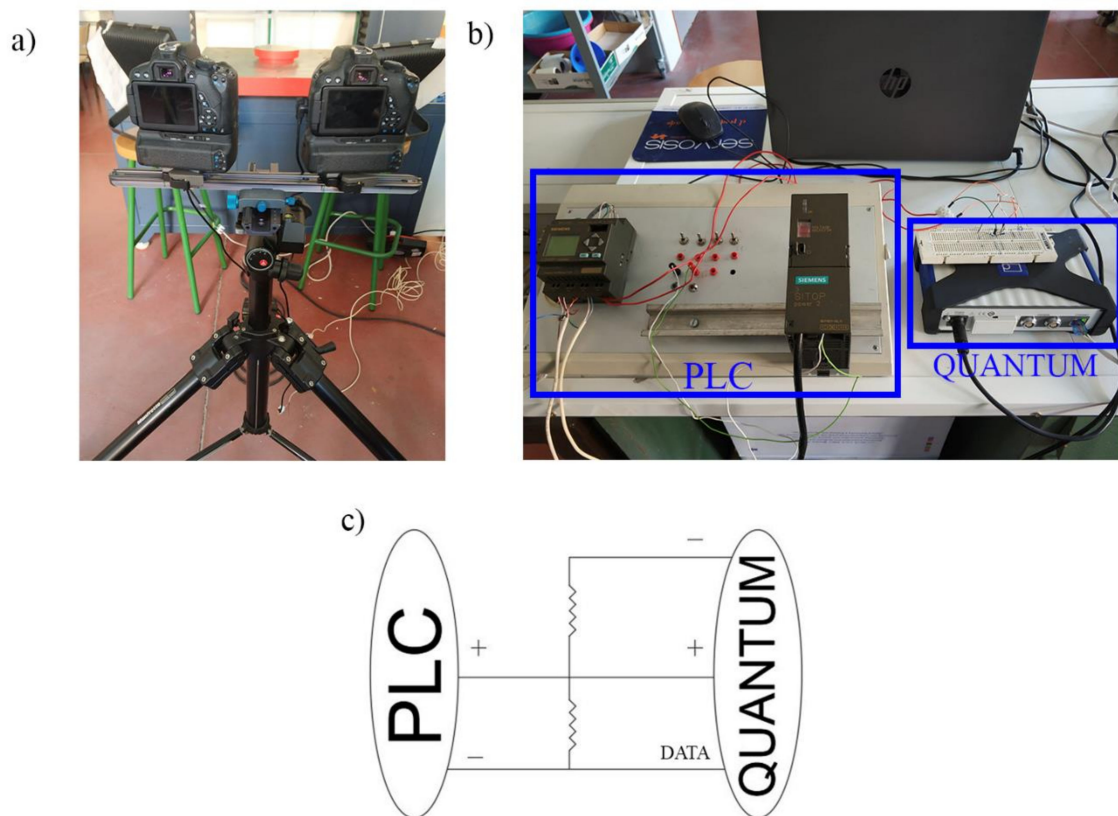
Figure 5. Data acquisition prototype: (**a**) platform of cameras and lighting units; (**b**) PLC and Quantum connections; and (**c**) single-line connection diagram.

Table 4. Canon 700D with macrolens technical specifications.

Sensor Type	CMOS APS-C
Sensor size	22.3×14.9 mm^2
Crop factor	1.61
Pixel size	4.3 μm
Image size	5184×3456 px
Total pixels	18.5 Mpx
Focal length	60 mm
Closer focused distance	254 mm
Lens magnification	1:1 (life size)
Dimensions	$133.1 \times 99.8 \times 78.8$ mm

2.2.2. Camera Orientation

An orientation phase was carried out ahead of the data acquisition. This phase allowed us to pass from the 2D images to a 3D point cloud. From the present case study, the Solav et al. [51] strategy was used. This approach integrates the Bundle Adjustment (BA) algorithm with the Direct Liner Transformation (DLT) algorithm to obtain the distortion, and internal and external parameters of the cameras.

Firstly, the inner calibration of the cameras was obtained by using the BA method. This method allowed us to minimize the overall re-projection error of the control points (corners of squares) extracted from a calibration pattern. Therefore, lens distortion can be corrected by using a non-linear distortion model, replacing the idealized coordinates with those corrected, according to a Gaussian radial distortion model (Equation (1)). In order to guarantee the accuracy and quality of this process, it is necessary to capture a set of images,

generally between 50 and 100 [51], of a flat calibration target so that different positions and orientations are captured throughout the FOV.

$$\begin{bmatrix} x_d \\ y_d \end{bmatrix} = \left(1 + k_1 r^2 + k_2 r^4 + k_3 r^6\right) \cdot \begin{bmatrix} x \\ y \end{bmatrix} + \begin{bmatrix} 2p_1 xy + p_2\left(r^2 + 2x^2\right) \\ p_1\left(r^2 + 2y^2\right) + 2p_2 xy \end{bmatrix} \tag{1}$$

where $r^2 = x^2 + y^2$ represents the radial distance, r, computed from the images' coordinates (x,y); (x_d, y_d) are the image coordinates corrected from lens distortion; k_1, k_2, k_3 are the radial distortion parameters; and p_1, p_2 are the decentering distortion parameters.

Once the lens distortion has been corrected, the DLT algorithm allows us to relate the image coordinates (x_d, y_d) and the object coordinates (X', Y', Z'). This algorithm provides a linear solution of 11 mathematical parameters equivalent to the non-linear model of 9 geometric parameters. The system can be solved knowing at least six points (Equation (2)). In this case a non-planar calibration object is used in which there are control points with their known 3D coordinates. Furthermore, the DLT algorithm allows us to obtain the 3D coordinates of a specific point by using the 2D coordinates of this point in at least two images.

$$x_p = \frac{L_1 X + L_2 Y + L_3 Z + L_4}{L_9 X + L_{10} Y L_{11} Z + 1}$$

$$\tag{2}$$

$$y_p = \frac{L_5 X + L_6 Y + L_7 Z + L_8}{L_9 X + L_{10} Y L_{11} Z + 1}$$

where x_p and y_p are the image point coordinates and L_1, L_2, L_3, L_4, L_5, L_6, L_7, L_8, L_9, L_{10}, L_{11} correspond to the 11 mathematical parameters of the DLT.

2.2.3. Correlation

As previously stated, the proper orientation of the cameras allowed us to reconstruct the common pixels between cameras in a common 3D space. Prior to this 3D reconstruction, it was required to use a correlation algorithm that allows matching homologous pixels captured at the time i and its homologous at the time $i + 1$ (Figure 6) in order to obtain the displacement vector (Figure 4).
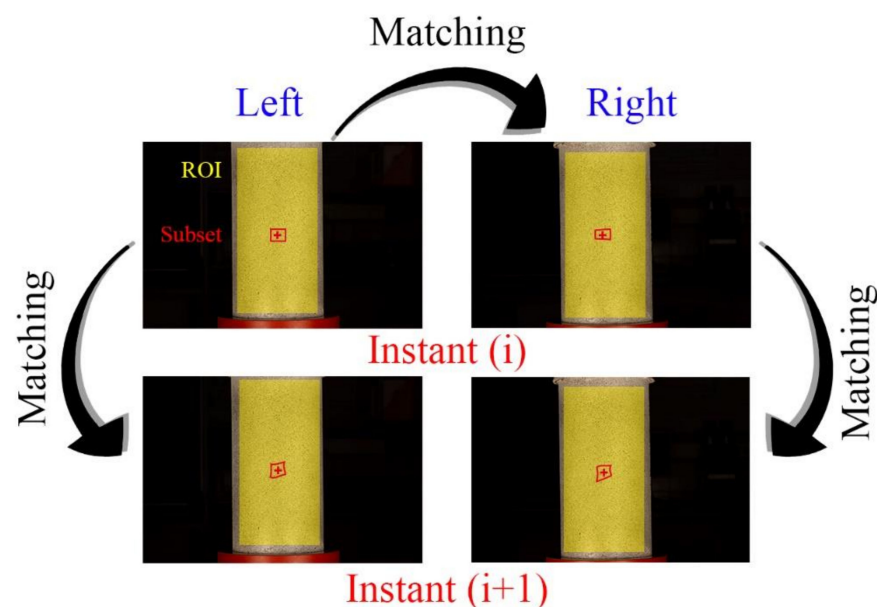

Figure 6. Image registration in 3D-DIC approach.

In order to carry out the matching procedure, it is necessary to divide the Region of Interest (ROI) into smaller areas called subsets (Figure 4). The degree of similarity between the subsets of each image is evaluated using the Zero mean Normalized Cross-Correlation

(ZNCC) criterion [52]. This correlation criterion is insensitive to the offset and linear scale in illumination lighting, offering the most robust noise-proof performance (Equation (3)).

$$C_{ZNCC} = \frac{\sum \overline{f}_i \overline{g}_i}{\sqrt{\sum \overline{f}_i^2 \sum \overline{g}_i^2}} \tag{3}$$

where $\overline{f} = \frac{1}{n} \sum_{i=1}^{n} f_i$, $\overline{g} = \frac{1}{n} \sum_{i=1}^{n} g_i$, $\overline{f}_i = f_i - \overline{f}$, $\overline{g}_i = g_i - \overline{g}$ with f_i, g_i representing the intensity value of the ith pixel point within reference subset and deformed subset, respectively.

The use of the ZNCC correlation allows for matching homologous points with pixel accuracy. In order to obtain a sub-pixel accuracy, the use of the following two-fold approach is required [53]: (i) a b-spline b-quantum interpolation scheme to pass from the discrete values of the images (0–255) to a continuous space [54]; and (ii) the Inverse Compositional Gauss-Newton method (IC-GN) for the minimization of the cost function that relates the reference subset to the deformed one. With the aim of minimizing the error accumulation due to the matching process, the Reliability-Guided Digital Image Correlation (RG-DIC) algorithm was used [55]. This algorithm starts from an initial point or seed and processes the rest of the subsets following an error minimization process.

Once the correlation process has been carried out, it is possible to perform the three-dimensional reconstruction of the corresponding points, thus obtaining a point cloud associated with the centres of the subsets placed within the ROI. To this end, the DLT parameters (L_1–L_{11}) obtained in the orientation process were used along with image coordinates (x_p, y_p) of the points obtained from DIC. In this way, the real coordinates of each of the points (X, Y, Z) can be calculated by means of Equation (4), following a least-square strategy. Since the external orientation was performed with a calibration object with known 3D coordinates, the X, Y, Z coordinates are obtained in the global coordinate system for all cameras.

$$P = \left[A^T A \right]^{-1} A^T U \tag{4}$$

$$A = \begin{bmatrix} L_1^{C_R} - L_9^{C_R} x_p^{C_R} & L_2^{C_R} - L_{10}^{C_R} x_p^{C_R} & L_3^{C_R} - L_{11}^{C_R} x_p^{C_R} \\ L_5^{C_R} - L_9^{C_R} y_p^{C_R} & L_6^{C_R} - L_{10}^{C_R} y_p^{C_R} & L_7^{C_R} - L_{11}^{C_R} y_p^{C_R} \\ L_1^{C_L} - L_9^{C_L} x_p^{C_L} & sL_2^{C_L} - L_{10}^{C_L} x_p^{C_L} & L_3^{C_L} - L_{11}^{C_L} x_p^{C_L} \\ L_5^{C_L} - L_9^{C_L} y_p^{C_L} & L_6^{C_L} - L_{10}^{C_L} y_p^{C_L} & L_7^{C_L} - L_{11}^{C_L} y_p^{C_L} \end{bmatrix}$$

where:

with C^R and C^L corresponding to the right and left cameras, respectively.

$$P = \begin{bmatrix} X \\ Y \\ Z \end{bmatrix} \quad U = \begin{bmatrix} x_p^{C_R} - L_4^{C_R} \\ y_p^{C_R} - L_8^{C_R} \\ x_p^{C_L} - L_4^{C_L} \\ y_p^{C_L} - L_8^{C_L} \end{bmatrix}$$

Once the three-dimensional coordinates of the homologous points for the entire ROI were obtained, these are used to calculate the displacements in 3D. In this way, it was possible to obtain a full field of displacements for each of the stereoscopic pairs.

2.3. Predictive Modelling Strategy

This section describes the strategy used for fitting both predictive models: (i) the predictive model for the unconfined compressive strength (UCS); and (ii) the predictive model for the maximum strain. As stated in the Introduction, the DIC approach is an added value in terms of the possibility of analysing the heterogeneous behaviour of the material and studying the maximum strains in the closest area to failure. This advantage allows us to establish a model to predict peak strain more precisely from the compressive strength of the concrete studied.

On the one hand, different models have been proposed for predicting the compressive strength [21–23] for different types and mix proportions of conventional and recycled concrete. However, the total replacement of coarse and fine aggregates represents a challenge that has not been addressed in the extensive bibliography and that aims to be solved with the predictive models proposed in this work.

Concerning the strain predictions, some design codes assumed a constant value of 0.002, meanwhile other models directly relate compressive strength with peak strain, such as the one provided by González-Fonteboa et al. [25] (Equation (5)), which has been established based on Eurocode 2 [24], considering the percentage of substitution of coarse aggregates for recycled aggregates:

$$\varepsilon_{c1} = 0.7 \cdot (f_{cm})^{0.31} \cdot (0.0021 \cdot \%RCA + 1) \tag{5}$$

where ε_{c1} is the peak strain; f_{cm} is the compressive strength at 28 days; and *%RCA* is the percentage of replacement with recycled coarse aggregates.

However, the strain at compressive strength depends on other variables that do not take into account models, such as mix composition, shape and size of specimen or age of curing [56]. The difference in the properties of the aggregates can be decisive in the final behaviour of the recycled concretes, so there are prediction models that incorporate other variables related to the properties of the aggregates, such as the mortar content, volume, density crushing strength and shape index [23]. In this sense, the properties with the greatest influence on the final result will be studied to incorporate them into the models.

2.3.1. Model Fitting

The model fitting strategy used was the Multiple Linear Regression (MLR) [57]. This fitting strategy allows us to predict the UCS and the maximum strain of the concretes by means of different inputs, such as the mix proportions and the specific characteristics of the concrete. This regression model was complemented by a variable transformation, which allows us to study the input-output relation from a non-linear perspective.

Complementary to both regression strategies, several statistical analyses were carried out with the aim of evaluating the statistical significance of the inputs. These tests were: (i) the analysis of variance (ANOVA) test, (ii) the Levene´s test; and (iii) *t*-Student test.

2.3.2. Sensitivity Analysis

The mathematical model can be finally expressed as a relationship in which there are three inputs bounded by the experimental data, which allows us to obtain a prediction of the final output value. According to this, a good practice compromises the analysis of the influence of each input in the final output. From the present study, it was decided to carry out a sensitivity analysis based on the Monte Carlo simulation (MCS). This method allows us to generate equiprobable situations, which could be considered as suitable sampling points for a subsequent sensitivity analysis. Within this context, one of the most used strategies to carry out sensitivity analysis is the estimation of the Sobol'indices [58]. These indices assume that the variance of the model (output) can be described as a sum of the variances of the inputs (Equation (6)). The normalized version of each variance with respect to the total one allows us to obtain de Sobol'indices with different orders (from 1 to 2^{n-1}) (Equation (7)). The sum of these indices is the total Sobol' index whose value is equal to 1.

$$V(Y) = \sum_i V_i + \sum_i \sum_{j>i} V_{ij} + \sum_i \sum_{j>i} \sum_{k>j} V_{ijk} + \dots V_{123..N} \tag{6}$$

where *V(Y)* is the variance of the model; $V_i = V(E(Y \mid X_i))$ is the first order partial variance; $V_{ij} = V(E(Y \mid X_i, X_j))$ is the second order partial variance, etc.

$$S_i = \frac{V_i}{V(Y)}, S_{ij} = \frac{V_{ij}}{V(Y)}, \tag{7}$$

where S_i is the first order Sobol' index and S_{ij} is the second-order Sobol'indices.

3. Experimental Results

3.1. Test Setup

A total of 38 tests were carried out following the guideline UNE-EN 12390-3 [48], 19 of which correspond to specimens with concrete aggregates (CDWRCon) and another 19 which correspond to specimens with ceramic aggregates (CDWRCer). For each type of concrete, four different mix proportions were used, and for each of these two different curing times were analysed (Table 5). Additionally, for dosages 2, 3 and 4, a specimen was reserved for testing with a longer curing age. It is worth mentioning the need to employ high water-cement ratios (w/c) in order to achieve good concrete workability. In addition, the variability in these values allows us to extend the validation range in modelling.

Table 5. Typology and characteristics of the tested specimens.

Dosage	Specimen	*w/c* Ratio	Curing Days
CDWRCon 1	CDWRCon 1-1	1.38	7
	CDWRCon 1-2		7
	CDWRCon 1-3		28
	CDWRCon 1-4		28
CDWRCer 1	CDWRCer 1-1	1.38	7
	CDWRCer 1-2		7
	CDWRCer 1-3		28
	CDWRCer 1-4		28
CDWRCon 2	CDWRCon 2-1	0.67	8
	CDWRCon 2-2		8
	CDWRCon 2-3		29
	CDWRCon 2-4		29
	CDWRCon 2-5		90
CDWRCer 2	CDWRCer 2-1	0.60	7
	CDWRCer 2-2		7
	CDWRCer 2-3		28
	CDWRCer 2-4		28
	CDWRCer 2-5		90
CDWRCon 3	CDWRCon 3-1	0.67	12
	CDWRCon 3-2		12
	CDWRCon 3-3		28
	CDWRCon 3-4		28
	CDWRCon 3-4		90
CDWRCer 3	CDWRCer 3-1	0.67	14
	CDWRCer 3-2		14
	CDWRCer 3-3		28
	CDWRCer 3-4		28
	CDWRCer 3-5		90

Table 5. *Cont.*

| Dosage	Specimen	*w/c* Ratio	Curing Days
CDWRCon 4	CDWRCon 4-1	0.60	21
	CDWRCon 4-2		21
	CDWRCon 4-3		28
	CDWRCon 4-4		28
	CDWRCon 4-5		90
CDWRCer 4	CDWRCer 4-1	0.67	21
	CDWRCer 4-2		21
	CDWRCer 4-3		28
	CDWRCer 4-4		28
	CDWRCer 4-5		90

In order to optimize the configuration to be used during the 3D-DIC test, a preparation stage was carried out. The steps followed in this process were as follows: (i) application of the speckle pattern; (ii) definition of the Ground Sampling Distance (GSD), lens aperture and stereo angle; and (iii) geometric calibration and orientation of the cameras.

Firstly, a speckle pattern was applied using the aerosol technique (Figure 7b). The quality of the pattern was evaluated through the covering factor [31] as well as the Mean Intensity Gradient (MIG) index [50]. For the first variable, an average value between 45–50% was obtained. Meanwhile the MIG values were comprised between 30–35, which was considered acceptable taking into account the method used [50].

The success of the 3D-DIC approach depends strongly on the GSD of the images and the stereo angle of the cameras. In this sense, an angle that is too high allows for a better precision in depth, but a lower precision in the plane, and an angle too small allows a better precision in the plane at the cost of a higher uncertainty in depth. Under this basis, the acquisition system was placed at 1.25 m with respect to the specimen (Figure 7a), achieving a GSD of 0.09 mm/px. The aperture of both lenses was established in f10, obtaining a good compromise between depth of field (which was of 180 mm) and sharpness. Additionally, a stereo angle of 10° was configured in order to avoid possible depth of field problems [59]. Taking into account that the loading speed was 0.4 MPa/s, the images were acquired each 0.6 MPa with a shutter speed of 1/100 s, capturing the first image without load in order to obtain the reference image.

Taking into account that the tests were performed on different days, the camera orientation procedure described in Section 2.2.2 was repeated for each of these days before carrying out the tests. The geometrical calibration of the camera was carried out by using a high-quality checkerboard target (Figure 7a). This target is made up of a matrix of 18×29 squares of 10 mm. Approximately 100 images were captured at different positions and angles, so that the BA algorithm allowed us to obtain the control points and calculate the lens distortion parameters, with an average re-projection error of 0.15 px for each camera.

The external orientation was carried out applying the DLT procedure, for which an image of a 125 mm diameter cylindrical object was captured (Figure 7c). The calibration object contains several control points. These points are placed on a 18 × 25 matrix with a spacing of 10 mm. It is worth mentioning that the re-projection of the control points allowed us to calculate the error associated with the reconstruction, obtaining a mean value between 0.010–0.015 mm and a Root Mean Square Error (RMSE) value between 0.155–0.179.
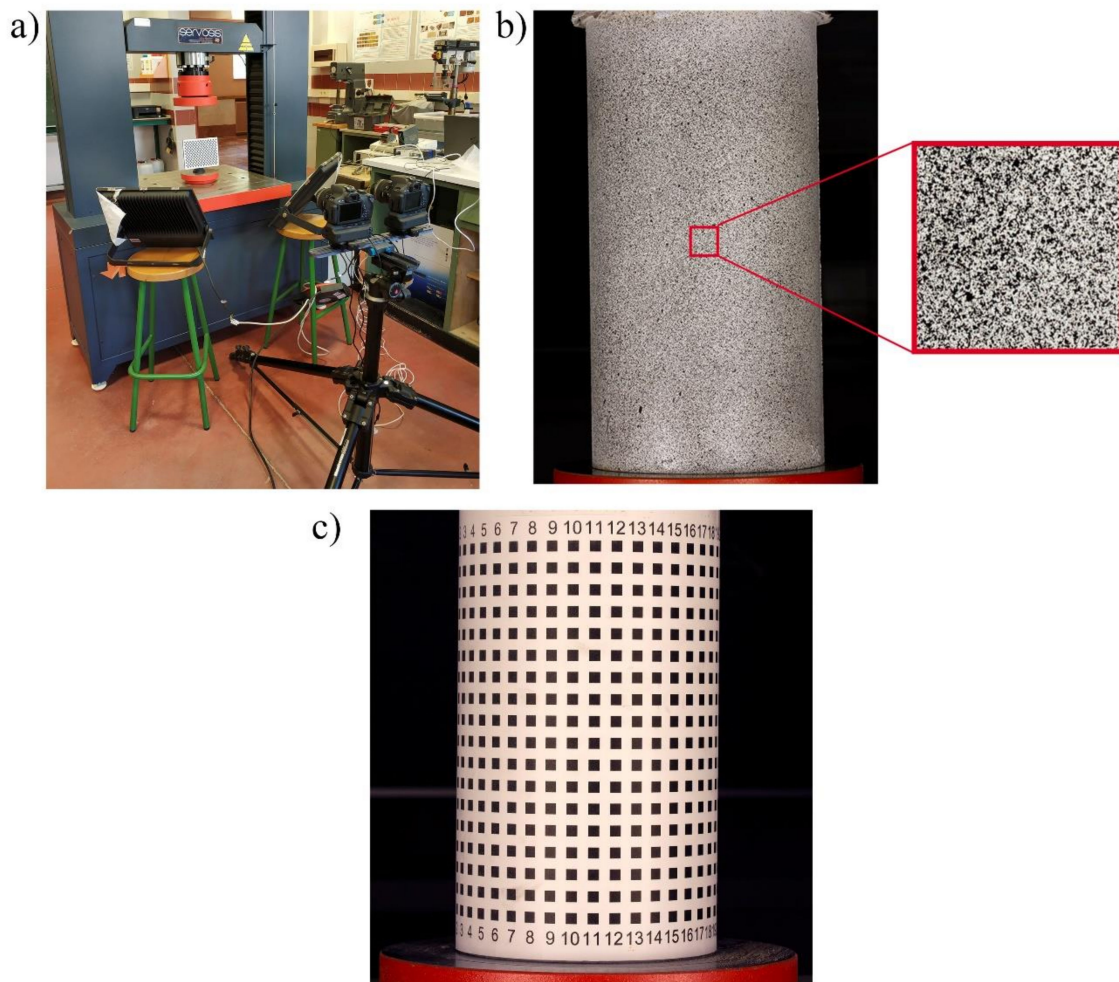
Figure 7. Digital Image Correlation campaign: (**a**) set-up used at the calibration stage; (**b**) detail of the speckle pattern applied; and (**c**) cylindrical calibration object.

3.2. Mechanical Properties of the Concrete Evaluated

In order to obtain the displacement and strain on each test specimen, the 3D-DIC approach defined in Section 2.2 was carried out by using the open-source software Multi-DIC [51]. This software integrates the open-source software Ncorr (Version 1.2, J. Blaber, Atlanta, GA, USA) [53]. Regarding DIC parameters, a subset size of 20×20 pixels and a 65% overlap (step of 7 pixels) were considered to ensure a proper DIC configuration [29]. The interpolation between points was carried out by considering a linear shape function. Finally, the 3D reconstruction of the sample was obtained by applying the DLT algorithm, allowing us to obtain a full field of displacements (Figure 8a).

The strains suffered by the specimen were captured at different locations. To this end the following strategy was used: (i) creation of several virtual extensometers to evaluate the longitudinal strains (Figure 8b); (ii) extraction the peak longitudinal strain in the state of load prior to failure; and (iii) selection of the virtual extensometer with the maximum peak strain, corresponding to the failure zone.
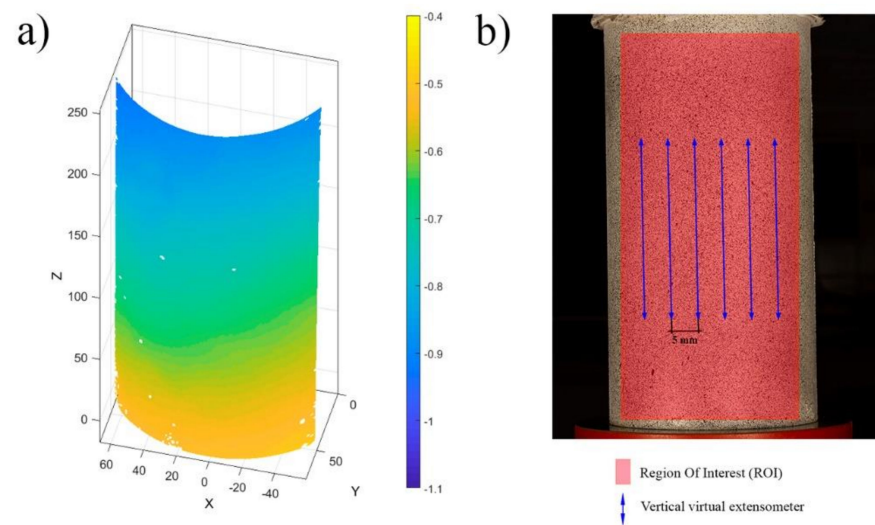
Figure 8. Results obtained during the 3D-DIC: (**a**) displacements obtained along the longitudinal axis; and (**b**) extraction of the maximum longitudinal strain by means of the virtual extensometer.

With the aim of obtaining a wide population, 22 virtual extensometers were placed in each specimen with a separation of 5 mm. In this sense, it is worth mentioning the high differences found between the values of the different virtual extensometers, which indicate the high heterogeneous behaviour of these materials. This heterogeneity can be seen in the high CoV corresponding to the virtual extensometers of some sample specimens shown in the Table 6. In order to establish a more precise model to predict strains, the virtual extensometers were analysed and those that corresponded to the failure zone were selected, such as peak strain.

Table 6. Results obtained from the mechanical characterization of some specimens analysed by the 3D-DIC approach.

Specimen	Mean	Lower Bound	Upper Bound	CoV (%)
CDWRCon 1-1	0.0017	0.0014	0.0020	9.90
CDWRCon 2-3	0.0025	0.0022	0.0031	7.19
CDWRCon 3-2	0.0020	0.0018	0.0025	10.16
CDWRCer 1-1	0.0019	0.0013	0.0024	16.76
CDWRCer 2-3	0.0028	0.0025	0.0030	5.44
CDWRCer 3-2	0.0024	0.0020	0.0026	6.37

4. Strength and Strain Models

4.1. Concrete Strength Model

The concrete strength model was obtained by using the MLR approach. This analysis was carried out with the assistance of the IBM SPSS Statistics software (Version 26.0, IBM Corp., Armonk, NY, USA). The input variables considered during this stage were: (i) the time (t); (ii) the water–cement ratio (w/c); and (iii) the percentage of material belonging to the class $Rc + Ru$ ($RcRu$) established by UNE-EN 13242 standard [38], where Rc corresponds to concrete, concrete products, mortar and concrete masonry parts, and Ru correspond to untreated aggregates and natural stone aggregates treated with hydraulic binders.

A total of 38 points were used to carry out the adjustment. Scatterplots with a trend line are showed in Figures 9–11, which express the correlation between each independent variable and the compressive strength. A positive correlation between the rupture time and $Rc + Ru$ with the maximum strength was observed. The water-cement ratio shows an inverse correlation with respect to the maximum strength.
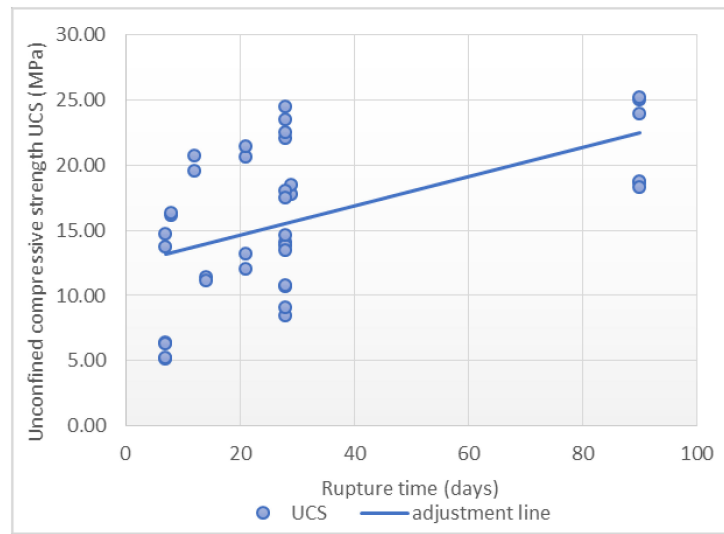
Figure 9. Relationship between rupture time and unconfined compressive strength.
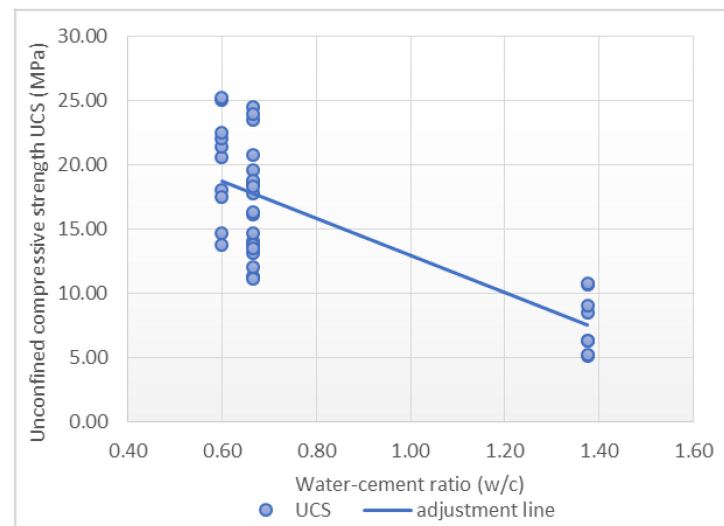

Figure 10. Relationship between water-cement ratio and unconfined compressive strength.
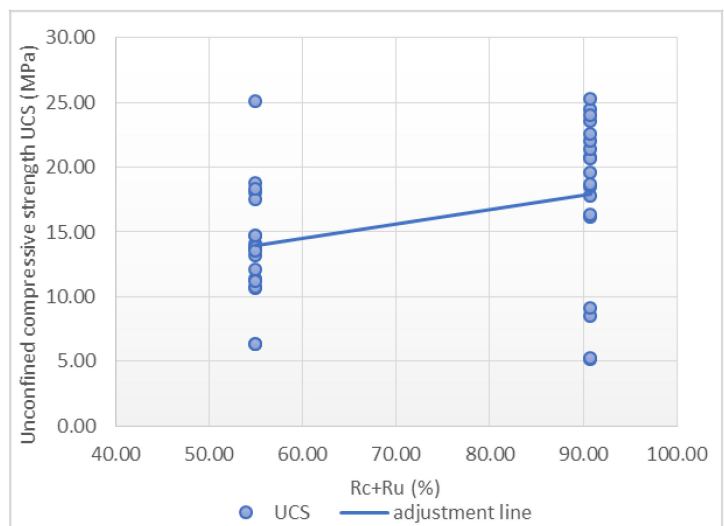

Figure 11. Relationship between *Rc + Ru* and unconfined compressive strength.

It is worth mentioning the low correlation between the individual inputs considered and the final output. Furthermore, in Figures 9–11 it can be seen how outliers can generate a correlation and a linear relationship between the variables that does not exist, according to the fourth case of Anscombe's quartet. As a result, a multilinear regression model was applied in order to consider all these variables in the same prediction model. In order to improve this regression, a transformation of the variables was carried out. In this case, the most satisfactory results correspond to the use of UCS as a cubic root and rupture time as a fifth root. The adjustment with the transformed variables resulted in a Pearson's correlation coefficient value of 0.921, representing a high correlation, and the determination coefficient is 0.848, with a standard error of 0.137, as is shown in Table 7.

Table 7. Determination coefficients for UCS model.

Summary Model			
R	R^2	Adjusted R^2	Standard Error
0.921 [a]	0.848	0.834	0.137

[a] predictors: constant, $\sqrt[5]{t}$ (days), *w/c*, *Rc* + *Ru* (%).

Table 8 shows the results obtained after applying the ANOVA strategy as well as Levene´s test. This test revealed a homoscedasticity with an F = 63.009 and a significance of 0.000 for 37 degrees of freedom. In this case, variances are significantly different and factors such as the rupture time, water-cement ratio and *Rc* + *Ru* have a statistical significance with the UCS.

Table 8. Analysis of variance for UCS model.

ANOVA [a]					
Model	Squares Sum	Degrees of Freedom	Average	F	sig.
regression	3.531	3	1.177	63.009	0.000 [b]
remainder	0.635	34	0.019		
Total	4.166	37			

[a] dependent variable: $\sqrt[3]{UCS}$ (MPa); [b] predictors: constant, $\sqrt[5]{t}$ (days), *w/c*, *Rc* + *Ru* (%).

The increase in the quality of the adjustment with the transformed variables, based on the value of the correlation coefficient, was not significantly high. However, it is considered advantageous to use the transformations in order to achieve the best possible approximation.

The obtained coefficients and the Student's t-test results are shown in Table 9 with a high value of the *t* statistic, between 4.211–10.069. All the variables are significant (sig. < 0.050).

Table 9. Determination coefficients for UCS model. Dependent variable: $\sqrt[3]{UCS}$.

Model	No Standard Coefficients		Standard Coefficients	*t*	sig.
	B	Standard Error	*β*		
Constant	1.983	0.197		10.069	0.000
t (days)	0.385	0.076	0.354	5.040	0.000
w/c	−0.774	0.077	−0.702	−9.991	0.000
RcRu (%)	0.005	0.001	0.282	4.211	0.000

Therefore, the equation that represents the best fit is Equation (8).

$$\sqrt[3]{UCS} = 0.385 \times \sqrt[5]{t} - 0.774 \times w/c + 0.005 \times RcRu + 1.983 \tag{8}$$

where, UCS is unconfined compressive strength (MPa), *t* is rupture time (days), *w/c* is water-cement ratio and *RcRu* is material belonging to the class *Rc + Ru*. There is a validity range to the significance of the model that is shown in Table 9. UCS has a range between 5.13 and 25.27 MPa. Rupture time is from 7 until 90 days. The water–cement ratio is from 0.60 until 1.38 and *Rc + Ru* is between 54.99 and 90.74.

In order to understand which variables are the most relevant in the strength prediction model of the recycled concrete, a Sobol sensitivity analysis was carried out. A total of 500,000 simulations were performed in order to carry out this analysis through a Monte Carlo Simulation. For each of the simulations, the input variables were modified within the ranges obtained from the experimental results.

Figure 12 indicates that the water/cement ratio is the most relevant parameter in the compressive strength prediction model. This property explains 71% of the total variance, agreeing with the Student's t-coefficients previously analysed. The rupture time has a greater influence in the final output with a Sobol index of 0.22 (22%), while *Rc + Ru* percentage is the variable that least affects the prediction. The great similarity between the first and the total Sobol'indices highlights the absence of a second-order effect.
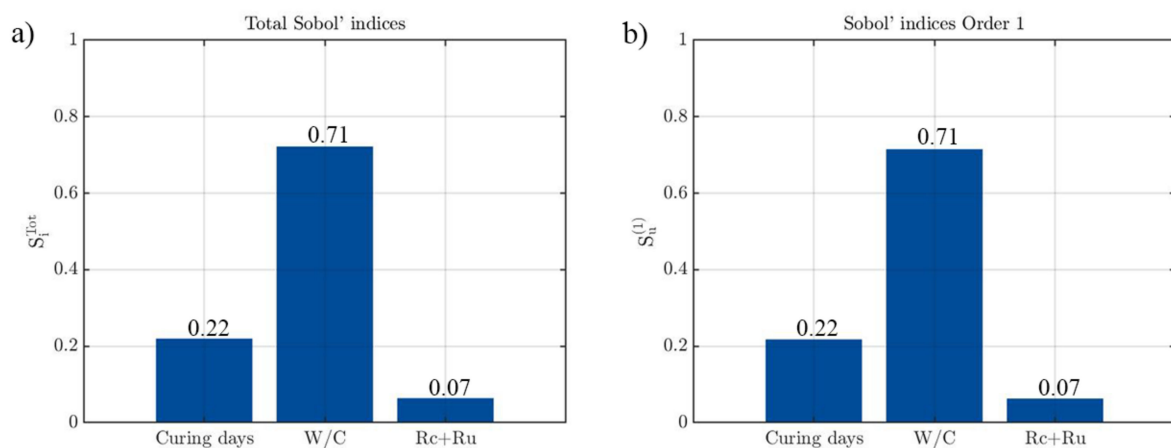
Figure 12. Results obtained during the sensitivity analysis of the strength model: (**a**) Total Sobol'indices and; (**b**) First-order Sobol'indices.

4.2. Concrete Strain Model

The inputs evaluated for predicting the maximum strain of the concretes were the compressive strength, the curing age and the water–cement ratio. Scatterplots with a linear trend are shown in Figures 13–15, which express the correlation between each independent variable and the peak strain.

The results in this case, for the simple regressions, also show a low correlation and outliers in Figure 15. Taking into consideration the values previously obtained, several multiple linear regressions with variable transformation were carried out. It is worth mentioning that a total of two maximum strain equations were obtained due to the dissimilarity of the data for the CDWRCon and CDWRCer. For this adjustment, a total of 32 samples were used.
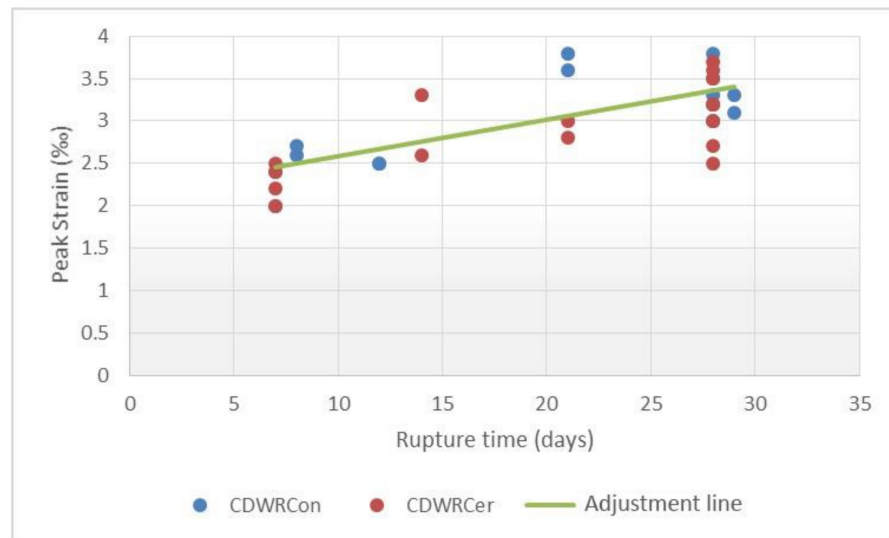
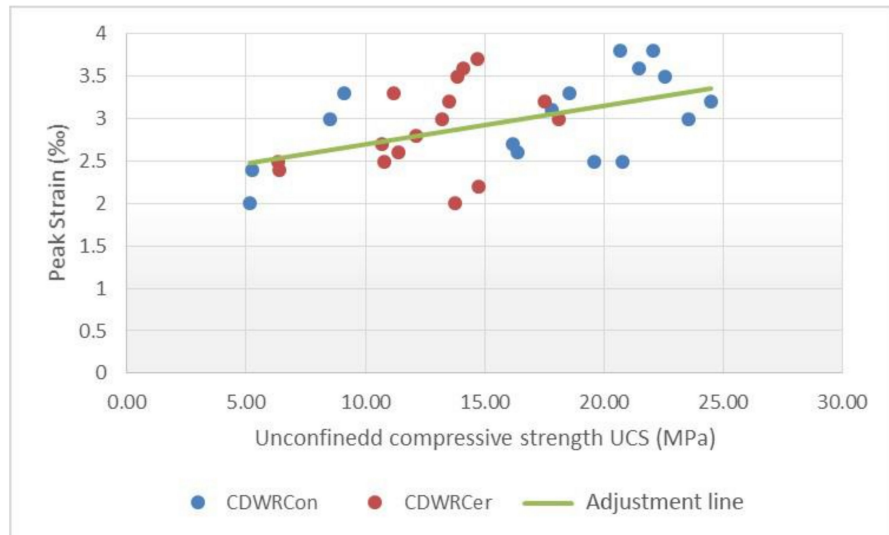**Figure 13.** Relationship between rupture time and peak strain.

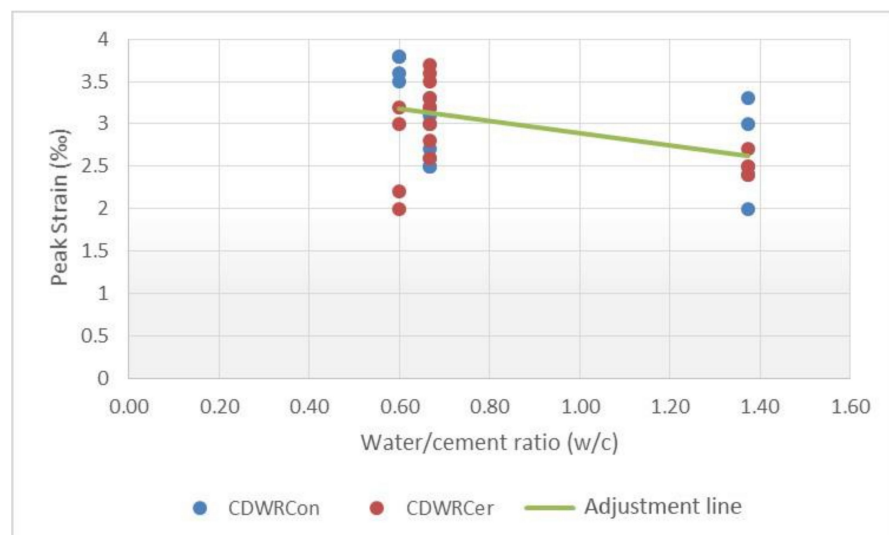**Figure 14.** Relationship between unconfined compressive strength and peak strain.

Figure 15. Relationship between water-cement ratio and peak strain.

The following transformations were used during the adjustment: (i) a square root for the peak strain; (ii) a cubic root for the UCS; and (iii) a fifth root for the rupture time. As a result of the transformations carried out, it was possible to obtain an adjustment for the concrete manufactured with CDWRCon with a Pearson's correlation coefficient value of 0.859, with the determination coefficient as 0.738 and a standard error of 0.090 (Table 10).

Table 10. Determination coefficients for strain model of CDWRCon.

Summary Model			
R	R^2	Adjusted R^2	Standard Error
0.859 [a]	0.738	0.673	0.090

[a] predictors: constant, $\sqrt[5]{t}$ (days), $\sqrt[3]{\text{UCS}}$ (MPa), w/c.

The analysis of variance (ANOVA) (Table 11) showed that the variables have variances significantly different and the predictors have a statistical significance on the peak strain prediction. The result in the Levene's test yielded a F = 11.272 with 0.001 of significance for 15 degrees of freedom.

Table 11. Analysis of variance for strain model of CDWRCon.

ANOVA [a]					
Model	Squares Sum	Degrees of Freedom	Average	F	sig.
regression	0.271	3	0.090	11.272	0.001 [b]
remainder	0.096	12	0.008		
Total	0.368	15			

[a] dependent variable: $\sqrt{\varepsilon_p}$ (‰); [b] predictors: constant, $\sqrt[5]{t}$ (days), $\sqrt[3]{\text{UCS}}$ (MPa), w/c.

The obtained coefficients and the Student's t-test results are shown in Table 12. They show low values, especially for the UCS and w/c ratio. The results show that these variables are not significant (sig. > 0.050). These values indicate the presence of anomalies that prevent obtaining an accurate prediction model for this type of concrete.

Table 12. Determination coefficients for strain model of CDWRCon. Dependent variable: $\sqrt{\varepsilon_p}$.

Model	No Standard Coefficients		Standard Coefficients	t	sig.
	B	Standard Error	β		
Constant	1.323	0.715		1.849	0.089
t (days)	0.692	0.181	0.885	3.816	0.002
UCS (MPa)	−0.213	0.271	−0.537	−0.787	0.447
w/c	−0.353	0.296	−0.740	−1.192	0.256

In order to determine what happens in the CDWRCon model, the data used to calculate the model were analysed individually and compared with the CDWRCer data. A greater data dispersion was found for the concretes made up by concrete waste, while ceramics have a more uniform distribution with no empty ranges (Figure 13). This issue could be attributed to an insufficient population. Thus, although the R^2 coefficient can be considered as acceptable, the parameters are not correct and the predictions for values of the inputs differ from those used to generate the model, which may result in erroneous predictions.

On the other hand, the model for the concrete manufactured with CDWRCer yielded a better adjustment with a Pearson's correlation coefficient value of 0.917, while the determination coefficient is 0.840 with a standard error of 0.085 (Table 13).

Table 13. Determination coefficients for strain model of CDWRCer.

	Summary Model		
R	R^2	Adjusted R^2	Standard Error
0.917 [a]	0.840	0.775	0.085

[a] predictors: constant, $\sqrt[5]{t}$ (days), $\sqrt[3]{UCS}$ (MPa), w/c.

The analysis of variance (ANOVA) (Table 14) is similar to the previous case, with a result in the Levene's test of F = 11.402 with 0.001 of significance for 15 degrees of freedom. This analysis shows that the variables have variances significantly different and the predictors have a statistical significance on the peak strain prediction.

Table 14. Analysis of variance for strain model of CDWRCer.

	ANOVA [a]				
Model	Squares Sum	Degrees of Freedom	Average	F	sig.
regression	0.244	3	0.081	11.402	0.001 [b]
remainder	0.086	12	0.007		
Total	0.330	15			

[a] dependent variable: $\sqrt{\varepsilon_p}$ (‰); [b] predictors: constant, $\sqrt[5]{t}$ (days), $\sqrt[3]{UCS}$ (MPa), w/c.

The Student's t-test results (Table 15) show a good value of the *t* statistic, between 2.442–5.036. These results indicate that all the variables are significant (sig. < 0.050) and the model seems to have a correct behaviour in this case.

Table 15. Determination coefficients for strain model of CDWRCer. Dependent variable: $\sqrt{\varepsilon_p}$.

Model	No Standard Coefficients		Standard Coefficients	*t*	sig.
	B	Standard Error	*β*		
Constant	1.963	0.485		4.044	0.002
t (days)	0.740	0.147	1.010	5.036	0.000
UCS (MPa)	−0.550	0.225	−0.803	−2.442	0.031
w/c	−0.386	0.127	−0.853	−3.030	0.010

Therefore, the peak strain prediction model can be represented by the Equation (9).

$$\sqrt{\varepsilon_p} = 1.963 + 0.740 \cdot \sqrt[5]{t} - 0.550 \cdot \sqrt[3]{UCS} - 0.386 \cdot w/c \tag{9}$$

where ε_p is the peak strain (‰); *t* is rupture time (days); UCS represents the unconfined compressive strength (MPa); and w/c is the water-cement ratio.

Further, the data obtained from the strain prediction model were subjected to a validation analysis. Thus, the predictions for the experimental data were simulated and compared with the results obtained during the campaign. A mean discrepancy of 6.1% was obtained for the CDWRCer model. These results were considered acceptable taking into account the low peak strain values as well as the precision required in this type of prediction.

In order to understand which variables are the most relevant in the strain prediction model of the recycled concrete, a Sobol sensitivity analysis was carried out. A total of 500,000 simulations were performed to carry out this analysis through a Monte Carlo Simulation. For each of the simulations, the input variables were modified within the ranges obtained from the experimental results (curing days [7–30 days]; strength [5–25 MPa]; and water-cement ratio [0.60–1.38]).

Figure 16 indicates that in the case of CDWRCer, the compressive strength of the concrete is the most relevant parameter in the peak strain prediction model. This mechanical

property explains 58% of the total variance, which agrees with other studies in which it is stated that strength is the main variable in this type of model [23,56]. The other two input parameters have a similar influence in the results, 24% corresponding to the curing age and 18% corresponding to water-cement ratio. The great similarity between the first and the total Sobol'indices highlights the absence of a second-order effect.
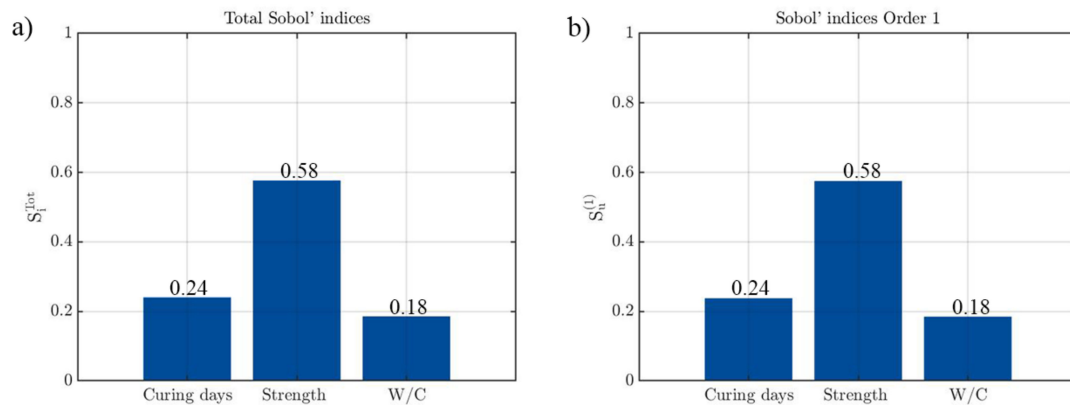
Figure 16. Results obtained during the sensitivity analysis of CDWRCer: (**a**) Total Sobol'indices and; (**b**) First-order Sobol'indices.

5. Conclusions

This work aimed at investigating a predictive model for the determination of the UCS and the maximum strain in non-structural concretes made up by two types of recycled waste: concrete and ceramic wastes. The inputs required for fitting these models have been obtained by means of an extensive experimental campaign, which include granulometric analysis, physical and chemical analysis, and compression test among others. It is worth mentioning the use of the 3D-DIC as a remote sensing approach able to obtain a full-field of strains. This property allows us to accurately determine the peak strain of the concrete, which showed a high heterogeneity depending on the area considered.

Within the predictive model strategy, the simple regressions yielded low correlation values for the individual variables, so finally an MLR model was adjusted and showed that there is a good correlation between all the variables considered together. In addition, the transformations of variables made it possible to minimize errors. This highlights the need to incorporate different variables to obtain a correct predictive model.

On the one hand, the adjustment obtained using MLR demonstrates that the variables' rupture time, water-cement ratio and $Rc + Ru$ are able to predict the UCS with a determination coefficient of 0.848 within the validity range, with a standard error of 0.137. The coefficients showed that the w/c ratio has the greatest influence on compressive strength.

On the other hand, the strain prediction model allows for estimating the peak strain as a function of three input variables: rupture time, unconfined compressive strength and water/cement ratio. The sensibility analysis showed that the UCS has the greatest influence on peak strain. Thus, the strength value obtained from the previous model can be employed to estimate the peak strain.

The results obtained for the concrete manufactured with ceramic waste can be considered satisfactory, since the R^2 coefficient of 0.840 is supported by several statistical analyses that verified the statistical significance of the inputs, as well as the low discrepancy in the verification with the experimental data. However, the results obtained for the concrete manufactured with concrete waste model show more anomalous values with a low R^2 coefficient and less satisfactory results during statistical analysis. These results show the complexity of establishing a prediction model for this type of concrete, making a larger population necessary to carry out the adjustment, which will try to be integrated into future research.

One of the main future works will focus on scaling up the data from experimental campaigns in order to achieve a database that allows us to contrast and scale the results of the modelling and check the error. Along with this, one of the main interests focuses on the use of the full-field data provided by the 3D-DIC approach to evaluate other properties that could be of great interest in this type of concrete, such as elasticity, shrinkage or behaviour at the aggregate-cement interface. For this purpose, other types of tests, such as bending tests, could give rise to greater possibilities regarding the analysis of these properties under a 3D-DIC approach. Additionally, further dosages will be carried out in order to improve the influence of the w/c in the compressive strength and maximum strain. To this end, the use of superplasticizers will be planned.

Additionally, the proposed methodology will be implemented in concrete with other types of recycled aggregates that allow for higher performance for structural uses and thus be possible to carry out numerical simulations with the properties obtained.

References

1. Akhtar, A.; Sarmah, A.K. Construction and demolition waste generation and properties of recycled aggregate concrete: A global perspective. *J. Clean. Prod.* **2018**, *186*, 262–281. [CrossRef]
2. Fernández-Canovas, M. *Hormigón*; Colegio de Ingenieros de Caminos, Canales y Puertos: Madrid, Spain, 2013.
3. Peduzzi, P. Sand, Rarer than One Thinks. *Environ. Dev.* **2014**, *11*, 208–218.
4. Eurostat. Waste Statistics. Available online: https://ec.europa.eu/eurostat/statistics-explained/index.php?title=Waste_statistics (accessed on 3 May 2021).
5. Medina, C.; Zhu, W.; Howind, T.; Frías, M.; de Rojas, M.I.S. Effect of the constituents (asphalt, clay materials, floating particles and fines) of construction and demolition waste on the properties of recycled concretes. *Constr. Build. Mater.* **2015**, *79*, 22–33. [CrossRef]
6. McNeil, K.; Kang, T.H.K. Recycled concrete aggregates: A review. *Int. J. Concr. Struct. Mater.* **2013**, *7*, 61–69. [CrossRef]
7. Nedeljković, M.; Visser, J.; Šavija, B.; Valcke, S.; Schlangen, E. Use of fine recycled concrete aggregates in concrete: A critical review. *J. Build. Eng.* **2021**, *38*, 102196. [CrossRef]
8. EHE-08. *Instrucción de Hormigón Estructural EHE-08*; Ministerio de Fomento, Gobierno de España: Madrid, Spain, 2008.
9. Martín-Morales, M.; Zamorano, M.; Ruiz-Moyano, A.; Valverde-Espinosa, I. Characterization of recycled aggregates construction and demolition waste for concrete production following the Spanish Structural Concrete Code EHE-08. *Constr. Build. Mater.* **2011**, *25*, 742–748. [CrossRef]
10. Juan-Valdés, A.; Rodríguez-Robles, D.; García-González, J.; Guerra-Romero, M.I.; Morán-del Pozo, J.M. Mechanical and microstructural characterization of non-structural precast concrete made with recycled mixed ceramic aggregates from construction and demolition wastes. *J. Clean. Prod.* **2018**, *180*, 482–493. [CrossRef]
11. Rodríguez, C.; Parra, C.; Casado, G.; Miñano, I.; Albaladejo, F.; Benito, F.; Sánchez, I. The incorporation of construction and demolition wastes as recycled mixed aggregates in non-structural concrete precast pieces. *J. Clean. Prod.* **2016**, *127*, 152–161. [CrossRef]
12. Guo, Z.; Tu, A.; Chen, C.; Lehman, D.E. Mechanical properties, durability, and life-cycle assessment of concrete building blocks incorporating recycled concrete aggregates. *J. Clean. Prod.* **2018**, *199*, 136–149. [CrossRef]
13. Martín-Morales, M.; Cuenca-Moyano, G.M.; Valverde-Espinosa, I.; Valverde-Palacios, I. Effect of recycled aggregate on physical-mechanical properties and durability of vibro-compacted dry-mixed concrete hollow blocks. *Constr. Build. Mater.* **2017**, *145*, 303–310. [CrossRef]

14. Sánchez Roldán, Z. *Utilización de Árido Reciclado para la Fabricación de Piezas de Hormigón Prefabricado de Mobiliario Urbano.* Ph.D. Thesis, Universidad de Granada, Granada, Spain, 2019.

15. Etxeberria, M.; Vázquez, E.; Marí, A.; Barra, M. Influence of amount of recycled coarse aggregates and production process on properties of recycled aggregate concrete. *Cem. Concr. Res.* **2007**, *37*, 735–742. [CrossRef]

16. Nepomuceno, M.C.S.; Isidoro, R.A.S.; Catarino, J.P.G. Mechanical performance evaluation of concrete made with recycled ceramic coarse aggregates from industrial brick waste. *Constr. Build. Mater.* **2018**, *165*, 284–294. [CrossRef]

17. Kumar, B.M.V.; Ananthan, H.; Balaji, K.V.A. Experimental studies on utilization of coarse and finer fractions of recycled concrete aggregates in self compacting concrete mixes. *J. Build. Eng.* **2017**, *9*, 100–108. [CrossRef]

18. Medina, C.; De Rojas, M.I.S.; Frías, M. Reuse of sanitary ceramic wastes as coarse aggregate in eco-efficient concretes. *Cem. Concr. Compos.* **2012**, *34*, 48–54. [CrossRef]

19. Mansur, M.A.; Wee, T.H.; Lee, S.C. Crushed bricks as coarse aggregate for concrete. *Mater. J.* **1999**, *96*, 478–484.

20. Kim, J.K.; Moon, Y.H.; Eo, S.H. Compressive strength development of concrete with different curing time and temperature. *Cem. Concr. Res.* **1998**, *28*, 1761–1773. [CrossRef]

21. Chidiac, S.E.; Moutassem, F.; Mahmoodzadeh, F. Compressive strength model for concrete. *Mag. Concr. Res.* **2013**, *65*, 557–572. [CrossRef]

22. Deng, F.; He, Y.; Zhou, S.; Yu, Y.; Cheng, H.; Wu, X. Compressive strength prediction of recycled concrete based on deep learning. *Constr. Build. Mater.* **2018**, *175*, 562–569. [CrossRef]

23. Cui, H.Z.; Lo, T.Y.; Memon, S.A.; Xing, F.; Shi, X. Analytical model for compressive strength, elastic modulus and peak strain of structural lightweight aggregate concrete. *Constr. Build. Mater.* **2012**, *36*, 1036–1043. [CrossRef]

24. EN 1992-1-1. *Eurocode 2: Design of Concrete Structures—Part 1-1: General Rules and Rules for Buildings*; CEN: Brussels, Belgium, 2004.

25. Belén, G.-F.; Fernando, M.-A.; Diego, C.L.; Sindy, S.-P. Stress-strain relationship in axial compression for concrete using recycled saturated coarse aggregate. *Constr. Build. Mater.* **2011**, *25*, 2335–2342. [CrossRef]

26. Rahal, K. Mechanical properties of concrete with recycled coarse aggregate. *Build. Environ.* **2007**, *42*, 407–415. [CrossRef]

27. Xiao, J.; Zhang, K.; Akbarnezhad, A. Variability of stress-strain relationship for recycled aggregate concrete under uniaxial compression loading. *J. Clean. Prod.* **2018**, *181*, 753–771. [CrossRef]

28. Hu, X.; Lu, Q.; Xu, Z.; Zhang, W.; Cheng, S. Compressive stress-strain relation of recycled aggregate concrete under cyclic loading. *Constr. Build. Mater.* **2018**, *193*, 72–83. [CrossRef]

29. Sutton, M.A.; Orteu, J.J.; Schreier, H.X. *Image Correlation for Shape, Motion and Deformation Measurements: Basic Concepts, Theory and Applications*; Springer Science & Business Media: New York, NY, USA, 2009.

30. Villarino, A.; López-Rebollo, J.; Antón, N. Analysis of Mechanical Behavior through Digital Image Correlation and Reliability of Pinus halepensis Mill. *Forests* **2020**, *11*, 1232. [CrossRef]

31. García-Martín, R.; López-Rebollo, J.; Sánchez-Aparicio, L.J.; Fueyo, J.G.; Pisonero, J.; González-Aguilera, D. Digital image correlation and reliability-based methods for the design and repair of pressure pipes through composite solutions. *Constr. Build. Mater.* **2020**, *248*, 118625. [CrossRef]

32. Abdulqader, A.; Rizos, D.C. Advantages of Using Digital Image Correlation Techniques in Uniaxial Compression Tests. *Results Eng.* **2020**, 100109. [CrossRef]

33. Le, D.B.; Tran, S.D.; Torero, J.L.; Dao, V.T.N. Application of digital image correlation system for reliable deformation measurement of concrete structures at high temperatures. *Eng. Struct.* **2019**, *192*, 181–189. [CrossRef]

34. Liu, B.; Guo, J.; Wen, X.; Zhou, J.; Deng, Z. Study on flexural behavior of carbon fibers reinforced coral concrete using digital image correlation. *Constr. Build. Mater.* **2020**, *242*, 117968. [CrossRef]

35. Kozicki, J.; Tejchman, J. Application of DIC technique to concrete—Study on objectivity of measured surface displacements. *Exp. Mech.* **2013**, *53*, 1545–1559.

36. Chen, Y.; Wei, J.; Huang, H.; Jin, W.; Yu, Q. Application of 3D-DIC to characterize the effect of aggregate size and volume on non-uniform shrinkage strain distribution in concrete. *Cem. Concr. Compos.* **2018**, *86*, 178–189. [CrossRef]

37. Dzaye, E.D.; Tsangouri, E.; Spiessens, K.; De Schutter, G.; Aggelis, D.G. Digital image correlation (DIC) on fresh cement mortar to quantify settlement and shrinkage. *Arch. Civ. Mech. Eng.* **2019**, *19*, 205–214. [CrossRef]

38. UNE-EN 13242:2003 + A1:2008. *Aggregates for Unbound and Hydraulically Bound Materials for Use in Civil Engineering Work and Road Construction*; AENOR: Madrid, Spain, 2008.

39. UNE-EN 933-1. *Test for Geometrical Properties of Aggregates—Part 1: Determination of Particle Size Distribution-Sieving Method*; AENOR: Madrid, Spain, 2012.

40. *Catalogue of Pavements and Work Units with Recycled Aggregates from Construction and Demolition Waste*; UCO Press Editorial Universidad de Córdoba: Córdoba, Spain, 2017.

41. UNE-EN 933-8:2012+A1:2015. *Tests for Geometrical Properties of Aggregates—Part 8: Assessment of Fines-Sand Equivalent Test*; AENOR: Madrid, Spain, 2016.

42. UNE-EN 1097-2. *Tests for Mechanical and Physical Properties of Aggregates—Part 2: Methods for the Determination of Resistance to Fragmentation*; AENOR: Madrid, Spain, 2010.

43. UNE-EN 933-9:2010+A1:2013. *Tests for Geometrical Properties of Aggregates—Part 9: Assessment of Fines—Methylene Blue Test*; AENOR: Madrid, Spain, 2013.

44. UNE 103204. *Organic Matter Content of a Soil by the Potassium Permanganate Method*; AENOR: Madrid, Spain, 2019.
45. UNE 103205. *Determination of Soluble Salts Content in Soils*; AENOR: Madrid, Spain, 2019.
46. UNE-EN 1097-6. *Tests for Mechanical and Physical Properties of Aggregates—Part 6: Determination of Particle Density and Water Absorption*; AENOR: Madrid, Spain, 2014.
47. UNE-EN 1744-1:2010+A1:2013. *Tests for Chemical Properties of Aggregates—Part 1: Chemical Analysis*; AENOR: Madrid, Spain, 2015.
48. UNE-EN 12390-3. *Ensayos de Hormigón Endurecido. Parte 3: Determinación de la Resistencia a Compresión de Probetas*; AENOR: Madrid, Spain, 2020.
49. Garcia-Martin, R.; Bautista-De Castro, A.; Sánchez-Aparicio, L.J.; Fueyo, J.G.; Gonzalez-Aguilera, D. Combining digital image correlation and probabilistic approaches for the reliability analysis of composite pressure vessels. *Arch. Civ. Mech. Eng.* **2019**, *19*, 224–239. [CrossRef]
50. Pan, B.; Lu, Z.; Xie, H. Mean intensity gradient: An effective global parameter for quality assessment of the speckle patterns used in digital image correlation. *Opt. Lasers Eng.* **2010**, *48*, 469–477. [CrossRef]
51. Solav, D.; Moerman, K.M.; Jaeger, A.M.; Genovese, K.; Herr, H.M. MultiDIC: An open-source toolbox for multi-view 3D digital image correlation. *IEEE Access* **2018**, *6*, 30520–30535. [CrossRef]
52. Pan, B.; Qian, K.; Xie, H.; Asundi, A. Two-dimensional digital image correlation for in-plane displacement and strain measurement: A review. *Meas. Sci. Technol.* **2009**, *20*, 062001. [CrossRef]
53. Blaber, J.; Adair, B.; Antoniou, A. Ncorr: Open-source 2D digital image correlation matlab software. *Exp. Mech.* **2015**, *55*, 1105–1122. [CrossRef]
54. Luu, L.; Wang, Z.; Vo, M.; Hoang, T.; Ma, J. Accuracy enhancement of digital image correlation with B-spline interpolation. *Opt. Lett.* **2011**, *36*, 3070–3072. [CrossRef]
55. Pan, B. Reliability-guided digital image correlation for image deformation measurement. *Appl. Opt.* **2009**, *48*, 1535–1542. [CrossRef]
56. Tasdemir, M.A.; Tasdemir, C.; Akyüz, S.; Jefferson, A.D.; Lydon, F.D.; Barr, B.I.G. Evaluation of strains at peak stresses in concrete: A three-phase composite model approach. *Cem. Concr. Compos.* **1998**, *20*, 301–318. [CrossRef]
57. Aiken, L.S.; West, S.G.; Pitts, S.C.; Baraldi, A.N.; Wurpts, I.C. Multiple Linear Regression. In *Handbook of Psychology*; John Wiley and Sons: Hoboken, NJ, USA, 2012; Volume 2.
58. Sobol, I.M. Sensitivity analysis for non-linear mathematical models. *Math. Model. Comput. Exp.* **1993**, *1*, 407–414.
59. Byrne, E.; Simonsen, M. Lens Selection and Stereo Angle. Available online: https://correlated.kayako.com/article/78-lens-selection-and-stereo-angle (accessed on 3 May 2021).

CAPÍTULO III
OPTIMIZACIÓN TÉRMICA USANDO TERMOGRAFÍA ACTIVA

3.1. Mejora de las propiedades térmicas mediante la introducción de aditivos reciclados

En esta primera parte del capítulo III se incluye el artículo "*Monitoring the thermal contribution of certain mortar additives as a way to optimize the energy performance of buildings*", publicado en la revista *Sustainable Energy Technologies and Assessments*.

Resumen

El elevado consumo energético es uno de los principales problemas de la industria de la construcción. Gran parte del consumo de energía y las emisiones de CO_2 es ocasionada por la edificación residencial. A este consumo energético se le suman efectos que alteran la estabilidad ambiental y contribuyen al calentamiento global como el de las islas de calor urbano. Cuando se construyen este tipo de infraestructuras se consideran las propiedades mecánicas de los materiales de construcción, prescindiendo de sus capacidades térmicas. En este sentido, el **objetivo** de este trabajo es avanzar en la mejora de materiales de construcción que permitan aumentar el rendimiento energético de los edificios. Por un lado, se busca una solución que favorezca el aislamiento de los edificios evitando los efectos de calentamiento producido por las islas de calor urbano y las pérdidas energéticas por calentamiento interior. A su vez, se busca un material con una elevada capacidad de conducción térmica con una función de intercambio de calor como aplicaciones geotérmicas.

La **metodología** seguida consistió en la evaluación del comportamiento térmico de morteros con aditivos procedentes del reciclaje o de otros materiales empleados en la construcción. Por un lado, se llevaron a cabo ensayos de laboratorio para determinar la conductividad y resistividad térmica. A partir de estos ensayos, se seleccionaron los morteros con mayor y menor conductividad para someterlos a ensayos experimentales para optimizar su función energética mediante técnicas de termografía activa.

La termografía activa consiste en la excitación de los materiales a través de una fuente de calor, de manera que la diferente composición de los morteros resulta en una diferente difusividad térmica y flujo de calor que es monitorizado por una cámara termográfica. Para este trabajo, se utilizó un simulador solar low-cost con el fin de reproducir las condiciones ambientales a las que los materiales son expuestos.

Los morteros seleccionados fueron sometidos a ciclos de calentamiento y enfriamiento con la estimulación del simulador solar para comparar su comportamiento respecto a un mortero de referencia fabricado sin aditivos. Tanto en la fase de calentamiento como enfriamiento, se extrajeron las curvas de evolución de la temperatura para diferentes regiones de interés con el fin de determinar también el efecto de borde producido durante los cambios térmicos.

Los **resultados** mostraron que los morteros con mayor conductividad térmica son aquellos que contienen yeso cristalizado como aditivo, mientras que los que incorporan fibras de poliéster presentaron una menor conductividad. Respecto a los ensayos experimentales, no se apreciaron diferencias en la fase de calentamiento ya que el aumento de temperatura se produce debido a la radiación. Sin embargo, si se apreció una mayor temperatura final tras la fase de enfriamiento para las muestras con yeso y una menor temperatura final para las muestras con fibras. Esto es debido a que la mayor conductividad térmica de las muestras con yeso permitió el calentamiento interno y por lo tanto mantener la temperatura tras el enfriamiento, mientras que el calentamiento en las muestras con fibras fue únicamente superficial al cumplir su función de aislamiento para el núcleo interno. El estudio de los efectos de borde determinó que no existieron diferencias entre la zona central y los bordes en el calentamiento, ya que se produjo de forma homogénea, mientras que sí se apreció una bajada de temperaturas más rápida durante el enfriamiento para las zonas externas.

Las principales **conclusiones** del trabajo resaltan la capacidad de los aditivos introducidos para modificar las propiedades térmicas de materiales de construcción básicos como los morteros. Considerando los aditivos seleccionados, además del ahorro energético que pueda suponer su implementación, el empleo de estos materiales promueve la sostenibilidad y economía circular en la construcción.

El enfoque de termografía activa adoptado permite una monitorización completa y precisa del comportamiento térmico, analizando tanto la evolución temporal como la distribución espacial de las temperaturas. Este tipo de técnicas junto con el empleo de simuladores solares low-cost permite además optimizar las propiedades térmicas de estos materiales garantizando la reproducibilidad y repetitividad de los ensayos en laboratorio simulando condiciones ambientales similares a las reales.
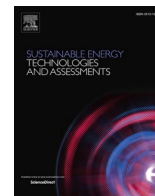
Monitoring the thermal contribution of certain mortar additives as a way to optimize the energy performance of buildings

Jorge López-Rebollo [a],[*], Natalia Nuño Villanueva [a], Ignacio Martín Nieto [a], Cristina Sáez Blázquez [a], Susana Del Pozo [a], Diego González-Aguilera [a]

[a] Department of Cartographic and Land Engineering. University of Salamanca, Higher Polytechnic School of Ávila, Hornos Caleros, 50, 05003 Ávila, Spain

ABSTRACT

Climate challenge requires developing approaches capable of improving the thermal capacities of building materials. These are the objectives of the new additive manufacturing industry in the building sector to mitigation of urban heat island. The objective of this work was to verify that the thermal properties of the additives are transferred to those of the final product, the mortar. For this purpose, several additives with different thermal conductivities, ranging from 0,038 to 130 W/m·K, were selected to include them in the matrix of a standard mortar with the same volume percentage. Once the mixtures were prepared, they were subjected to two thermal tests: a first thermal conductivity test, and a second heat transfer test. For the last test, a low-cost solar simulator was used to heat the mortar samples. Both the heating and cooling of the samples were monitored with a thermographic camera. After analysis, it was found that the mortar samples with additives modified their thermal behaviour by up to 30 % compared to the mortar sample without additives. These are encouraging results that open up new research possibilities that could materialize in studying the thermal behaviour of mortars with other kind of additives and with different dosage percentages.

Introduction

The increasing concern about climate change and its devastating effects constitutes a stimulus pushing the research towards the identification of novel alternatives to decrease the world energy consumption. The possibilities of mitigating its undesired effects can no longer depend solely on the implementation of emission reduction policies; it is necessary to adopt coordinated measures on other fronts of action [1].

In the climate challenge, building sector must be considered as one of the main key players involved. According to the statistics of the International Energy Agency (IEA), the building sector is one of the largest energy consumers (40 % worldwide). Within this sector, 27 % of energy consumption belongs to residential buildings, with an associated CO_2 emission rate of 17 % of global emissions [2]. The large energy consumption by this sector results in a greater depletion of resources and greater pollution and degradation of the environment.

In this context, one of the undesirable effects produced by high energy consumption in buildings and by the thermal properties of their construction materials is the creation of Urban Heat Islands (UHI) that

significantly alter the environmental stability of these areas [3,4]. Therefore, the energy efficiency of buildings is today a primary objective of energy policies at regional, national, and international level [5]. Thus, different mitigation actions must be considered for the sustainable planning of urban spaces. In this sense, the inclusion of green areas has proven to be one of the fundamental favourable factors [6]. Lately, the inclusion of climate change mitigation measures in building construction procedures has also been considered. Ideally, a combination of measures to mitigate unwanted effects together with energy saving measures could even be proposed, such as the energy use approach based on the residual heat stored by the heat island effect [7,8].

Focusing on improving the energy efficiency of buildings, the development of novel construction materials is gaining increasing interest in industrial and domestic communities. In this sense, different solutions have been introduced to minimize heating and cooling loads through the building envelope towards more energy-efficient buildings [9]. In this context, the incorporation of Phase Change Materials (PCM) translates into significant energy savings [10,11]. Considering the specific requirements of each building, and with the aim of going a step

further, the approach can be directed in two different ways. On the one hand, in some places, it will be preferable for the material to conduct and/or store heat more efficiently, while in other locations buildings can be configured to reduce the heat island effect. Different research works address the improvement of the thermal properties of mortars from the point of view of thermal conductive [12] or the absorption of solar radiation [13], including tests of materials for the thermal energy storage [14] without neglecting their mechanical properties [15]. Nevertheless, these studies mainly focus on extracting thermal properties without testing how the materials actually behave under real or simulated environmental conditions. Moreover, expensive and sometimes polluting materials are often added to achieve thermal improvements. This highlights the need to find a cost-effective and environmentally friendly solution that is monitored and tested in environmental conditions similar to those of its potential use.

To advance in this field, this research aims to evaluate the thermal behaviour of mortars with different additives that allow these construction materials to fulfil not only a structural function, but an energy function. With that objective, this work includes a series of commonly used thermographic analyses with promising results in other materials [16,17]. In this sense, a novel experiment is proposed that combines a low-cost solar simulator to reproduce the environmental conditions of use with the application of active thermography for monitoring its behaviour. The different composition of the mortar samples results in different thermal diffusivity and heat flux [18] which can be monitored by a thermographic camera. This technique is an improvement over point measurements in conventional studies as it allows full-field thermal measurements to be made to analyse the overall behaviour, obtaining results that are closer to reality.

Consequently, an experimental campaign is performed on mortars with different additives, subjecting them to conductivity and thermographic tests to analyse their thermal behaviour. After this Introduction, Section 2 describes these materials and techniques employed. In Section 3, the experimental results for each test performed are shown. A discussion of the results is given in Section 4. Finally, in Section 5, the main conclusions are drawn about the suitability of using certain material as additives of mortar mixtures to modify their thermal behaviour, as well as discuss the feasibility of introducing these compounds in the construction industry.

Materials and methods

This work focuses on the use of additives particularly selected to alter the thermal properties of mortars. Once the additives materials for the mixtures were selected, samples for subsequent tests were prepared. Respecting the mortar setting period, the samples were first subjected to thermal conductivity test using the needle probe method [19]. Those samples that showed the desired thermal result in the first test were subsequently subjected to thermal distribution tests by means of a thermographic camera [20]. Fig. 1 shows a schematic diagram of the workflow followed.

Selection of additives and sample preparation

Due to the importance of the properties of construction materials in the energy aspect of buildings, trying to modify these in order to achieve a change in their thermal behaviour is an interesting and challenge aspect. In this line of research, mortar has been the construction material selected due to its wide use in the construction sector and because it is easy to mix with different additives.

For the selection of additives, some factors have been considered key. For example, the ease of obtaining them, the possibility of reusing them and giving them a second use, and even, in the case of additives of the same nature and different form (powder and liquid, for example), the possibility of using both types. In the latter case, it is interesting to analyse whether its form can cause different thermal behaviour in the mortar sample with such material. Finally, it should be mentioned that the additives used in this study cannot currently be used commercially.
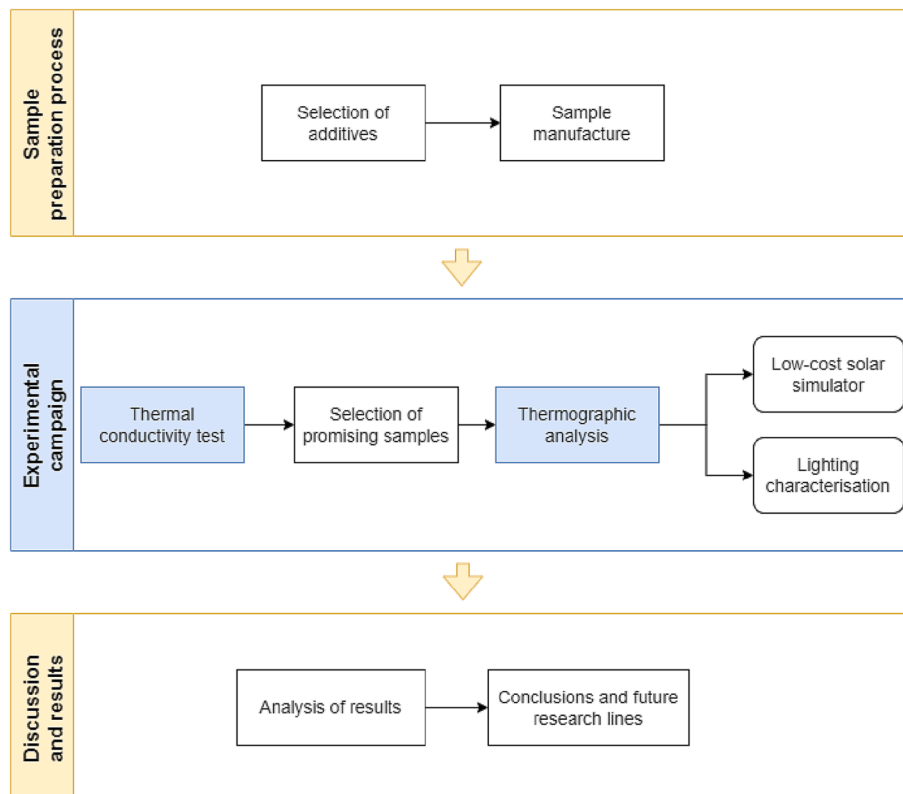

Fig. 1. Workflow diagram.

In this sense, five different materials were chosen to be added to the mortar as additives: polyester fibres, polystyrene, graphite, gypsum powder and crystallised gypsum. All of them are relatively easy to obtain and with the possibility of being reused in the construction industry.

Polyester fibres were chosen due to their high availability, and due to their possible reuse and have been used as an additive in photochromic mortars [21]. Polystyrene shares the key factors respect to the polyester fibres as it is commonly used in sample packaging and has been shown to influence cement for heat cycling [22]. Graphite is a mineral used in various industries such as the pharmaceutical industry, construction or even electrical industry (electrodes), so it would be another use given to this widely available material, already used in mortars with electromagnetic properties [23]. Gypsum, for its part, is a material commonly used in combination with cement [24] and that could be used as an additive in different forms. In this research its crystal and powder forms have been considered. Crystallised gypsum is its base mine form while the powdered form is the gypsum form that has been processed for its use in construction as moulding paste, as a bonding and joint paste, and even for artistic purposes. It is, therefore, a material that is present in the construction sector and that could be reused to improve the thermal properties of mortars.

Regarding the amount of additive to add to each mortar sample and given the variability in the nature and form of each one, it was decided to measure its amount in % volume so as not to exceed the amount of mortar used per sample. This would happen if the quantification method were mass, and in the specific case of additives such as polystyrene (low density). A value of 5% by volume of the total mixture was determined so that the mechanical properties of the resulting mortar are not altered. Taking into account the densities of the raw materials measured in the laboratory, the mortar mix compositions were 7 kg/m^3 for polyester fibre, 2,5 kg/m^3 for polystyrene, 105 kg/m^3 for graphite, 115 kg/m^3 for gypsum in its crystallised form and 60 kg/m^3 for powdered gypsum. Table 1 presents a summary with the characteristics of the additives used.

Once the additives have been selected and their quantity has been decided, the mortar base mix to which they will be added must be determined. In this study, the mortar was a mixture of natural siliceous aggregates, Portland cement and water in a ratio of 3:1:0,5 respectively. The characteristics of the components of the mortar mixture are the following:

- The cement used was white Portland cement with limestone (EN 197-1:2011 [28]) and a compressive strength of 42,5 N.
- The natural aggregates were siliceous sand treated with a 2 mm test sieve (UNE 7050-3 [29]).
- The sample water was non-aggressive according to UNE 83952 [30].

For the manufacture of the samples, prismatic moulds of 160 × 40 × 40 mm, described in the UNE-EN 196-1 standard [31], were used. The curing conditions were respected by keeping the samples in the moulds for the first 24 h. Subsequently the specimens were kept in water at a temperature of 293,15 ± 2 K.

A total of 18 samples were manufactured, so that three specimens were obtained for each of the six mixtures (5 with additives and 1 without additive). One of the three specimens per mixture was used for the thermal conductivity test, another for the heating–cooling tests, and the remaining one was kept for safety and for future research.

Thermal conductivity procedure

The theoretical principle on which the thermal conductivity measurement procedure is based is known as the infinite line heat source theory, in which thermal conductivity is calculated from monitoring the dissipation of heat in the needle probe. Heat is injected to the needle for an established heating time t_h, and temperature is then measured in the monitoring needle during heating and for an extra time equal to t_h after heating. Equation (1) describes how the temperature during heating is obtained [32].

$$T = m_0 + m_2 t + m_3 lnt \tag{1}$$

Where m_0 is the ambient temperature during the heating stage; m_2 is the rate of background temperature drift; and m_3 is the slope of a line relating temperature rise to logarithm of temperature.

The model during cooling is described in Equation (2).

$$T = m_1 + m_2 t + m_3 ln \frac{t}{t - t_h} \tag{2}$$

The thermal conductivity of the sample is finally obtained from Equation (3), which also considers the heat flux (q).

$$k = \frac{q}{4m_3} \tag{3}$$

For carrying out the necessary measurements based on this principle on a laboratory scale, a DECAGON analyser was used: TEMPOS. This analyser complies with the following regulations that guarantee the standardization of the results: ISO 2008, ASTM 5334, IEEE 442 and is also capable of making accurate measurements not only of thermal conductivity but also of thermal resistance, specific heat, and thermal diffusivity of materials [33].

Considering the material of the samples and their size, the RK-3 needle was chosen due to its size sensor de 3,9 mm diameter y 60 mm length. This needle has a resistivity range of 17 to 1000 °C·cm/W and a conductivity range of 0.1 to 6 W/(m·K). Its accuracy is ± 10% from 0.1 to 6 W/(m·K).

For the thermal conductivity test with the described TEMPOS analyser, samples were radially drilled for the introduction of RK-3 needle. The contact between the needle and the material was ensured by inserting thermal grease in the mentioned hole.

Before the measuring process, RK-3 sensor was accordingly calibrated with the specific sample supplied by the manufacturer. Once calibrated, three measurements (of around 2 min each) were carried out on each mixture to evaluate possible measuring uncertainties and errors.

It should be also mentioned that ambient temperature was kept as constant as possible at 298,15 K during the measurement process to obtain the most accurate data possible. In this sense, to minimize these sources of error, about 15 min for samples and needle to equilibrate with the ambient temperature was required before taking measurements, and around 15 min between readings for temperatures to be equilibrated.

Table 1
Summary table of additives, their thermal conductivity (λ), and their image.

	Polyester	Polystyrene	Graphite	Gypsum (crystal)	Gypsum (powder)
λ (W/m·K)	0,038 [25]	0,035 [26]	130 [27]	0,56 [26]	0,30 [26]
Image					

Heating test and temperature monitoring

The characterisation of thermal behaviour of the samples was carried out under active thermography and by a step heating approach. The procedure followed for these tests was as follows: i) design and manufacture of a low-cost solar simulator; ii) characterisation of the low-cost simulator; ii) set the configuration and calibration of the thermographic camera; and finally iv) perform the heating and cooling tests.

For that purpose, a low-cost solar simulator was used in order to replicate under laboratory conditions, the real state to which mortars can be subjected during their useful life. In this way, an attempt was made to manufacture a lighting system with similar characteristics to solar lighting using a metal arc halide lamp that simulates the heating produced by the sun's rays [34,35]. In this case, a Philips HPI-T Plus 250W/645 bulb was selected, so it was installed on a platform designed ad-hoc to hold it at different heights. A polished aluminium plate was used to concentrate the lighting on a lower surface to ensure uniformity and stability of the luminous flux.

In order to check the characteristics of the illumination obtained by the solar simulator, a Sekonic C7000 spectrometer was used to obtain its luminance, correlated colour temperature (CCT) and spectral power distribution (SPD). This device has a measurement range of 1 to 200.000 lx for illuminance with an accuracy of ± 5 %. The CCT allows values between 1.563 and 100.000 K to be obtained. Regarding the SPD, it is possible to obtain output wavelength increments of 1 nm in the range from 380 to 780 nm.

The monitoring of the temperature was carried out with a FLIR T540 thermographic camera. This camera integrates a 5 Mpx RGB sensor and a 464 × 348 px thermal sensor with a 42° lens along with a laser sensor that detects the distance between the object and the camera to improve focusing. The measuring temperature range is from 253,15 to 393,15 K with a temperature sensitivity < 30 mK at 303,15 K. In addition, it is possible to correct the emissivity in steps of 0,01 to adjust the temperature measurement according to the type of material.

The experimental campaign was carried out with the three samples selected after conductivity tests. In this way, the materials with the highest and lowest thermal conductivity were selected, in addition to the reference mortar. The tests for each material were carried out individually, placing the samples in such a way that the illumination had a vertical incidence on the surface to be studied, with a distance of 0,5 m. The camera was placed at the same distance with the least possible inclination to avoid errors in the measurement (Fig. 2a).

With the aim of guaranteeing the same initial conditions in each test, the samples were kept isolated at a temperature of 298,15 K until they were placed under the solar simulator. To ensure that the illumination was stable and to avoid deviations during heating, the lamp was turned on for 10 min until the sample was placed. Once the sample is placed, the thermographic image acquisition stars during the heating stage, with duration of 15 min. Once this time has elapsed, the solar simulator is switched off and the cooling stage begins, maintaining image acquisition for an additional 30 min. No additional device was used during this stage, so the sample was cooled by natural convection.

Regarding the acquisition of thermographic images, a frequency of 1 fps was used and taking into account heating and cooling, a total of 2700 images were acquired (45 min).

For each of these images, in order to evaluate if there were significant differences between the inside and outside of the sample due to edge effects, three Region of Interest (ROI) were selected (Fig. 2b): i) full sample, corresponding to the entire study surface; ii) edges, corresponding to the outer region with a width of 10 mm; and iii) centre, corresponding to the inner area with dimensions of 60 × 20 mm.
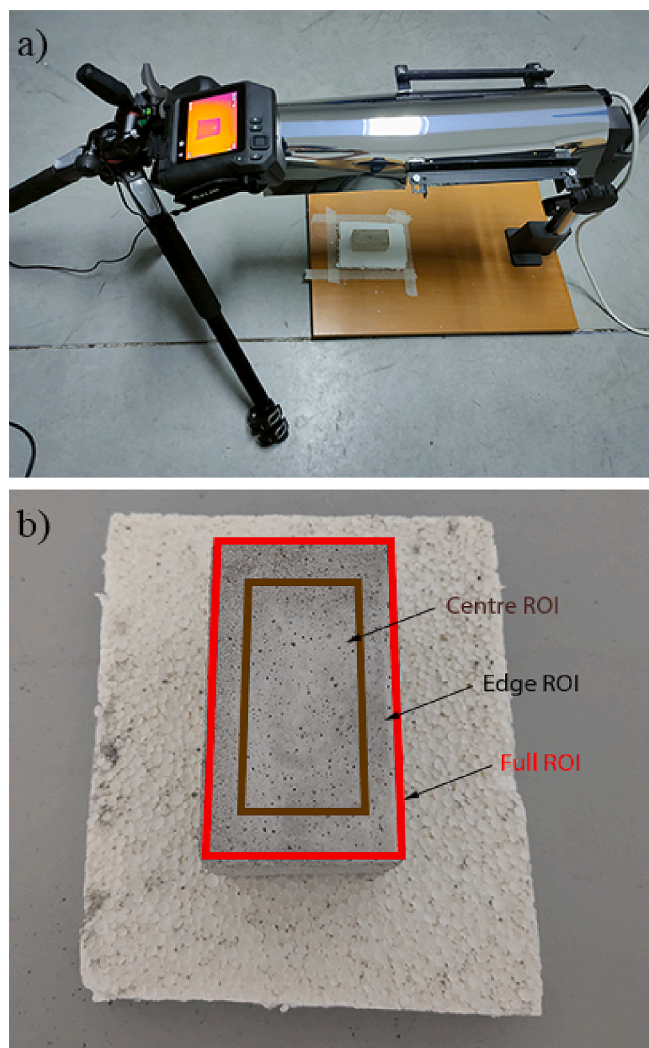
Fig. 2. Heating and cooling test. a) Test set up; b) Selected ROIs for thermographic analysis.

Experimental results

Thermal conductivity

The thermal conductivity test was carried out for all the samples, including the reference mortar and the five mortars with additives. For each of the samples, three tests were performed in order to eliminate possible uncertainties or measurement errors, so that a total of 18 tests were performed. Thermal conductivity and thermal resistance were obtained in each of these measurements and their results are shown in Table 2.

The results show differences between thermal conductivity and thermal resistance for mortars with different additives with respect to

Table 2

Results of the thermal conductivity and thermal resistance of the samples.

Sample	Thermal conductivity (W/m·K)		Thermal resistance (m·K/W)	
	$\overline{X}$	δ	$\overline{X}$	δ
Mortar	0,584	0,041	1,717	0,121
Polyester	0,386	0,027	2,603	0,178
Polystyrene	0,912	0,025	1,097	0,032
Graphite	0,861	0,087	1,170	0,114
Gypsum (C)	1,061	0,177	0,959	0,155
Gypsum (P)	0,446	0,042	2,257	0,210

the reference mortar. Taking into account that the difference for some materials is not very high, it was decided to select the two samples with the most extreme behaviours: mortar with crystallised gypsum as the mixture with the highest thermal conductivity and mortar with polyester fibres as the mixture with the lowest thermal conductivity. Along with them, the mortar without additives was kept as reference material to carry out the heating and cooling tests.

Heating test and temperature monitoring

In order to carry out the heating and cooling test properly, the first step was to characterise the low-cost solar simulator. The lamp was switched on and its behaviour during the first 15 min was analysed with the spectrometer. The results for CCT are shown in Fig. 3a, while the corresponding results for luminance can be seen in Fig. 3b.

After 6 or 7 min a stable CCT of approximately 5600 K and a constant luminance of 22000 lx is reached. Nevertheless, it was decided to set a more conservative lamp warm-up time of 10 min to avoid possible disturbances. Thus, it is considered that once this time is reached the illumination is sufficiently stable that the samples can start to heat up homogeneously both spatially and temporally.

Once this stable illumination was achieved, the SPD normalised to 1 shown in Fig. 4 was obtained. A peak wavelength of 537 nm was obtained, together with two other peaks at wavelengths 453 nm and 549 nm with a value close to it.

The tests were analysed using two different approaches. On the one hand, the temperature evolution curve was analysed, both in the heating and cooling phases in order to study the differences in the behaviour of each material. On the other hand, the ROIs described above were studied to determine the possible influence of edge effects and effectiveness of

the heating device.

The heating and cooling curves (Fig. 5) were obtained for each of the samples. For this purpose, the mean value of the full ROI was calculated for each of the thermal images to eliminate point errors or defective pixels. Then, a moving average filter was applied to eliminate anomalous values caused by erroneous frames or measurement disturbances.

Once the curves were plotted, the values corresponding to the end of heating and cooling were extracted. These values correspond to the maximum temperature increase and the final temperature variation of the sample (Table 3). In order to study the possible temperature differences between the inside and outside of the samples, the analyses described in Section 2.3. and exemplified in Fig. 2b were performed.

Discussion

Thermal conductivity

The study of thermal conductivity and thermal resistance showed the differences produced by the introduction of additives in the manufacture of the mortars. Compared to the reference mortar, with a value of 0,584 W/m·K for thermal conductivity and 1,717 m·K/W for thermal resistance, the influence of the materials is detailed below:

- The mortar additivated with polyester fibres obtained the lowest thermal conductivity, with a decrease of 0,199 W/m·K. In addition, the thermal resistance was also 0,89 m·K/W higher with respect to the reference mortar. In this case, the low thermal conductivity of the additive was also transferred to the result of the mortar.
- Initially, polystyrene had a similar thermal conductivity to polyester fibres. Nevertheless, an opposite effect occurred, so that the thermal
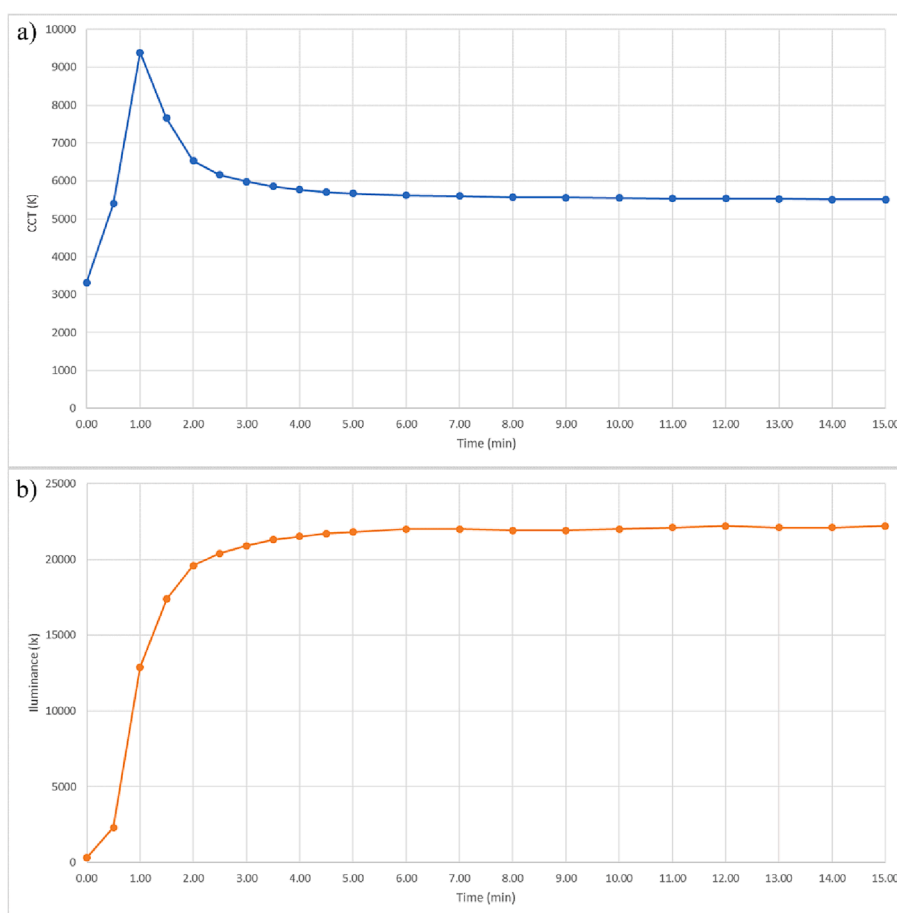

Fig. 3. Behaviour of the solar Simulator during the first 15 min. a) Correlated colour temperature (CCT); b) Luminance on the sample platform.
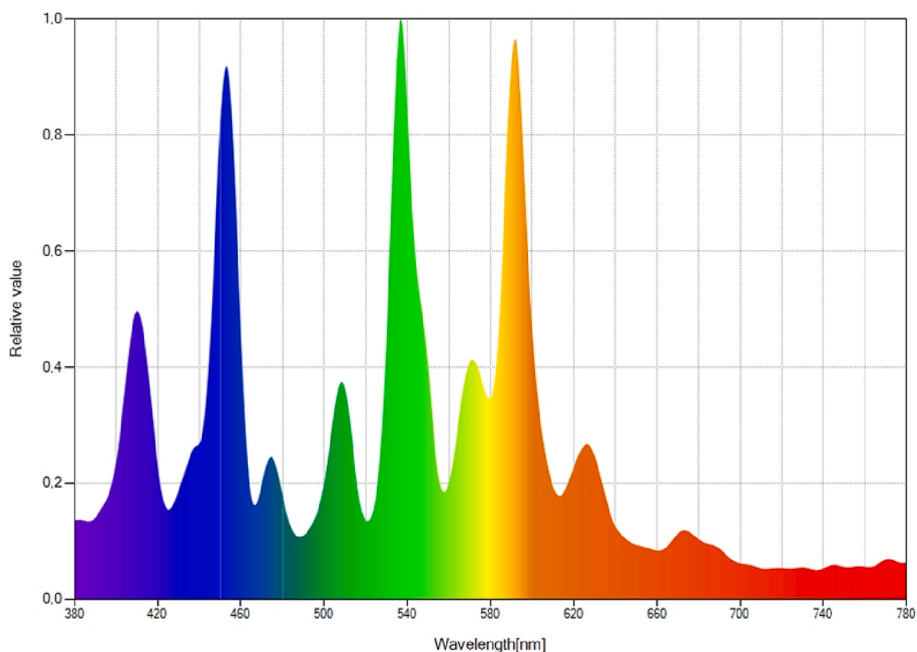
Fig. 4. Spectral power distribution of the solar simulator with stable illumination.
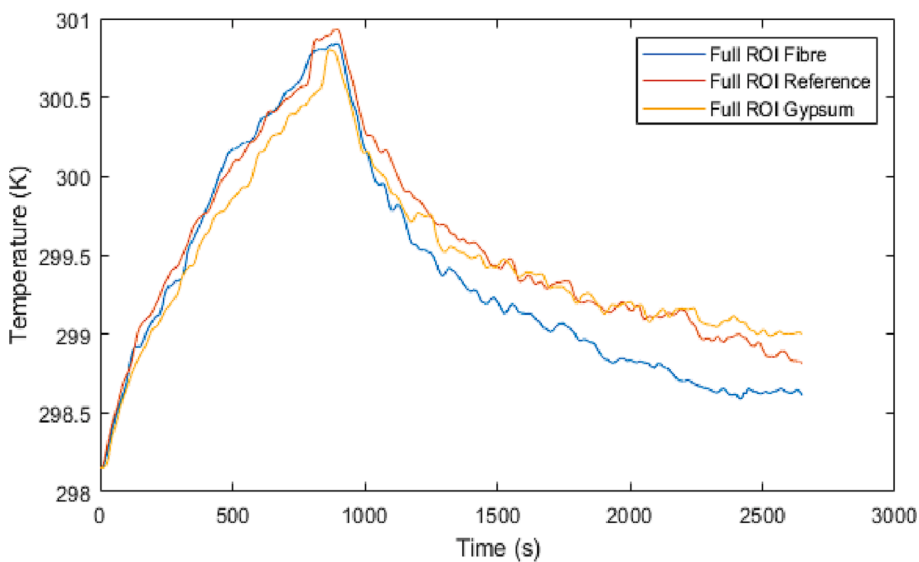

Fig. 5. Heating and cooling curves of thermal tests.

Table 3
Results for the heating and cooling tests for each ROI. ΔT_M refers to maximum temperature increase. ΔT_F refers to final temperature variation. *Temperature increase in K.

Sample	Full ROI		Centre ROI		Edge ROI	
	ΔT_M	ΔT_F	ΔT_M	ΔT_F	ΔT_M	ΔT_F
Fibre	2,69	0,46	2,70	0,50	2,68	0,41
Reference	2,78	0,66	2,79	0,72	2,76	0,61
Gypsum	2,65	0,85	2,65	0,89	2,64	0,80

conductivity of the mortar with this additive increased with respect to the reference mortar in 0,328 W/m·K. Furthermore, the thermal resistance was reduced in 0,62 m·K/W. In this case, the shape and arrangement of the particles as well as their interaction with the mortar may be the cause of this effect.

- Graphite was initially the material with the highest conductivity of the selected materials by a considerable margin. Nevertheless, although its mixture was able to increase the thermal conductivity in 0,276 W/m·K and to reduce the thermal resistance in 0,547 m·K/W, it was not the most influential additive and did not reach the most extreme values.
- Beforehand, gypsum in its crystalline form had a thermal conductivity similar to that of the mortar. Nevertheless, the mixture of both reached the highest value for thermal conductivity with an increase of 0,476 W/m·K and the lowest thermal resistance with a decrease of 0,76 m·K/W, both referred to the reference mortar.
- Powdered gypsum had a slightly lower thermal conductivity than the mortar and was the material that produced the least changes in the mortar, reducing its thermal conductivity in only 0,139 W/m·K and increasing its thermal resistance in 0,54 m·K/W. Although its initial value was practically similar to that of crystalline gypsum, it has

been shown that the different forms in which the same material is presented can produce notable differences.

This study allowed obtaining a valid approximation for the thermal conductivity in order to select the samples with the most extreme behaviour as mentioned above. In the case of polyester fibres, which for the dosage studied ($7 \, \text{kg/m}^3$) manage to reduce the thermal conductivity of the mortar by 34 %, it has been estimated that the cost of one m^3 of mortar is increased by 15 %. It is worth mentioning that, for the elderly, betting on the use of polyester fibres from, for example, the reuse of industrial bags made with this material is presented as a highly economical, sustainable and environmentally friendly option in the circular economy framework. This measure offers not only a solution that minimizes the problems associated with recycling these materials, but also allows for a more complete and responsible approach in terms of resource management and reduction of environmental impact.

For its part, crystallized gypsum, which for the dosage studied (115 kg/m^3) manages to increase thermal conductivity by 82 %, has a high cost associated with great variability depending on its origin, method of extraction and purity. In this sense, due to the high quantity required, its use as a mortar additive would be limited to specific cases in which the energy benefits derived from its application are associated with economic benefits higher than the manufacturing cost.

Thermal behaviour

The characterisation of the solar simulator made it possible to analyse its temporal behaviour in order to determine the time required to achieve stable illumination. In the case of the CCT, during the first minute, a maximum value of 9388 K is reached and then it begins to drop to a temperature of approximately 5600 K, which remains stable after approximately 7 min. The luminance also undergoes the greatest increase during the first two minutes, and after approximately 6 min it remains constant with a value of 22000 lx. As mentioned above, in order to avoid possible changes in the conditions that could modify this behaviour and delay the stabilisation time, it was decided to adopt a more conservative time of 10 min to start the heating tests. The SPD study showed a similar behaviour to that defined by the manufacturer and which is close to the real behaviour of sunlight.

With regard to heating test and temperature monitoring, the curves for each of the materials are practically similar in the heating phase, reaching a similar maximum temperature increase. The slight differences in this value are barely significant (0,1 K) and may be due to causes associated with the measurement process, such as the slight thermal oscillations caused by natural convection. In this sense, it must be considered that the heating is produced by radiation and that only surface heating is produced because the time is not very long, so it is difficult for the difference in conductivity to have an influence.

In the case of the cooling phase, significant differences can be observed. There is a difference of 0,4 K between the fibre sample and the crystallised gypsum sample, corresponding to those with the lowest and highest conductivity respectively. The reference sample is practically equidistant between the two. Due to the fact that the heating is carried out by radiation and in a short period of time as mentioned above, there is mainly surface heating, which means that the difference in conductivity does influence the final temperature of the sample in this case. In the case of the mortar with fibre, as it has a lower conductivity, the heating is only superficial without heating the whole sample, which causes a greater reduction in temperature during the cooling phase. On the other hand, the sample corresponding to the mortar with crystallised gypsum can heat up inside due to the higher conductivity, not only being a superficial heating. In this case, the heating of the whole sample causes the final surface temperature to be higher.

Regarding the edge effect test, the results show a similar behaviour during the heating phase as the difference between the centre and edge region does not exceed 0,03 K in any case. Edge effects were not visible during the heating phase and it seems reasonable to assume that the heating of the solar simulator is homogeneous, since the temperature of the sample does not show spatial irregularities.

In the case of the results for the final temperature, differences can be seen between the temperatures corresponding to the central region and the edge region, while the temperatures for the full ROI are logically situated between the two. In this case, the differences reach 0,1 K, so that the edge ROI cools more than the centre ROI in all cases.

Conclusions

This research has sought to influence basic construction materials, such as mortar, in terms of their thermal properties through the use of additives for their future adaptation to the needs of use. This is an advantage not only in terms of energy efficiency, but considering the type of additives selected; it results in cost savings in materials and promotes sustainability within the construction ecosystem.

The additives that have generated the greatest variations in the thermal properties of the final mortar mix were: polyester fibres, achieving a 34 % reduction in thermal conductivity; and gypsum in its crystallised form, which achieved a thermal conductivity value 82 % higher, being the highest among the mixtures manufactured, although the value of the additive is similar to that of the mortar.

The first analysis on the two selected additives has been a heating–cooling test carried out with a low-cost solar simulator that has been characterized using a spectrometer, which determined an optimal heating time of 10 min. After this time, the illumination is considered stable with a CCT of 5600 K and a luminance of 22,000 lx with a peak wavelength of 453 nm.

The heating and cooling test allows the extreme thermal behaviour of the mortar to be analysed. Differences were found in the cooling phase of the test where the mixture with fibres acted as an insulator and caused the surface temperature variation at the end of the test to be 30 % lower than the reference sample, while for the mixture with crystallised gypsum this variation was 29 % higher than the reference sample. Regarding the heating phase, there were no significant differences.

The next test carried out was the analysis of the possible influence of the edge effect. The results showed that the heating device produced homogeneous heating and hardly affected the spatial distribution of temperatures. Nevertheless, there was more cooling at the edges of the sample, which will require increasing the sample size and differentiating between the two areas in future tests.

Therefore, the influence of the selection and use of additives on the thermal behaviour of the mortar is highlighted. In many cases, the desired effect will be thermal insulation of the exterior, in order to promote sustainability in the building ecosystem and to contribute to savings in building heating/cooling systems. The application of the materials with the lowest conductivity studied as cladding for buildings could result in a decrease in their temperature during cooling periods (night) and the consequent decrease in the heating–cooling sequence by starting from a lower initial temperature, thus contributing to the reduction of the heat island effect in cities. On the other hand, there are applications of ceramic and stone materials where the ability to transmit heat or to reduce the temperature as quickly as possible is important. An example of this is the backfilling of geothermal heat boreholes, where the aim is to allow the heat to pass from the ground to the borehole heat exchangers as quickly as possible. Another example can be found in service structures in cities with high summer temperatures, it is desirable that as the sun goes down their temperature is reduced more quickly to mitigate the heat island effect, increase their functional life and allow their use (e.g. street furniture benches, pavements, railings, etc.).

In both cases, it can be considered that the work yields promising results for the sector that motivate the continuation of this line of research. Future work will focus on carrying out more exhaustive analyses of the behaviour of these materials, carrying out tests with different

configurations. In this sense, it will be interesting to check their behaviour over longer heating–cooling times, and it will also be possible to carry out thermal profile studies to analyse temperatures at different depths.

CRediT authorship contribution statement

Jorge López-Rebollo: Methodology, Investigation, Formal analysis, Writing – original draft, Writing – review & editing. **Natalia Nuño Villanueva:** Conceptualization, Investigation, Formal analysis, Writing – review & editing. **Ignacio Martín Nieto:** Investigation, Formal analysis, Writing – review & editing. **Cristina Sáez Blázquez:** Investigation, Formal analysis, Writing – review & editing. **Susana Del Pozo:** Investigation, Formal analysis, Writing – review & editing. **Diego González-Aguilera:** Supervision, Funding acquisition, Writing – review & editing.

Declaration of Competing Interest

The authors declare that they have no known competing financial interests or personal relationships that could have appeared to influence the work reported in this paper.

Data availability

Data will be made available on request.

Acknowledgements

References

[1] Medved S, Medved S. Urban environment and local climate. Building physics: heat, ventilation, moisture, light, sound, fire, and urban microclimate. 2022:453-72 3030743896.

[2] Afolabi LO, Ariff ZM, Megat-Yusoff PSM, Al-Kayiem HH, Arogundade AI, Afolabi-Owolabi OT. Red-mud geopolymer composite encapsulated phase change material for thermal comfort in built-sector. Sol Energy 2019;181:464–74. 0038-092X.

[3] Halder B, Bandyopadhyay J, Banik P. Evaluation of the climate change impact on urban heat island based on land surface temperature and geospatial indicators. Int J Environ Res 2021;15:819–35. 1735-6865.

[4] Kim SW, Brown RD. Urban heat island (UHI) intensity and magnitude estimations: A systematic literature review. Sci Total Environ 2021;779:146389. 0048-9697.

[5] Mirabella N, Roeck M, Ruschi Mendes Saade M, Spirinckx C, Bosmans M, Allacker K, et al. Strategies to improve the energy performance of buildings: A review of their life cycle impact. Buildings 2018;8:105. 2075-5309.

[6] Shishegar N. The impact of green areas on mitigating urban heat island effect: A review. Int J Environ Sustain. 2014;9:119-30 2325-1077.

[7] Jiang Y, Huang J, Shi T, Wang H. Interaction of urban rivers and green space morphology to mitigate the urban heat island effect: Case-based comparative analysis. Int J Environ Res Public Health 2021;18:11404. 1660-4601.

[8] Gao M, Chen F, Shen H, Barlage M, Li H, Tan Z, et al. Efficacy of possible strategies to mitigate the urban heat island based on urbanized high-resolution land data assimilation system (U-HRLDAS). J Meteorol Soc Japan Ser II 2019;97(6):1075–97. 0026-1165.

[9] Lotfabadi P, Hançer P. A comparative study of traditional and contemporary building envelope construction techniques in terms of thermal comfort and energy efficiency in hot and humid climates. Sustainability. 2019;11:3582, 2071-1050.

[10] Alam M, Zou PXW, Sanjayan J, Ramakrishnan S. Energy saving performance assessment and lessons learned from the operation of an active phase change materials system in a multi-storey building in Melbourne. Appl Energy 2019;238: 1582–95. 0306 2619.

[11] Nada SA, Alshaer WG, Saleh RM. Thermal characteristics and energy saving of charging/discharging processes of PCM in air free cooling with minimal temperature differences. Alexandria Eng J. 2019;58:1175-90 10-0168.

[12] Corinaldesi V, Mazzoli A, Moriconi G. Mechanical behaviour and thermal conductivity of mortars containing waste rubber particles. Mater Des 2011;32: 1646–50. 0261-3069.

[13] López-Rebollo J, Del Pozo S, Nieto IM, Blázquez CS, González-Aguilera D. Experimental study on the thermal properties of pigmented mortars for use in energy efficiency applications. J Clean Prod 2023;382:135280. 0959-6526.

[14] Rathore PKS, Shukla SK, Gupta NK. Synthesis and characterization of the paraffin/expanded perlite loaded with graphene nanoparticles as a thermal energy storage material in buildings. J Sol Energy Eng 2020;142:041006. 0199-6231.

[15] Berardi U, Gallardo AA. Properties of concretes enhanced with phase change materials for building applications. Energ Buildings 2019;199. 402-14 0378 7788.

[16] Lizaranzu M, Lario A, Chiminelli A, Amenabar I. Non-destructive testing of composite materials by means of active thermography-based tools. Infrared Phys Technol 2015;71:113–20. 1350-4495.

[17] Rodríguez-Martín M, Fueyo JG, Pisonero J, López-Rebollo J, Gonzalez-Aguilera D, García-Martín R, et al. Step heating thermography supported by machine learning and simulation for internal defect size measurement in additive manufacturing. Measurement 2022;205:112140. 0263-2241.

[18] Maldague X. Theory and practice of infrared technology for nondestructive testing. 2001.

[19] Yun TS, Jeong YJ, Han T-S, Youm K-S. Evaluation of thermal conductivity for thermally insulated concretes. Energy Build 2013;61:125–32. 0378-7788.

[20] Holland SD, Reusser RS. Material evaluation by infrared thermography. Annu Rev Mat Res 2016;46:287–303. 1531-7331.

[21] Sikandar MA, Mubeen G, Baloch Z, El-barbary AA, Hamad M. Comparative study on the performance of photochromic cement, epoxy, and polyester mortars. J Build Eng 2023;70:106394. 2352-7102.

[22] Ferrándiz-Mas V, García-Alcocel E. Durability of expanded polystyrene mortars. Constr Build Mater. 2013;46:175-82 0950-618.

[23] Stefaniuk D, Sobótka M, Jarczewska K, Logoń D, Majcher K, Musiał M, et al. Microstructure properties of cementitious mortars with selected additives for electromagnetic waves absorbing applications. Cem Concr Compos 2022;134: 104732. 0958-9465.

[24] Silva DBP, Lima NB, Lima VME, Estolano AML, Nascimento HCB, Vilemen P, et al. Producing a gypsum-based self-leveling mortar for subfloor modified by polycarboxylate admixture (PCE). Constr Build Mater 2023;364:130007. 0950-0618.

[25] Ceimat. Fibras poliester no tejidas. Available online: https://ceimates/es/productos/producto-2 [Accessed February 20, 2023].

[26] Fomento Md. Catálogo de Elementos Constructivos del CTE (CEC). España 2011.

[27] GmbH GN. Propiedades grafito. Available online: https://wwwgab-neumanncom/Grafito-impermeable-Propiedades [Accessed February 20, 2023].

[28] AENOR. UNE-EN 197-1. Cement - Part 1: Composition, specifications and conformity criteria for common cements. Madrid, Spain2011.

[29] AENOR. UNE 7050-3. Test sieves. Technical requirements and testing. Part 1. Test sieves of metal wire cloth. Madrid, Spain1997.

[30] AENOR. UNE 83952. Concrete durability. Water for mixing and aggressive waters. Determination of the pH. Potentiometric method. Madrid, Spain 2008.

[31] AENOR. UNE-EN 196-1. Methods of testing cement - Part 1: Determination of strength. Madrid, Spain2018.

[32] Sáez Blázquez C, Farfán Martín A, Martín Nieto I, Carrasco García P, Sánchez Pérez LS, González-Aguilera D. Efficiency analysis of the main components of a vertical closed-loop system in a borehole heat exchanger. Energies. 2017;10:201 1996-073.

[33] Devices D. KD2 Pro thermal properties analyzer operator's manual. USA: WA; 2016.

[34] Tawfik M, Tonnellier X, Sansom C. Light source selection for a solar simulator for thermal applications: A review. Renew Sustain Energy Rev. 2018;90:802-13 1364-0321.

[35] Colarossi D, Tagliolini E, Principi P, Fioretti R. Design and validation of an adjustable large-scale solar simulator. Appl Sci 2021;11:1964.

3.2. Mejora de las propiedades térmicas mediante la introducción de pigmentos

En esta segunda parte del capítulo III se incluye el artículo *"Experimental study on the thermal properties of pigmented mortars for use in energy efficiency applications"*, publicado en la revista *Journal of Cleaner Production*.

Resumen

Los pigmentos son empleados en la construcción y arquitectura generalmente con fines estéticos u ornamentales y no suelen considerarse sus capacidades colorimétricas para otros fines. Dadas las necesidades de mejora de las propiedades térmicas de los materiales de construcción, en este estudio se plantea su incorporación como aditivos. En este sentido, el **objetivo** de este trabajo es avanzar en la mejora de las propiedades térmicas de materiales de construcción desde el punto de vista de la absorción de radiación solar en lugar de la modificación de su conductividad térmica. De igual forma que en el trabajo anterior, se tratará de buscar soluciones que permitan una mayor captación de radiación solar para funciones relacionadas con la acumulación de calor a la par que soluciones que permitan repeler la radiación para mitigar el calentamiento de las infraestructuras y los efectos de las islas de calor urbano.

La **metodología** seguida consistió en la evaluación del comportamiento térmico de morteros fabricados con cemento blanco y cemento gris con diferentes dosificaciones de pigmento blanco y negro. Previo al análisis térmico, se llevaron a cabo ensayos mecánicos con el fin de determinar la influencia del pigmento en las propiedades mecánicas como la resistencia a compresión. A su vez, se realizaron también ensayos de laboratorio para determinar la conductividad y resistividad térmica.

Los ensayos del comportamiento térmico se llevaron a cabo bajo en enfoque de termografía activa propuesto en el trabajo anterior. Las muestras fueron sometidas a ciclos de calentamiento y enfriamiento bajo un simulador solar y monitorizadas mediante cámara termográfica. La evolución temporal de la temperatura superficial fue obtenida en cada una de las muestras estudiadas, analizando también el posible efecto de borde. En este caso, dado que el objetivo se centró en la absorción de radiación solar, el análisis se focalizó en la fase de calentamiento.

Por último, se realizó un análisis de reflectividad óptica para determinar de la influencia del pigmento en la respuesta espectral así como su correlación con el comportamiento térmico. Se analizó la reflectividad y absorción de los morteros con diferente composición de pigmento tanto el rango visible (VIS) como el infrarrojo cercano (NIR). Para ello, se empleó un láser escáner terrestre (TLR) que permitió

escanear las muestras obteniendo información radiométrica visual y del infrarrojo cercano, además del color gracias a la cámara RGB.

Los **resultados** mostraron que la adicción de pigmentos en los porcentajes establecidos por el fabricante no afecta a la resistencia a compresión de los morteros estudiados, tanto el fabricado con cemento blanco como cemento gris. Estos mismos porcentajes de pigmento suponen alteraciones muy leves en cuanto a la conductividad térmica, con un ligero incremento en la conductividad para los morteros con cemento blanco y pigmento blanco y valores algo más bajos para las muestras con pigmento negro y cemento gris.

Los ensayos de calentamiento mostraron una diferencia significativa en la temperatura superficial alcanzada por cada una de las muestras. Por un lado, el pigmento blanco apenas redujo la temperatura, especialmente en el caso de los morteros fabricados con cemento blanco. Sin embargo, el pigmento negro permitió alcanzar temperaturas más altas, especialmente cuando se trata de mortero fabricado con cemento blanco. En cuanto al análisis de radiación reflejada, mostró una mayor absorción para los morteros con pigmento negro, corroborando los resultados obtenidos en el análisis térmico.

Las principales **conclusiones** del trabajo resaltan la elevada influencia del uso de pigmentos para la mejora de las propiedades térmicas de los morteros sin alterar su capacidad mecánica. Especialmente el empleo de pigmentos negros proporciona notables capacidades de absorción de radiación que pueden resultar útiles para funciones de eficiencia energética como almacenamiento de calor.

La técnica de termografía activa aplicada con simulador solar ha sido validada por medio de análisis ópticos, que han ratificado la contribución de los aditivos a una mayor absorción de radiación solar. Este enfoque además ha permitido cuantificar la ganancia térmica, por lo que resulta de gran utilidad para estudios de mejora y optimización de estos materiales en cuanto a mejora térmica y eficiencia energética.
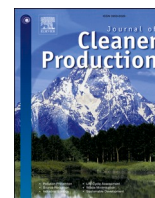
Experimental study on the thermal properties of pigmented mortars for use in energy efficiency applications

Jorge López-Rebollo [a,*], Susana Del Pozo [a], Ignacio Martín Nieto [a], Cristina Sáez Blázquez [a,b], Diego González-Aguilera [a]

[a] Department of Cartographic and Land Engineering. University of Salamanca, Higher Polytechnic School of Ávila, Hornos Caleros, 50, 05003, Ávila, Spain
[b] Department of Electric, System and Automatic Engineering, Universidad de León, León, Spain

ARTICLE INFO

ABSTRACT

This study aims at investigating the application of pigments on mortars and evaluating how it affects their thermal properties. In addition, it was analysed whether the addition of this type of substance affects the mechanical and optical properties of the mortars. For this purpose, several mortar samples were made with grey and white cement to which different concentrations of black and white pigment were added. The mechanical characterization tests showed that the compressive strength is not affected by the addition of pigments in the proportions supplied. On the other hand, the thermal conductivity tests also showed a negligible relationship between the proportion of pigment added and the change in the mortar conductivity. Then, the thermal behaviour of these mortar samples subjected to heating with a low-cost solar simulator was also monitored. Results revealed a significant increase in temperature for the mortar samples with black pigments, while those with white pigments barely reduced this temperature. Finally, after performing a spectral reflectance test, a correlation was found between the reflectivity of the pigmented mortars in the optical spectrum and their thermal behaviour.

1. Introduction

The excessive consumption of resources and the generation of a large amount of waste in the construction industry point to the need to use materials with properties that allow their full potential to be exploited in a sustainable way. The inclusion of capabilities on construction materials that go beyond their mechanical properties necessary to ensure the integrity of structures, is a challenge faced by this sector. One of the development paths in the concrete market, accompanied by numerous investigations on its characteristics and capabilities, is the suitability of its use in a recycled manner (Verian et al., 2018; Matias et al., 2020; Teijón-López-Zuazo et al., 2021). One of the recent lines of research is based on the introduction of self-healing capabilities in construction materials (Gupta and Naval, 2020). This line aims to increase the safety and durability of structures that are difficult to monitor and/or maintain. Finally, it is necessary to mention those research lines that analyse the thermal capacities of construction materials on which the present work is focused (Basha et al., 2020; Sukontasukkul et al., 2019).

The thermal requirements in construction materials are beginning to gain importance within the framework of the environmental and energy transition policies adopted by many countries. Among others, the possibilities of improving the performance of air conditioning systems based on the selection of construction materials, means that a great development of this type of solutions is expected in the future. It is also worth mentioning the importance that the thermal properties of construction materials have, for example, in the generation of heat islands that occurs in many urban centres mainly during the summer season (Deilami et al., 2018). An adequate modification of the thermal properties of the concrete could contribute to significantly mitigate this undesirable effect. On the other hand, in certain climatic scenarios, the opposite action can result in an energy advantage. For example, managing to improve the thermal capacities of concrete to increase its energy storage capacity can result in significant savings in the heating systems used (Xaman et al., 2019).

As for granting certain thermal capacities to construction materials, it entails using different additives capable of conferring them the desired

properties without affecting their mechanical properties. The economic, environmental and safety considerations on these additives are an important part of the investigation. In this sense, numerous pigments have been tested with very diverse compositions (Cellat et al., 2019; Berktas et al., 2020; Nocuń-Wczelik and Stolarska, 2019).

The main developments focused on improving the thermal capabilities of construction materials are focused on the use of paint coatings made of Near Infrared (NIR) reflective pigments (Rosati et al., 2021; Divya and Das, 2021), which allow the temperature of buildings to be reduced by applying them to façades and roofs (Puesan and Mestre, 2017). So far, the introduction of pigments as additives for mortars or concrete has been done mainly for architectural and visual design purposes (Corinaldesi et al., 2012), while its addition to other materials, such as asphalt, has been shown to be effective in considerably reducing the temperatures reached without affecting its performance (Badin et al., 2020, 2021). In this sense, the addition of pigments as additives hardly affects the mechanical performance of the mortars, as some research has shown that the differences in their mechanical properties are very slight (Heerah et al., 2021).

Nevertheless, there is a lack of knowledge regarding the thermal performance of this type of mortars with pigmented additives, as research in this field is very scarce and therefore the use of multidisciplinary techniques is presented as an opportunity to study their thermal behaviour.

Traditionally, the improvement of the thermal properties of mortars has been tested from the point of view of thermal conductivity (Corinaldesi et al., 2011; Yun et al., 2013). Thermal conductivity can be measured by applying the infinite line heat source model (Healy et al., 1976) from the heating/cooling process undergone by the samples (Lockmuller et al., 2004). However, from a thermographic point of view, some studies on NIR reflective coatings have shown the feasibility of measuring surface temperature with thermal imaging (Thejus et al., 2021). In this case, the active thermography (Lizaranzu et al., 2015) applied by means of a solar simulator is intended to reveal the difference between the materials due to the alteration of thermal diffusivity and heat flow caused by their composition (Maldague, 2001). The use of solar simulators is widespread in the field of renewable energies, and more specifically to carry out performance tests on solar thermal and photovoltaic systems (Tawfik et al., 2018). There is an extensive review on the types of solar lamps and their performance (Colarossi et al., 2021) as well as on the use of low-cost solar simulators for multiple applications (Tawfik et al., 2018; Colarossi et al., 2021; Codd et al., 2010; Meng et al., 2011).

Together with thermal conductivity and thermographic analysis, the use of optical spectrum sensors allows the analysis of the radiation absorbed/reflected by the samples and has been used in many works to study this type of behaviour in other construction materials, generally related to heritage (Sánchez-Aparicio et al., 2018; Del Pozo et al., 2016; Rodriguez-Gonzalvez et al., 2015). For this purpose, multi and hyperspectral imaging (Santos et al., 2018; Bonifazi et al., 2018) are other widely used techniques while spectroscopy (Reuben et al., 2018; Watanabe et al., 2019; Florian, 2022) allows to reach the highest level of detail given its precision and resolution.

As consequence, this work aims to advance in the knowledge of the thermal behaviour of pigmented mortars through the application of multidisciplinary techniques to study their thermal properties and their heating and cooling performance. To this end, an experimental campaign is carried out on mortars with different dosages of pigment using thermal, optical and mechanical tests. After this Introduction Section, the materials and the description of the techniques employed are described in the Materials and Methods (Section 2). In Section 3, the experimental results for each test are shown, the connections between the results of the different thermal tests are analysed and some explanations are proposed. Finally, in Section 4, a series of conclusions are exposed, some of which were expected (the addition of pigments in the percentages established does not affect the compressive strength of the

mortar), while others are promising for the construction and building sector and open new engaging research lines.

2. Materials and methods

This work focuses on the use of additives particularly designed to alter the colour of cement and, specifically, on the study of their effect on the thermal properties of mortars. In addition to this study, it has been considered to evaluate the conservation of its mechanical properties and to analyse the influence they have on the reflectance in the optical spectrum (visible and infrared).

To carry out these tests, two different types of cement (grey and white) have been used, which different proportions of white and black pigments have been added in order to study the effects of the pigmentation on its mechanical, thermal and optical properties. With these pigmented cements, and following the procedure described in the following subsections, mortars have been prepared to produce the samples on which the following tests have been performed. Fig. 1 shows a scheme of the workflow followed.

- Mechanical characterization. In order to verify whether the mechanical properties are maintained or whether the addition of pigments has any effect on their behaviour, compressive strength tests were carried out.
- Thermographic analysis. The active thermography applied allows analysing the thermal behaviour of the sample against heating and cooling processes, so that a continuous monitoring of its surface temperature is carried out.
- Optical reflectivity test. To analyse the radiation absorbed/reflected by the mortar samples in the optical spectrum, a Terrestrial Laser Scanning (TLS) operating in the NIR spectrum (at 905 nm) with an integrated Red-Green-Blue (RGB) camera was used.
- Thermal conductivity test. The main objective is to study the possible connections between the variations in thermal conductivity from the different samples, with the results obtained in the other tests carried out. In addition, the test will reveal if the different dosages of pigments in the mortars could have an effect on this thermal parameter.

2.1. Materials for the pigmented mortars

Pigmented mortars are mostly used for functional and aesthetic applications buildings, so their mechanical behaviour is not a limiting factor for their manufacture, though it is advisable that its properties and durability remain unchanged. They have a dosage made up by of water, natural siliceous aggregates, Portland cement and chemical additives such as pigments in this case. Within the scope of this study, the focus was on evaluating the use of different dosages of pigment and its influence on the properties of mortars. In order to analyse the thermal behaviour and achieve notable differences, two types of cement and two types of pigment were used on this research. The fine natural aggregate used in all the mixes was silica sand, 0–4 mm fraction. No additives other than pigment were used.

On the one hand, the blinder used for manufacturing the grey mortar was a cement type BL II/B-LL 32.5 R. This Grey Cement (GrC) has the following components: i) a Clinker content comprised between 65 and 79%; ii) a Limestone content of 21–35%; iii) a Chloride content: ≤ 0.10; iv) a Sulphate content: ≤ 4.0; and v) a soluble toilet chromium VI content $\leq 0.0002\%$. It has a beginning of setting: ≥ 60 min and an end of setting: ≤ 720 min. The expansion is less than 10 mm. Resistance at 28 days ≤ 32.5 MPa.

On the other hand, White Cement (WhC) with a whiteness content $\geq 85\%$ was chosen, looking for the best contrast with the dark pigment dosages. This cement is type BL II/B-LL 42.5 R and its composition is similar to that of GrC. In this case, resistance at 28 days ≤ 42.5 MPa.

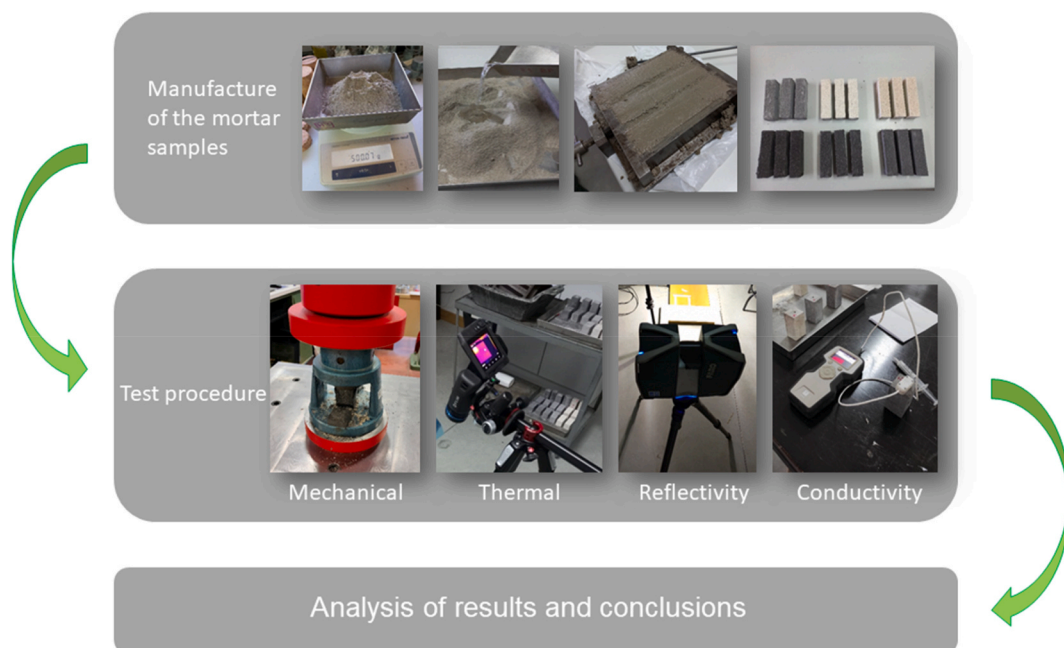Regarding the pigments, white and black dyes were used in different

Fig. 1. Workflow scheme for the mechanical, thermal and physical characterization of pigmented mortars.

proportions (Table 1). The White Pigment (WhPig) used belongs to Oxined® and the Black Pigment (BlPig) used belongs to HobbyColor. Both contain synthetic metal oxides, inorganic, insoluble in water, resistant to alkalis and unaltered by the effect of sunlight and any other atmospheric agent.

A total of 12 mortar samples were made with the same proportions of sand (3), cement (1) and water (0.5), so that only the amount of pigment was modified. A high percentage of pigment was used in order to achieve greater coloration, so that 10% corresponding to the weight of the cement was added. Although the proportions of each pigment were varied in each specimen, the same total weight was maintained in each sample, except in the reference ones (G5-Ref and W5-Ref).

2.2. Mechanical characterization

With the aim of verifying the influence of the pigment on the mechanical properties, mechanical characterization tests were carried out. These tests allow us to know if the strength of the mortar increases or decreases depending on the type and amount of pigment for each of the dosages with respect to the reference. The mortar solutions were evaluated by means of compression tests according to guideline UNE-EN 196-1 (AENOR. UNE-EN). In order to carry out these tests, an electromechanical test machine Servosis ME-405/50/5 was used with a load cell of 500 kN and the corresponding compression plates. It was

necessary to use an auxiliary device (Fig. 2) to carry out the compression tests on specimens with standardized dimensions. This device consists of two 40 × 40 mm plates on which the sample is placed, so that the upper plate of the machine transmits the load to the upper plate of the device by means of a spherical joint.

The specimens for the mechanical characterization were manufactured following the guideline UNE-EN 196-1. Initially, moulds to manufacture three 160 × 40 × 40 mm specimens were used for each of the mixtures. The specimens were kept for 24 h in the moulds in conditions of 20 ± 2 °C and relative humidity greater than 90%. Subsequently, the moulds were removed, and the specimens were kept in water at a temperature of 20 ± 2 °C until reaching 28 days of curing.

In order to reduce and adapt the dimensions to the regulations, each of the specimens was cut, obtaining two semi-prisms of approximately 80 mm in length. In this way, one of the halves was used for the compression tests while the other half was reserved for the rest of the tests.

2.3. Thermographic analysis

With the objective of carrying out a thermographic analysis to

Table 1
Pigment proportions of each mixture.

Nomenclature	Cement Colour	BlPig (g)	WhPig (g)
G1	Grey	50	0
G2	Grey	37.5	12.5
G3	Grey	25	25
G4	Grey	12.5	37.5
G5-Ref	Grey	0	0
G6	Grey	0	50
W1	White	50	0
W2	White	37.5	12.5
W3	White	25	25
W4	White	12.5	37.5
W5-Ref	White	0	0
W6	White	0	50

Fig. 2. Test Machine and auxiliary device.

determine the behaviour of the mortars, the active thermography technique and the step heating was used. This method consists of applying heat to the specimens by means of a lighting system under controlled conditions and for a certain time, so that their heating and cooling phases can be monitored. This monitoring was carried out with equipment made up of: i) a thermographic camera FLIR T540; and ii) a lighting system with a low-cost solar simulator.

In this case, the FLIR T540 camera with a 42° lens was used, which allows a field of view of 42° × 32°. The camera has an infrared resolution of 464 × 348 pixels in addition to incorporating a 5 MPx visible sensor that allows both images to be superimposed. It also has a laser sensor to measure the distance to the object and perform autofocus. It has a thermal sensitivity <30 mK at 30 °C and is calibrated for a temperature range of −20 to 120 °C. Finally, it allows a shooting speed of 30 frames per second. The acquisition of images was carried out using FLIR ResearchIR software, which allows us to configure test parameters and environmental conditions, as well as defining image capture protocols.

Considering that the mortars are intended to be used in real environmental conditions, an attempt was made to use a solar simulator that could resemble as much as possible the heating produced by the sun's rays. The lighting system consists of a developed low-cost solar simulator (Fig. 3). The most widely used lamps to create solar simulators are usually argon arc, metal halide, tungsten halogen or xenon arc (Tawfik et al., 2018; Colarossi et al., 2021). In this case, a 250 W metal arc halide lamp (Table 2) was chosen. Thus, the solar simulator consists of a metal halide lamp, a ballast to regulate the continuous flow of the arc and to provide the appropriate voltage to the lamp, a support for the lamp with an aluminium plate to concentrate the radiation, and a sample tray.

Solar simulators are devices capable of approximately simulating, by means of artificial light, the natural light of the sun. Thanks to them, studies and simulations can be carried out under controlled laboratory conditions, guaranteeing a certain stability in environmental conditions. In addition, this type of test allows planning, programming, and taking ad-hoc data, guaranteeing reproducibility and repeatability. As for the main aspects to consider in the design of solar simulators are the spectral correspondence, the uniformity of irradiation and its temporal stability. In this study, the uniformity and temporal stability of the luminous flux received by the samples is guaranteed because they were always located in the same place with respect to the lamp (Fig. 3), in addition to the fact that the heating-cooling tests were carried out under the same conditions (same turn-on and turn-off duration for all simulations). Regarding the optical spectrum, as Fig. 4 shows, metal halide lamps have a spectral coverage close to the global solar radiation spectrum.

2.4. Optical reflectivity test

In order to analyse and quantify the part of radiation reflected by the samples in the Visible (VIS) and NIR spectrum, it was decided to carry out a data acquisition with a Faro Focus 3D 120 terrestrial laser scanner equipped with an integrated RGB camera (specifications are shown in Table 3). This sensor is an active phase shift device that emits electromagnetic radiation (at a wavelength of 905 nm) and collects the reflected back from objects. Thanks to this, not only can objects be reconstructed in three dimensions with millimetric accuracy, but also the intensity reflected from them can be measured. This information will be useful to analyse the amount of radiation absorbed by the mortar samples and, therefore, likely to be subsequently emitted and recorded by the thermographic camera.

2.5. Thermal conductivity test

Thermal measurements were performed using the thermal properties analyser TEMPOS. This device, developed by the commercial group "METERgroup" complies with the ISO 2008 standards and the ASTM 5334 and IEEE 442 and is specifically designed for taking accurate readings of thermal conductivity, thermal resistivity, thermal diffusivity, and specific heat in different types of materials.

For the mentioned readings, different specific needles are used based on the nature of the material and the measuring test. Each needle produces a discrete amount of heat, virtually eliminating the moisture movement (or free convection in the case of liquids) that could influence the reading. In addition, the short heating times required by TEMPOS (around 1 min) allows to measure frozen materials and even fluids (George et al., 2020).

The operation of this equipment is based on the infinite line heat source theory, so the thermal conductivity is obtained by monitoring the dissipation of heat from the needle probe. Heat is inserted to the needle for an established heating time *th*, and temperature is then measured in
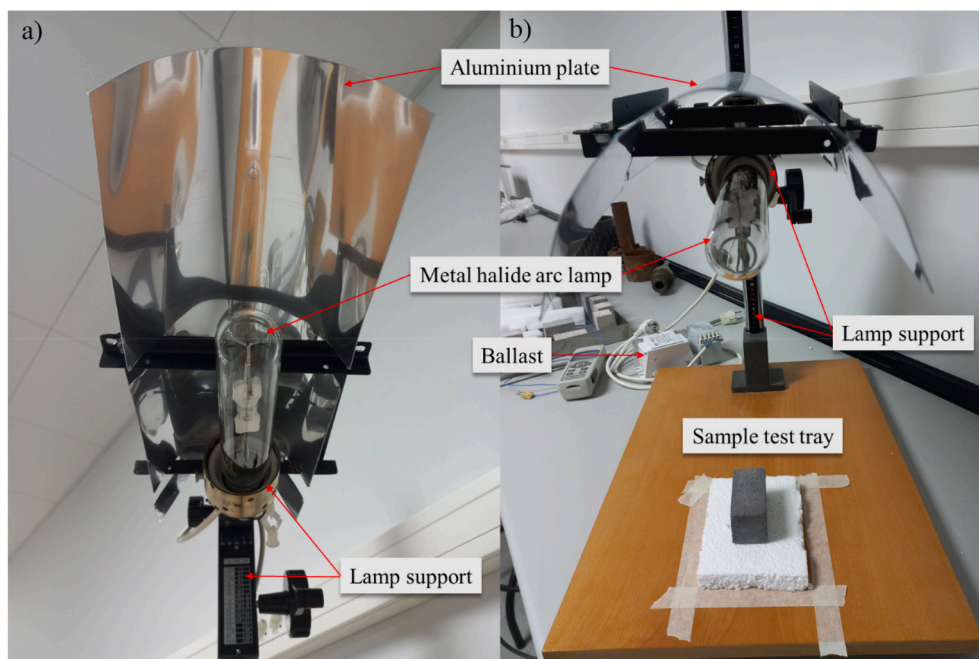

Fig. 3. Low-cost solar simulator device. (a) Bottom view of the lamp and reflective aluminium coating; (b) Configuration of the device together with the test sample.

Table 2

Metal halide arc lamp main features.

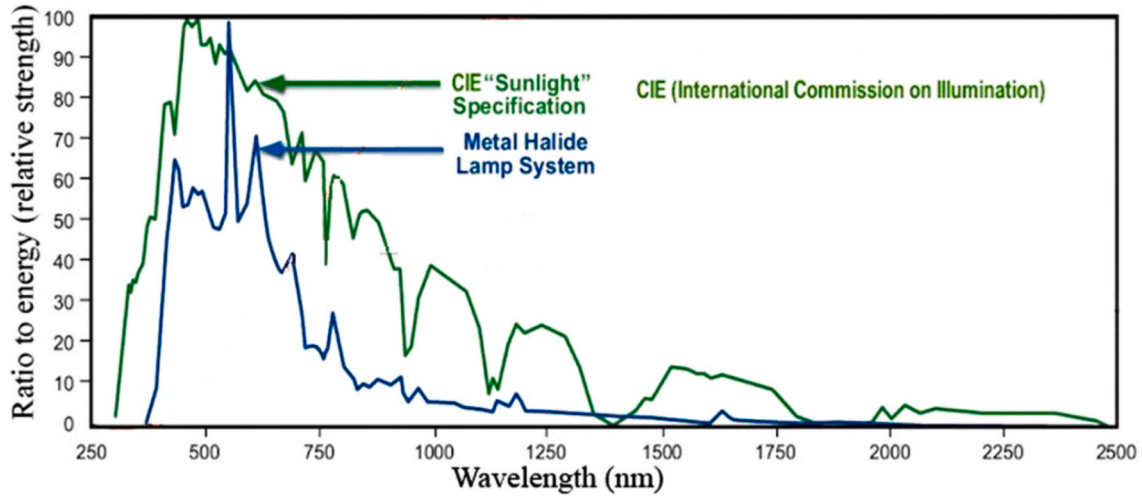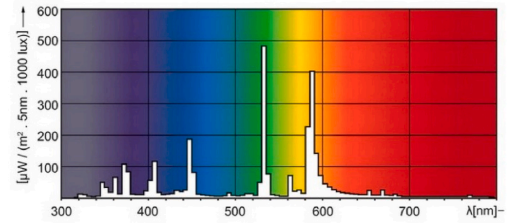| Attribute	Value
Product name	HPI-T Plus 250W/645
Nominal luminous flux	19500 lm
Colour temperature	4500 K
Length	255 mm
Diameter	47 mm

Fig. 4. Spectral distribution chart comparing metal halide lamps with sunlight (PublicLab, 2022).

the monitoring needle during heating and for an extra time equal to *th* after heating (Carslaw and Jaeger, 1959). The following Eq. (1) shows how the temperature during heating is obtained.

$$T = m_0 + m_2 t + m_3 lnt \tag{1}$$

where m_0 is the ambient temperature during heating; m_2 is the rate of background temperature drift; and m_3 is the slope of a line relating temperature rise to logarithm of temperature.

In the same way, the model during cooling is described in Eq. (2).

$$T = m_1 + m_2 t + m_3 \ ln\frac{t}{t - t_h} \tag{2}$$

Finally, the thermal conductivity parameter is calculated from Eq. (3), which also considers the heat flux (*q*).

$$k = \frac{q}{4m_3} \tag{3}$$

In the case of the present research, conductivity measurements were performed using the RK-3 single needle, conceived for solid and rocky materials. The specifications of this sensor are included in the following Table 4.

3. Experimental results

3.1. Mechanical properties

A total of 36 tests were carried out following the guideline UNE-EN 196-1, 18 of which correspond to specimens with grey cement (GrC) (Table 5) and another 18 which correspond to specimens with white cement (WhC) (Table 6). For each type of cement, six different dosages were used (Table 1) and for each of these three specimens were tested. According the guideline UNE-EN 196-1 (AENOR. UNE-EN), the specimens were centred in the plates and the speed test was set at 2400 ± 200 N/s. Taking in account that the dimensions of the plates are 40 × 40 mm, the compressive strength was calculated as follow (Eq. (4)).

$$UCS = \frac{F_c}{1600} \tag{4}$$

where *UCS* is the unconfined compressive strength (Mpa); F_c is the maximum breaking load (N) and 1600 is the area of the plates (mm^2).

Taking into account that the two types of cement have differences in their mechanical properties, the compressive strength analyses were carried out separately, although the procedure was similar in both cases.

Table 3

Faro Focus-3D 120 main features.

Attribute	Value
Physical principle	Phase shift
Wavelength (nm)	905 - near infrared
Measurement range (m)	0.6–120
Field of view (degrees)	360 H × 320 V
Accuracy nominal value at 25 m (mm)	2
Beam divergence (mrad)	0.19
Capture rate (points/s)	122,000/976,000
Radiometric resolution (bits)	11

Table 4

Specifications of the single needle RK-3 used with TEMPOS device.

RK-3 needle specifications	
Size	3.9 mm diameter x 60 mm length
Range	Resistivity: 17–1000 °C·cm/W
	Conductivity: 0.1–6 W/(m·K)
Accuracy	Conductivity: ±10% from 0.1 to 6 W/(m·K)

Table 5
Results obtained of the mechanical characterization of the grey cement.

Nomenclature	UCS (Mpa)	Dosage Average (Mpa)	Dosage Deviation (%)	Total Deviation (%)
G1-1	29.1	29.1	0.1	0.8
G1-2	28.5		1.9	2.6
G1-3	29.7		2.0	1.2
G2-1	29.1	29.3	0.5	0.6
G2-2	30.0		2.3	2.3
G2-3	28.8		1.8	1.8
G3-1	29.8	29.3	1.7	1.7
G3-2	28.5		2.6	2.6
G3-3	29.6		0.9	0.9
G4-1	27.4	29.1	6.0	6.5
G4-2	30.7		5.2	4.6
G4-3	29.4		0.8	0.3
G5-Ref-1	30.4	31.2	2.6	3.7
G5-Ref-2	29.5		5.4	0.7
G5-Ref-3	33.7		8.0	15.0
G6-1	27.5	27.8	0.9	6.1
G6-2	28.4		2.2	3.1
G6-3	27.4		1.3	6.4

Table 6
Results obtained of the mechanical characterization of the white cement.

Nomenclature	UCS (Mpa)	Dosage Average (Mpa)	Dosage Deviation (%)	Total Deviation (%)
W1-1	43.6	44.8	2.7	3.1
W1-2	44.4		0.9	5.1
W1-3	46.4		3.6	9.8
W2-1	44.6	43.1	3.5	5.6
W2-2	41.7		3.1	1.2
W2-3	42.9		0.5	1.5
W3-1	43.0	41.0	4.9	1.7
W3-2	40.1		2.1	5.0
W3-3	39.8		2.8	5.7
W4-1	39.8	41.7	4.4	5.7
W4-2	42.6		2.2	0.8
W4-3	42.6		2.2	0.8
W5-Ref-1	42.5	43.2	1.6	0.7
W5-Ref-2	43.2		0.1	2.2
W5-Ref-3	43.9		1.6	4.0
W6-1	39.5	39.8	0.5	6.4
W6-2	41.3		3.9	2.2
W6-3	38.4		3.4	9.1

First, the compressive strength was obtained for each of dosages, so that an average value was calculated, as well as the deviations of each of the samples with respect to this mean value. In accordance with the requirements of the guideline, all the values presented deviations of less than ±10%, so the tests can be considered as valid. Next, it was decided to take all the samples as if they belonged to the same group, so the deviation of each one of them with respect to the total mean value was calculated.

The deviations from the total mean value are within the limits ± 10% for each of specimens in both GrC and WhC (Fig. 5, Fig. 6). Only one abnormal value was found that exceeded the upper limit for GrC (G5-Ref-3). This value corresponds to a sample of the reference dosage, which could lead one to think that the application of pigments reduces the compressive strength. Despite this anomaly, the other two values are within limits and are consistent with the rest of samples, being very close to the mean value. In addition, it is worth mentioning that the value that exceeds the limits also has a high deviation (8%) with respect to the values of this same dosage, so it can be taken as a disposable value as it corresponds to a single specimen as indicated in the guideline.

The rest of the GrC specimens as well as all those corresponding to WhC have a similar behaviour, whose deviation falls within the established limits. In addition, the small variations do not seem to have any relationship with the pigment content, since some values are above and others below without a clear trend. These variations may be due to heterogeneities caused in the material by small differences or by human action during the manufacturing or curing stages. In this way, it can be stated that the application of pigments does not have an influence on the compressive strength of this type of mortar.

3.2. Thermal behaviour

3.2.1. Tests setup

For the thermal study, a sample of each dosage was used, so a total of 12 specimens were analysed. The specimens correspond to the remaining semi-prism from the compression tests and their size is 40 × 40 mm with an approximate length of 80 mm.

The tests were carried out individually and under the same conditions, so that the specimens were placed under the solar simulator at a distance of 0.5 m (Fig. 3). In order to avoid heat transfer to the support surface, the samples were placed on a polystyrene panel. The camera was placed at a distance of 0.5 m, focusing on the upper surface of the sample on which the heating is caused. The angle of incidence of the
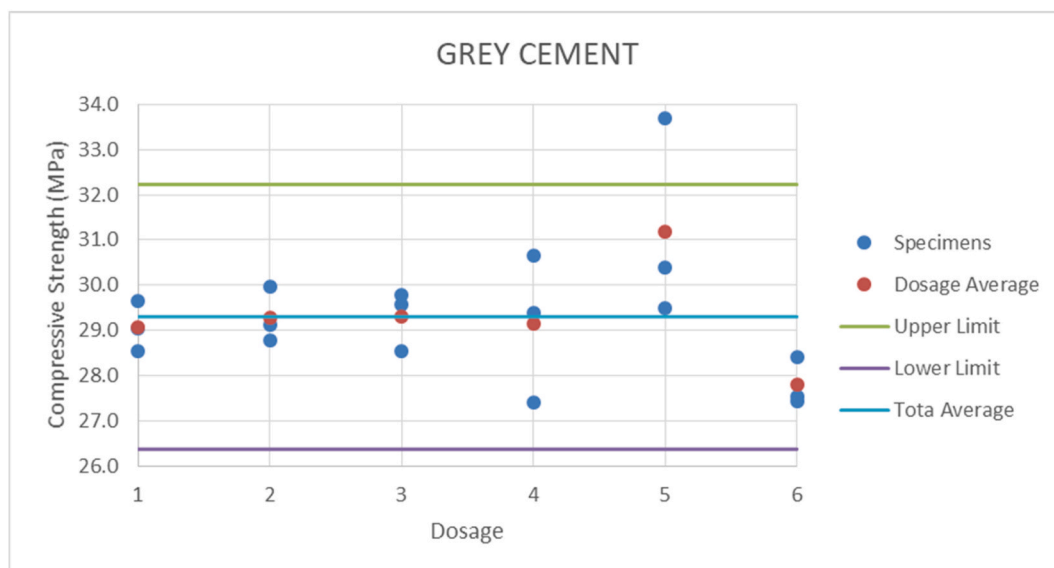
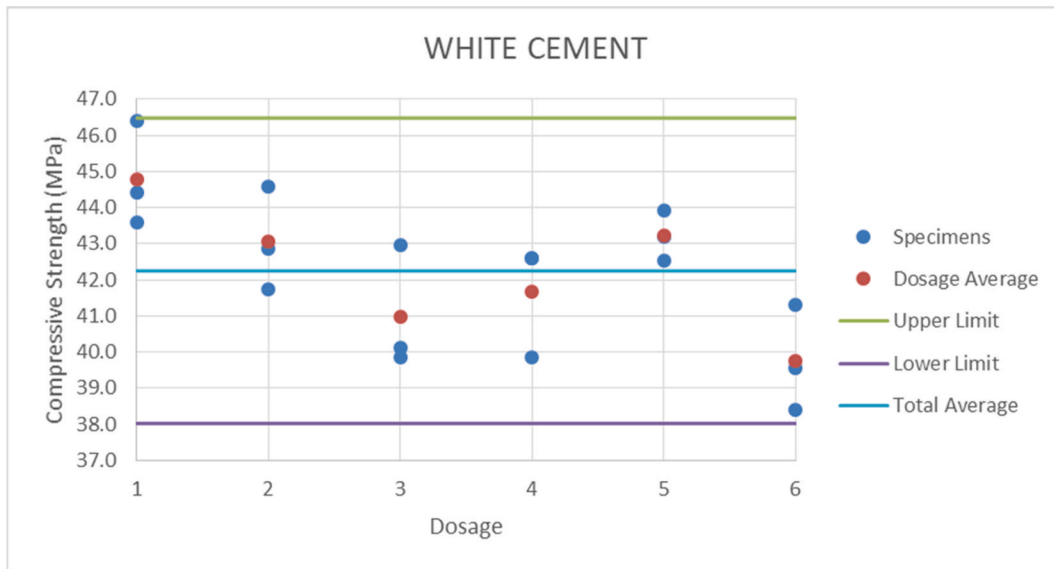**Fig. 5.** Compressive Strength and deviation limits of Grey Cement.

Fig. 6. Compressive Strength and deviation limits of White Cement.

light rays was tried to be as perpendicular as possible, as well as the direction of the camera, which had a slight angle of inclination due to the position of the solar simulator.

In order to all the tests were carried out under the same conditions, the samples were kept isolated at a constant temperature of 23 °C until the start of the tests. Initially, the solar simulator was turned on for 10 min before each test, so that it reached stable illumination. Next, the sample was placed under the simulator, starting the capture of thermographic images while heating for 15 min. Finally, the samples were allowed to cool for 30 min, continuing the acquisition of images. Considering that the time test was long, the thermographic images were acquired every second.

Taking into account that the samples have a reduced size and the edge effect can produce differences between the central zone and the outer zone of the samples, three approaches were carried out for these tests: i) full sample; ii) centre; and iii) edges (Fig. 7). On the one hand, the analysis of the thermographic images was carried out by selecting a rectangular Region Of Interest (ROI) that covered the full sample. In order to determine if the aforementioned edge effects exist, a central ROI, corresponding to a size of 60 × 20 mm, was selected. Finally, the inverse ROI was selected, that is, a rectangle corresponding to the full sample in which the inner ROI selected in step 2 is extracted.

3.2.2. Thermal results

For each of the tests and their corresponding approach, a similar procedure was carried out to extract the maximum temperature increments for the selected ROI in the samples. First, the average temperature value of the ROI was calculated for each of the frames, which made it possible to eliminate the pixels with anomalous values and thus eliminate the errors of a punctual nature. Then, the heating and cooling curves were obtained with a total of 2700 points corresponding to each of the images acquired in the test (Fig. 8, Fig. 9). To reduce the noise of the curve due to the sensitivity of the camera, a moving average filter was applied to smooth the curve and eliminate the peaks produced by those frames that could present anomalous values. Finally, the maximum temperature increases (Table 7, Table 8) were obtained from these curves, which correspond to the time immediately prior to switching off the solar simulator.
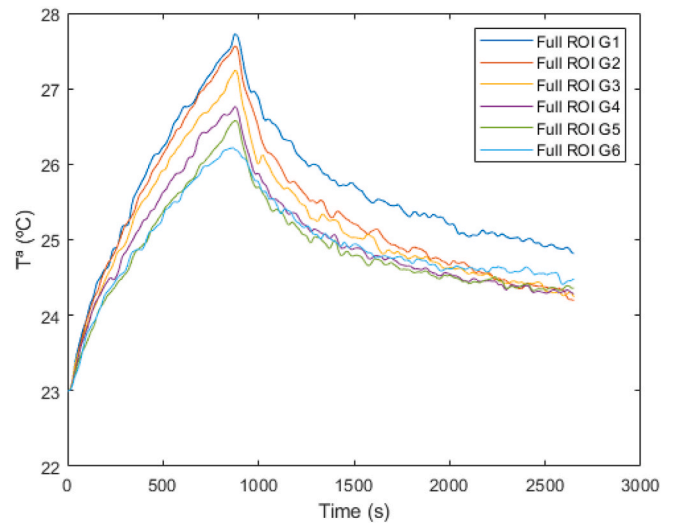

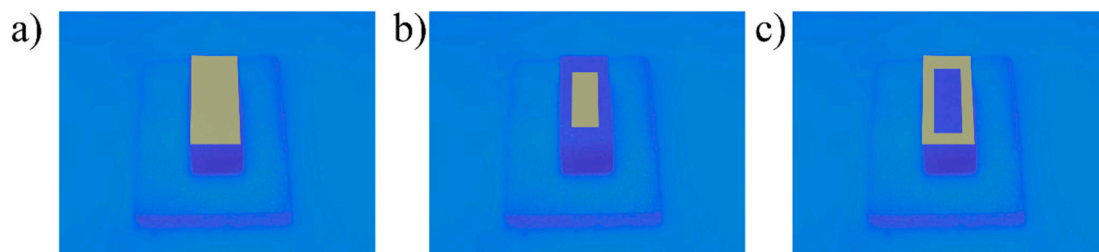**Fig. 8.** Heating and cooling curves of Grey Cement.

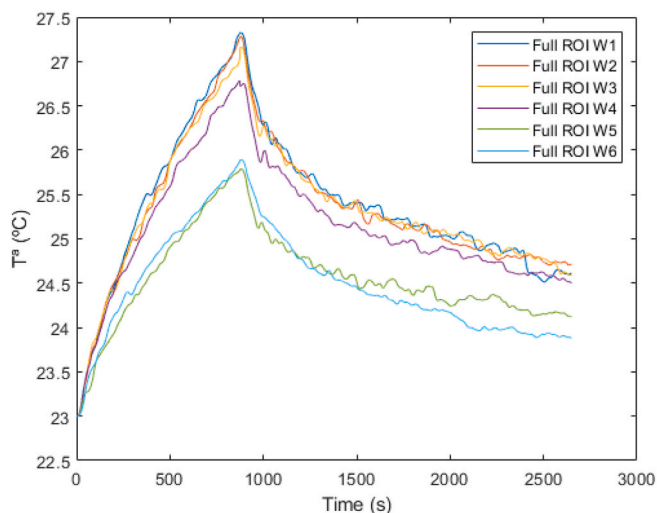**Fig. 7.** Region Of Interest for each of the approaches. a) Full sample. b) Centre. c) Edges.

Fig. 9. Heating and cooling curves of White Cement.

Table 7
Temperature increments (°C) for each ROI of Grey Cement.

Nomenclature	Full ROI	Centre ROI	Edge ROI
G1	4.73	4.75	4.71
G2	4.57	4.6	4.55
G3	4.24	4.28	4.21
G4	3.77	3.78	3.75
G5-Ref	3.58	3.59	3.57
G6	3.22	3.22	3.21

Since the differences between each of ROIs were minimal, it can be considered that the edges of the samples do not cause any significant heat loss effect, at least during the heating stage. This means that the heating produced with the solar simulator is homogeneous, as the coefficient of variation of the values for each pixel within the Full ROI was approximately 1% for all samples, which can be attributed to the noise produced in the thermographic images. For this reason, it was decided to show only the results corresponding to the Full ROI, as they are representative of the behaviour of the entire sample surface. In order to compare the two types of cement and each of the mixtures manufactured, the results obtained for each of them are shown below (Fig. 10).

Comparing the two types of cement used, it can be seen that, in general, the temperature increase is higher for the samples manufactured with grey cement. However, the colours produced by the different dosages seem to have a significant influence beyond the original colour of the cement.

On the one hand, the higher percentage of BlPig produces a higher temperature increase, so that mortars with full BlPig reach a higher heating. In this sense, for the mortar manufactured with GrC, the samples corresponding to dosage 1 have achieved 32% more heating compared to the reference dosage (5) (Fig. 10). In the case of the mortar manufactured with WhC, the heating corresponding to dosage 1 was 55% higher than the reference dosage (5) (Fig. 10). This temperature

Table 8
Temperature increments (°C) for each ROI of White Cement.

Nomenclature	Full ROI	Centre ROI	Edge ROI
W1	4.33	4.35	4.31
W2	4.28	4.32	4.23
W3	4.16	4.19	4.14
W4	3.78	3.82	3.75
W5-Ref	2.79	2.81	2.78
W6	2.89	2.89	2.88

increase can be considered as significant and comparable in both cases, taking into account that the mortar with grey cement started from a darker colour.

However, the full WhPig does not have the same effect on the two types of mortar. While for the mortar manufactured with GrC the temperatures reached are lower with WhPig, for the mortar manufactured with WhC the increase is very similar, even slightly higher in the mixture containing full WhPig. This may be due to the fact that the type of cement used has a high whiteness content, so that the pigment hardly causes any whitening.

The results obtained for full BlPig and WhPig are significant and can be further analysed with the other techniques used in the experimental campaign. Nevertheless, the results for the intermediate mixtures only allow us to know the influence of the pigment type, resulting in intermediate values with less interpretation, as the mixture of the two inverse pigments (BlPig and WhPig) does not generate a proportional and comparable colour.

3.3. VIS and NIR reflected radiation

3.3.1. Tests setup

The data acquisition with the TLS was perform by one scan as orthogonally as possible to the mortar samples. For the TLS data collection, the 12 mortar samples were placed at such a height that the laser beam hit them as orthogonally as possible, since the geometry of the acquisition affects the backscattered intensity, both distance and angle of incidence. Thus, the samples were placed on a support (Fig. 11) and the TLS was fitted onto a tripod stand so that both the mortar samples and the TLS laser beam were at the same height. The distance between the mortar samples and the TLS was about 5 m.

Regarding the TLS configuration, it was established a spatial resolution of 6 mm at 10 m, enough to extract redundant and representative radiometric information (400 points per mortar sample). In addition, the data acquisition was performed with photorealistic colour thanks to the parallax-free RGB camera of 70 megapixels with 8-bit radiometric resolution that the Faro Focus 3D 120 has integrated.

After data collection, the point cloud with *X, Y* and *Z* coordinates, visual and near infrared radiometric information, was segmented and analysed. Specifically, the median of the digital values of each of the 12 samples was calculated for the 4 wavelengths registered: 450 nm (blue band of the integrated camera), 550 nm (green band of the integrated camera), 650 nm (red band of the integrated camera) and 905 nm (TLS near infrared wavelength). Since the radiometric resolutions of the integrated camera and the laser scanner differ, 8 and 11 bits respectively, the values were normalized to 11 bits to be able to make comparisons and even be able to extract the spectral behaviour of the 12 samples at the visible and near infrared spectrum.

3.3.2. Reflected radiation analysis

The analysis of the radiation reflected by the specimens in the visible and near infrared is very important since it explains the energetic behaviour of the samples. Thus, the more radiation reflected in the visible and infrared, the less radiation absorbed and therefore less radiation emitted and vice versa. Thanks to the data collection with the TLS the spectral response of the mortar samples in the visible and near infrared can be extracted (Fig. 12) even though the analysis is carried out at digital levels (11 bits).

In this sense, the mortar samples can be ordered according to their spectral behaviour (Fig. 13) from greater to lesser reflection of radiation in the visible: W6, W5, G6, G5, G4, W4, G3 and W3, G2 and W2, W1, and G1. In the case of its spectral behaviour in the near infrared, the order followed is practically the same: W6, W5, G6, G5, G4 and W4, G3 and W3, G2 and W2, W1 and G1.

Finally, it is worth mentioning that all the mortar samples reflect more radiation in the near infrared than in the visible.
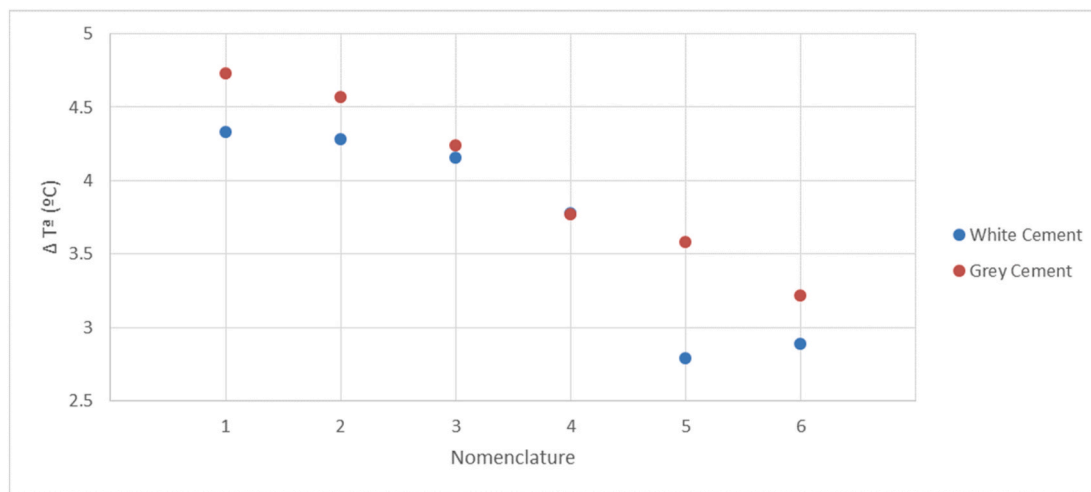
Fig. 10. Temperature increments (°C) for Full ROI of each cement.

3.4. Thermal conductivity test

3.4.1. Tests setup

The 12 mixtures evaluated in this work were accordingly drilled with the aim of introducing the RK-3 needle and measuring the thermal conductivity. During this process, it is important to ensure the contact between needle and tested material by placing thermal grease in the hole where the needle is situated (Blázquez et al., 2017a, 2017b). After the calibration of the sensor with the specific sample supplied by the manufacturer, three measurements were made on each sample to evaluate possible uncertainties.

It is also convenient to mention that, to obtain the most accurate data possible, ambient temperature was kept as constant as possible during the measurement process. Thus, to minimize these sources of error, about 15 min for samples and needle to equilibrate with the ambient temperature before taking measurements and around 15 min between readings for temperatures to equilibrate. Fig. 14 shows the drilling of the samples and the measuring process with TEMPOS.

3.4.2. Thermal conductivity results

As commented before, 3 thermal conductivity tests were carried out on each of the samples (6 specimens of grey cements and 6 specimens of white cements), so a total of 36 measurements were globally performed. After following the steps already described with the TEMPOS device, the thermal conductivity parameter was measured for each sample. These results, together with the deviation of each measuring are presented in Table 9 and Table 10.

As shown in the previous Tables 9 and 10, deviations are all below the usual acceptable values (±10%), and no abnormal values were detected. Analysing now the thermal conductivity results, it is possible to observe that, in general terms, white cement samples present higher conductivity values, but without notable differences with respect to the grey cement. In the case of this last group of specimens, it is clearly observable how the addition of pigment for its darkening (black pigment) contributes to decrease the thermal conductivity. Thus, the reference sample of this grey cement is the most thermally conductive of the set of samples analysed. Regarding the white cement samples, a small reduction in the thermal conductivity value is also observed in the first two samples (with a greater amount of black pigment), while the sample with only white pigment (W6) is the most conductive from a thermal point of view. Generally speaking, it can be established that the pigments do not have a significant influence on the thermal behaviour of
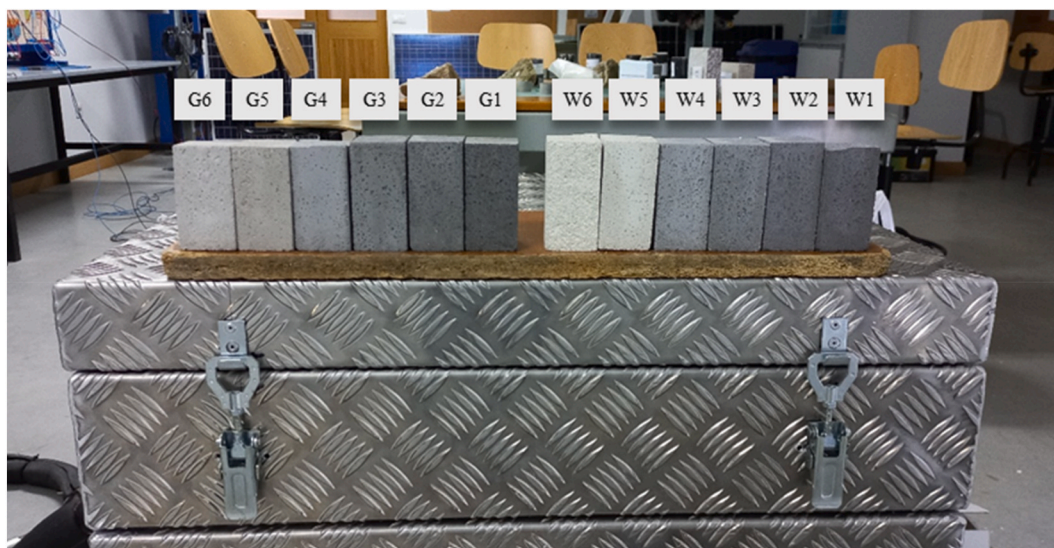

Fig. 11. Arrangement of the 12 mortar samples for the TLS data acquisition with the Faro Focus 3D 120. The 6 samples on the left correspond to the grey mortar samples and the 6 on the right correspond to the white mortar samples.
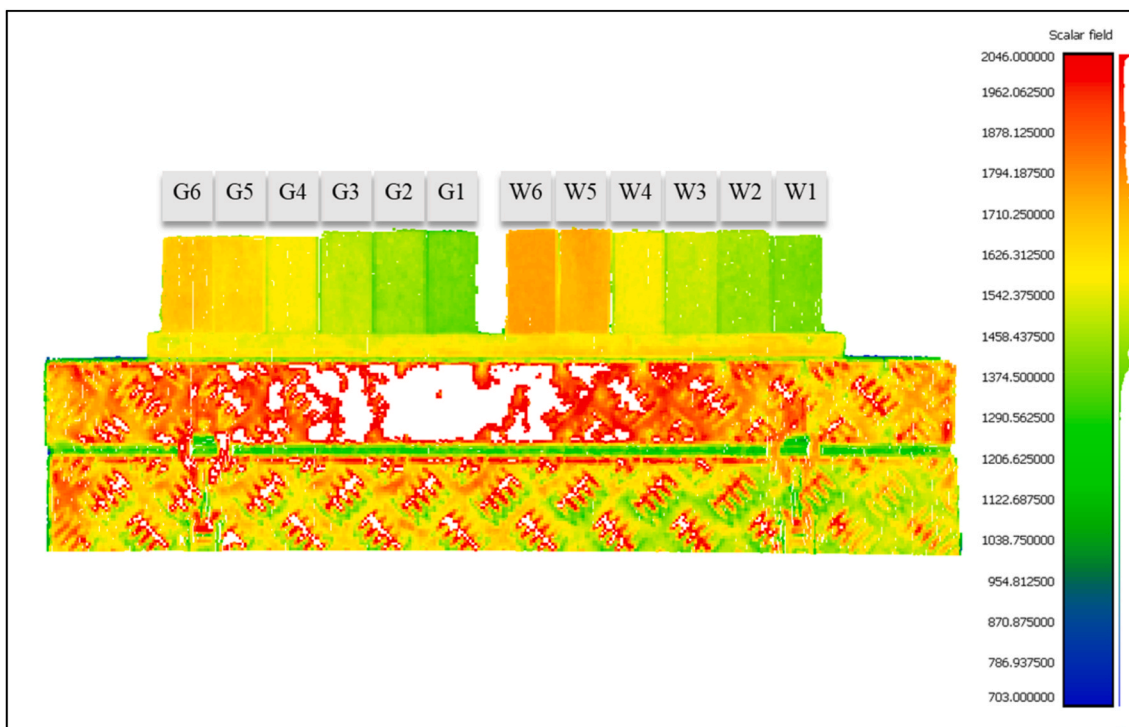
Fig. 12. Data acquired with the Faro Focus 3D 120: Point cloud with backscattered intensity values at 905 nm for the 12 mortar samples analysed.
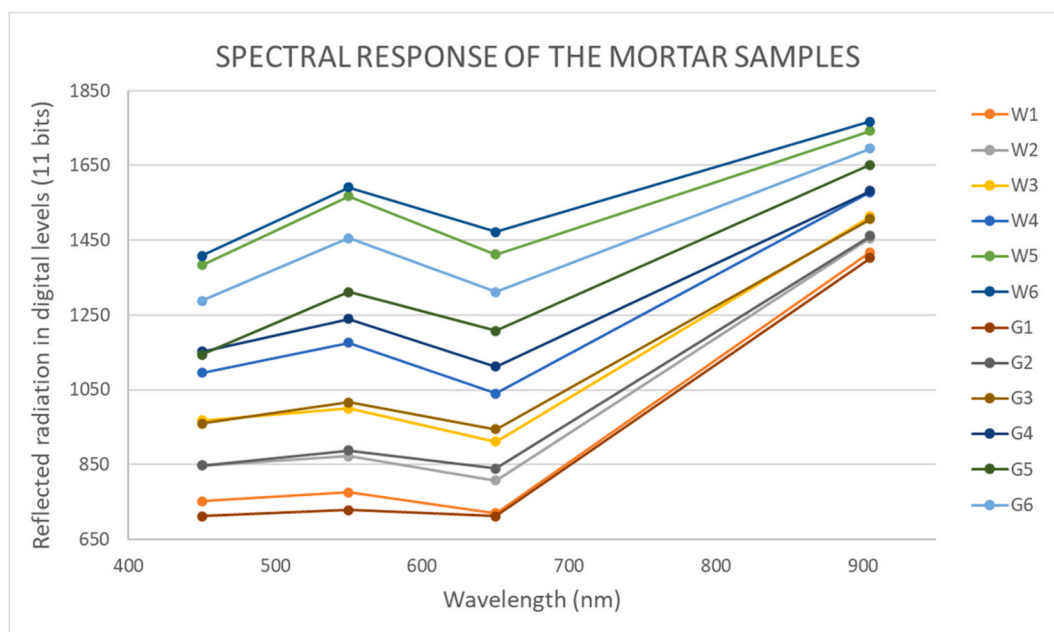

Fig. 13. Spectral response of the 12 mortar samples analysed for the VIS-NIR spectral range.

the tested materials, and that in any case, the trend is the reduction of the thermal conductivity with the addition of black pigment, especially in the grey cement samples. A slight increase in this thermal parameter could be also noticeable when white pigment is added, and black pigment is omitted.

4. Conclusions

This works aims at investigating the use of additive pigments to provide mortars with better thermal properties. To this end, two types of

cement and six dosages with different proportions of pigment were evaluated by means of mechanical, thermal and optical tests.

First, the mechanical properties of each of the samples were analysed, which allowed us verifying that the addition of pigments in the percentages established by the manufacturer does not affect the compressive strength of the mortar. All the deviations found were within the limits established by the standards, which guarantees its use without modifying its performance.

The thermal heating tests of the samples showed that there are significant variations in the surface temperature reached at the different
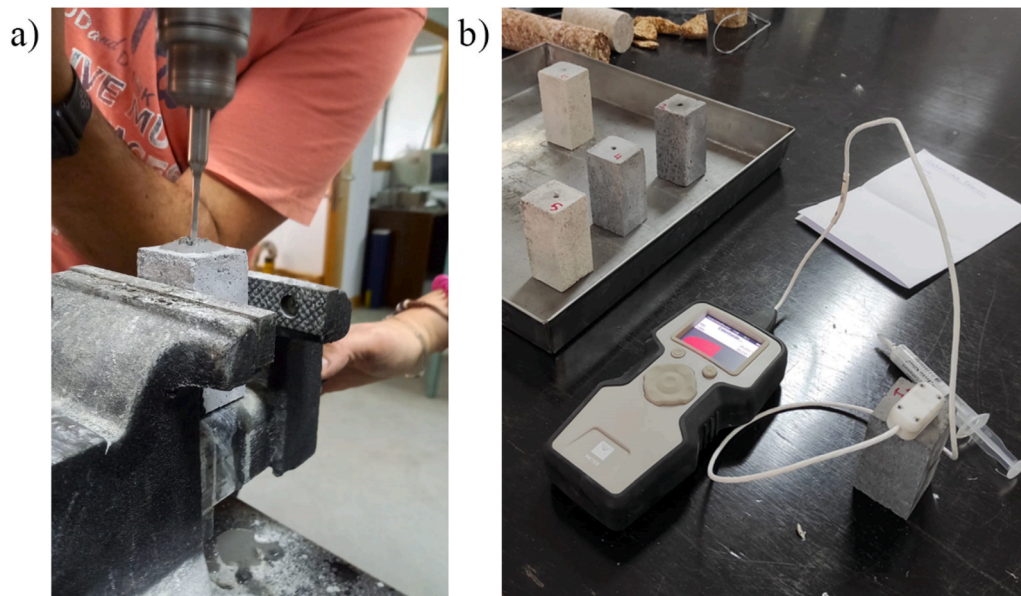
Fig. 14. Thermal conductivity test. a) Drilling; b) Measuring with TEMPOS and RK-3 needle.

Table 9
Thermal conductivity results obtained with TEMPOS for the Grey Cement.

Nomenclature	Measurement	Thermal Conductivity (W/m·K)	Deviation	Thermal Conductivity Average (W/m·K)	Deviation Average
G1	M-1	1.042	0.0035	1.041	0.0031
	M-2	1.121	0.0029		
	M-3	0.961	0.0029		
G2	M-1	1.242	0.0002	1.273	0.0003
	M-2	1.348	0.0003		
	M-3	1.230	0.0005		
G3	M-1	1.986	0.00036	1.884	0.0004
	M-2	1.876	0.00045		
	M-3	1.789	0.00040		
G4	M-1	1.419	0.021	1.363	0.022
	M-2	1.301	0.033		
	M-3	1.369	0.013		
G5-Ref	M-1	1.983	0.010	2.063	0.009
	M-2	1.996	0.008		
	M-3	2.211	0.0098		
G6	M-1	1.682	0.0001	1.626	0.0002
	M-2	1.594	0.0003		
	M-3	1.603	0.00025		

Table 10
Thermal conductivity results obtained with TEMPOS for the White Cement.

Nomenclature	Measurement	Thermal Conductivity (W/m·K)	Deviation	Thermal Conductivity Average (W/m·K)	Deviation Average
W1	M-1	1.593	0.003	1.596	0.003
	M-2	1.586	0.005		
	M-3	1.610	0.002		
W2	M-1	1.633	0.0007	1.621	0.0009
	M-2	1.549	0.0009		
	M-3	1.682	0.001		
W3	M-1	1.879	0.0002	1.918	0.0002
	M-2	1.967	0.0004		
	M-3	1.907	0.0001		
W4	M-1	1.739	0.0008	1.725	0.0007
	M-2	1.589	0.0009		
	M-3	1.846	0.0005		
W5-Ref	M-1	1.983	0.0007	1.774	0.009
	M-2	1.785	0.0009		
	M-3	1.554	0.001		
W6	M-1	1.959	0.002	2.103	0.001
	M-2	2.106	0.0005		
	M-3	2.243	0.0009		

dosages. On the one hand, WhPig hardly reduce the temperature of mortars, especially in the case of using WhC due to its high percentage of whiteness. Nevertheless, BlPig allow higher temperatures to be reached in the mortar samples. Thus, the surface temperature increases in those samples with the highest amount of BlPig. Specifically, it increases 32% with respect to the reference sample temperature in the case of GrC and 55% when using WhC. The rest of the samples containing BlPig also achieve a higher temperature rise, although the specific proportionality corresponding to the amount of pigment cannot be determined due to the mixing of two opposite colour pigments. In this sense, future work will focus on optimising similar pigments in different proportions in order to estimate the saturation point beyond which there is no significant temperature increase for an increase in pigment.

The optical reflectivity test showed a higher reflected radiation in the VIS and NIR for mortars with WhPig, i.e., mortars with BlPig have a higher radiation absorption. This behaviour agrees with the results obtained in the thermal analyses described above.

Finally, thermal conductivity tests were carried out in which small differences were found, showing that the effect of the pigments is very slight. Nevertheless, a lower thermal conductivity was found for samples with BlPig corresponding to GrC, while mortars with WhPig corresponding to WhC showed a higher thermal conductivity. This behaviour would help to reinforce the idea that the darker samples allow a higher temperature to be reached and stored while the whiter samples reach a lower temperature and could dissipate it earlier due to the higher thermal conductivity.

The results obtained for thermal behaviour highlight the high influence of the use of pigments, which could be useful for energy efficiency and heat storage functions such as solar chimneys or hot water tanks. Future work will focus on carrying out studies under real solar conditions and testing the effect of this increase in surface temperature on indoor fluids such as air or water.

CRediT authorship contribution statement

Jorge López-Rebollo: Methodology, Investigation, Formal analysis, Writing – original draft, Writing – review & editing. **Susana Del Pozo:** Conceptualization, Investigation, Formal analysis, Writing – review & editing. **Ignacio Martín Nieto:** Investigation, Formal analysis, Writing – review & editing. **Cristina Sáez Blázquez:** Investigation, Formal analysis, Writing – review & editing. **Diego González-Aguilera:** Supervision, Funding acquisition, Writing – review & editing.

Declaration of competing interest

The authors declare that they have no known competing financial interests or personal relationships that could have appeared to influence the work reported in this paper.

Data availability

Data will be made available on request.

Acknowledgements

References

AENOR. UNE-EN 196-1. Methods of testing cement - Part 1: Determination of strength. Madrid, Spain2018.

Badin, G., Ahmad, N., Ali, H.M., 2020. Experimental investigation into the thermal augmentation of pigmented asphalt. Phys. Stat. Mech. Appl. 551, 123974 0378-4371.

Badin, G., Ahmad, N., Ali, H.M., Ahmad, T., Jameel, M.S., 2021. Effect of addition of pigments on thermal characteristics and the resulting performance enhancement of asphalt. Construct. Build. Mater. 302, 124212, 0950-0618.

Basha, S.I., Ali, M.R., Al-Dulaijan, S.U., Maslehuddin, M., 2020. Mechanical and thermal properties of lightweight recycled plastic aggregate concrete. J. Build. Eng. 32, 101710 2352-7102.

Berktas, I., Ghafar, A.N., Fontana, P., Caputcu, A., Menceloglu, Y., Okan, B.S., 2020. Facile synthesis of graphene from waste tire/silica hybrid additives and optimization study for the fabrication of thermally enhanced cement grouts. Molecules 25, 886.

Blázquez, C.S., Martín, A.F., Nieto, I.M., García, P.C., Pérez, L.S.S., Aguilera, D.G., 2017a. Thermal conductivity map of the Avila region (Spain) based on thermal conductivity measurements of different rock and soil samples, 71 0375 Geothermics 65, 60–6505.

Blázquez, C.S., Martín, A.F., Nieto, I.M., García, P.C., Pérez, L.S.S., González-Aguilera, D., 2017b. Analysis and study of different grouting materials in vertical geothermal closed-loop systems. Renew. Energy 114, 1189–1200, 0960-1481.

Bonifazi, G., Palmieri, R., Serranti, S., 2018. Evaluation of attached mortar on recycled concrete aggregates by hyperspectral imaging. Construct. Build. Mater. 169, 835-42 0950-618.

Carslaw, H.S., Jaeger, J.C., 1959. Conduction of Heat in Solids. Clarendon press.

Cellat, K., Tezcan, F., Kardaş, G., Paksoy, H., 2019. Comprehensive investigation of butyl stearate as a multifunctional smart concrete additive for energy-efficient buildings. Int. J. Energy Res. 43, 7146, 58 0363-907X.

Codd, D.S., Carlson, A., Rees, J., Slocum, A.H., 2010. A low cost high flux solar simulator. Sol. Energy 84, 2202–2212, 0038-092X.

Colarossi, D., Tagliolini, E., Principi, P., Fioretti, R., 2021. Design and validation of an adjustable large-scale solar simulator. Appl. Sci. 11, 1964.

Corinaldesi, V., Mazzoli, A., Moriconi, G., 2011. Mechanical behaviour and thermal conductivity of mortars containing waste rubber particles, 50 0261 Mater. Des. 32, 1646–3069.

Corinaldesi, V., Monosi, S., Ruello, M.L., 2012. Influence of inorganic pigments' addition on the performance of coloured SCC. Construct. Build. Mater. 30, 289–293, 0950-618.

Deilami, K., Kamruzzaman, M., Liu, Y., 2018. Urban heat island effect: a systematic review of spatio-temporal factors, data, methods, and mitigation measures. Int. J. Appl. Earth Obs. Geoinf. 67, 30, 42 0303-2434.

Del Pozo, S., Herrero-Pascual, J., Felipe-García, B., Hernández-López, D., Rodríguez-Gonzálvez, P., González-Aguilera, D., 2016. Multispectral radiometric analysis of façades to detect pathologies from active and passive remote sensing. Rem. Sens. 8, 80 2072-4292.

Divya, S., Das, S., 2021. New red pigments based on Li3AlMnO5 for NIR reflective cool coatings. Ceram. Int. 47, 30381, 30390 0272-8842.

Florian L. Interlacing the Evaluation of Mechanical Properties of Mortar Cement with Near-Infrared Spectroscopy Using Multivariate Data Analysis 2022.

George, M., Pandey, A.K., Abd Rahim, N., Tyagi, V.V., Shahabuddin, S., Saidur, R., 2020. A novel polyaniline (PANI)/paraffin wax nano composite phase change material: superior transition heat storage capacity, thermal conductivity and thermal reliability. Sol. Energy 204, 448–458, 0038-092X.

Gupta, A., Naval, S., 2020. A critical literature on auto repair behaviour of bio concrete. LIAST [International Journal of Advanced Science and Technology 29, 2043–2047.

Healy, J.J., De Groot, J.J., Kestin, J., 1976. The theory of the transient hot-wire method for measuring thermal conductivity, 408 0378 Phys. B+C 82, 392–4363.

Heerah, M.Z., Galobardes, I., Dawson, G., 2021. Characterisation and control of cementitious mixes with colour pigment admixtures. Case Stud. Constr. Mater. 15 e00571 2214-5095.

Lizaranzu, M., Lario, A., Chiminelli, A., Amenabar, I., 2015. Non-destructive testing of composite materials by means of active thermography-based tools, 20 1350 Infrared Phys. Technol. 71, 113–4495.

Lockmuller, N., Redgrove, J., Kubicar, L., 2004. Measurement of thermal conductivity with the needle probe, 38 0018 High. Temp. - High. Press. 36, 127–1544.

Maldague, X., 2001. Theory and Practice of Infrared Technology for Nondestructive Testing.

Matias, G., Torres, I., Rei, F., Gomes, F., 2020. Analysis of the functional performance of different mortars with incorporated residues. J. Build. Eng. 29, 101150 2352-7102.

Meng, Q., Wang, Y., Zhang, L., 2011. Irradiance characteristics and optimization design of a large-scale solar simulator. Sol. Energy 85, 1758–1767, 0038-092X.

Nocuń-Wczelik, W., Stolarska, K., 2019. Calorimetry in the studies of by-pass cement kiln dust as an additive to the calcium aluminate cement. J. Therm. Anal. Calorim. 138, 4561, 9 1588-2926.

PublicLab. Ultraviolet spectrometry. https://publiclab.org/wiki/uv-spectrometry. (Accessed 3 July 2022).

Puesan, C.-W.P., Mestre, J.-L.Z., 2017. Technical evaluation of an improved paint coating with NIR pigments designed to reduce thermal discomfort caused by incident solar radiation: application in the Caribbean area, 79 1876 Energy Proc. 115, 463–6102.

Reuben, N.O., Perez, P.A., Josiah, M.A., Abdul, M.M., 2018. Towards enhancing sustainable reuse of pre-treated drill cuttings for construction purposes by near-infrared analysis: a review, 39 2141 J. Civ. Eng. Construct. Technol. 9, 19–634.

Rodriguez-Gonzalvez, P., Gonzalez-Aguilera, D., Gonzalez-Jorge, H., Hernandez-Lopez, D., 2015. Low-cost reflectance-based method for the radiometric calibration of kinect 2. IEEE Sensor. J. 16, 1975, 1985 530-437X.

Rosati, A., Fedel, M., Rossi, S., 2021. NIR reflective pigments for cool roof applications: a comprehensive review. J. Clean. Prod. 313, 127826, 0959-6526.

Sánchez-Aparicio, L.J., Del Pozo, S., Ramos, L.F., Arce, A., Fernandes, F.M., 2018. Heritage site preservation with combined radiometric and geometric analysis of TLS data, 39 0926 Autom. ConStruct. 85, 24–5805.

Santos, B.O., Valença, J., Júlio, E., 2018. Classification of Biological Colonization on Concrete Surfaces Using False Colour HSV Images, Including Near-Infrared Information. SPIE, pp. 13–22.

Sukontasukkul, P., Uthaichotirat, P., Sangpet, T., Sisomphon, K., Newlands, M., Siripanichgorn, A., et al., 2019. Thermal properties of lightweight concrete incorporating high contents of phase change materials. Construct. Build. Mater. 207, 431–439, 0950-618.

Tawfik, M., Tonnellier, X., Sansom, C., 2018. Light source selection for a solar simulator for thermal applications: a review. Renew. Sustain. Energy Rev. 90, 802, 13 1364-0321.

Teijón-López-Zuazo, E., López-Rebollo, J., Sánchez-Aparicio, L.J., Garcia-Martín, R., Gonzalez-Aguilera, D., 2021. Compression and strain predictive models in non-structural recycled concretes made from construction and demolition wastes. Materials 14, 3177.

Thejus, P.K., Krishnapriya, K.V., Nishanth, K.G., 2021. NIR reflective, anticorrosive magenta pigment for energy saving sustainable building coatings. Sol. Energy 222, 103–114, 0038-092X.

Verian, K.P., Ashraf, W., Cao, Y., 2018. Properties of recycled concrete aggregate and their influence in new concrete production. Resour. Conserv. Recycl. 133, 30, 49 0921-3449.

Watanabe, A., Furukawa, H., Miyamoto, S., Minagawa, H., 2019. Non-destructive chemical analysis of water and chlorine content in cement paste using near-infrared spectroscopy. Construct. Build. Mater. 196, 95, 104 0950-618.

Xaman, J., Vargas-Lopez, R., Gijon-Rivera, M., Zavala-Guillen, I., Jimenez, M.J., Arce, J., 2019. Transient thermal analysis of a solar chimney for buildings with three different types of absorbing materials: copper plate/PCM/concrete wall. Renew. Energy 136, 139–158, 0960-1481.

Yun, T.S., Jeong, Y.J., Han, T.-S., Youm, K.-S., 2013. Evaluation of thermal conductivity for thermally insulated concretes, 32 0378 Energy Build. 61, 125–7788.

CAPÍTULO IV
HORMIGÓN RECICLADO ESTRUCTURAL CON CAPACIDAD TÉRMICA

4.1. Depósito de agua acumulador de calor fabricado a partir de hormigones con áridos reciclados y aditivos pigmentados

En este capítulo IV se incluye el artículo "*Enhancing thermal efficiency in water storage tanks using pigmented recycled concrete*", publicado en la revista *Materials*.

Resumen

Tal y como se ha demostrado en los trabajos anteriores, es posible sustituir los áridos naturales por áridos reciclados para la fabricación de hormigón con capacidad estructural. Del mismo modo, la incorporación de pigmentos permite una mejora de las propiedades térmicas en cuanto a la mayor absorción de radiación solar. Este estudio tratará de aunar el conocimiento y los avances obtenidos en los trabajos previos para obtener un hormigón reciclado con capacidad estructural y propiedades térmicas mejoradas. En este sentido, el **objetivo** de este trabajo es fabricar y validar una solución de depósito de agua acumulador de calor a partir de hormigones reciclados y aditivos pigmentados. Por un lado, se tratará de contribuir a la circularidad de los materiales de construcción al incorporar rechazos de prefabricado en sustitución de áridos naturales. Por otro lado, se pretende promover el ahorro energético y de emisiones al mejorar el rendimiento térmico gracias a la mejora térmica que el pigmento colorante proporciona a los elementos de hormigón, cuya principal aplicación es la acumulación de calor para industrias que requieran agua caliente.

La **metodología** seguida consistió en la evaluación del comportamiento mecánico y térmico de hormigones fabricados con áridos reciclados procedentes de rechazos de prefabricados de hormigón y aditivos pigmentados. En primer lugar, se llevaron a cabo ensayos mecánicos de tracción, compresión y módulo de elasticidad para evaluar la eficacia del hormigón fabricado con áridos reciclados. A continuación, se llevó a cabo un proceso de evaluación del comportamiento térmico del hormigón con el fin de optimizar el pigmento a emplear como aditivo. Para ello, se fabricaron muestras con porcentajes de pigmento que van desde el 0% (hormigón de referencia) hasta un máximo del 10%. Estas muestras fueron también sometidas a ensayos de laboratorio para determinar la conductividad y resistividad térmica.

La optimización del pigmento se llevó a cabo bajo un enfoque de termografía activa similar al propuesto en los trabajos anteriores. Un simulador solar fue fabricado ad-hoc y caracterizado para someter a las muestras a ciclos de calentamiento y enfriamiento, monitorizando su comportamiento mediante una cámara termográfica. Con el fin de determinar cuál de las muestras permitía una mayor absorción de la radiación solar, se

evaluó la evolución temporal de la temperatura superficial en cada una de las muestras durante la fase de calentamiento.

Dos prototipos de depósitos de agua de dimensiones reducidas (50×50×50 cm) fueron fabricados con el hormigón reciclado caracterizado: uno de ellos como referencia sin pigmento y otro como solución con el porcentaje de pigmento determinado como óptimo. Para comparar ambos depósitos y validar la solución, se expusieron a condiciones ambientales reales durante un mes, monitorizando la temperatura ambiental, la temperatura superficial y la temperatura del agua en el interior de ambos depósitos.

Los **resultados** mostraron que el hormigón reciclado fabricado con áridos procedentes de rechazos de prefabricados de hormigón es adecuado para su uso estructural y puede ser utilizado para la fabricación de los depósitos propuestos. Las muestras fabricadas con este hormigón y diferentes concentraciones de pigmento presentaron unos resultados de conductividad y resistividad térmica variables debido a la heterogeneidad de la composición de los agregados reciclados, pero se demostró que el pigmento no tuvo un efecto significativo en estas propiedades. Esto permite afirmar que las mejoras térmicas del hormigón pigmentado son consecuencia únicamente de la absorción de radiación solar.

Los ensayos de calentamiento para la optimización del pigmento mostraron una mayor temperatura a medida que la concentración de pigmento era aumentada. A partir del método de descenso de gradiente, se determinó que la muestra con el 1% de pigmento era la solución más adecuada para fabricar los depósitos.

En cuanto a los depósitos de agua fabricados, los resultados mostraron una diferencia notable en cuanto a la temperatura superficial, siendo hasta 8.2 ℃ mayor para la solución optimizada. La temperatura del agua en el interior también fue notablemente más alta, especialmente durante las horas de sol, con un aumento medio de 1.98 ℃. Esto fue debido a que no toda la radiación absorbida por el material fue transferida al agua debido a su alto calor específico y la baja conductividad térmica del hormigón.

Por último, se llevó a cabo un estudio económico y ambiental considerando el coste para las industrias que requieren de procesos de calentamiento de agua. Los ahorros asociados al estudio de un mes indicaron un ahorro potencial de 8625 kWh, lo que a su vez supone un considerable ahorro económico en función del tipo de energía empleado.

Las principales **conclusiones** del trabajo resaltan las ventajas fabricar hormigones reciclados a partir de rechazos de prefabricados de hormigón, así como de emplear pigmentos para mejorar el rendimiento térmico de los mismos. La investigación tiene un doble beneficio: la reducción de residuos en la industria de la construcción a través del fomento del uso de materiales reciclados, y la mejora de la competitividad de estos materiales gracias a la mejora de sus propiedades térmicas que permiten ahorros económicos y ambientales para las industrias que dependen de procesos de calentamiento de agua.

Article

Enhancing Thermal Efficiency in Water Storage Tanks Using Pigmented Recycled Concrete

Jorge López-Rebollo *[iD], Ignacio Martín Nieto [iD], Cristina Sáez Blázquez [iD], Susana Del Pozo [iD] and Diego González-Aguilera *[iD]

Department of Cartographic and Land Engineering, Higher Polytechnic School of Ávila, University of Salamanca, Hornos Caleros, 50, 05003 Ávila, Spain
* Correspondence: jorge_lopez@usal.es (J.L.-R.); daguilera@usal.es (D.G.-A.)

Abstract: The present work investigated the manufacture of elements such as water tanks from recycled concrete for applications where industries require water heating. This proposal leverages precast rejects for recycled concrete and incorporates colouring pigments. It is expected to contribute to the circularity of construction materials (due to the total replacement of natural aggregates by recycled aggregates) as well as to energy and emissions savings, which are attributed to improved thermal performance driven by the thermal behaviour that the coloration pigment gives to the manufactured concrete elements. To assess the efficacy of the proposed solution, on the one hand, mechanical tests were carried out in tensile, compression and modulus of elasticity, which showed a suitable concrete dosage for HA-30 structural concrete. Simultaneously, in search for a material that would increase the internal temperature of the tanks, thermal tests were carried out in a controlled laboratory environment on samples with different percentages of pigment, and an optimum concentration of 1% was obtained. It was also found that the thermal conductivity remained almost unaffected. Finally, two water tank prototypes were manufactured and tested under real environmental conditions: one with the optimised pigment concentration solution and other (the reference tank) without pigment. The results revealed that the colourised tank with the optimal concentration resulted in an average water temperature increase of 2 °C with respect to the reference tank. Finally, the economic and environmental benefits of this temperature increase were studied for industrial processes requiring water heating with a potential saving of 8625 kWh per month.

Keywords: pigmented concrete; recycled concrete; thermographic properties; heat storage; water tank

1. Introduction

With the aim of responding to the devastating effects of climate change, efforts have been focused towards mitigating greenhouse gas (GHG) emissions in all industrial and residential areas characterised by substantial fossil fuel and material consumption. In this context, considering the growing integration of renewable energy sources, the circular economy (CE) paradigm plays an imperative role. The core of CE is the "restorative resource utilization" concept, which seeks to eliminate the wastage of raw materials [1]. This approach not only provides new pathways for resources but also contributes to the effective management of the waste generated in initial activities.

The construction industry stands out as one of the most resource-intensive sectors, accounting for the significant generation of solid waste worldwide [2]. Construction and demolition waste (CDW) comprises different materials, such as bricks, concrete, wood, mortar, tiles or materials left unused during the construction process for external reasons. The recycling and reuse of such waste is favourable for its potential to mitigate pollution and decrease the demand of new natural aggregates, which in turn reduces energy consumption and CO_2 emissions [3,4]. In this sense, the use of recycled concrete has garnered substantial attention across different applications. Given the nature of these compounds, it

is essential to know their mechanical properties and limitations in order to determine their suitability in line with specific sample composition [5–7]. Among the different types of recycled aggregates, prior studies [8,9] have demonstrated the viability of precast concrete in the manufacture of structural elements, providing a sustainable alternative with an adequate performance.

In the quest for environmentally sustainable solutions, the incorporation of other additives into recycled concretes is a common practice. This aims to enhance different mechanical, structural or thermal properties of the base mixture while preserving its fundamental attributes. Depending on the intended application, several elements have been introduced into the concrete mix: paint-based coatings to reduce the temperature of facades and roofs [10]; waste or recycled materials to improve thermal conductivity and increase the thermal performance of buildings [11]; composites or phase change materials to increase the conductivity and improve the compressive strength for building applications [12]; mineral aggregates to improve the self-compaction of concrete at high temperatures [13]; and steel fibres, polypropylene or basalt to improve fracture properties [14,15].

Focusing on improving the thermal performance of concrete compounds, which aligns with the current emphasis on energy efficiency, these additives are designed to increase the energy efficiency of the spaces or structures where the concrete mixture is included. In this context, pigmented mortars emerge as a compelling solution due to their capacity to not only improve thermal characteristics (extending beyond the aesthetic appeal) but also ensure the preservation of the concrete's mechanical properties [16]. The incorporation of pigments into concrete offers advantages compared to alternative options such as paints, owing to their greater durability and environmental attributes. Nevertheless, optimising the pigment dosage is imperative to minimise costs while maximising material performance [17].

Starting from a proper composition of the concrete and the inclusion of pigmented additives, the enhanced properties of the resultant compound can be of great contribution to the optimisation of energy consumption across different applications and sectors [18,19]. Depending on the intended use, these pigments can be strategically employed to either increase or decrease thermal absorption from external sources, which will have a direct impact on the internal environment. Therefore, this approach can lead to reduced cooling or heating requirements for a specific space or element, resulting in substantial cost savings and the derived environmental benefits.

This type of pigmented additive has traditionally been used for aesthetic or colorimetric purposes, such as in the case of heritage restoration [20]. Nevertheless, more recent works have investigated their use to improve some physical or mechanical properties of concrete: de Oliveira et al. pointed out the improvement of compressive strength by adding iron oxide-based inorganic pigments in concentrations of 2–5% [21]; Hatami et. al. improved the properties of coloured self-compacting mortars using intensely coloured nanoparticles [22]; Lermen et al. studied the substitution of sands with pigments from acid mine drainage as a sustainable alternative in civil construction [23]. Nevertheless, despite their potential in thermal applications, their use is very limited, so a comprehensive exploration of their influence on the thermal behaviour is imperative. To address this, the present research proposes a multidisciplinary investigation encompassing thermal conductivity measurements [24] combined with thermographic analysis [19]. In particular, the active thermography technique, widely used for evaluating a broad spectrum of materials [25,26], is here proposed. To simulate real-world conditions, a solar simulator was used to reproduce the environmental stresses conditions imposed by solar radiation [27].

Based on all the previously stated reasons, this paper aims to develop an innovative solution that enhances the energy and environmental performance attributes of concrete by combining recycled concrete and certain pigments. Specifically, this research pursues the optimisation of concrete pigment dosages to increase the internal temperature of the tanks by absorbing solar radiation. On the one hand, the total replacement of natural aggregates with recycled aggregates represents an economic and environmental saving in terms of

materials and contributes to the circular economy. Furthermore, the heating of water due to the improved material properties saves energy and emissions in industrial applications that require water heating. In pursuit of this objective, concrete samples with different pigment dosages are manufactured in laboratory conditions. These samples are subjected to rigorous examination of their thermal behaviour during controlled heating facilitated by a low-cost solar simulator purpose-built with this aim. After identifying the optimal percentage of pigment for this purpose, a prototype water tank is built with this pigment dosage, and the thermal dynamics of the enclosed water is monitored under different external environmental conditions.

The manuscript is organised into the following sections. Section 2 describes the methodology and materials used for the testing and characterisation of the optimised pigmented concrete solution. Section 3 addresses the experimental laboratory tests performed on the pigmented concrete specimens as well as on the final water tanks. In Section 4, the optimised solution is revealed considering both economic and environmental aspects. And, finally, Section 5 briefly summarises the main findings of the research and outlines the expected future work.

2. Materials and Methods

To fulfil the objectives of this study, a systematic and rigorous methodology (Figure 1) was developed. This methodology has been designed to safeguard the integrity of concrete samples manufactured with varying pigment dosages, assuring their mechanical and structural stability. Additionally, it guarantees precision in the subsequent analyses, encompassing the thermal evaluation as well as the assessment of economic and environmental aspects associated with the water tank construction employing the optimal pigment dosage.
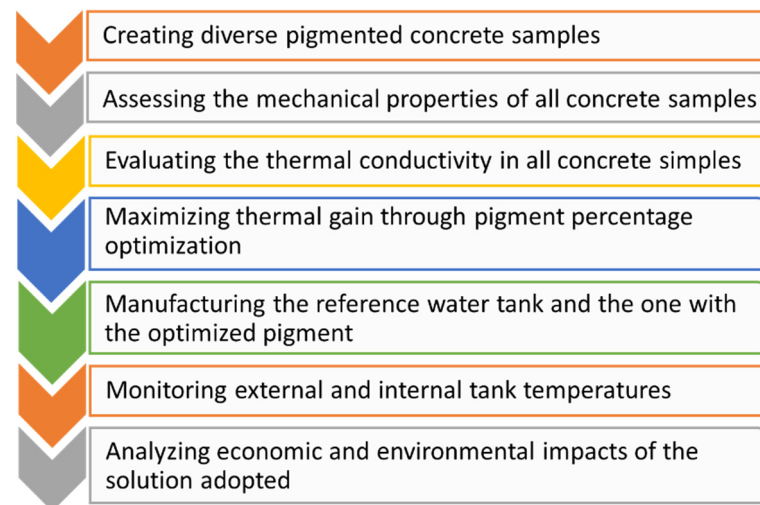
Figure 1. Workflow of the methodology and analysis performed.

2.1. Pigmented Concrete Samples

This first phase focuses on the incorporation of pigments into the concrete manufacturing process with the goal of enhancing its thermal properties. Given the intended application of the proposed concrete tanks, the use of structural concrete, typically designed to withstand compressive stresses exceeding 25 MPa after 28 days of curing, is required [28]. Such concrete is generally composed of natural siliceous aggregates (both coarse and fine), Portland cement, and water. Nevertheless, the present research introduces a novel approach by substituting natural aggregates with recycled aggregates to promote environmental sustainability. These recycled aggregates come from rejected precast concrete elements, including concrete blocks, kerbs, and pipes that do not meet the minimum quality standards for market placement, which is usually due to production accidents or other factors. In this case, the recycled aggregates come from the precast concrete plant in

Toro (Zamora, Spain), and they have been crushed and filtered through a 40 mm sieve in order to ensure proper sizing. Notably, the study employs a unified approach, replacing all the natural aggregates (both coarse and fine) with recycled aggregates.

Taking into account the origin of the aggregates, an exhaustive characterisation of the aggregates was not necessary. As they had already been used in the production of concrete, it was assumed that their shape, resistance to fragmentation, cleanliness and chemical composition met the quality standards. A particle size analysis was carried out to compare the particle size with the Fuller method. The particle size of the recycled aggregates corresponded to the ideal sizes, except between 2 and 1 mm, where there is a slight deviation between 6 and 14%. Nevertheless, these sizes have the least impact on the compactness and strength of the concrete, which allows these aggregates to be considered in the production of structural concrete.

The binder used in this case was a white cement of type BL I/B-LL 42.5 R [29], which is known for achieving a compressive strength of more than 20 MPa after two days and a compressive strength ranging from 42.5 to 62.5 MPa after 28 days. To provide a greater contrast with the pigmented mixtures, white cement with a whiteness content exceeding 85%, due to a very low content of metal oxides, was chosen.

Regarding the pigment, a black pigment HobbyColor by Europigments (Barcelona, Spain) was used. Taking into account that the purpose of the pigmentation is the highest heat accumulation, the black colour was chosen for a higher absorption of solar radiation. This synthetic pigment, composed of metal oxides, is inorganic and insoluble in water. The pigment has a composition of over 90% Fe_2O_3 with an average density of 4.60 g/cm^3 and a predominant particle size of 0.15 microns. Unlike other coatings such as paints, this type of pigment exhibits resistance to alkalis and remains unaltered when exposed to sunlight or other atmospheric agents [30].

Consistency in concrete dosage was ensured throughout the study, encompassing mechanical tests, pigmented concrete formulations, and final manufactured tanks. Specifically, for every 100 kg of all-in-one aggregates, 30 kg of cement, and 16 L of water were added, yielding a water–cement ratio of 0.53. The water used for all the concrete manufacturing was non-aggressive water with a pH > 5, which is in accordance with the durability requirements of the standard used [28] and measured according to the Spanish UNE 83952 [31].

2.2. Mechanical Properties Characterisation

With the aim of analysing the suitability of concrete incorporating recycled aggregates for the construction of the test water tanks, a mechanical characterisation was carried out. Specifically, test were carried out to obtain compressive strength in accordance with the Spanish UNE-EN 12390-3 guideline [32], indirect tensile strength in accordance with UNE-EN 12390-6 [33], and modulus of elasticity in accordance with UNE-EN 12390-13 [34]. A Servosis electromechanical testing machine equipped with a 1500 kN load cell and corresponding compression platens was used for these tests.

Cylindrical specimens, with a diameter of 150 mm and a height of 300 mm, were manufactured in accordance with the Spanish UNE-EN 12390-2 guideline [35]. The specimens were kept in their moulds for 24 h under controlled conditions of 20 ± 5 °C. Subsequently, moulds were removed, and the specimens were transferred to a humid chamber maintained at a temperature of 20 ± 2 °C and a relative humidity exceeding 95% throughout the 28-day curing period.

It is noteworthy that for the mechanical tests, the concrete was manufactured without the inclusion of any pigment. Since the pigment percentage in all cases was equal to or lower than 10%, it was determined that the addition of pigment would not affect the concrete´s mechanical properties, as demonstrated in previous research [17].

2.3. Thermal Conductivity Test

Since the thermal performance of the material is to be analysed, it was decided to include the measurement of the thermal conductivity of the different samples prepared

with different pigment concentrations. A significant variation of this parameter is not expected, but it is still considered interesting to know its behaviour, since it has been observed that this parameter varies considerably depending on the additive added, with significant changes at different dosages, even if the densities are kept similar [36,37].

In order to find out the thermal conductivity of the different manufactured mixtures, the transient line-source model [38] was selected as the theoretical substrate for the conducted test. This approach establishes an automated protocol to measure the heat dissipation provided by a linear source within a medium where thermal conductivity needs to be known. The temperature during the process was monitored, and the sample´s thermal conductivity was obtained using Equation (1):

$$k = \frac{q}{m_3} \tag{1}$$

where k is the thermal conductivity, q signifies the heat flow and m_3 is a constant derived in the process of measuring the evolution of temperature according to this model [39]:

Heating cycle (Equation (2)):

$$T = m_0 + m_2 t + m_3 \ln t \tag{2}$$

Cooling cycle (Equation (3)):

$$T = m_1 + m_2 t + m_3 \ln \frac{t}{t - t_h} \tag{3}$$

Here, m_0 and m_1 are the initial temperatures of the corresponding cycle, m_2 is the rate of temperature variation, and m_3 is the slope of the line resulting from plotting the variation in temperature against its logarithm.

For the thermal conductivity measurements, the TEMPUS model analyser from the company DECAGON DEVICES (Pullman, WA, USA) [40] (Figure 2), which complies with standardisation standards such as ISO 9000:2008 [41], ASTM D5334 [42], and IEEE 442 [43], was employed to ensure the rigour and reliability of the results. To connect the measurement and control device with the samples, the RK-3 sensor has been chosen. This sensor, measuring 60 mm in length and 3.9 mm in width at its widest point, requires the creation of corresponding drill holes in the samples for insertion. To ensure optimal thermal contact between the samples and the sensor, a mixture of diamond powder with thermal grease was used. The sensor operates within a conductivity range of 0.1 to 6 W/(m·K) and a precision of ±10%.
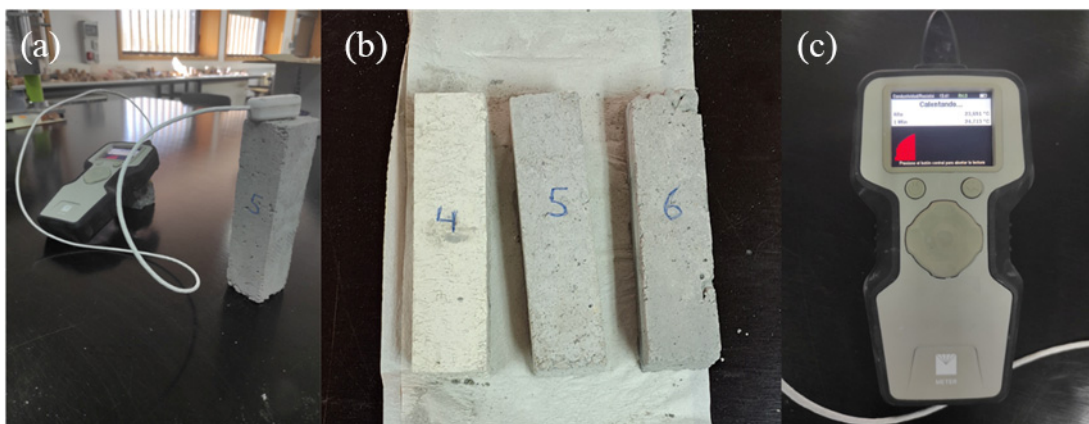
Figure 2. (**a**) Ongoing measuring process, (**b**) samples 4 to 6, (**c**) Decagon device recording the heating cycle.

The measurements were conducted on 9 different samples, prepared as described in the correspondent Section 3.2, under constant ambient conditions at 22 °C. To minimise errors and significant deviations, the sensor was calibrated prior to each sample measurement, and a sufficient time interval between each of the 3 different measurements performed was ensured to achieve thermal equilibrium with the environment.

2.4. Maximising Thermal Gain through Pigment Percentage Optimisation

To optimise the appropriate pigment dosage, thermal tests were conducted, involving the exposure of different pigment concentrations to control heating using a solar simulator. The thermal response of these mixtures was analysed with a thermographic camera. The heating caused by the solar simulator and the absorption of solar radiation were monitored to compare the temperature reached by each of the samples with different percentages of pigment. Optimisation was carried out using the gradient descent method. This method is based on analysing the magnitude of the temperature increments to improve convergence to the optimal solution. In this case, the highest temperature increase was sought for the lowest pigment percentage increase.

In total, 9 different pigment dosages were investigated taking into account the maximum amount recommended by the manufacturer (10%) (Figure 3): an initial reference sample devoid of pigment, and incremental dosages comprising 0.5%, 1%, 2%, 3%, 4%, 5%, 7% and 10% pigment relative to the cement content. Smaller increments were considered for lower percentages and larger increments were considered for higher percentages, as the greatest colour change occurs at the beginning until saturation. The dimensions of the samples were $100 \times 100 \times 50$ mm to maximise the heated surface area, ensuring uniform and consistent testing conditions.

Figure 3. Samples for assessing the optimisation of pigment concentrations through thermal testing.

Monitoring the thermal behaviour of the 9 specimens involved the utilisation of specific equipment. Central to this process was an FLIR T540 (Wilsonville, OR, USA) thermographic camera (Figure 3), equipped with a 42° lens and an integrated RGB sensor, capable of capturing 30 frames per second. This camera offers a Thermal Infrared (TIR) resolution of 464×348 pixels and 5-megapixel visible (VIS) spectrum resolution. Additionally, it incorporates a laser sensor for pre-acquisition distance measurement, facilitating autofocus. Notably, the camera has a remarkable thermal sensitivity of less than 30 m·K at 30 °C, and it is calibrated for a temperature range from −20 to 120 °C. The FLIR software was

used to manage the image acquisition, configure test parameters, control environmental conditions, and establish image capture protocols [11].

In the pursuit of replicating real-world environmental conditions for the concrete specimens under examination, a cost-effective solar simulator was custom-designed and employed. This setup allowed for the precise control of heat application to the specimens using an integrated lighting system. Consequently, this setup allowed to systematically monitor their subsequent heating and cooling phases by combining the thermographic camera with the solar simulator.

The light source of the solar simulator (Figure 4) comprises three metal halide bulbs embedded in a prismatic aluminium structure with dimensions of 400×400 mm and a height of 700 mm. The design concentrates the lighting on the specimen. Specifically, three Philips Master HPI-T Plus 400W/645 E40 1SL/12 bulbs by Philips (Amsterdam, The Netherlands) [44] were used in conjunction with a ballast for precise regulation of arc current and voltage. This configuration was set after conducting a thorough lighting characterisation test [45], conclusively demonstrating that the stability and performance of this solar simulator were significantly enhanced when three bulbs were employed, as opposed to one or two. Additionally, the test confirmed the necessity of allowing a minimum of 5 min for light stabilisation to attain the maximum illuminance output from the cost-effective solar simulator. A spectrophotometer and a pyranometer were used for photometric and radiometric characterisation. According to the characterisation carried out, the output flux of the solar simulator was measured to be 270 W/m^2 with an illuminance of 20,100 lx in the area where the samples were placed.
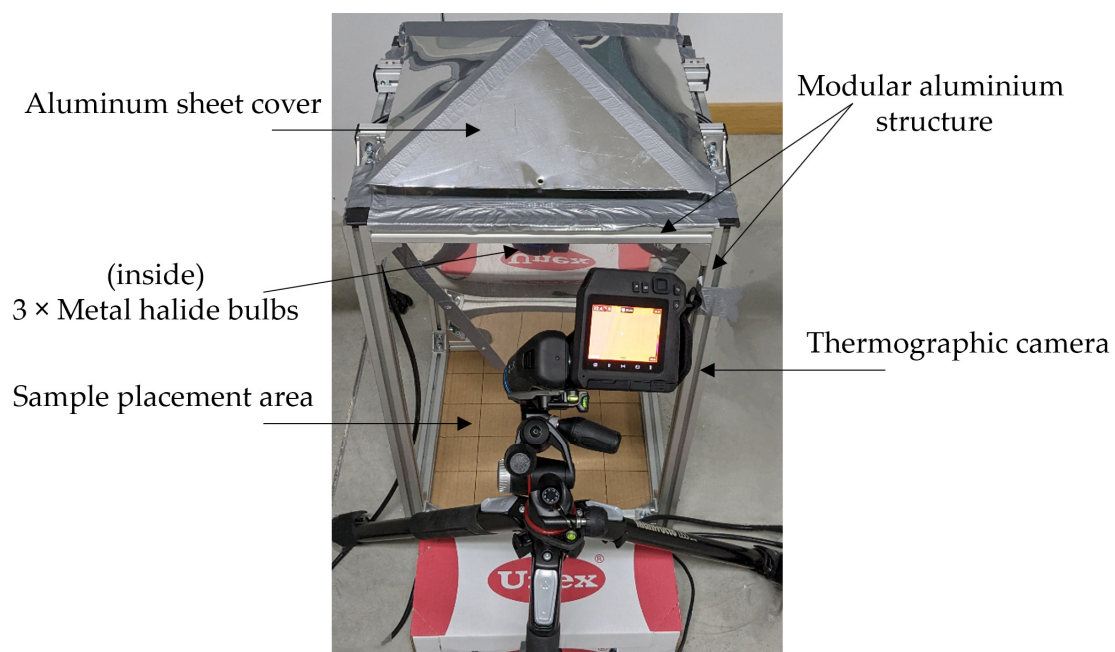
Figure 4. Temperature monitoring system consisting of a solar simulator and a thermographic camera.

Prior to the initiation of the heating test, samples were kept isolated at a constant temperature of 22 °C, ensuring uniform initial conditions for each of the samples.

According to the specifications of the solar simulator, the device was powered up 10 min before placing the samples to achieve a stable illumination and spectral power distribution. Subsequently, samples were positioned at the centre of the incident area of the solar simulator, maintaining a vertical orientation at a distance of 50 cm. To minimise distortion, the thermographic camera was placed at the same distance with the least possible inclination.

The heating test started upon sample placement, and the thermographic image acquisition was initiated at a rate of 1 fps. The heating phase was maintained for 20 min, after which the solar simulator was turned off. Image acquisition was continued for an additional 40 min to capture the cooling phase, which was primarily driven by natural convection. It should be noted that despite efforts to maintain constant ambient temperature, heating by the solar simulator can induce slight alterations and oscillations during the cooling phase.

2.5. Manufacturing of the Water Tanks

Two prototypes of recycled concrete tanks were manufactured to carry out the experimental validation in real conditions. Although they were manufactured and subjected to real environmental conditions, a smaller scale than the industrial scale was used due to the limitations of the material and the study. Despite the complexity of direct scaling or extrapolation of results, the construction of two tanks of similar size will allow the comparative study that is the objective of this research.

The tank manufacturing process encompassed several critical stages conducted within a controlled laboratory setting. The initial phase was the design and warehouse planning, where attention was given to tank external dimensions ($500 \times 500 \times 500$ mm with a 50 mm thickness), shape, and the necessary rebar reinforcements. Notably, a steel grating reinforcement was devised for both the tank base and sides (Figure 5a).
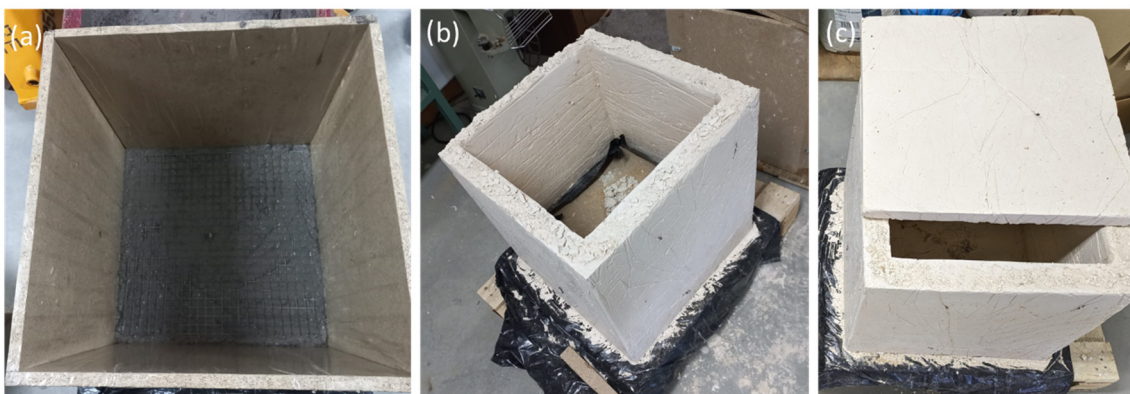
Figure 5. Manufacturing of tanks. (**a**) Formwork and rebar on the base, (**b**) finished tank in the absence of removing the base formwork piece, and (**c**) final reference tank with its lid.

Following the design phase, custom-cut wooden planks were employed to construct precision formwork moulds, integrating rebar reinforcements (Figure 5a). Subsequently, the concrete mixture was meticulously prepared using a concrete mixer, sequentially adding its components: water, cement, and pigment (only for the pigmented tank), which was followed by the introduction of recycled aggregates.

To ensure uniformity in the mixture, the concrete was carefully poured into the formwork, which was then subjected to vibration and compaction measures to mitigate air bubble formation. Subsequently, a well-established 7-day curing period was adhered to, ensuring that the concrete reached its peak strength. Finally, the wooden planks enclosing both the tanks and their lids were carefully removed (Figure 5b), unveiling the final tanks (Figure 5c).

To monitor the thermal behaviour of the water tanks and the influence of the pigmented dosage on the internal water temperature, both tanks were filled and placed in identical ambient conditions. Specifically, tanks were placed on an outdoor terrace at the roof of a building, maintaining a distance of 1.5 m to prevent casting of shadows (Figure 6). They were then filled with water, while water temperature thermometers were strategically positioned to monitor the internal water temperature for one month.
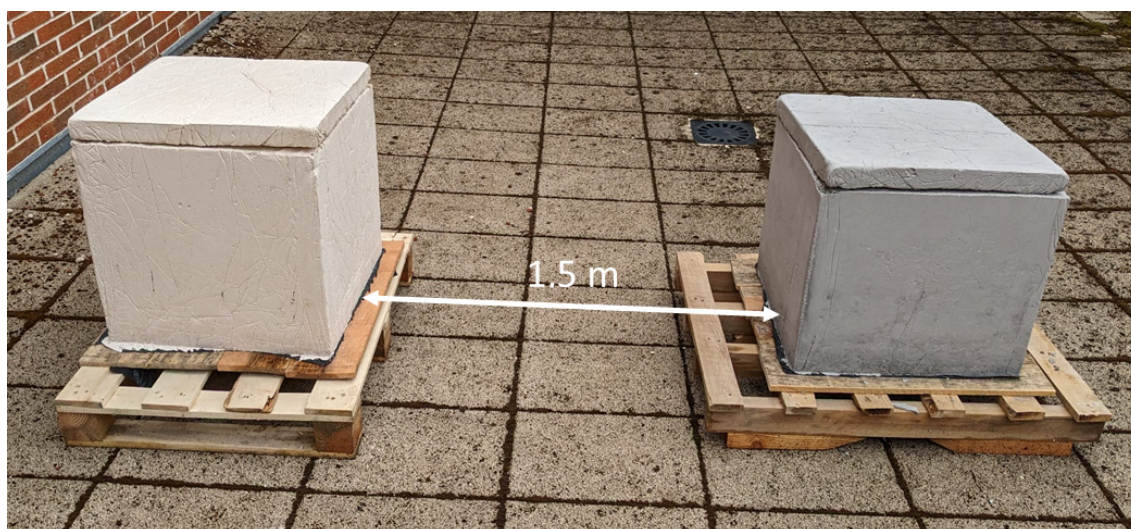
Figure 6. Geometric arrangement of the two tanks on the terrace.

For this purpose, two DS18B20 by Analog Devices (Wilmington, MA, USA) submersible temperature sensors with a functional measuring range of -10 to 85 °C and decimal accuracy in absolute values were used. To minimise this error and ensure greater accuracy in measuring relative temperature increases, the instruments were calibrated to the same temperature prior to immersion. In addition, ambient temperature and humidity sensors were placed between the two tanks to monitor the surrounding environmental conditions. To ensure seamless data collection, all sensors were interconnected by sending real-time data at a 5 min interval through a LoRaWAN Gateway. In addition, a Grafana 10.0.0 platform was configured to visualise and manage the acquired data.

In addition to the water temperature monitoring, the surface temperature of the tanks was also monitored. For this purpose, thermographic images were taken with the thermographic camera described in Section 2.4. Given the time of the year in which the tests were performed and the slight inclination of the sun's rays, it was established that the upper surface of the tank received the most sunlight exposure. Thus, vertical images were taken from a height of 1 m for each of the tanks. This capture process spanned 12 h with an image recorded every 40 min.

3. Experimental Results

3.1. Mechanical Properties

A total of 20 samples were subjected to mechanical tests. Ten of them were used to determine their compressive strength; following the guideline outlined in UNE-EN 12390-3 [32], the specimens were centred in the plates, and the test speed was set at 0.6 ± 0.2 MPa/s. Five of them were used to determine the indirect tensile strength; following the guideline UNE-EN 12390-6 [33], the specimens were placed in a horizontal position, applying a loading rate of 0.6 ± 0.2 MPa/s in a thin strip along their entire length. The other five samples were used to determine the secant modulus of elasticity in compression; following the guideline UNE-EN 12390-13 [34], three loading cycles were applied at a rate of 0.6 ± 0.2 MPa/s, ranging from 10% to one third of the compressive strength.

Once the mechanical properties was obtained for each specimen, essential statistical parameters, including the mean value, standard deviation, coefficient of variation to measure dispersion expressed as a percentage, and maximum and minimum values, were calculated. These results are presented in Table 1.

Table 1. Results of the mechanical characterisation.

Property	Mean	STD	CoV (%)	Minimum	Maximum
f_c	38.5	3.87	10.0	29.1	43.5
f_{ti}	2.8	0.3	11.2	2.5	3.1
E	27,615.5	4562.0	16.5	21,179.9	36,816.0

f_c = Compressive strength (MPa). f_{ti} = Indirect tensile strength (MPa). E = Secant modulus of elasticity in compression (MPa).

The tests yielded satisfactory results to consider the manufactured concrete as a structural concrete, since all the values were above 25 MPa. Furthermore, considering that the concrete was made of recycled aggregates, a coefficient of variation of about 10% was observed for the compressive and indirect tensile strength and around 16.5% was observed for the modulus of elasticity. This value can be considered acceptable for this particular type of concrete given the greater inherent heterogeneity of recycled aggregates when compared to natural aggregates [7]. Taking into account these results, it can be stated that the concrete can be used for structural purposes, which is classified as HA-30.

3.2. Thermal Conductivity Test

Three separate measurements of thermal conductivity were conducted for each sample. The results obtained for each of them, along with the mean values and the standard deviations, are presented in Table 2.

Table 2. Thermal conductivity results.

Sample	Measure 1	Measure 2	Measure 3	Mean Value	Std. Dev.	*p*-Value
Ref	1.14	1.11	1.14	1.13	0.01	-
0.5%	0.81	0.91	0.76	0.83	0.08	0.0999029
1%	1.41	1.43	1.41	1.41	0.01	0.1364058
2%	1.26	1.08	1.09	1.14	0.10	1.0000000
3%	1.26	1.52	1.47	1.41	0.14	0.1364058
4%	1.38	1.28	1.28	1.31	0.05	0.6234869
5%	1.29	0.99	1.01	1.09	0.17	0.9999902
7%	1.58	1.21	1.23	1.34	0.21	0.4596789
10%	1.43	1.29	1.18	1.30	0.13	0.7054091

Units in W/(m·K).

Upon careful examination of the results, it becomes evident that with the possible exception of sample 2, there was minimal variation in thermal conductivities among the samples, encompassing a range of approximately 0.25 W/(m·K). In general, this level of variance is within the acceptable range the measuring device employed.

To investigate these results further, an ANOVA test was performed to assess whether the incorporation of the pigment changed the thermal conductivity. A *p*-value of 0.00016 was obtained, indicating the existence of significant differences in the overall data. A one-way Tukey test was then performed to compare the results of the reference sample with the other pigmented samples, and the *p*-values obtained are shown in Table 2. These results show that the mean of the reference sample is not significantly different from the other samples (*p*-values > 0.05). The evidence provided by the ANOVA test refers to the fact that the mean of the sample with 0.5% pigment shows a significant difference as it is the sample with the lowest value and its *p*-value is less than 0.05. Considering that the recycled aggregate used to manufacture the concrete can introduce certain heterogeneity to exist in their local composition, we can conclude that the concentration of the additive has a negligible impact on the conductivity measurement.

These findings enable the analysis of the thermal behaviour under standardised conditions for all samples. In this way, any heating or cooling of the material will not be attributed to variations in thermal conductivity but will depend on the radiation absorption caused by the difference in pigment concentration.

3.3. Thermal Behaviour

The heating tests were conducted individually for each of the nine samples ensuring the same initial conditions as previously described.

Although the test considers both heating and cooling phases, the study focused mainly on the heating phase and the maximum temperature increase, as the aim was to find the sample that would enable the highest temperature accumulation.

For this analysis, thermographic images were analysed using a Region of Interest (ROI) covering the entire sample surface. This approach was justified by the uniform illumination provided by the solar simulator, rendering the consideration of edge effects during heating unnecessary [11].

A total of 3600 frames were obtained, 1200 for the 20-min heating phase and 2400 for the 40-min cooling phase. From each frame, the average surface temperature within the selected ROI was extracted to minimise the impact of potential surface irregularities leading to anomalous pixels. Then, the temperature evolution curves were generated, as shown in Figure 7.
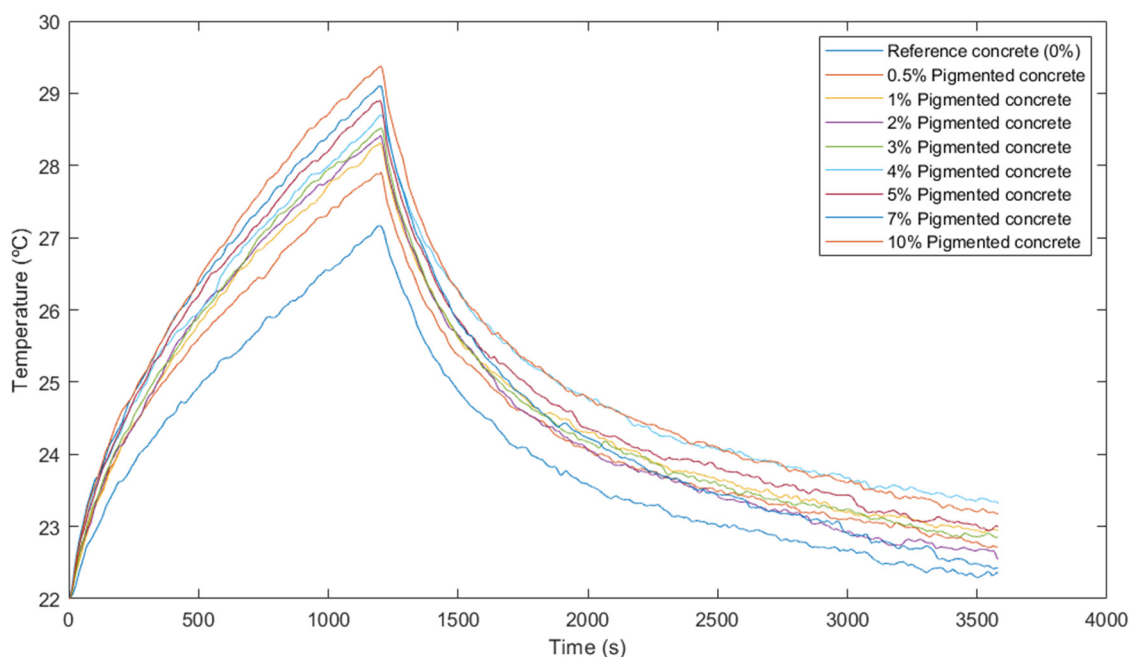
Figure 7. Heating and cooling curves of thermal tests.

Due to the high sensitivity of the camera and the effects introduced by the shutter and the rapid capture frequency, some frames presented variations compared to their neighbours. To overcome this, an attempt was made to smooth the curves by applying a moving average filter.

Once the temperature curves were plotted, the maximum temperature values reached during the heating phase were extracted for each sample, resulting in the temperature increase. Relative increases were then calculated for each sample, representing the temperature difference between a sample and the one with the lowest dosage. These findings are shown in Table 3.

Table 3. Temperature and temperature increase in concrete samples in thermal tests.

Nomenclature	Maximum Temperature	Maximum Temperature Increase	Relative Increase
Ref	27.16	5.16	-
0.5%	27.91	5.91	0.74
1%	28.31	6.31	0.41
2%	28.41	6.41	0.10
3%	28.52	6.52	0.10
4%	28.70	6.70	0.19
5%	28.90	6.90	0.20
7%	29.11	7.11	0.20
10%	29.38	7.38	0.27

Units in °C.

In general, an increase in pigment dosage corresponded to a higher temperature rise at the end of the heating phase. The higher the pigment content, the darker the colour of the concrete. As dark materials have a greater capacity to absorb radiation in the visible and infrared wavelengths, the higher absorbed radiation in blacker concretes results in greater heating, as shown by spectral analysis in previous studies [17].

The results in Table 3 highlight the significant temperature increase observed for the first two dosages. The addition of 0.5% pigment led to a 14.3% increase in temperature rise compared to the non-pigmented dosage, while the 1% dosage improved this temperature increase by 6.9% compared to the previous dosage. Nevertheless, beyond the 1% dosage, the relative temperature increases diminished to less than 2%.

During the cooling phase, the temperature curves were practically similar for all dosages with no significant differences observed. Minor variations may be attributed to causes associated with the measurement process and the nature of cooling, potentially causing slight thermal oscillations caused by natural convection.

Considering the temperatures reached by each dosage and trying to achieve cost and resource efficiency, it was determined that the 1% dosage was the optimal solution to build the water tank.

3.4. Monitoring Water Tanks Temperatures

3.4.1. Monitoring Surface Temperature

A comprehensive analysis of surface temperature was conducted involving the capture of 19 pairs of images from the reference and from the 1% dosage pigmented tank (Figure 8). These image pairs were taken at 40-min intervals over a 12 h period, coinciding with sunrise and sunset.
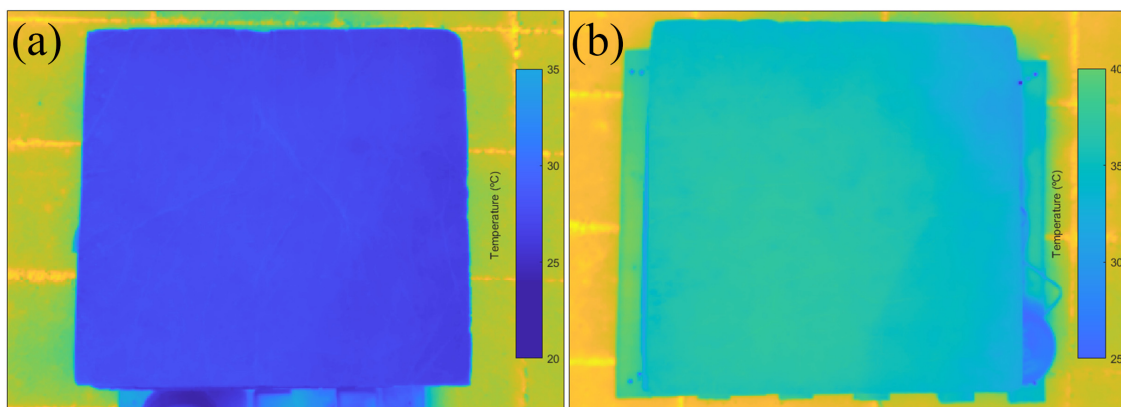
Figure 8. Thermographic images at the time of highest surface temperature for both tanks. (**a**) Reference tank and (**b**) pigmented tank.

For each image, the same procedure as that employed in the previous thermographic analysis was followed. This process involved extracting the average temperature from the ROI corresponding to the upper surface of the tank.

The temperature obtained from these thermographic images was correlated with the ambient temperature at the time of each corresponding capture; its evolution over time is shown graphically in Figure 9.
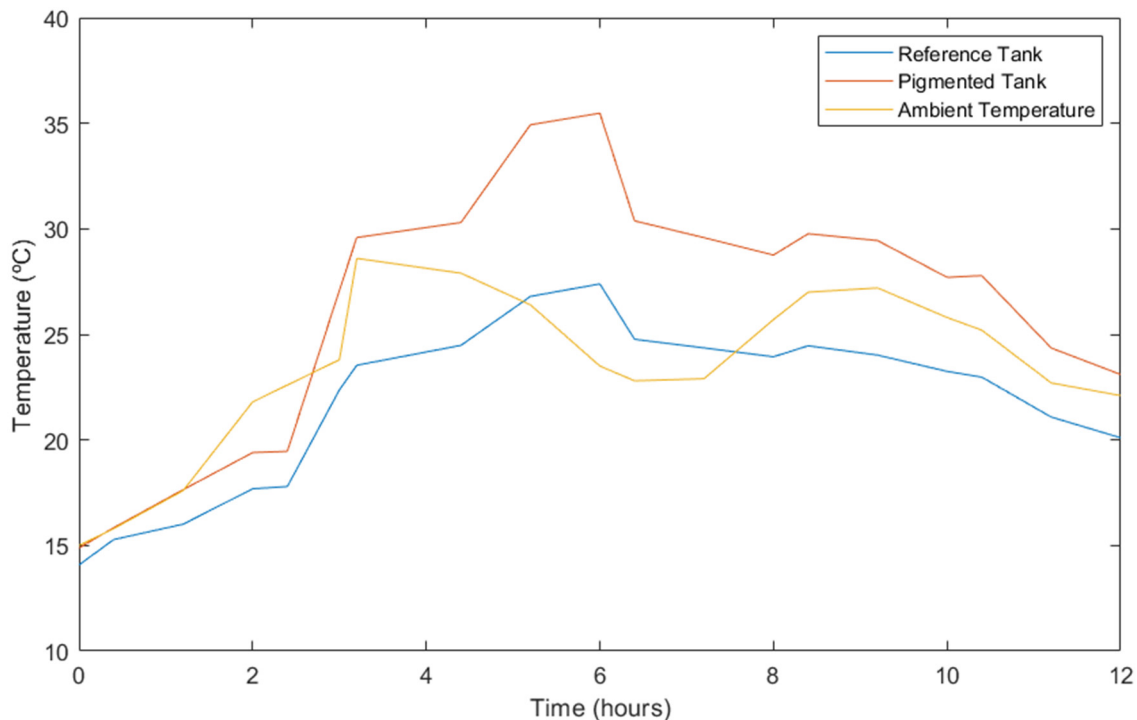
Figure 9. Evolution of tank surface and ambient temperature.

According to Figure 9, a significant disparity exists between the surface temperature of the reference tank and the one pigmented. While the pigmented tank reached a maximum temperature of 35.5 °C, the reference tank only reached 27.3 °C. In other words, there was an 8.2 °C difference in surface temperature. Furthermore, the reference tank did not exceed the maximum ambient temperature.

As mentioned in the previous section, the effect of the pigment is based on the increased absorption of solar radiation, which causes an increase in the temperature of the material, which is in this case measured at the surface. Meanwhile, in the laboratory samples, a temperature difference of 1.15 °C was reached after 20 min of heating between the reference concrete and the concrete with 1% pigment; in real conditions, this difference was seven times higher and was reached after about 6 h. Nevertheless, heating in this case was not homogeneous and constant, as more complex external factors could intervene during this process, such as ambient temperature, wind cooling and the fact that solar radiation is not constant due to the movement of the sun and the possible presence of cloud cover.

Additionally, upon comparing the surface temperature evolution with the corresponding ambient temperature, it was observed that both tanks reached their maximum surface temperatures approximately two hours after the ambient temperature peaks. Furthermore, in the case analysed, a temporal correlation between a decline in ambient temperature during the day and a corresponding decrease in surface temperature was observed. Afterwards, as the ambient temperature raised again, there was a slight increase in surface temperature.

For most of the observation period, the surface temperature of the pigmented tank was above the ambient temperature, while the reference tank consistently registered lower temperatures than the ambient environment. Nevertheless, it should be mentioned that the measurements did not account for cloud cover. The presence of cloud cover at certain

times could potentially influence surface temperature fluctuations, as it may obstruct the sun's rays from heating the tank surfaces.

3.4.2. Monitoring Water Temperature

As part of the research, water temperature measurements were conducted within each of the tanks. For this purpose, the above-described sensors installed in the tanks were used to capture data at 5-min intervals. In this sense, Figure 10 shows a comprehensive depiction of the water temperature measurements taken over a 30-day period in both tanks. This figure also includes records of the ambient temperature, which were collected at the same time intervals.
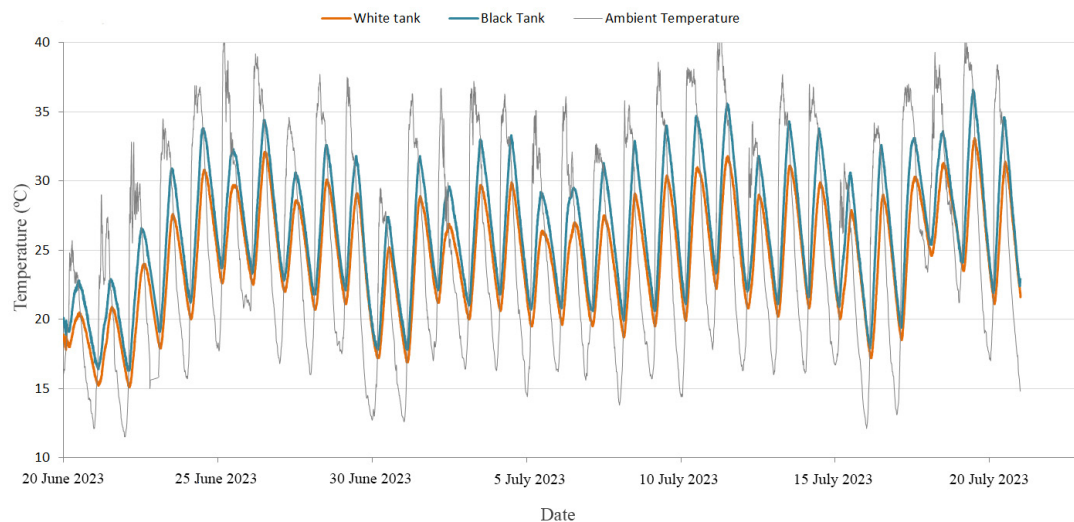
Figure 10. Registers of the water temperature in the developed tanks and the ambient temperature during the established 30-day period.

In addition to the data presented in Figure 10, it is crucial to evaluate the temperature differences observed in the water accumulated in both tanks especially during periods of exposure to solar radiation. Taking into account the solar radiation hours in the study area, the daily average temperature difference during this solar period was calculated. Figure 11 illustrates the temporal evolution of these temperature differentials in water over the 30-day analysis period. Based on these values, the overall average water temperature in the tanks during the considered solar period was 1.98 °C.
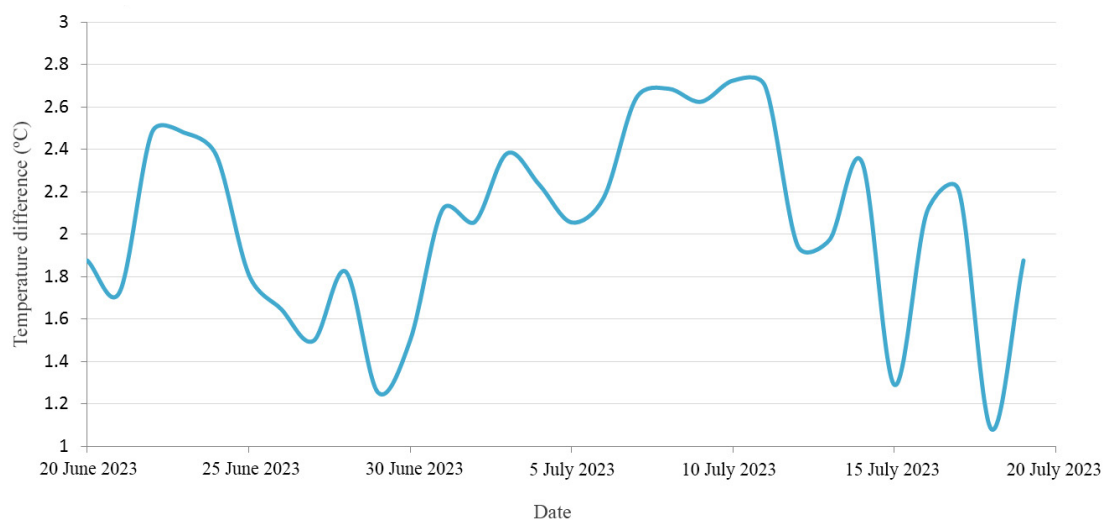
Figure 11. Evolution of the average daily differences in the water temperatures of both tanks.

4. Economic and Environmental Analysis

The results of this research suggests that under specific seasonal climatic conditions, a temperature increase of 1.98 °C can be obtained in the water stored by the tank with the optimal pigmented mixture. This can mean energy savings in thermal processes requiring heated water. For every litre of water, the energy savings needed for these thermal processes can be estimated at 8.05 J. Depending on the method chosen to achieve the temperature increase can lead to varying economic savings.

To quantitatively assess thermal performance and emission reduction, a segment of the agri-food industry was selected as a reference for water consumption in thermal processes. An estimate of approximately 45,000 cubic meters of water annually, evenly distributed over 12 months, can be attributed to a typical plant in the fruit-and-vegetable processing industry [46]. Considering that this work focused on a one-month period, achieving the proposed benefits would require an appropriate scheduling of processes. With a monthly water consumption of 3750 m^3 for medium-temperature thermal processes, the energy savings, based on the initial water temperature difference, amount to 31,066.2 MJ (8625 kWh). The corresponding economic and environmental savings, including CO_2 emissions, considering different energy sources, are shown in Table 4.

Table 4. Prices and monthly savings per energy sources [47].

Energy Source	Price (€/kWh)	Monthly Saving (€)	CO_2 Emissions Saved (kg) *
Electricity	0.18	1552.5	2854.9
Natural gas	0.07	603.8	2173.5
Gasoil	0.09	776.3	2682.3
LPG	0.08	690.0	2190.6

* For the estimation of the emissions saved with electricity as energy source, a standard location has been selected to consult the existing electricity mix and to establish an emissions factor per kWh of energy consumed. The electricity mix used was the conventional Spanish peninsular mix [48].

Due to the changing climatic conditions in central Spain throughout the year, the data in Table 4 cannot be extrapolated to annual yields and emissions savings. Nevertheless, it can be noted that the calculations use an average temperature difference between the two tanks, and with an optimised process schedule, even greater temperature differences can be achieved. Furthermore, the average thermal difference may vary in other months of the year. In this context, future research will encompass longer monitoring periods, spanning one or several years, to analyse temperature evolution in the tanks further.

Considering that the average energy required to produce a conventional concrete element of 1 m^3 is 29.4 kWh [49] and that the energy saved in the reference month is 8625 kWh, the inclusion of an analysis of the energy used to produce the pigment does not seem very relevant. The largest energy consumption in recycled concrete is related to the production of cement, the pigment represents only 1% by weight of this component, and the energy consumption in its production is much lower. It should also be noted that the addition of pigment is a one-off energy cost as opposed to a cumulative saving over time (e.g., over a lifetime of about 25 years).

Regarding the CO_2 emission savings related to water heating, it is essential to highlight the environmental benefits of using recycled aggregates in concrete production. Conventional coarse and fine aggregates are associated with emissions of approximately 54 kg per cubic meter of concrete, while recycled aggregates are linked to emissions of around 30 kg [50]. This signifies a reduction of 24 kg of CO_2 per cubic meter of concrete along with a preservation of 1100 kg/m^3 of natural resources and a reduction in waste destined for landfills.

5. Conclusions

This research focused on investigating the thermal properties of recycled concrete with the aim of optimising the percentage of pigment as an additive to enhance its thermal

performance. Experimental laboratory tests were complemented by tests on prototype water tanks to facilitate the comparison between the optimised solution and a reference one. This research carries a twofold significance. On the one hand, it advances the cause of sustainable construction by promoting the use of recycled materials, thereby contributing to waste reduction in the construction industry. On the other hand, it enhances the competitiveness of these materials, offering economic and environmental savings for industries reliant one water heating processes.

To begin, mechanical characterisation tests determined that concrete composed of recycled aggregates from precast waste can achieve structural properties and can be used for the manufacture of the proposed tanks, as it can be categorised as HA-30 structural concrete. Nine different mixtures were produced using this recycled concrete and black pigment: one as a reference without pigment and the remaining eight incorporating black pigment in percentages ranging from 0.5 to 10%.

Thermal conductivity tests demonstrated that the percentage of pigment had negligible effects on this conductivity properties with minor variations attributed to the heterogeneity of the recycled aggregate composition.

Thermal tests were carried out in the laboratory by monitoring the heating and cooling of samples using a low-cost solar simulator. These tests allowed for the selection of the optimal mixture using the gradient descent method, which was found to be 1% pigment. Under these conditions, the optimal mixture reached a temperature 1.15 °C higher than the reference mixture due to the greater radiation absorbed by the pigmented effect. This solution verified the initial hypothesis of higher heating for the pigmented concrete and also provided the highest temperature increases in relation to the percentage of pigment used.

Subsequently, two prototype water tanks were fabricated, one with the optimised pigment dosage and the other with the reference mixture, and exposed to ambient conditions for one month. Surface temperature monitoring revealed temperature differences of up to 8.2 °C for the optimised solution. The water temperature indoors was also notably higher, especially during sunny hours, with an average increase of 1.98 °C. Although the higher radiation absorption resulted in a significant increase in the surface temperature of the material, this was transferred to the water to a lesser extent due to its high specific heat and the low thermal conductivity of the concrete as well as other external factors such as ambient temperature or wind cooling.

The study also involved an economic and environmental evaluation, considering costs for industries requiring water heating. The savings associated for the one-month study indicated potential savings of 8625 kWh, which can be translated into substantial economic savings depending on the energy typically used.

In conclusion, this research highlighted the advantages of using both waste materials in concrete manufacturing and pigment for the enhancing thermal performance. Future investigations will expand to year-long monitoring and in-depth studies, facilitating comparisons between seasons. These analyses will help demonstrate the practicality of this solution, particularly in cold regions during winter months, where it could prevent water freezing. Additionally, forthcoming research will explore modifications to thermal conductivity properties to facilitate the transfer of higher surface temperatures to the water and will also incorporate numerical simulations to further refine the prototype under real environmental conditions and on an industrial scale.

Institutional Review Board Statement: Not applicable.

References

1. Sharma, R.R. Green management and circular economy for sustainable development. *Vision* **2020**, *24*, 7–8. [CrossRef]
2. Janani, R.; Kaveri, V. A critical literature review on reuse and recycling of construction waste in construction industry. *Mater. Today Proc.* **2021**, *37*, 3077–3081. [CrossRef]
3. Shaikh, F.U.A.; Nath, P.; Hosan, A.; John, M.; Biswas, W.K. Sustainability assessment of recycled aggregates concrete mixes containing industrial by-products. *Mater. Today Sustain.* **2019**, *5*, 100013. [CrossRef]
4. Yazdani, M.; Kabirifar, K.; Frimpong, B.E.; Shariati, M.; Mirmozaffari, M.; Boskabadi, A. Improving construction and demolition waste collection service in an urban area using a simheuristic approach: A case study in Sydney, Australia. *J. Clean. Prod.* **2021**, *280*, 124138. [CrossRef]
5. McNeil, K.; Kang, T.H.K. Recycled concrete aggregates: A review. *Int. J. Concr. Struct. Mater.* **2013**, *7*, 61–69. [CrossRef]
6. Nedeljković, M.; Visser, J.; Šavija, B.; Valcke, S.; Schlangen, E. Use of fine recycled concrete aggregates in concrete: A critical review. *J. Build. Eng.* **2021**, *38*, 102196. [CrossRef]
7. Teijón-López-Zuazo, E.; López-Rebollo, J.; Sánchez-Aparicio, L.J.; Garcia-Martín, R.; Gonzalez-Aguilera, D. Compression and strain predictive models in non-structural recycled concretes made from construction and demolition wastes. *Materials* **2021**, *14*, 3177. [CrossRef]
8. Thomas, C.; Setién, J.; Polanco, J.A. Structural recycled aggregate concrete made with precast wastes. *Constr. Build. Mater.* **2016**, *114*, 536–546. [CrossRef]
9. Zhao, Z.; Courard, L.; Groslambert, S.; Jehin, T.; Leonard, A.; Xiao, J. Use of recycled concrete aggregates from precast block for the production of new building blocks: An industrial scale study. *Resour. Conserv. Recycl.* **2020**, *157*, 104786. [CrossRef]
10. Puesan, C.-W.P.; Mestre, J.-L.Z. Technical evaluation of an improved paint coating with NIR pigments designed to reduce thermal discomfort caused by incident solar radiation: Application in the Caribbean area. *Energy Procedia* **2017**, *115*, 463–479. [CrossRef]
11. López-Rebollo, J.; Villanueva, N.N.; Nieto, I.M.; Blázquez, C.S.; Del Pozo, S.; González-Aguilera, D. Monitoring the thermal contribution of certain mortar additives as a way to optimize the energy performance of buildings. *Sustain. Energy Technol. Assess.* **2023**, *57*, 103268. [CrossRef]
12. Berardi, U.; Gallardo, A.A. Properties of concretes enhanced with phase change materials for building applications. *Energy Build.* **2019**, *199*, 402–414. [CrossRef]
13. AzariJafari, H.; Amiri, M.J.T.; Ashrafian, A.; Rasekh, H.; Barforooshi, M.J.; Berenjian, J. Ternary blended cement: An eco-friendly alternative to improve resistivity of high-performance self-consolidating concrete against elevated temperature. *J. Clean. Prod.* **2019**, *223*, 575–586. [CrossRef]
14. Kazemi, M.; Hajforoush, M.; Talebi, P.K.; Daneshfar, M.; Shokrgozar, A.; Jahandari, S.; Saberian, M.; Li, J. In-situ strength estimation of polypropylene fibre reinforced recycled aggregate concrete using Schmidt rebound hammer and point load test. *J. Sustain. Cem.-Based Mater.* **2020**, *9*, 289–306. [CrossRef]
15. Ahmed, W.; Lim, C.W. Production of sustainable and structural fiber reinforced recycled aggregate concrete with improved fracture properties: A review. *J. Clean. Prod.* **2021**, *279*, 123832. [CrossRef]
16. Calis, G.; Yildizel, S.A.; Keskin, U.S. Investigation of color pigment incorporated roller compacted high performance concrete as a mitigation tool against urban heat island. *Case Stud. Constr. Mater.* **2022**, *17*, e01479. [CrossRef]
17. López-Rebollo, J.; Del Pozo, S.; Nieto, I.M.; Blázquez, C.S.; González-Aguilera, D. Experimental study on the thermal properties of pigmented mortars for use in energy efficiency applications. *J. Clean. Prod.* **2023**, *382*, 135280. [CrossRef]
18. Thejus, P.K.; Nishanth, K.G. Rational approach to synthesis low-cost BiVO4–ZnO complex inorganic pigment for energy efficient buildings. *Sol. Energy Mater. Sol. Cells* **2019**, *200*, 109999. [CrossRef]
19. Thejus, P.K.; Krishnapriya, K.V.; Nishanth, K.G. NIR reflective, anticorrosive magenta pigment for energy saving sustainable building coatings. *Sol. Energy* **2021**, *222*, 103–114. [CrossRef]
20. Miranda, J.; Costa, H.; Valença, J.; Carmo, R.d.; Júlio, E. Design and durability assessment of restoring mortar for concrete heritage. *Materials* **2021**, *14*, 4508. [CrossRef] [PubMed]
21. de Oliveira, G.F.F.; de Souza, E.J.; de Lima Gomes, A.J. Study of the technical feasibility of using colored mortar for coating. *Int. J. Geosci. Eng. Technol.* **2023**, *7*, 8–15.
22. Hatami, L.; Jamshidi, M.; Yavari, M. Improving mechanical/colorimetric properties of self-compacting mortar using an intensively colored-nanoparticle containing polymeric paste. *J. Build. Eng.* **2023**, *66*, 105841. [CrossRef]
23. Lermen, R.T.; Orlando, G.d.O.; Silva, R.d.A. Development of Decorative Mortars with Pigments from Acid Mine Drainage: Analysis of Physical and Mechanical Properties. *Mining* **2023**, *3*, 696–711. [CrossRef]

24. Yun, T.S.; Jeong, Y.J.; Han, T.-S.; Youm, K.-S. Evaluation of thermal conductivity for thermally insulated concretes. *Energy Build.* **2013**, *61*, 125–132. [CrossRef]

25. Yumnam, M.; Gupta, H.; Ghosh, D.; Jaganathan, J. Inspection of concrete structures externally reinforced with FRP composites using active infrared thermography: A review. *Constr. Build. Mater.* **2021**, *310*, 125265. [CrossRef]

26. Rodríguez-Martín, M.; Fueyo, J.G.; Pisonero, J.; López-Rebollo, J.; Gonzalez-Aguilera, D.; García-Martín, R.; Madruga, F. Step heating thermography supported by machine learning and simulation for internal defect size measurement in additive manufacturing. *Measurement* **2022**, *205*, 112140. [CrossRef]

27. Tawfik, M.; Tonnellier, X.; Sansom, C. Light source selection for a solar simulator for thermal applications: A review. *Renew. Sustain. Energy Rev.* **2018**, *90*, 802–813. [CrossRef]

28. *EHE-08*; Instrucción de Hormigón Estructural EHE-08. Ministerio de Fomento: Madrid, Spain, 2008.

29. *UNE-EN 197-1*; Cement—Part 1: Composition, Specifications and Conformity Criteria for Common Cements. AENOR: Madrid, Spain, 2011.

30. Corinaldesi, V.; Monosi, S.; Ruello, M.L. Influence of inorganic pigments' addition on the performance of coloured SCC. *Constr. Build. Mater.* **2012**, *30*, 289–293. [CrossRef]

31. *UNE 83952*; Concrete Durability. Water for Mixing and Aggresives Waters. Deter-Mination of the pH. Potentiometric Method. AENOR: Madrid, Spain, 2008.

32. *UNE-EN 12390-3:2020*; Ensayos de Hormigón Endurecido. Parte 3: Determinación de la Resistencia a Compresión de Probetas. AENOR: Madrid, Spain, 2020.

33. *UNE-EN 12390-6:2010*; Ensayos de Hormigón Endurecido. Parte 6: Resistencia a Tracción Indirecta de Probetas. AENOR: Madrid, Spain, 2010.

34. *UNE-EN 12390-13:2022*; Ensayos de Hormigón Endurecido. Parte 13: Determinación del Módulo Secante de Elasticidad en Compresión. AENOR: Madrid, Spain, 2022.

35. *UNE-EN 12390-2:2020*; Ensayos de Hormigón Endurecido. Parte 2: Fabricación y Curado de Probetas Para Ensayos de Resistencia. AENOR: Madrid, Spain, 2020.

36. Carman, A.P.; Nelson, R.A. Thermal conductivity and diffusivity of concrete. *Univ. Illinois. Eng. Exp. Station. Bull.* **1921**, *XVIII*, 122.

37. Asadi, I.; Shafigh, P.; Hassan, Z.F.B.A.; Mahyuddin, N.B. Thermal conductivity of concrete—A review. *J. Build. Eng.* **2018**, *20*, 81–93. [CrossRef]

38. Sass, J.H.; Stone, C.; Munroe, R.J. Thermal conductivity determinations on solid rock—A comparison between a steady-state divided-bar apparatus and a commercial transient line-source device. *J. Volcanol. Geotherm. Res.* **1984**, *20*, 145–153. [CrossRef]

39. Jaeger, J.C.; Carslaw, H.S. *Conduction of Heat in Solids*; Clarendon Press: Oxford, UK, 1959.

40. Devices, D. *TEMPUS Thermal Properties Analyzer Operator's Manual*; DECAGON DEVICES: Pullman, WA, USA, 2016.

41. *ISO 9001:2008*; Quality Management Systems—Requirements. ISO: Geneva, Switzerland, 2008.

42. *ASTM D5334*; Standard Test Method for Determination of Thermal Conductivity of Soil and Rock by Thermal Needle Probe Procedures. ASTM: West Conshohocken, PA, USA, 2008.

43. *IEEE 442-2017*; IEEE Guide for Thermal Resistivity Measurements of Soils and Backfill Materials. IEEE: New York, NY, USA, 2017.

44. Philips, L. MASTER HPI-T Plus 400W/645 E40 1SL/12. Available online: https://www.lighting.philips.com/main/prof/conventional-lamps-and-tubes/high-intensity-discharge-lamps/quartz-metal-halide/master-hpi-t-plus/928481600096_EU/product (accessed on 30 October 2023).

45. López-Rebollo, J.; Molada-Tébar, A.; Del Pozo, S. Diseño y caracterización de simulador solar low-cost para monitorización termomecánica de materiales. In Proceedings of the XXIV Congreso Nacional de Ingeniería Mecánica, Las Palmas de Gran Canaria, Spain, 25–27 October 2023.

46. Strzelczyk, M.; Steinhoff-Wrześniewska, A.; Rajmund, A. Indicators of water consumption and the quantity of wastewater formed in selected branches of food industry. *Pol. J. Chem. Technol.* **2010**, *12*, 6–10. [CrossRef]

47. Martín del Toro, E. El Coste de los Vectores Energéticos. Sustentable & Sostenible Magazine. 2022. Available online: https://blog.deltoroantunez.com/ (accessed on 30 October 2023).

48. *Factores de Emisión de CO$_2$ y Coeficientes de Paso a Energía Primaria de Diferentes Fuentes de Energía Final Consumidas en el Sector de Edificios en España*; Ministerio de Industria, E.y.T.; IDAE (Instituto Para la Diversificación y Ahorro de la Energía): Madrid, Spain, 2014.

49. Heravi, G.; Nafisi, T.; Mousavi, R. Evaluation of energy consumption during production and construction of concrete and steel frames of residential buildings. *Energy Build.* **2016**, *130*, 244–252. [CrossRef]

50. Nayana, A.Y.; Kavitha, S. Evaluation of C02 emissions for green concrete with high volume slag, recycled aggregate, recycled water to build eco environment. *Int. J. Civ. Eng. Technol* **2017**, *8*, 703–708.

CAPÍTULO V

CONCLUSIONES Y

TRABAJOS FUTUROS

5.1.   Conclusiones

La presente Tesis Doctoral se ha centrado en el empleo de técnicas de caracterización avanzada para la mejora de los materiales de construcción con el fin de alcanzar soluciones innovadoras y eficaces desde el punto de vista de la sostenibilidad, salvaguardando su función estructural y mejorando su eficiencia energética. Los cinco artículos científicos de impacto publicados mostraron la integración de estas técnicas ópticas de campo completo para el análisis y caracterización de nuevos materiales que contribuyan a la construcción sostenible. En concreto, la correlación digital de imágenes ha permitido llevar a cabo la medición de desplazamientos y deformaciones con el fin de caracterizar mecánicamente los materiales, mientras que la termografía infrarroja ha permitido su optimización térmica a través de la monitorización de la temperatura superficial. Tal y como se estableció en el objetivo principal, las investigaciones presentadas proporcionan un panorama integral sobre el uso de materiales de construcción sostenibles y la aplicación de técnicas avanzadas de caracterización para mejorar tanto las propiedades mecánicas como térmicas de estos materiales.

En primer lugar, las investigaciones han confirmado la viabilidad y eficacia de desarrollar nuevos materiales de construcción alineados con los conceptos de sostenibilidad y economía circular. En primera instancia, se demostró que, a pesar de su menor capacidad estructural, la construcción con materiales de tierra supone una alternativa medioambientalmente adecuada. Se trata de una solución especialmente relevante para aquellos lugares donde la disponibilidad de recursos es limitada, favoreciendo así la construcción con materias primas locales y reduciendo los elevados costes y emisiones asociados al transporte y a los procesos de fabricación de materiales convencionales como el cemento o acero.

En busca de una solución estructuralmente viable a la par que respetuosa con el medioambiente, la utilización de residuos de construcción y demolición como materia prima para la fabricación de hormigones reciclados ha demostrado ser una solución adecuada. En este sentido, los áridos procedentes de residuos de construcción y demolición pueden ser empleados para la fabricación de hormigones sostenibles de carácter no estructural, mientras que los áridos procedentes de rechazos de prefabricados pueden ser empleados para la fabricación de hormigón estructural.

En ambos casos se ha puesto de manifiesto el potencial de la correlación digital de imágenes como técnica de caracterización avanzada. En el primero de los trabajos se ha implementado su enfoque bidimensional para la evaluación de bloques de tierra comprimida con superficies planas, mientras que en el segundo de los trabajos se ha implementado su enfoque tridimensional para caracterizar las probetas cilíndricas de hormigón con curvatura en su superficie. Estos estudios han mostrado que la DIC es una herramienta eficaz para medir desplazamientos y deformaciones de campo completo, lo que ha permitido obtener una comprensión más completa del comportamiento mecánico de los nuevos materiales de construcción. Gracias a los datos proporcionados por esta

técnica se han podido llevar a cabo análisis de la fisuración o rotura, determinando su comportamiento espacial e incluso desarrollando modelos predictivos que permiten obtener las deformaciones a partir de las propiedades y composición del material.

Por otro lado, se ha mostrado que la incorporación de aditivos en los materiales de construcción puede mejorar significativamente sus propiedades térmicas. En un primer trabajo en el ámbito térmico, la incorporación de residuos ha mostrado modificar la conductividad térmica en los materiales de construcción. En el siguiente trabajo se ha planteado estudiar su comportamiento térmico desde el punto de vista de la absorción de radiación solar a través de la incorporación de pigmentos. Estos aditivos han mostrado una alteración en la absorción de radiación solar y, por lo tanto, una alternativa para mejorar el rendimiento en términos de eficiencia energética, ya sea para mitigar los efectos de las islas de calor urbano o, en contraposición, para aumentar la capacidad de acumulación de calor de las infraestructuras.

La termografía infrarroja ha demostrado ser útil para analizar este comportamiento térmico de estos materiales, lo que facilita la optimización de sus propiedades térmicas y su aplicación en la mejora de la eficiencia energética. Para facilitar esta implementación, se ha desarrollado un simulador solar que ha permitido reproducir las condiciones ambientales reales para replicar los ensayos bajo condiciones controladas en laboratorio. La integración del simulador solar junto con la termografía infrarroja ha mostrado que el calentamiento de las muestras a través de la radiación solar simulada puede ser monitorizado mediante imágenes termográficas para evaluar su comportamiento térmico.

Por último, el trabajo final respalda la idea de que es posible desarrollar y utilizar materiales de construcción sostenibles con propiedades mecánicas y térmicas mejoradas para obtener beneficios en el sector de la ingeniería civil e industrial. A través del desarrollo y testeo de un prototipo de depósito de agua acumulador de calor se ha mostrado que es posible fabricar elementos estructurales con hormigón reciclado y que es posible dotar a este material de propiedades térmicas que favorezcan la eficiencia energética. Todo ello supone un beneficio tanto económico como ambiental que se manifiesta con los correspondientes ahorros energéticos como consecuencia de un mayor aumento de la temperatura del agua interior de los depósitos, lo que genera un menor consumo en procesos donde se requiere agua caliente.

Estos hallazgos tienen importantes implicaciones tanto para la industria de la construcción como para la investigación en materiales, y sugieren que la integración de enfoques multidisciplinarios puede ser clave para abordar los desafíos ambientales y sociales asociados con la construcción y el desarrollo urbano. El empleo de estas técnicas no solo permite caracterizar las propiedades mecánicas y térmicas de los materiales de forma precisa y completa, sino que también facilita el desarrollo de nuevos materiales con propiedades mejoradas, promoviendo así la economía circular y la eficiencia energética en la industria de la construcción.

5.2. Trabajos futuros

En el contexto de la construcción sostenible, donde se busca reducir el impacto ambiental y promover prácticas más eficientes, los avances obtenidos en la presente Tesis Doctoral abren un amplio abanico de perspectivas futuras. Estos avances representan un punto de partida sólido para futuras investigaciones que pueden contribuir aún más al desarrollo de materiales y técnicas innovadoras en la construcción. Estas investigaciones tienen el potencial de contribuir significativamente a generar una industria de la construcción más sostenible y eficiente energéticamente.

Una de las principales líneas de investigación futura se centra en la optimización y mejora continua de los materiales desarrollados. Si bien los estudios actuales han demostrado la viabilidad de emplear áridos reciclados y aditivos para mejorar las propiedades mecánicas y térmicas de los materiales de construcción, aún queda espacio para explorar nuevas combinaciones de materiales y aditivos que puedan ofrecer un rendimiento aún mayor. En este sentido, la sustitución del cemento como material aglomerante supone un reto en el sector del hormigón. Se trata de un material cuya producción tiene un alto impacto medioambiental con una elevada huella de carbono, por lo que la reducción de este material preservando las propiedades mecánicas del hormigón es una de las principales perspectivas futuras del sector de la construcción. Materiales generalmente considerados de desecho como las cenizas volcánicas pueden ser una solución para realizar sustituciones parciales del cemento y aprovechar estos materiales que se originan en desastres naturales como las erupciones volcánicas.

En línea con el objetivo de implementar técnicas de campo completo para la caracterización de materiales, futuras investigaciones podrían centrarse el aprovechamiento del potencial de estas técnicas para optimizar el diseño de infraestructuras. En los estudios presentados se han empleado los datos de campo completo para realizar análisis exhaustivos y profundizar en el conocimiento del comportamiento mecánico de los materiales. No obstante, su combinación con técnicas de ingeniería robusta y análisis estocásticos pueden suponer una ventaja a la hora de diseñar y optimizar infraestructuras elaboradas con este tipo de materiales. Se pretende continuar avanzando en este campo, de manera que puedan integrarse estas metodologías con técnicas de simulación como el método de elementos finitos.

Respecto a los equipos para la caracterización mecánica, las campañas experimentales pueden complementarse con instrumentación avanzada como el prototipo desarrollado y mostrado en el Apéndice II, del cual se ha solicitado patente. Este prototipo permitiría reconstruir y caracterizar la totalidad de las probetas empleando la técnica DIC y colocando cámaras en todo su entorno en lugar de monitorizar únicamente la superficie frontal. Además, gracias a este prototipo y su sistema de calibración podrían evaluarse tanto probetas como infraestructuras de mayor complejidad empleando sistemas de coordenadas globales que permiten capturas de pares de cámaras independientes.

En el ámbito de la mejora de las propiedades térmicas de los materiales, hay un gran potencial para la investigación futura en el diseño de materiales con capacidades de almacenamiento de calor aún más eficientes. Además de la incorporación de pigmentos para la absorción de radiación solar, se podrían explorar otros enfoques, como la incorporación de materiales de cambio de fase o la mejora de la conductividad térmica de estos materiales para maximizar su capacidad de almacenamiento térmico y transferir esta ganancia al interior, bien sea para un mayor aumento de la temperatura en depósitos de almacenamiento de agua o para aplicaciones en edificación de alta eficiencia energética.

En cuanto a la instrumentación y las técnicas de medición, futuras investigaciones podrían centrarse en el desarrollo de dispositivos y sistemas más avanzados para la caracterización de materiales en condiciones más realistas. Por ejemplo, se podrían diseñar simuladores solares más sofisticados que permitan reproducir con mayor precisión las condiciones de iluminación solar y las variaciones estacionales. Del mismo modo, podrían explorarse nuevas configuraciones de termografía infrarroja que permitan una monitorización más detallada y precisa del comportamiento térmico de los materiales, incluso en condiciones de funcionamiento dinámico o en aplicaciones reales a gran escala.

Además de los aspectos técnicos y científicos, las futuras investigaciones también deben abordar cuestiones relacionadas con la viabilidad económica y la implementación práctica de los nuevos materiales y técnicas desarrollados para una mayor transferencia al sector de la construcción. Esto incluye la evaluación del costo-beneficio de la adopción de estos materiales en comparación con las prácticas de construcción convencionales, así como la consideración de factores como la disponibilidad de materias primas, los procesos de fabricación y la compatibilidad con las normativas y estándares de la industria de la construcción.

REFERENCIAS

1. Akhtar, A. and A.K. Sarmah, *Construction and demolition waste generation and properties of recycled aggregate concrete: A global perspective.* Journal of Cleaner Production, 2018. **186**: p. 262-281.
2. Peduzzi, P., *Sand, rarer than one thinks.* Environmental Development, 2014. **11**: p. 208-218.
3. Eurosat, *Generation of waste by waste category, hazardousness and NACE Rev. 2 activity.* Available online: https://ec.europa.eu/eurostat/databrowser/view/env_wasgen/default/table?lang=en [Accessed April 4, 2024].
4. Revilla-Cuesta, V., et al., *Assessment of longitudinal and transversal plastic behavior of recycled aggregate self-compacting concrete: A two-way study.* Construction and Building Materials, 2021. **292**: p. 123426.
5. Abdulqader, A. and D.C. Rizos, *Advantages of using digital image correlation techniques in uniaxial compression tests.* Results in Engineering, 2020. **6**: p. 100109.
6. Sutton, M.A., J.J. Orteu, and H.X. Schreier, *Image correlation for shape, motion and deformation measurements: basic concepts, theory and applications*. 2009: Springer Science & Business Media.
7. Corinaldesi, V., A. Mazzoli, and G. Moriconi, *Mechanical behaviour and thermal conductivity of mortars containing waste rubber particles.* Materials & Design, 2011. **32**(3): p. 1646-1650 0261-3069.
8. Thejus, P.K., K.V. Krishnapriya, and K.G. Nishanth, *NIR reflective, anticorrosive magenta pigment for energy saving sustainable building coatings.* Solar Energy, 2021. **222**: p. 103-114.
9. Lizaranzu, M., et al., *Non-destructive testing of composite materials by means of active thermography-based tools.* Infrared Physics & Technology, 2015. **71**: p. 113-120.
10. Maldague, X., *Theory and practice of infrared technology for nondestructive testing.* 2001.
11. Fernández-Canovas, M., *Hormigón (cuarta edición).* Colegio de Ingenieros Caminos Canales y Puertos, Servicio de Publicaciones, Madrid, 1996.
12. Costa, C., et al., *The sustainability of adobe construction: past to future.* International Journal of Architectural Heritage, 2019. **13**(5): p. 639-647.
13. Herrmann, C.J. and E.O. Zappettini, *Recursos minerales, minería y medio ambiente*, ed. S. Serie Publicaciones Nº 173. Instituto de Geología y Recursos Minerales. 2014, Buenos Aires, Argentina.
14. de Brito, J. and R. Kurda, *The past and future of sustainable concrete: A critical review and new strategies on cement-based materials.* Journal of Cleaner Production, 2021. **281**: p. 123558
15. Deboucha, S. and R. Hashim, *A review on bricks and stabilized compressed earth blocks.* Scientific Research and Essays, 2011. **6**(3): p. 499-506.
16. Rigassi, V., *Compressed earth blocks: Manual of production.* Network. GATE/BASIN, 1985.

17. Etzion, Y. and M. Saller, *Earth construction—a review of needs and methods.* Architectural Science Review, 1987. **30**(2): p. 43-48.

18. Gálvez-Martos, J.-L., et al., *Construction and demolition waste best management practice in Europe.* Resources, conservation and recycling, 2018. **136**: p. 166-178.

19. ECC, *Regulation, E.U., No 305/2011 of the European Parliament and of the Council of 9 March 2011 laying down harmonised conditions for the marketing of construction products and repealing Council Directive 89/106.* 2011.

20. Gonçalves, P. and J.d. Brito, *Recycled aggregate concrete (RAC)–comparative analysis of existing specifications.* Magazine of Concrete Research, 2010. **62**(5): p. 339-346.

21. Travush, V., et al., *Mechanical safety and survivability of buildings and building structures under different loading types and impacts.* Procedia engineering, 2016. **164**: p. 416-424.

22. Pacheco-Torgal, F., et al., *Cost-effective energy efficient building retrofitting: materials, technologies, optimization and case studies.* 2017: Woodhead publishing.

23. Morel, J.-C., A. Pkla, and P. Walker, *Compressive strength testing of compressed earth blocks.* Construction and Building materials, 2007. **21**(2): p. 303-309.

24. Rodríguez, C., et al., *The incorporation of construction and demolition wastes as recycled mixed aggregates in non-structural concrete precast pieces.* Journal of Cleaner Production, 2016. **127**: p. 152-161.

25. Thomas, C., J. Setién, and J.A. Polanco, *Structural recycled aggregate concrete made with precast wastes.* Construction and Building Materials, 2016. **114**: p. 536-546

26. Teixeira, E.R., et al., *Mechanical and thermal performance characterisation of compressed earth blocks.* Energies, 2020. **13**(11): p. 2978.

27. Rahal, K., *Mechanical properties of concrete with recycled coarse aggregate.* Building and environment, 2007. **42**(1): p. 407-415.

28. Mirabella, N., et al., *Strategies to improve the energy performance of buildings: A review of their life cycle impact.* Buildings, 2018. **8**(8): p. 105 2075-5309.

29. Kim, S.W. and R.D. Brown, *Urban heat island (UHI) intensity and magnitude estimations: A systematic literature review.* Science of the Total Environment, 2021. **779**: p. 146389 0048-9697.

30. Xaman, J., et al., *Transient thermal analysis of a solar chimney for buildings with three different types of absorbing materials: Copper plate/PCM/concrete wall.* Renewable Energy, 2019. **136**: p. 139-158 0960-1481.

31. Badin, G., et al., *Effect of addition of pigments on thermal characteristics and the resulting performance enhancement of asphalt.* Construction and Building Materials, 2021. **302**: p. 124212 0950-0618.

32. Calis, G., S.A. Yildizel, and U.S. Keskin, *Investigation of color pigment incorporated roller compacted high performance concrete as a mitigation tool against urban heat island.* Case Studies in Construction Materials, 2022. **17**: p. e01479.

33. Hoffmann, K., *Applying the wheatstone bridge circuit.* 1974: HBM Darmstadt, Germany.

34. Chen, T.C., W.Q. Yin, and P.G. Ifju, *Investigation of shrinkage behaviour and cracks in cement paste using moiré interferometry.* The Journal of Strain Analysis for Engineering Design, 2010. **45**(1): p. 19-31.

35. Hover, E., S. Psomas, and C. Eddie, *Estimating crack widths in steel fibre-reinforced concrete.* Proceedings of the Institution of Civil Engineers-Construction Materials, 2017. **170**(3): p. 141-152.

36. Kumar, P., et al., *Experimental study of dry stone masonry walls using digital reflection photoelasticity.* Strain, 2020. **56**(6): p. e12372.

37. Gehri, N., J. Mata-Falcón, and W. Kaufmann, *Automated crack detection and measurement based on digital image correlation.* Construction and Building Materials, 2020. **256**: p. 119383.

38. Clauß, F., M.A. Ahrens, and P. Mark, *A comparative evaluation of strain measurement techniques in reinforced concrete structures–A discussion of assembly, application, and accuracy.* Structural Concrete, 2021. **22**(5): p. 2992-3007

39. Kang, J., et al., *Digital image correlation studies for microscopic strain distribution and damage in dual phase steels.* Scripta Materialia, 2007. **56**(11): p. 999-1002.

40. Villarino, A., J. López-Rebollo, and N. Antón, *Analysis of Mechanical Behavior through Digital Image Correlation and Reliability of Pinus halepensis Mill.* Forests, 2020. **11**(11): p. 1232.

41. Garcia-Martin, R., et al., *Digital image correlation and reliability-based methods for the design and repair of pressure pipes through composite solutions.* Construction and Building Materials, 2020. **248**: p. 118625.

42. María, R.-M., et al., *Improvement of tensile properties of carbon fibre-reinforced cementitious matrix composites with coated textile and enhanced mortars.* Construction and Building Materials, 2023. **369**: p. 130552.

43. Berfield, T.A., et al., *Micro-and nanoscale deformation measurement of surface and internal planes via digital image correlation.* Experimental Mechanics, 2007. **47**: p. 51-62.

44. Tian, L. and B. Pan, *Remote bridge deflection measurement using an advanced video deflectometer and actively illuminated LED targets.* Sensors, 2016. **16**(9): p. 1344.

45. Peters, W.H. and W.F. Ranson, *Digital imaging techniques in experimental stress analysis.* Optical engineering, 1982. **21**(3): p. 427-431.

46. Pan, B., *Digital image correlation for surface deformation measurement: historical developments, recent advances and future goals.* Measurement Science and Technology, 2018. **29**(8): p. 082001.

47. Pisonero, J., et al., *A comparative study of 2D and 3D digital image correlation approaches for the characterization and numerical analysis of composite materials.* IEEE Access, 2021. **9**: p. 160675-160687.

48. Pan, B., Z. Lu, and H. Xie, *Mean intensity gradient: an effective global parameter for quality assessment of the speckle patterns used in digital image correlation.* Optics and Lasers in Engineering, 2010. **48**(4): p. 469-477.

49. Triggs, B., et al. *Bundle adjustment—a modern synthesis.* 2000. Springer.

50. Reu, P.L., *A study of the influence of calibration uncertainty on the global uncertainty for digital image correlation using a Monte Carlo approach.* Experimental mechanics, 2013. **53**: p. 1661-1680.

51. Pan, B., et al., *Two-dimensional digital image correlation for in-plane displacement and strain measurement: a review.* Measurement science and technology, 2009. **20**(6): p. 062001.

52. Luu, L., et al., *Accuracy enhancement of digital image correlation with B-spline interpolation.* Optics letters, 2011. **36**(16): p. 3070-3072.

53. Pan, B., K. Li, and W. Tong, *Fast, robust and accurate digital image correlation calculation without redundant computations.* Experimental Mechanics, 2013. **53**: p. 1277-1289.

54. Pan, B., *Reliability-guided digital image correlation for image deformation measurement.* Applied optics, 2009. **48**(8): p. 1535-1542.

55. Xiao, Z., et al., *An accurate stereo vision system using cross-shaped target self-calibration method based on photogrammetry.* Optics and Lasers in Engineering, 2010. **48**(12): p. 1252-1261.

56. Abdel-Aziz, Y.I. *Direct linear transformation from comparator coordinates in close-range photogrammetry. In Proceedings American Society of Photogrammetry Symposium on Close-Range Photogrammetry. Falls Church, VA.* 1971.

57. Faugeras, O., *Three-dimensional computer vision: a geometric viewpoint.* 1993: MIT press.

58. Teijón-López-Zuazo, E., et al., *Compression and strain predictive models in non-structural recycled concretes made from construction and demolition wastes.* Materials, 2021. **14**(12): p. 3177.

59. Yun, T.S., et al., *Evaluation of thermal conductivity for thermally insulated concretes.* Energy and Buildings, 2013. **61**: p. 125-132.

60. Speakman, J.R. and S. Ward, *Infrared thermography: principles and applications.* Zoology-Jena-, 1998. **101**: p. 224-232.

61. Kylili, A., et al., *Infrared thermography (IRT) applications for building diagnostics: A review.* Applied Energy, 2014. **134**: p. 531-549.

62. Rodríguez-Martín, M., et al., *Step heating thermography supported by machine learning and simulation for internal defect size measurement in additive manufacturing.* Measurement, 2022. **205**: p. 112140.

63. Barreira, E. and V.P. de Freitas, *Evaluation of building materials using infrared thermography.* Construction and building materials, 2007. **21**(1): p. 218-224.

64. Hung, Y.Y., et al., *Review and comparison of shearography and active thermography for nondestructive evaluation.* Materials Science and Engineering: R: Reports, 2009. **64**(5-6): p. 73-112.

65. Colarossi, D., et al., *Design and validation of an adjustable large-scale solar simulator.* Applied Sciences, 2021. **11**(4): p. 1964.

66. Tawfik, M., X. Tonnellier, and C. Sansom, *Light source selection for a solar simulator for thermal applications: A review.* Renewable and Sustainable Energy Reviews, 2018. **90**: p. 802-813.

67. CIE15:2018, *Colorimetry, Fourth ed.* Commission Internationale de l'Eclairage, Vienna, 2018.

68. Ma, X., S. Bader, and B. Oelmann, *Characterization of indoor light conditions by light source classification.* IEEE Sensors Journal, 2017. **17**(12): p. 3884-3891.

69. Luo, M.R., *Encyclopedia of color science and technology.* 2016: Springer New York.

70. Codd, D.S., et al., *A low cost high flux solar simulator.* Solar energy, 2010. **84**(12): p. 2202-2212 0038-092X.

APÉNDICES

APÉNDICE I: INDEXACIÓN Y FACTOR DE IMPACTO DE LAS REVISTAS

Este Apéndice I incluye la información relativa a la indexación y principales medidas de impacto de las revistas en las cuales se han publicado los artículos de la presente Tesis Doctoral. Todas las revistas cuentan con su correspondiente indexación (JCR, del inglés "Journal Citation Report") en la base de datos *Web of Science (WoS)* de *Clarivate Analytics*.

Los cinco artículos han sido publicados en modalidad de acceso abierto (OA, del inglés "Open Access"), de manera que es posible acceder a su contenido en línea de manera libre y universal, sin costo alguno para el lector.

- Los artículos 1 y 5 (Epígrafes 2.1 y 4.1) se han publicado en la revista *Materials* de la editorial MDPI, de acceso abierto.
- El artículo 2 (Epígrafe 2.2) se ha publicado en la revista *Buildings* de la editorial MDPI, de acceso abierto.
- El artículo 3 (Epígrafe 3.1) se ha publicado en la revista *Sustainable Energy Technologies and Assessments* de la editorial ELSEVIER, en la modalidad Gold Open Access.
- El artículo 4 (Epígrafe 3.2) se ha publicado en la revista *Journal of Cleaner Production* de la editorial ELSEVIER, en la modalidad Gold Open Access.

A continuación, se describen los principales parámetros métricos que se incluyen para cada una de las revistas:

- **Journal Impact Factor (JIF) Trend.** El factor de impacto es una métrica a nivel de revista calculada a partir de los datos indexados en la WoS. Este parámetro se obtiene de dividir el número de citas recibidas por una revista entre el recuento de sus artículos y/o reseñas publicadas. Los gráficos muestran la evolución del factor de impacto y su rango de percentil durante los últimos años.
- **Journal Citation Indicator (JCI).** El indicador de citas es la media del impacto normalizado de las citas por categoría (CNCI, del inglés "Category Normalized Citation Impact") de los elementos citables (artículos y revisiones) publicados por una revista en los últimos tres años. El JCI medio de una categoría es 1.
- **Citas totales.** Este parámetro hace referencia al número total de veces que una revista ha sido citada por todas las revistas incluidas en la base de datos JCR.

- **Distribución de citas.** Este parámetro muestra la frecuencia con la que los artículos publicados en el año o los dos años anteriores fueron citados en el año de datos del JCR (para el cual se calcula el JIF).

- **5 year Impact Factor.** El factor de impacto de los últimos cinco años es la media de veces que los artículos de la revista publicados en los últimos cinco años han sido citados en el año JCR. Se calcula dividiendo el número de citas en el año JCR por el número total de artículos publicados en los cinco años anteriores.

- **Eigenfactor score.** La puntuación del factor propio refleja la densidad de la red de citas en torno a la revista utilizando 5 años de contenidos citados por el año en curso. Considera tanto el número de citas como la fuente de esas citas, de modo que las fuentes muy citadas influirán en la red más que las fuentes menos citadas. El cálculo del factor propio no incluye las autocitas de la revista.

- **Normalized Eigenfactor.** La puntuación normalizada del factor propio se obtiene reescalando el número total de revistas en el JCR cada año, de modo que la revista media tenga una puntuación de 1. De este modo, las revistas pueden compararse y la influencia puede medirse por su puntuación en relación con 1.

- **Article influence score.** La puntuación de la influencia del artículo normaliza la puntuación del factor propio en función del tamaño acumulado de la revista citada en los cinco años anteriores. La puntuación media de la influencia de cada artículo es de 1. Una puntuación superior a 1 indica que cada artículo de la revista tiene una influencia superior a la media.

- **Immediacy Index.** El índice de inmediatez es el número de citas de la revista en el año en curso que hacen referencia a contenidos de ese mismo año.

A.1.1. Buildings

Buildings es una revista internacional de acceso abierto, revisada por pares, sobre ciencias de la edificación, ingeniería de la edificación y arquitectura. La revista se publica mensualmente en línea por MDPI desde el año 2011.

Se ha publicado el siguiente artículo de la presente Tesis Doctoral en la revista *Buildings*:

Artículo 1 - Improvement of mechanical properties of compressed earth blocks with stabilising additives for self-build of sustainable housing.

Tabla 2: Principales medidas de impacto e indexación de la revista Buildings.

Revista	Buildings
Editorial	MDPI
EISSN	2075-5309
Factor de Impacto (2022)	3.8
Ranking	23/68
Cuartil	Q2
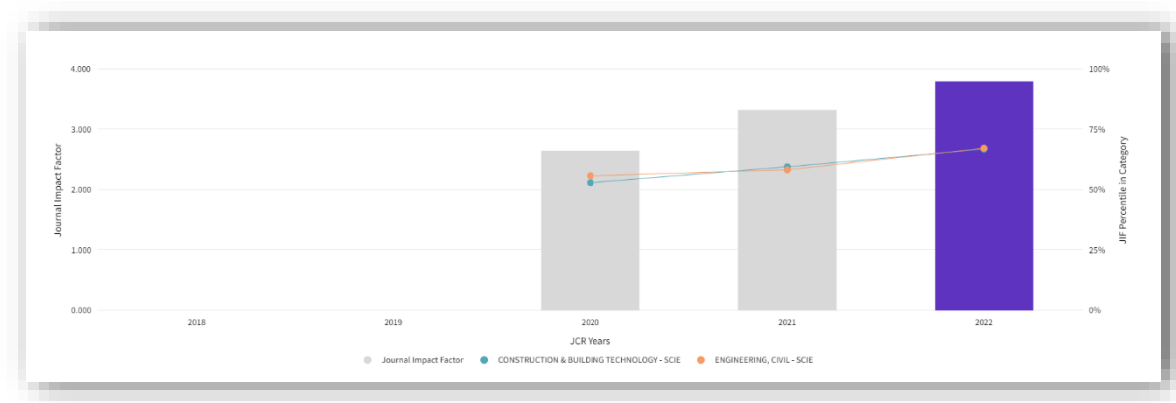
Figura 8: Buildings: Journal Impact Factor (JIF) Trend.
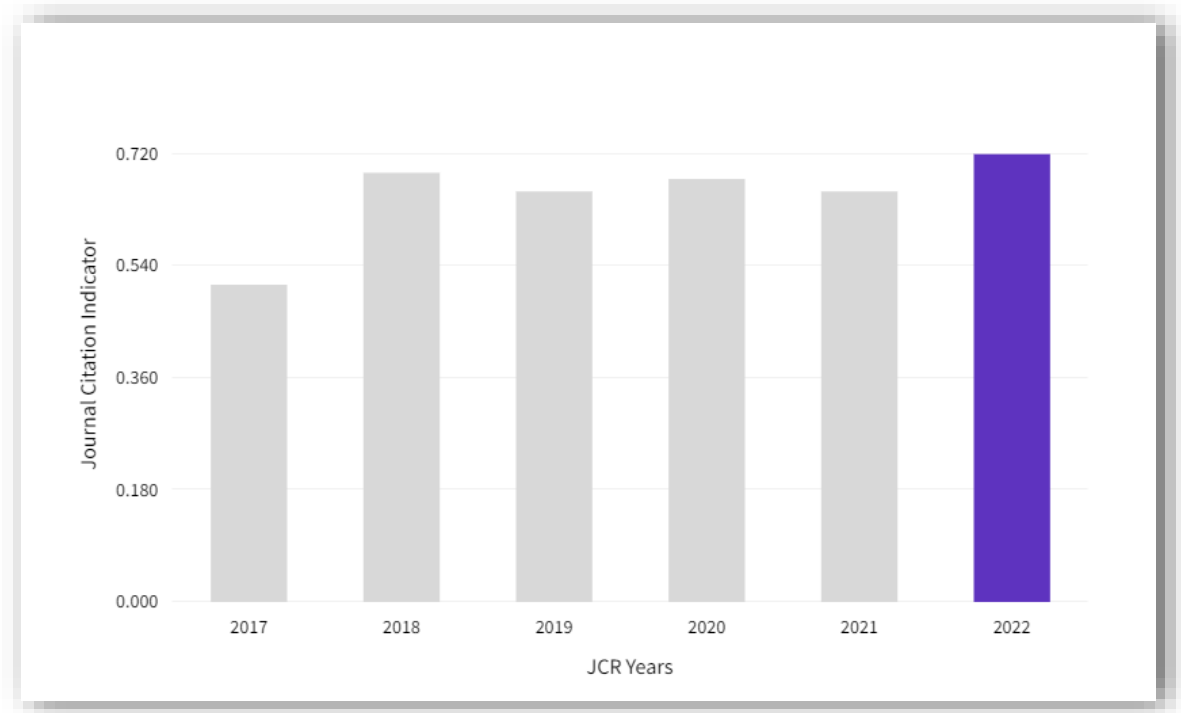
Figura 9: Buildings: Journal Citation Indicator (JCI).
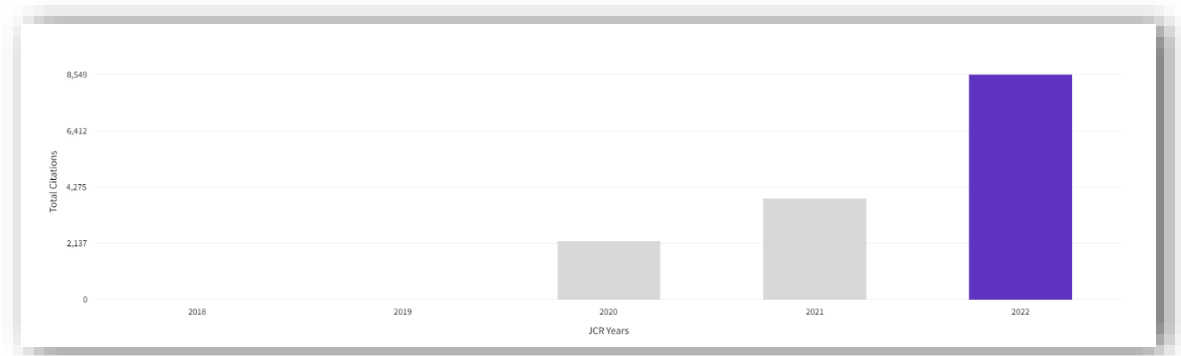

Figura 10: Buildings: Total Citations.
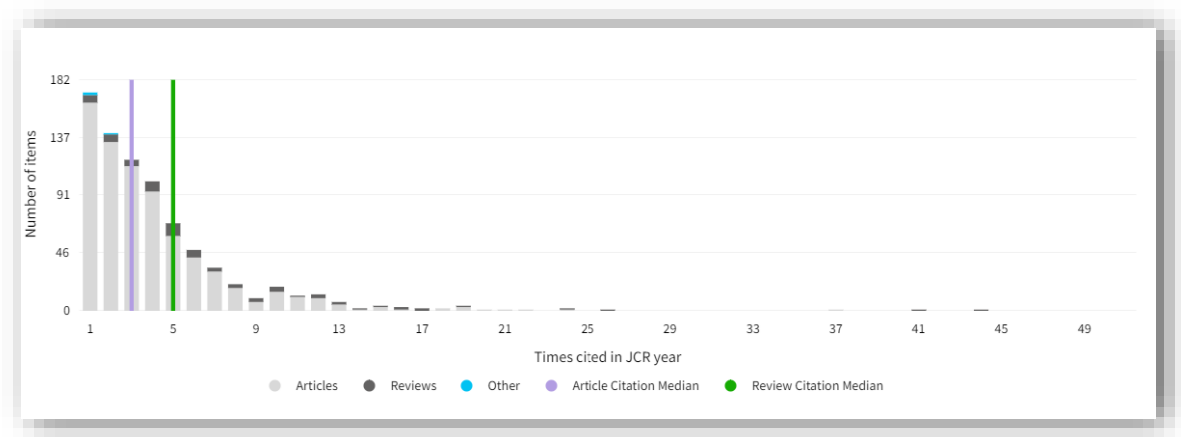
Figura 11: Buildings: Citation Distribution.
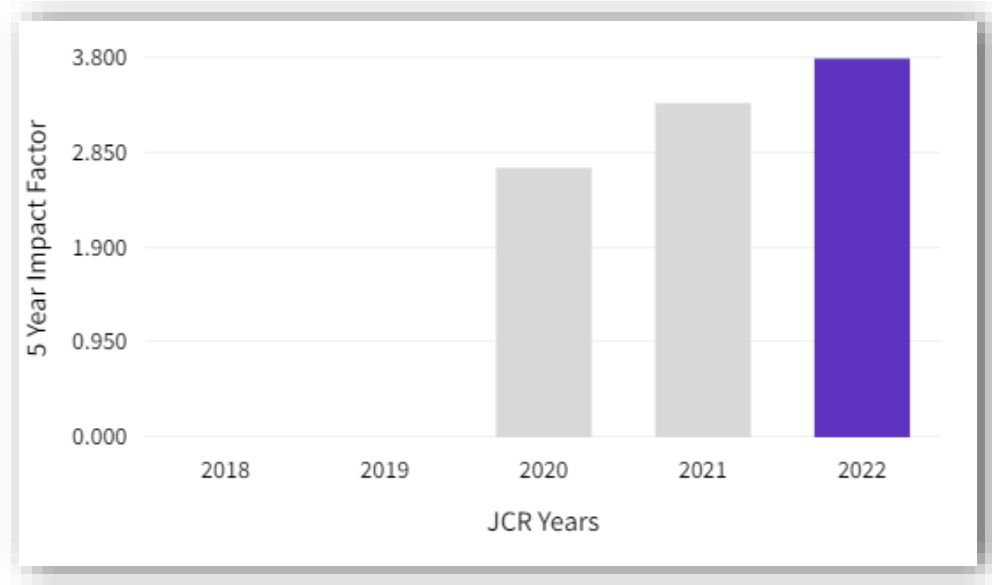
Figura 12: Buildings: 5 year Impact Factor.
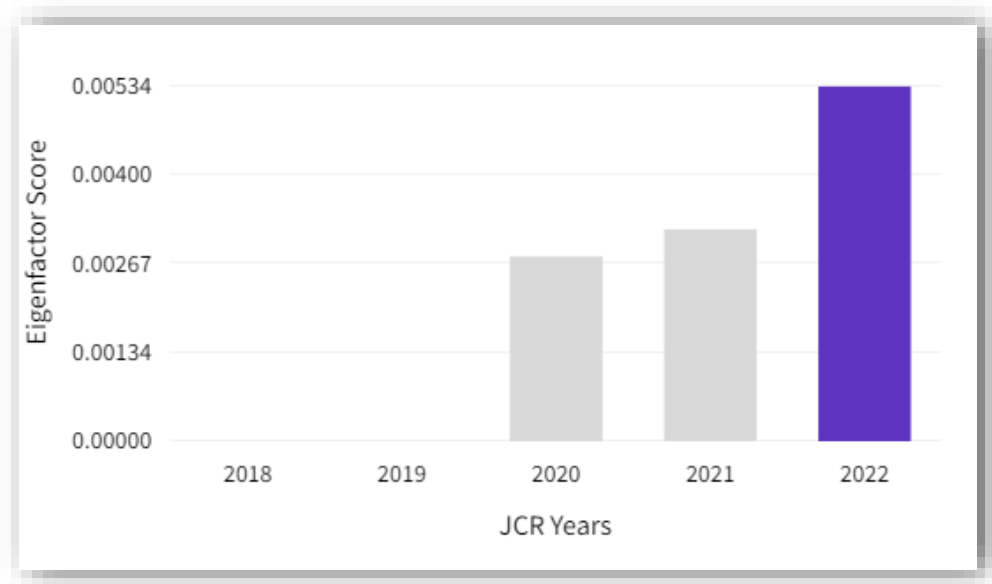
Figura 13: Buildings: Eigenfactor score.
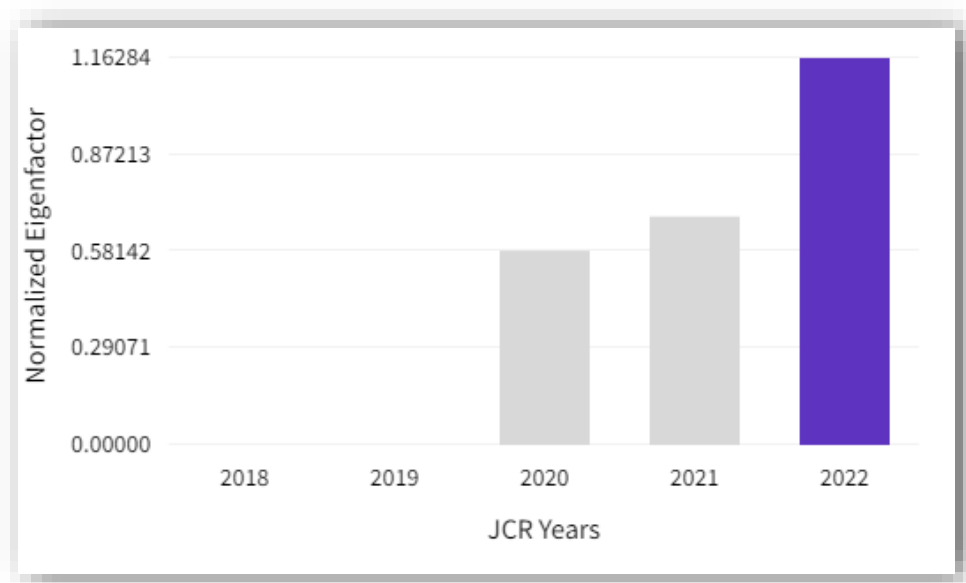
Figura 14: Buildings: Normalized Eigenfactor.
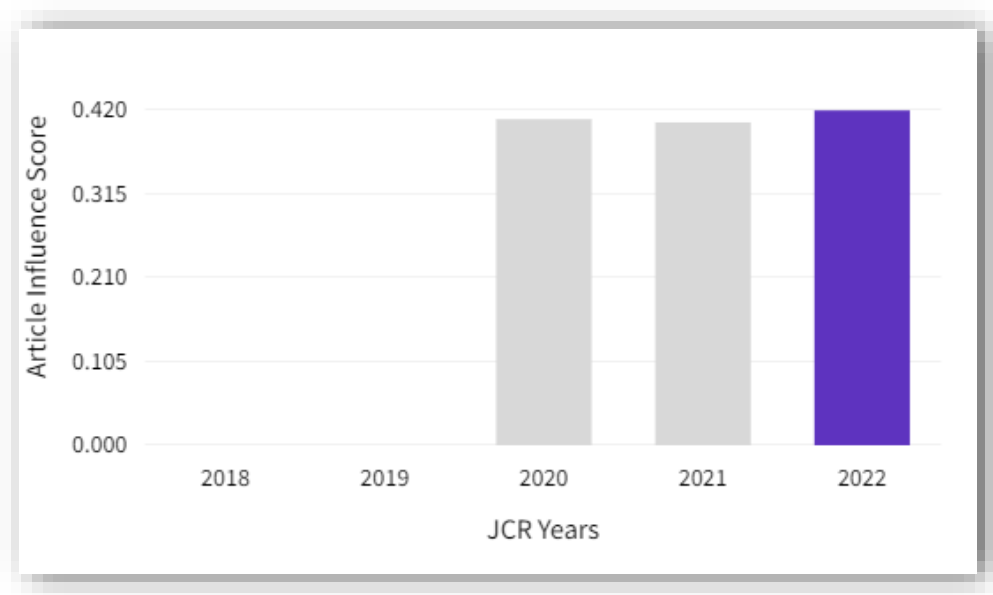
Figura 15: Buildings: Article influence score.
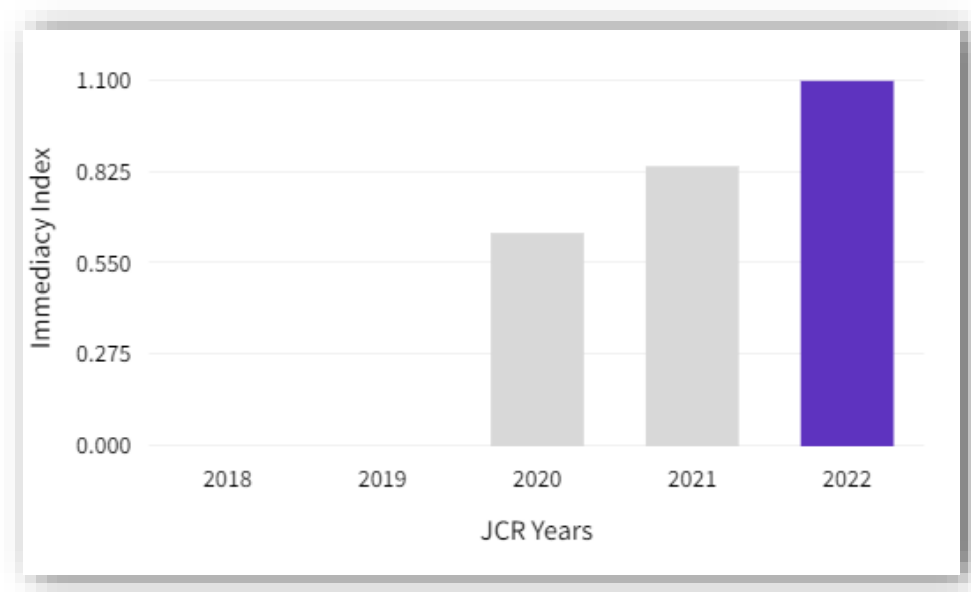
Figura 16: *Buildings: Immediacy Index.*

A.1.2. Materials

Materials es una revista internacional de acceso abierto, revisada por pares, sobre ciencia e ingeniería de materiales. La revista se publica quincenalmente en línea por MDPI desde el año 2008.

Se han publicado los siguientes dos artículos de la presente Tesis Doctoral en la revista *Materials*:

Artículo 2 - Compression and strain predictive models in non-structural recycled concretes made from construction and demolition wastes.

Artículo 5 - Enhancing thermal efficiency in water storage tanks using pigmented recycled concrete.

Dado que los artículos se publicaron en diferentes años (2021 y 2024), se han incluido en la Tabla 3 el Factor de Impacto, Ranking y Cuartil disponible en el momento de ambas publicaciones (2020 y 2022).

***Tabla 3:** Principales medidas de impacto e indexación de la revista Materials.*

Revista	Materials
Editorial	MDPI
EISSN	1996-1944
Factor de Impacto (2020-2022)	3.62 - 3.4
Ranking	17/80 - 20/79
Cuartil	Q1 - Q2

***Figura 17:** Materials: Journal Impact Factor (JIF) Trend.*
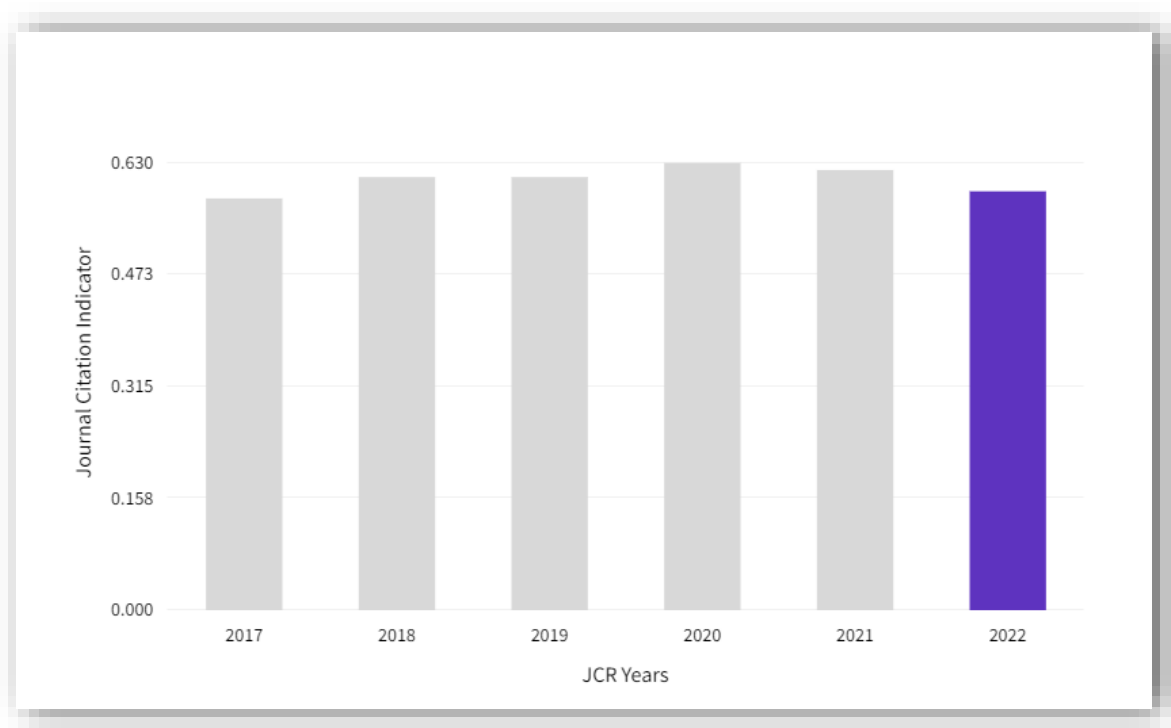
Figura 18: *Materials: Journal Citation Indicator (JCI).*
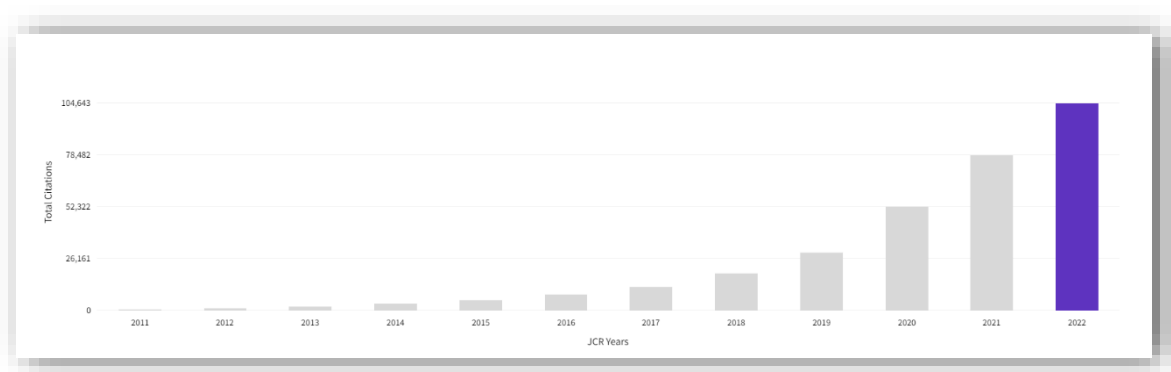
Figura 19: *Materials: Total Citations.*
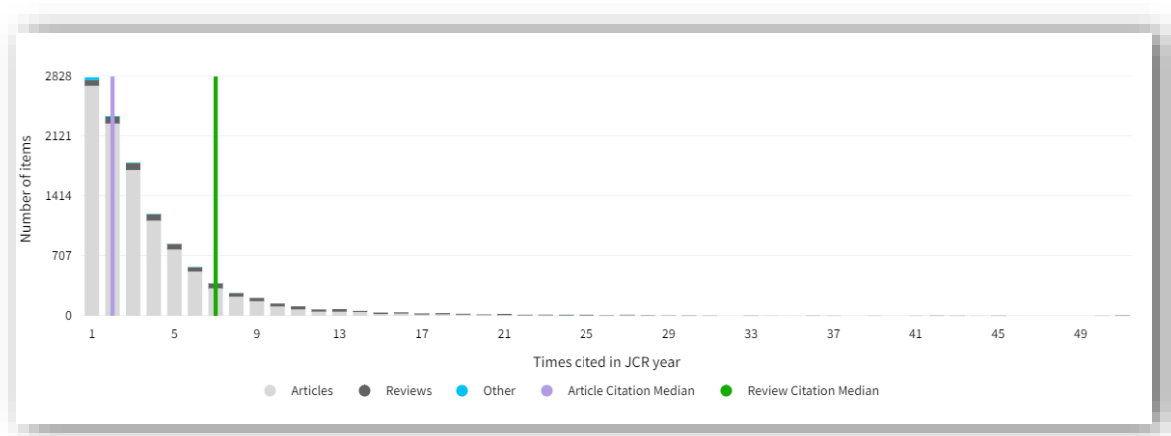
Figura 20: *Materials: Citation Distribution.*
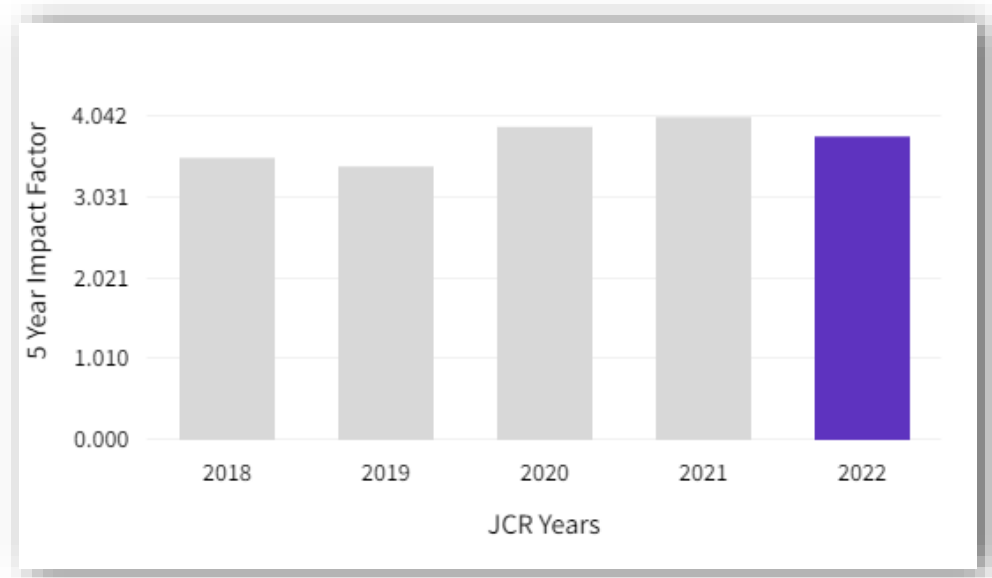
Figura 21: Materials: 5 year Impact Factor.
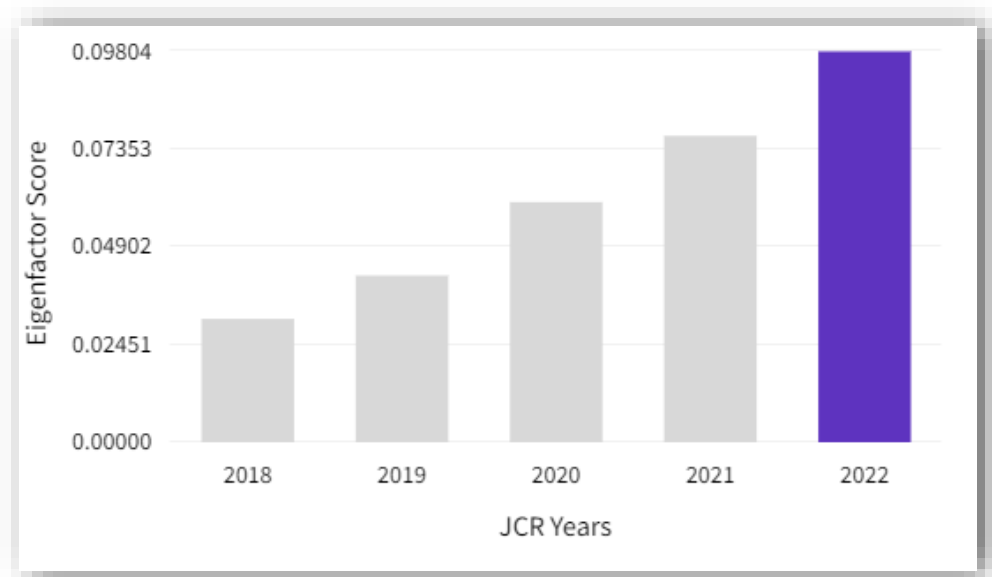
Figura 22: Materials: Eigenfactor score.
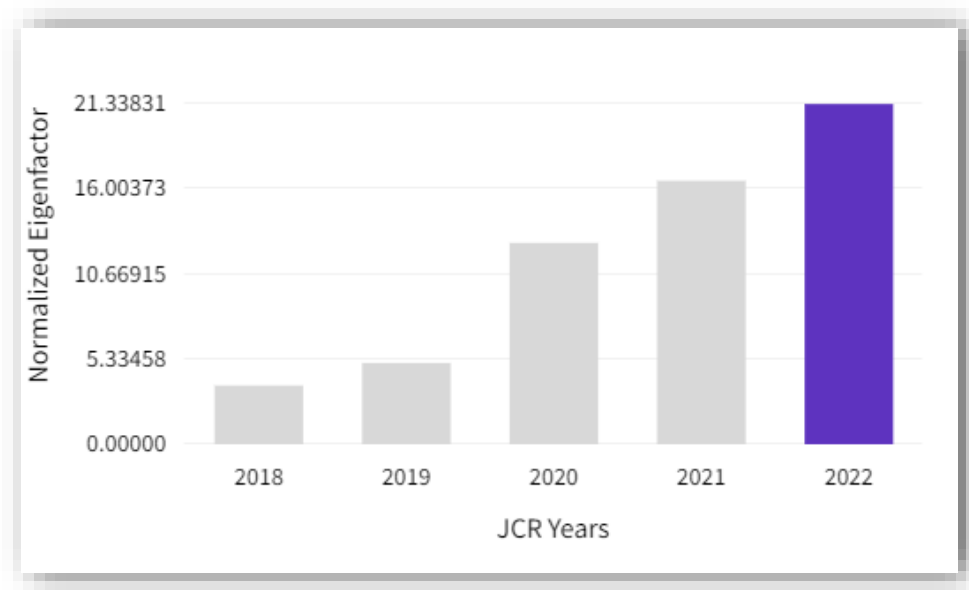
Figura 23: *Materials: Normalized Eigenfactor.*
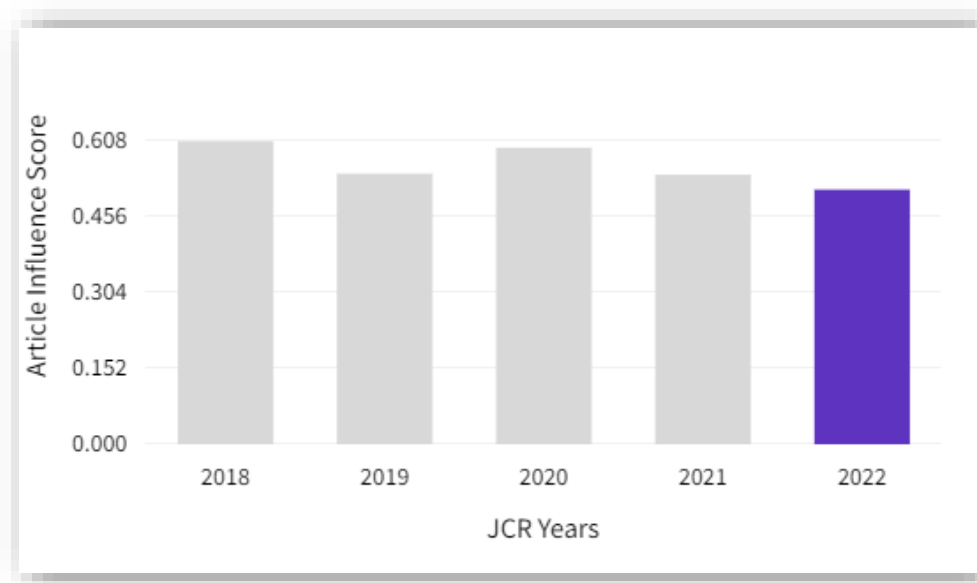
Figura 24: *Materials: Article influence score.*
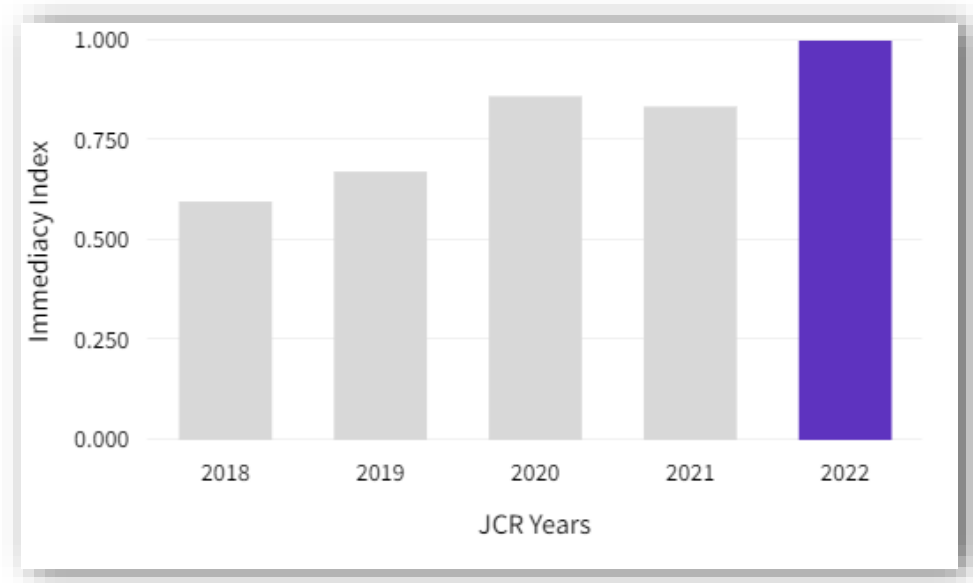
Figura 25: Materials: Immediacy Index.

A.1.3. Sustainable Energy Technologies and Assessments

Sustainable Energy Technologies and Assessments (SETA) es una revista internacional, revisada por pares, sobre tecnologías para la generación y/o utilización de energía que disminuyan el impacto en la producción y uso. La revista se publica bimensualmente en línea por ELSEVIER desde el año 2013.

Se ha publicado el siguiente artículo de la presente Tesis Doctoral en la revista *Sustainable Energy Technologies and Assessments*:

Artículo 3 - Monitoring the thermal contribution of certain mortar additives as a way to optimize the energy performance of buildings.

Tabla 4: Principales medidas de impacto e indexación de la revista SETA.

Revista	Sustainable Energy Technologies and Assessments
Editorial	ELSEVIER
EISSN	2213-1396
Factor de Impacto (2022)	8.0
Ranking	28/119
Cuartil	Q1
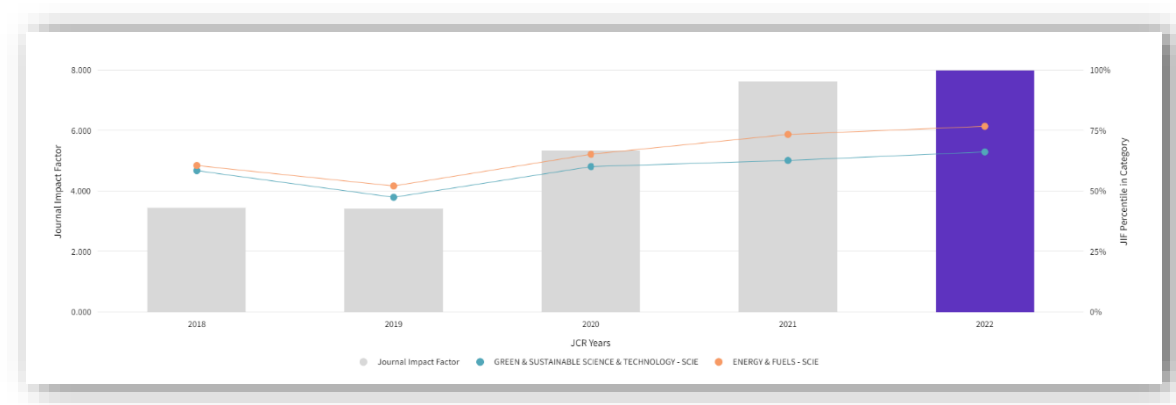
Figura 26: SETA: Journal Impact Factor (JIF) Trend.
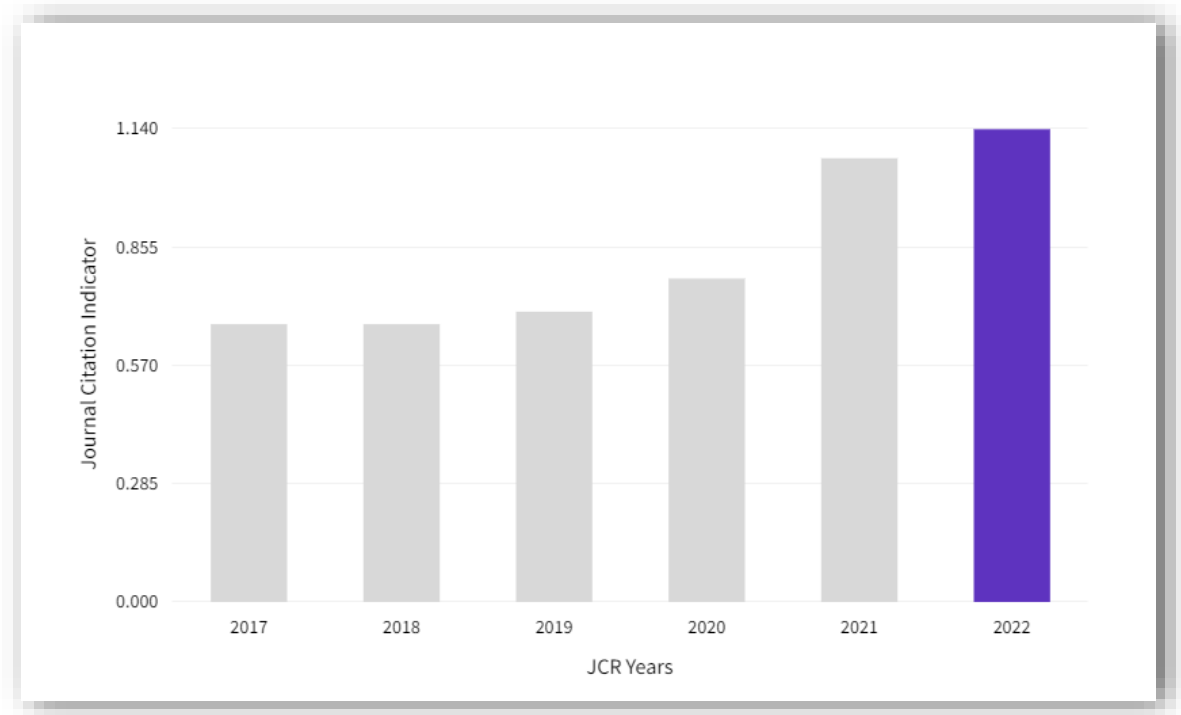
Figura 27: SETA: Journal Citation Indicator (JCI).
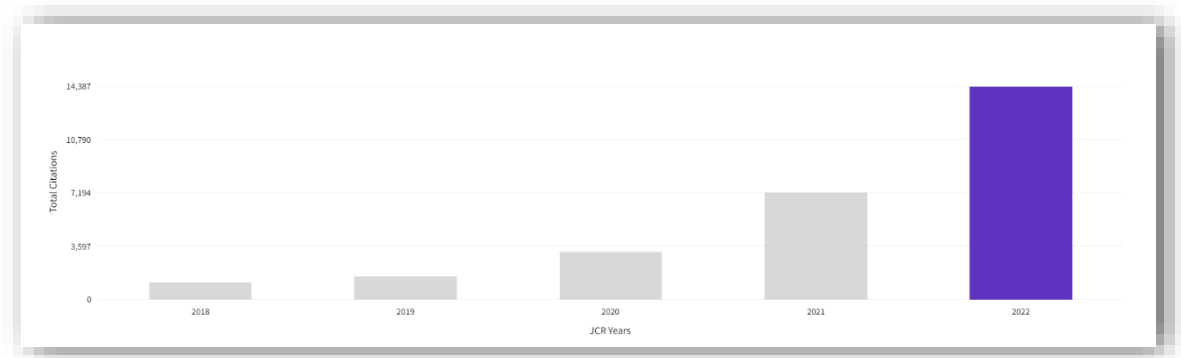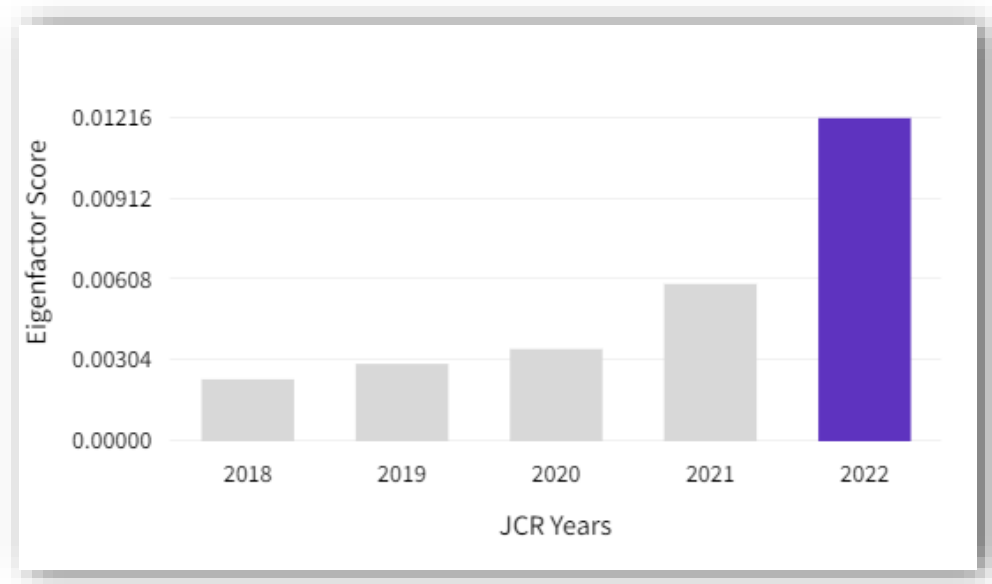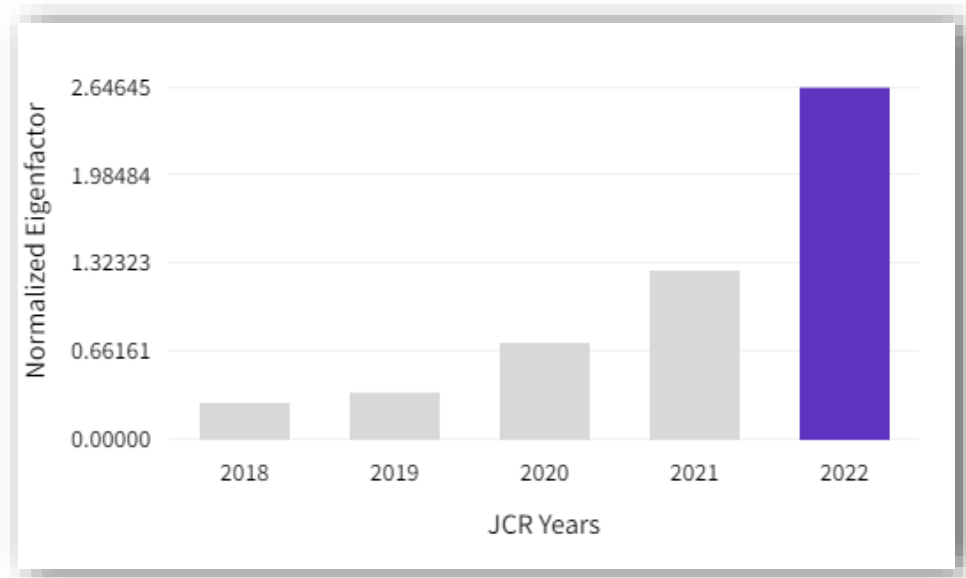

Figura 28: SETA: Total Citations.
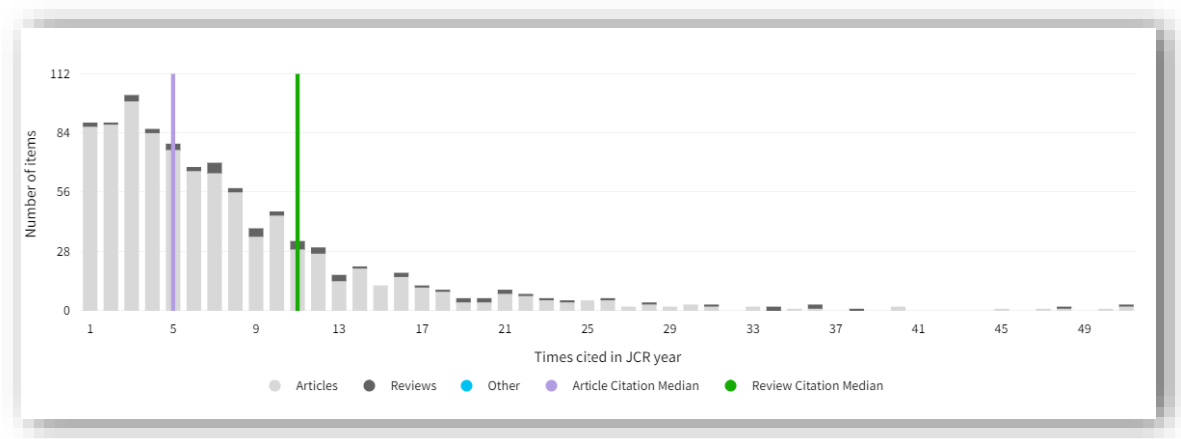
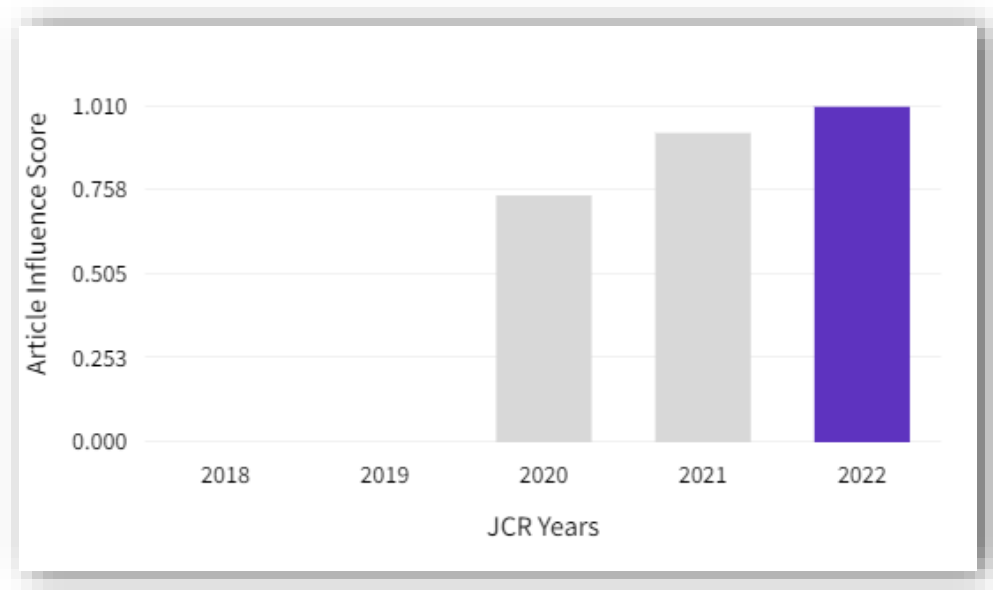*Figura 29: SETA: Citation Distribution.*
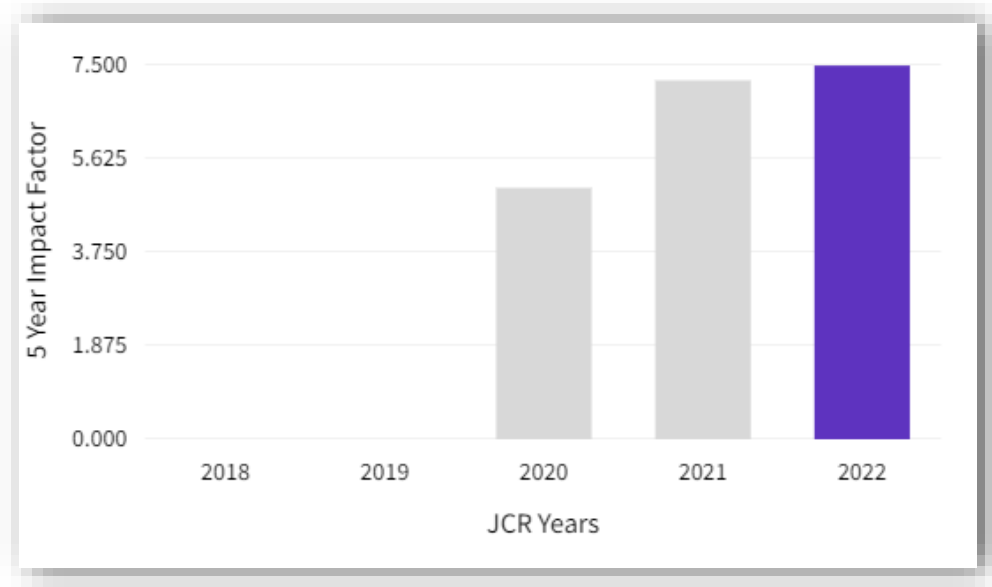
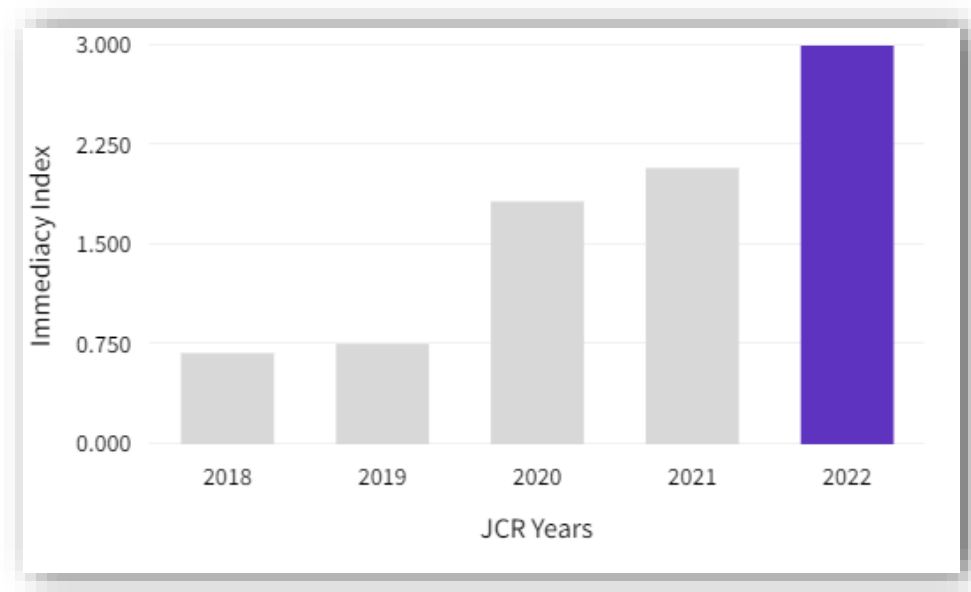*Figura 30: SETA: 5 year Impact Factor.*

Figura 31: SETA: Eigenfactor score.

Figura 32: SETA: Normalized Eigenfactor.

Figura 33: SETA: Article influence score.

Figura 34: SETA: Immediacy Index.

# A.1.4. Journal of Cleaner Production

Journal of Cleaner Production (JCP) es una revista internacional, revisada por pares, transdisciplinaria que se centra en la investigación y la práctica de producción más limpia, medio ambiente y sostenibilidad. La revista se publica semanalmente en línea por ELSEVIER desde el año 1993.

Se ha publicado el siguiente artículo de la presente Tesis Doctoral en la revista *Journal of Cleaner Production*:

Artículo 4 - Experimental study on the thermal properties of pigmented mortars for use in energy efficiency applications.

Tabla 5: Principales medidas de impacto e indexación de la revista JCP.

Revista	Journal of Cleaner Production
Editorial	ELSEVIER
EISSN	1879-1786
Factor de Impacto (2022)	11.1
Ranking	8/55
Cuartil	Q1
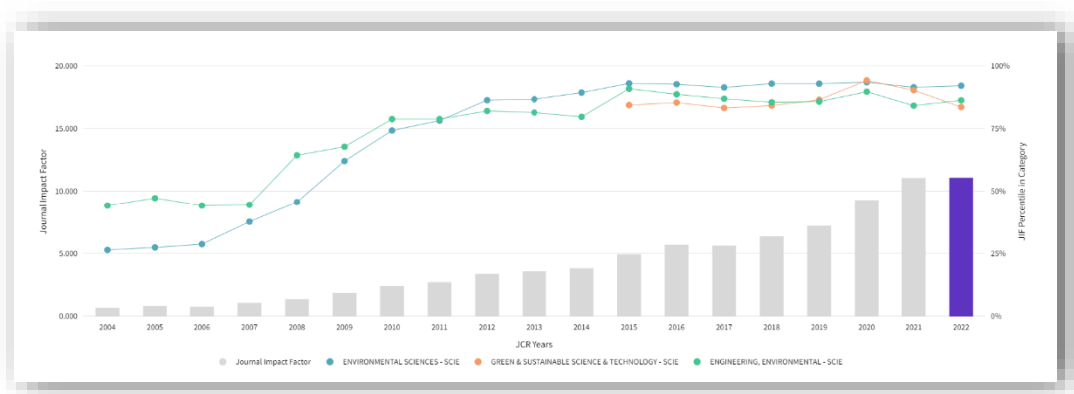
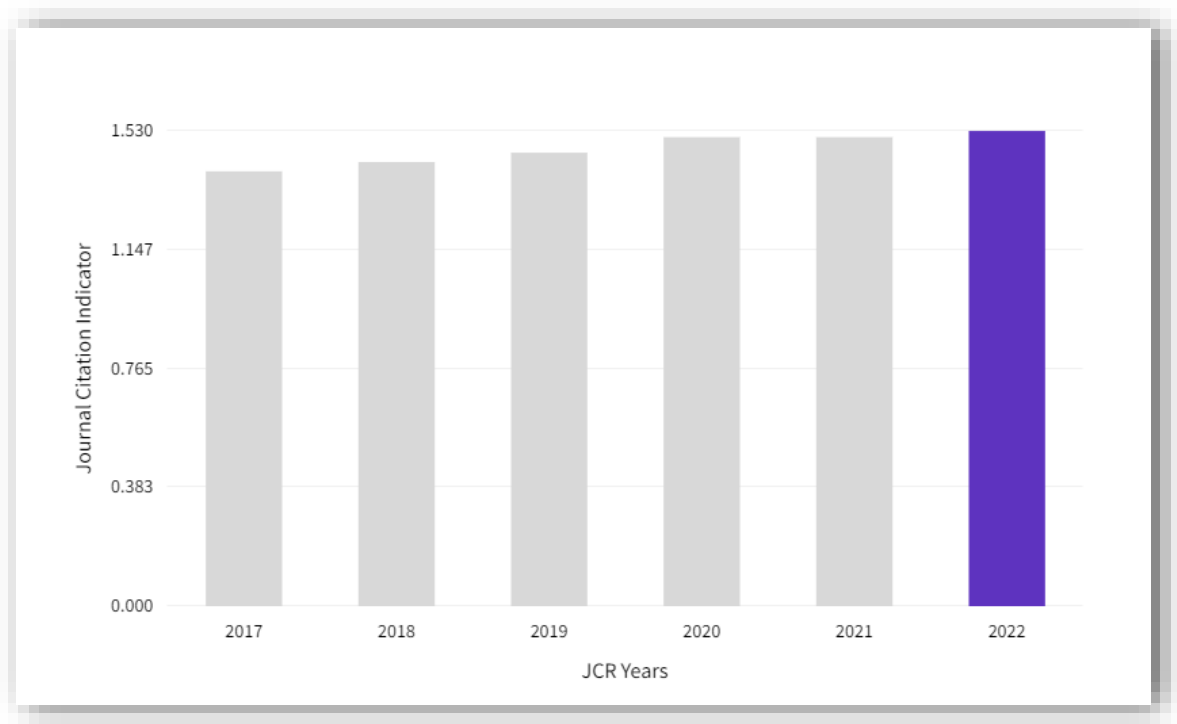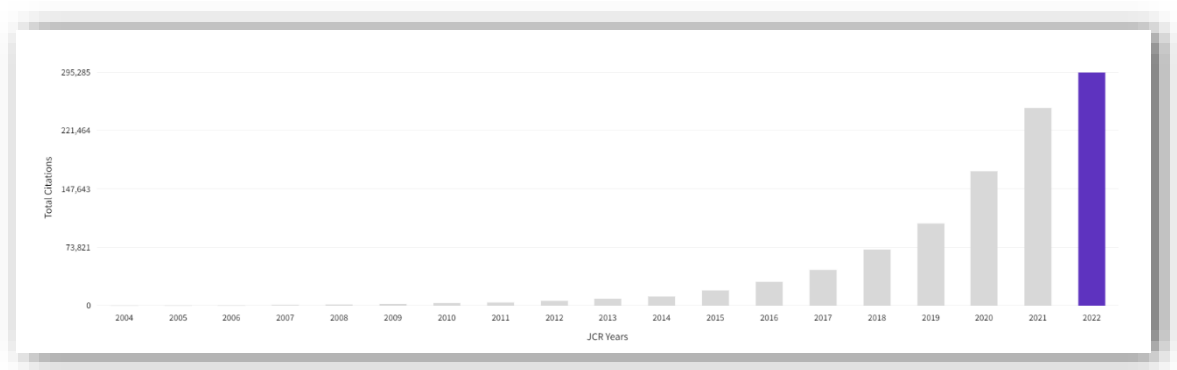*Figura 35: JCP: Journal Impact Factor (JIF) Trend.*

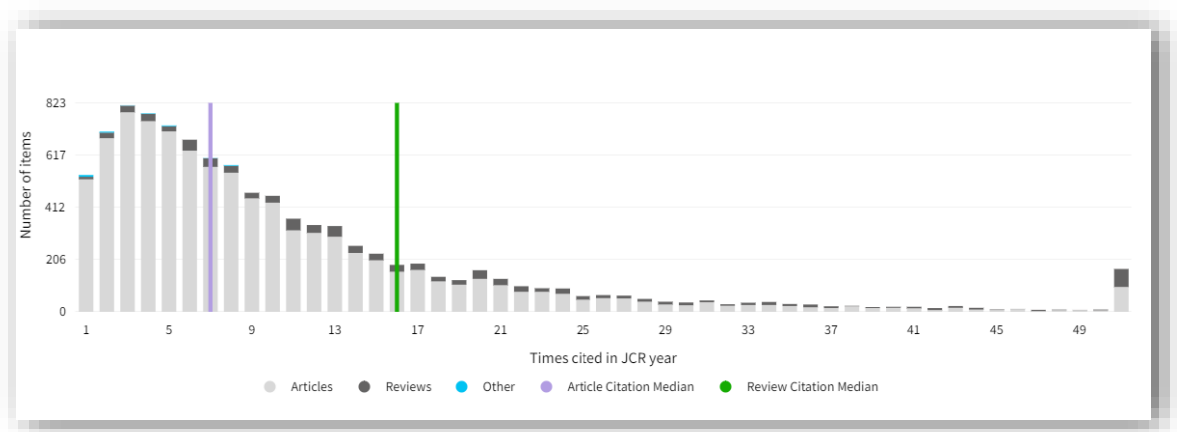*Figura 36: JCP: Journal Citation Indicator (JCI).*
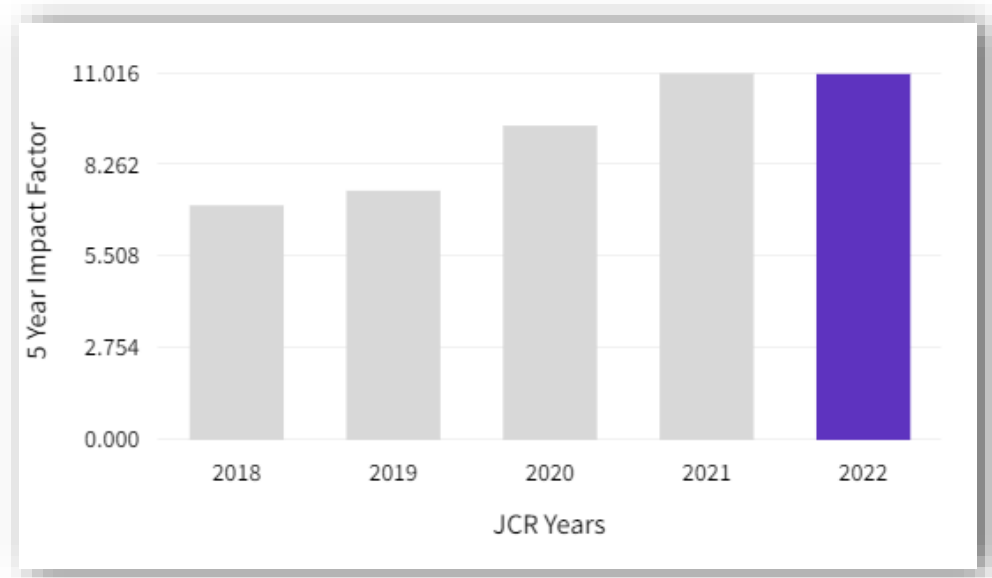

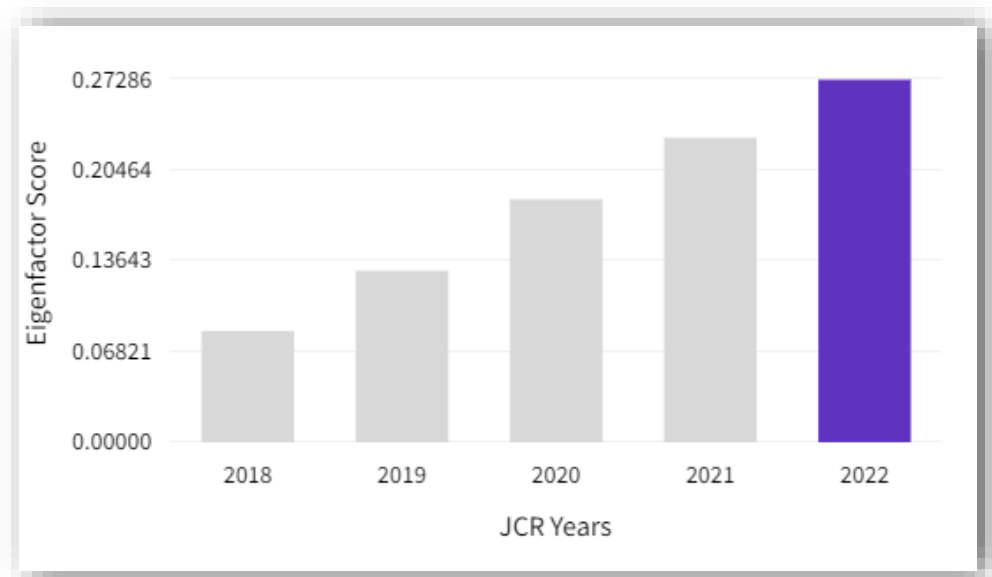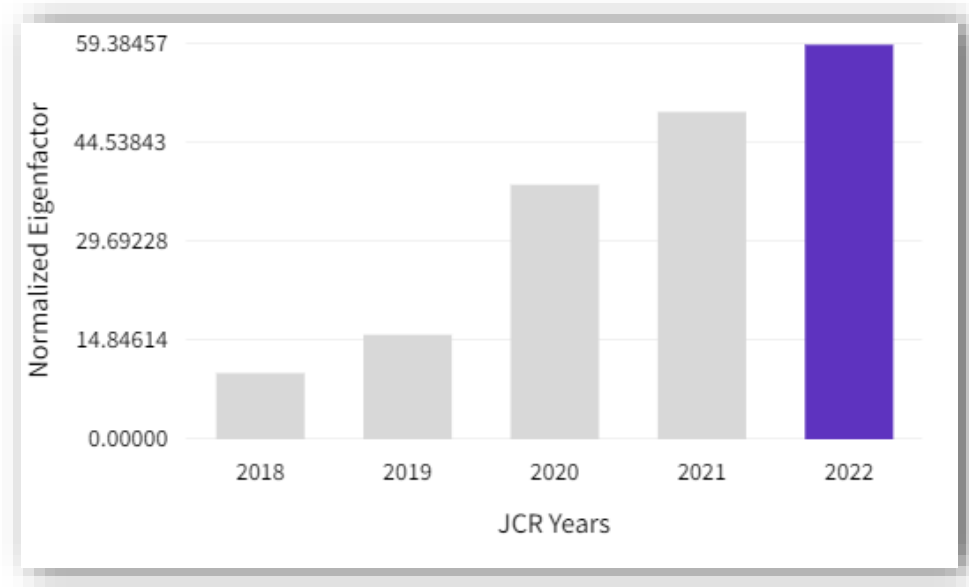*Figura 37: JCP: Total Citations.*

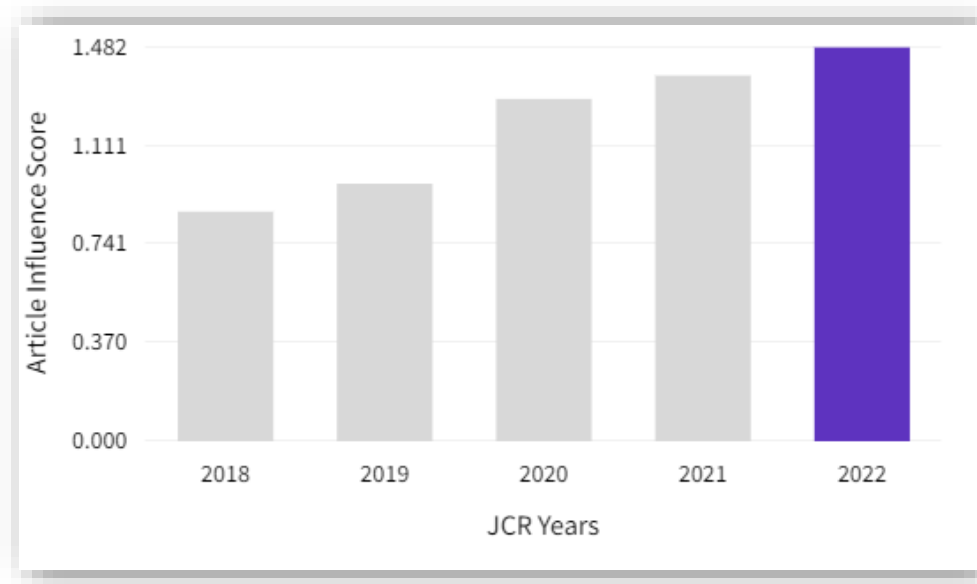
Figura 38: JCP: Citation Distribution.

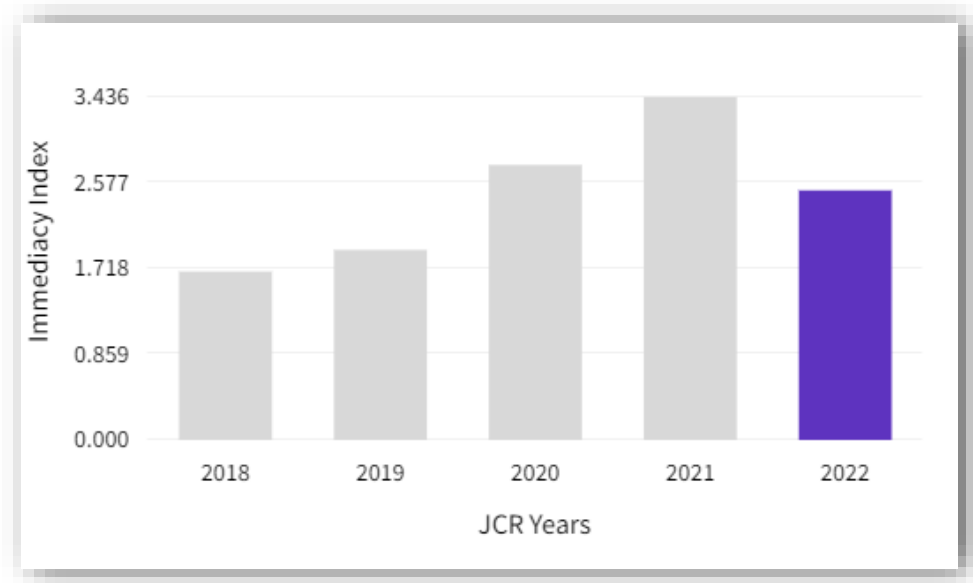*Figura 39:* JCP: 5 year Impact Factor.

Figura 40: JCP: Eigenfactor score.

Figura 41: JCP: Normalized Eigenfactor.

Figura 42: JCP: Article influence score.

Figura 43: JCP: Immediacy Index.

APÉNDICE II: PATENTE

Este Apéndice II incluye la información relativa a la solicitud de patente presentada del prototipo para la caracterización mecánica de materiales a partir de DIC y reconstrucción tridimensional, desarrollado durante la elaboración de la Tesis Doctoral.

Se adjuntan los documentos presentados en la solicitud relativos a (i) la descripción del objeto de invención, (ii) las reivindicaciones, (iii) los dibujos correspondientes y (iv) el resumen.

Título:	Sistema de caracterización de objetos a partir de su reconstrucción en 360 grados mediante generación de imágenes
Número de solicitud:	P202230901
Estado:	En trámite
Solicitante:	Universidad de Salamanca
Inventores:	Jorge López Rebollo
	Javier Pisonero Carabias
	Roberto José García Martín
	Luis Javier Sánchez Aparicio
	Diego González Aguilera

SISTEMA DE CARACTERIZACIÓN DE OBJETOS A PARTIR DE SU RECONSTRUCCIÓN EN 360 GRADOS MEDIANTE GENERACIÓN DE IMÁGENES

D E S C R I P C I Ó N

OBJETO DE LA INVENCIÓN

La presente invención se refiere al campo de la caracterización de objetos, para el cual se emplean sistemas de generación de imágenes y algoritmos de reconstrucción de objetos mediante imágenes.

Así, un objeto de la invención es un sistema de caracterización de objetos a partir de su reconstrucción en 360 grados mediante la generación de imágenes.

ANTECEDENTES DE LA INVENCIÓN

Hoy en día, los procesos de caracterización de materiales se llevan a cabo de manera general a través de dispositivos de contacto, como las galgas extensiométricas, que tienen un carácter local realizando únicamente mediciones puntuales y necesitando estar en contacto directo con el espécimen, lo que puede suponer un problema al sufrir daños a la hora de la rotura del material.

Además, las galgas extensiométricas han de ser desechadas tras un único uso, incrementando notablemente el coste de los ensayos, de modo general la preparación del ensayo consume recursos económicos y gran cantidad de tiempo. Cabe destacar que este tipo de dispositivo es muy sensible a la temperatura, por lo que sería un factor extra a tener en cuenta.

Existen algunas tipologías de ensayos en los que, por la propia geometría de los especímenes, es muy complicado predecir la zona en la que se producirá la rotura. Esto dificulta la elección de colocación de los sensores o la definición de las regiones que suponen un mayor interés para el estudio.

En este sentido, la correlación digital de imágenes puede considerarse como una técnica no destructiva y no invasiva, permitiendo obtener resultados muy precisos de alta

calidad con un coste reducido a partir del análisis de imágenes capturadas durante el proceso de caracterización.

Aunque existen aplicaciones fotogramétricas en las que se incorpora la técnica de correlación digital de imágenes, su integración en los ensayos y el procedimiento para llevar a cabo su aplicación generalmente requieren de un conocimiento profundo y una preparación específica por parte del personal. Además, la interacción del operario durante los procedimientos de calibración añade una fuente de incertidumbre que puede provocar la pérdida de precisión en los datos.

En la actualidad, los equipos comerciales que integran la técnica de correlación digital de imágenes para la caracterización de materiales disponen de una o dos cámaras para su aplicación bidimensional o tridimensional. Sin embargo, en muchas ocasiones la propia geometría de los prototipos a ensayar o la tipología de ensayo impide conocer la región de interés sobre la que focalizar el estudio, no existiendo dispositivos, y menos de bajo coste, capaces de obtener una reconstrucción en 360º de la escena.

DESCRIPCIÓN DE LA INVENCIÓN

La invención se refiere a un sistema de caracterización de objetos a partir de la reconstrucción en 360 grados mediante la generación de imágenes que permiten hacer uso de una técnica de correlación digital de imágenes.

El sistema de la invención permite obtener una reconstrucción completa de un objeto y, por tanto, analizar de manera global su comportamiento, sin necesidad de restringir las mediciones a una región de interés concreta, ya que puede captarse todo el proceso de ensayo tanto de manera temporal como de manera espacial.

Además, el sistema permite mejorar y agilizar la etapa experimental a través de la automatización de la captura de datos y los procesos de calibración mediante un sistema que integra tanto sensores fotogramétricos como sistemas de control y automatización.

En conjunto, el sistema permite llevar a cabo los procesos de caracterización y análisis de soluciones industriales mediante la reconstrucción completa de objetos y la aplicación de la técnica de correlación digital de imágenes de forma automática.

El sistema de la invención comprende una plataforma modular. La plataforma, a su vez, comprende un conjunto módulos conectables destinados a ser dispuestos en forma circular.

Los módulos conectables comprenden cada uno un trípode, una estructura, preferiblemente conformada por perfiles de aluminio, montada sobre el trípode, y un soporte para la integración de los sensores fotogramétricos, preferiblemente obtenido mediante impresión aditiva en ácido poliláctico (PLA), conectados al trípode mediante la estructura. Preferiblemente, cada trípode del conjunto de módulos conectables está configurado para posicionar cada estructura a diferentes alturas e inclinaciones.

De este modo se obtienen plataformas modulares ligeras y robustas que permiten albergar sensores fotogramétricos e iluminación.

El sistema de la invención también comprende un conjunto de sensores fotogramétricos montados sobre cada soporte de los módulos conectables.

Los sensores fotogramétricos usados son preferiblemente de bajo coste, pues la configuración usada permite garantizar una alta calidad y precisión, requerida para llevar a cabo la técnica de correlación digital de imágenes.

El sistema descrito también comprende un conjunto de módulos de iluminación LED montados sobre cada una de las estructuras y, preferentemente, conectados en un circuito en línea.

Los sensores fotogramétricos y los módulos de iluminación tienen asociados un conjunto de controladores conectados, preferiblemente de forma inalámbrica, en una red controlada de tipo Maestro-Esclavo que controla simultáneamente todos los sensores fotogramétricos y los módulos de iluminación.

Además, el uso de la red controlada de tipo Maestro-Esclavo permite conectar y sincronizar todos los sensores de manera que el procedimiento de captura de datos pueda simplificarse y automatizarse.

Preferiblemente, la red controlada será inalámbrica, pudiendo también crear una red cableada donde los controladores estarán conectados a una red de relés, donde la precisión temporal será superior.

Adicionalmente, el sistema de la invención puede comprender un módulo de calibración, el cual comprende:

- un brazo robótico que comprende un conjunto de servomotores de 180º y 360º;
- un soporte conectado al brazo robótico;
- una placa de calibración montada sobre el soporte; y
- un controlador configurado para actuar sobre los servomotores del brazo robótico con el fin de reproducir una rutina automatizada de calibración en la placa de calibración.

La configuración del módulo de calibración permite definir un protocolo para la automatización de la calibración de las cámaras.

Así, el sistema de la invención permite la generación de modelos 3D de campo completo de manera que pueden obtenerse geometrías completas de objetos y llevar a cabo un análisis de manera global.

Además, el sistema permite generar modelos 3D densos del objeto que pueden ser empleados para llevar a cabo técnicas de ingeniería inversa y posteriormente ser integrados en sistemas de ingeniería asistida por ordenador (CAE). De esta manera, pueden abordarse procesos de simulación numérica en base a una representación fidedigna del objeto estudiado y posteriormente llevar a cabo la verificación experimental en prototipos reales.

El sistema generado permite llevar a cabo procedimientos de caracterización y verificación industrial de manera más rápida y económica que las soluciones actuales bajo las premisas de la flexibilidad y robustez.

Esta tecnología podrá ser transferida a otros sectores como la construcción u obra civil, ya que el dispositivo puede emplearse en diferentes escenarios y sin necesidad de que sea manejado por personal experto.

El prototipo no solo reduce los costes de ensayo de producto, dado que se trata de una técnica de no contacto donde no se destruyen los sensores, sino que además incorpora funciones de auto calibración que reducen los tiempos asociados a la preparación de ensayos.

El sistema descrito permite su uso en cualquier proceso de caracterización de materiales y comportamiento mecánico de elementos sometidos a esfuerzo.

Además, el sistema cuenta con una gran capacidad de adaptación a diferentes técnicas gracias a su diseño modular. Por ejemplo, en una realización alternativa, es posible aplicar con el mismo sistema otras técnicas de adquisición de imágenes con sensores fuera del espectro visible, como podría ser el uso de imágenes termográficas.

También es destacable que este tipo de sistema puede ser utilizado como un nuevo nodo en una red del Internet de las Cosas, IoT, gracias a la creación de una red propia que puede ser acoplada a otra red existente.

DESCRIPCIÓN DE LOS DIBUJOS

Para complementar la descripción que se está realizando y con objeto de ayudar a una mejor comprensión de las características de la invención, de acuerdo con un ejemplo preferente de realización práctica de la misma, se acompaña como parte integrante de dicha descripción, un juego de dibujos en donde con carácter ilustrativo y no limitativo, se ha representado lo siguiente:

Figura 1.- muestra un ejemplo de realización del sistema de generación de imágenes de la invención con una plataforma modular compuesta por cuatro módulos conectables.

Figura 2.- muestra un ejemplo de realización del sistema de generación de imágenes de la invención con una plataforma modular compuesta por cuatro módulos conectables, incluyendo un módulo de calibración.

Figura 3.- muestra un ejemplo de realización de un módulo conectable, de acuerdo con la invención, que comprende un trípode, una estructura de perfiles de aluminio, montada sobre el trípode, y un soporte conectado al trípode mediante los perfiles de aluminio; sobre

el soporte se montan tres sensores fotogramétricos y un conjunto de módulos de iluminación LED.

Figura 4.- muestra un ejemplo de realización del módulo de calibración, de acuerdo con la invención, que comprende un brazo robótico con servomotores de 180º y 360º, un soporte y una diana de calibración montada sobre el soporte.

REALIZACIÓN PREFERENTE DE LA INVENCIÓN

La invención se refiere a un sistema de caracterización de objetos a partir de su reconstrucción en 360 grados mediante generación de imágenes que permiten hacer uso de una técnica de correlación digital de imágenes y que comprende:

- una plataforma modular (1) que comprende un conjunto de módulos conectables (2) destinados a ser dispuestos en forma circular, los cuales a su vez comprenden cada uno:
  - o un trípode (3),
  - o una estructura (4), montada sobre el trípode (3), y
  - o un soporte (5) conectado al trípode (3) mediante la estructura (4);
- un conjunto de sensores fotogramétricos (6), montados sobre cada soporte (5) de los módulos conectables (2);
- un conjunto de módulos de iluminación (7) LED montados sobre cada una de las estructuras (4); y
- un módulo de control (8) que comprende un conjunto de controladores asociados a los sensores fotogramétricos (6), conectados de forma inalámbrica o cableada en una red controlada de tipo Maestro-Esclavo que controla simultáneamente todos los sensores fotogramétricos (6) y los módulos de iluminación (7).

En una realización preferente de la invención, la plataforma modular (1) está compuesta de perfiles de aluminio, que combinan un fácil ensamblaje junto con ligereza y rigidez.

Los sensores fotogramétricos (6) son preferiblemente sensores de imagen de bajo coste y microcontroladores compatibles con los mismos.

En una realización preferente, los soportes (5), tanto de los sensores fotogramétricos (6) como de los controladores, son obtenidos mediante impresión aditiva en ácido poliláctico (PLA), por ser una forma económica y viable para adaptarse al diseño.

La figura 1 muestra una realización preferente del sistema de la invención que comprende la plataforma, cuya mecanización y ensamblaje se realiza de forma que la plataforma sea modular. Para ello, se disponen cuatro módulos conectables (2) que conforman la plataforma de forma circular. En cada uno de los módulos conectables (2) se disponen tres sensores de imagen y su correspondiente controlador.

El uso de perfiles de aluminio facilita la labor de ensamblaje, permitiendo la adaptación a diferentes ángulos y la conexión entre los módulos conectables (2).

En esta realización preferente, los soportes (5) y carcasas diseñadas para los controladores se unieron mediante tornillería estándar para facilitar el montaje y desmontaje de los mismos.

Preferentemente, también se pueden incorporar trípodes (3), que permiten la nivelación de la plataforma a diferentes alturas e inclinaciones, permitiendo una mayor versatilidad a la hora de llevar a cabo ensayos en diferentes entornos y condiciones.

En este caso, se incorporó iluminación a cada uno de los módulos conectables (2), constituyendo un circuito en línea a lo largo de toda la estructura (4) de aluminio. De esta manera, se pueden conectar únicamente las unidades de iluminación (7) que se requieran en función de los módulos conectables (2) a utilizar.

Además, los sensores fotogramétricos (6) y los módulos de iluminación (7) se conectan y sincronizan, de manera que pudiera trabajarse como si de un dispositivo único se tratara.

En una realización preferente, los controladores estarán dentro de una red cableada por ser una forma simple y sencilla de sincronización

La tecnología usada permite un uso extenso de múltiples dispositivos creando una red controlada, teniendo información y monitorizando cualquier tipo de elemento de manera remota.

La calibración del sistema comprende las etapas de seleccionar posiciones predeterminadas para el panel de calibración, activar el brazo robótico (10) para situar la placa de calibración (13) en cada una de las posiciones predeterminadas, y estabilizar la placa de calibración (13) para tomar una imagen en cada una de las posiciones.

La figura 3 muestra un ejemplo de realización de la plataforma modular (1), en este caso, compuesta por perfiles de aluminio. La plataforma modular (1) permite albergar tanto los sensores fotogramétricos (6) como los módulos de iluminación (7).

La figura 1 muestra una plataforma con 4 módulos conectables (2) que permite su uso en diferentes escenarios en función de los objetos y el tipo de ensayo a realizar. Así, en los escenarios en los que por la propia geometría no sea posible llevar a cabo la reconstrucción de los 360º, podrán emplearse los módulos conectables (2) correspondientes para realizar la reconstrucción con un menor número de sensores fotogramétricos (6) y abarcando un menor ángulo de visión.

El uso combinado de perfiles de aluminio junto con trípodes (3), también de aluminio, permite garantizar la estabilidad de los sensores fotogramétricos (6) durante los ensayos.

Además, se han integrado los sensores fotogramétricos (6) y los controladores mediante soportes (5) diseñados ad-hoc y fabricados mediante impresión aditiva en ácido poliláctico (PLA).

Por su parte, los sensores fotogramétricos (6) seleccionados en este caso son sensores de imagen de la tipología Raspberry Pi HQ Camera y lentes de 16mm que permiten obtener la mayor calidad y precisión en los resultados tratando de garantizar el principio de low-cost.

Como se muestra en la Figura 3, la plataforma está constituida por cuatro módulos conectables (2) que integran tres sensores de imagen cada uno de ellos, separados por un ángulo de 30º, de manera que sea posible reconstruir la escena en 360º. El uso de estos sensores fotogramétricos (6) permite la sincronización y automatización de todos los elementos del sistema.

Los módulos de iluminación (7) permiten que el sistema pueda emplearse tanto en interiores como exteriores, pues garantizan las condiciones lumínicas requeridas para la aplicación de las técnicas fotogramétricas.

En este caso, se han incorporado unidades de iluminación (7) LED en toda la estructura (4) modular, de manera que se facilite su conexión para los diferentes módulos conectables (2) y que, a su vez, permita cubrir los 360º obteniendo una iluminación uniforme a fin de evitar brillos y reflejos en la superficie de los objetos a ensayar.

El control del sistema se lleva a cabo mediante un módulo de control (8) que incorpora una conexión entre sensores fotogramétricos (6) mediante una red propia de microcontroladores, del tipo Maestro-Esclavo en estrella, en este caso, usando dispositivos RaspBerry Pi.

Cada uno de los sensores fotogramétricos (6) (Esclavo) incorpora un microcontrolador RaspBerry Pi 3B+ que permite la captura y almacenamiento de imágenes, mientras que un dispositivo más potente (Maestro), es empleado para controlar todas las cámaras de manera simultánea creando una red propietaria.

La conexión inalámbrica permite evitar un mayor cableado, así como obtener una plataforma modular (1) al conectar únicamente aquellos dispositivos necesarios para cada ensayo.

La conexión cableada permite mejorar la precisión temporal y poner a punto las cámaras de manera previa a la toma de datos.

Con el fin de lograr una mayor automatización, se ha diseñado un módulo de calibración (9) automatizado que permite llevar a cabo la calibración de las cámaras sin necesidad de intervención de un operario.

Como se muestra en la figura 4, en este caso, se hace uso de un brazo robótico (10) compuesto por servomotores (11) de 180º y 360º que permiten abarcar seis grados de libertad. Además, se ha diseñado y fabricado mediante impresión aditiva un soporte de brazo (12) específico para la introducción de una placa de calibración (13).

El dispositivo incorporara también un controlador de calibración (14) que permite automatizar totalmente el proceso de calibración sin necesidad de intervención humana, reduciendo así los tiempos de preparación del equipo, lo cual redunda en el ahorro de costes.

Para este proceso de calibración, se ha diseñado una rutina automatizada que traslada los movimientos asociados a la placa de calibración (13) mediante una plataforma Arduino.
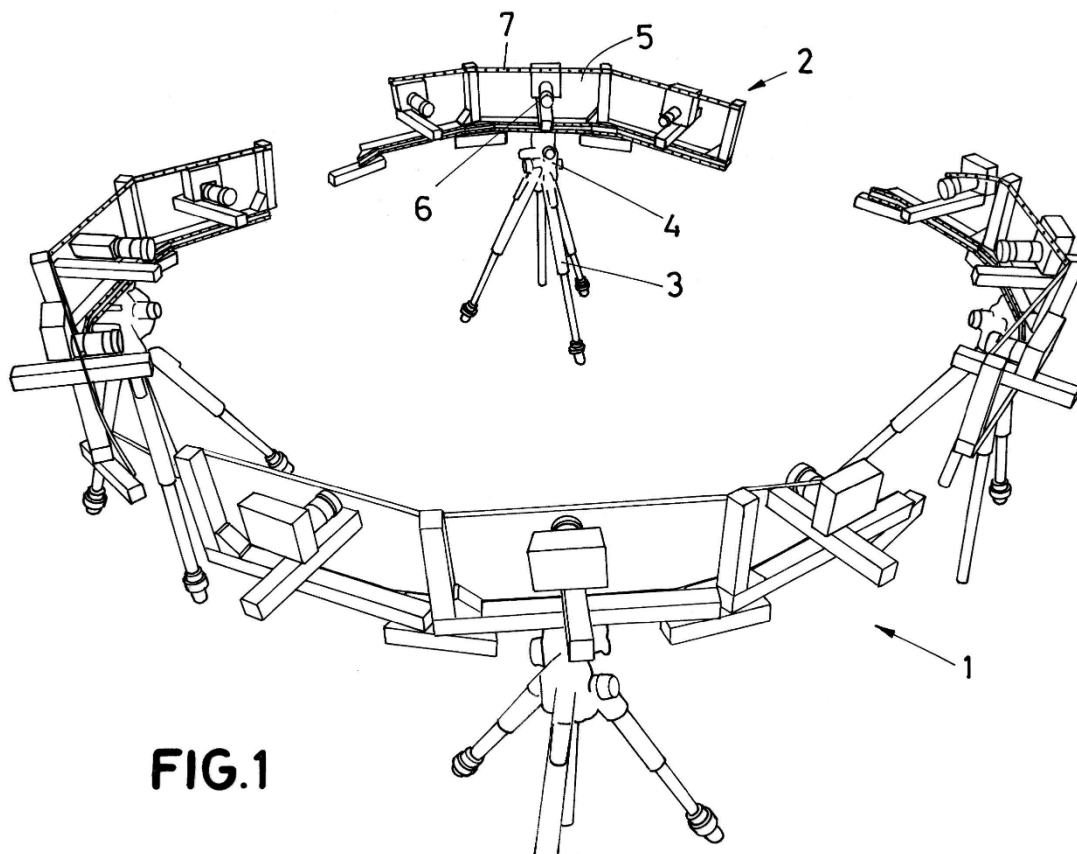
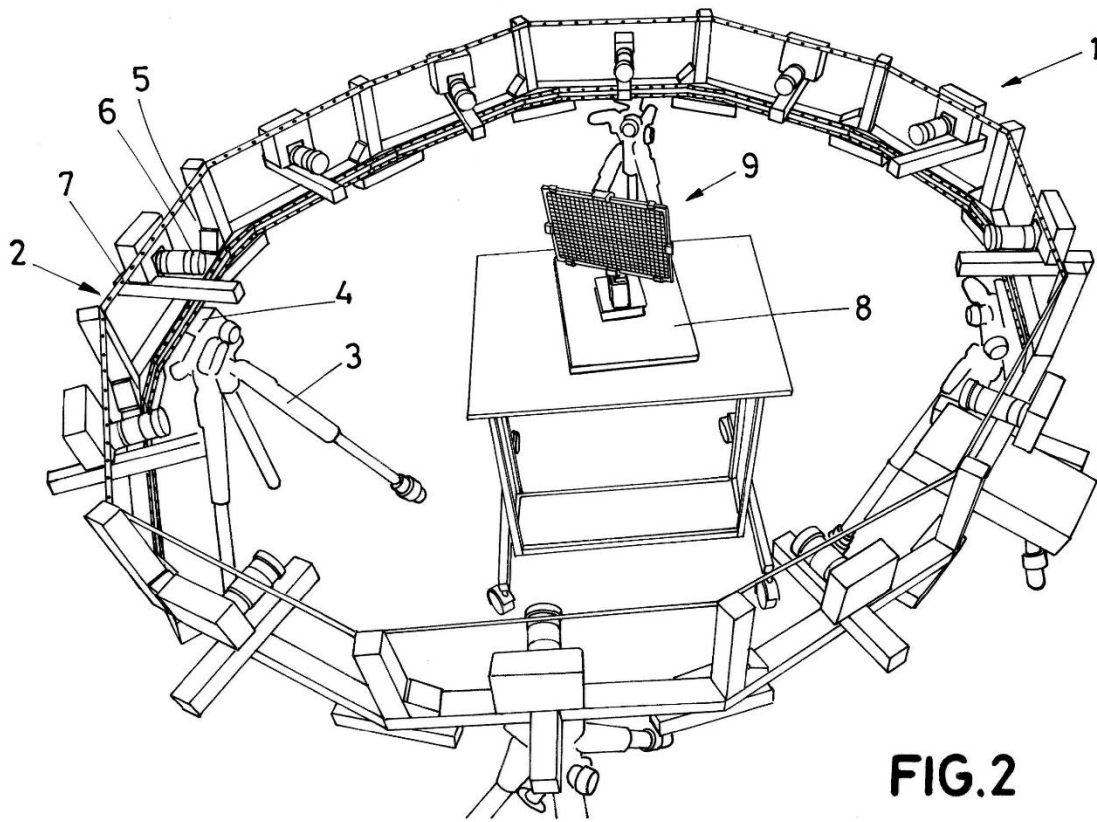# R E I V I N D I C A C I O N E S

1. Sistema de caracterización de objetos a partir de su reconstrucción en 360 grados mediante generación de imágenes que hace uso de una técnica de correlación digital de imágenes, que comprende:
   - una plataforma modular (1) que comprende un conjunto módulos conectables (2) destinados a ser dispuestos en forma circular, los cuales a su vez comprenden cada uno:
     o un trípode (3),
     o una estructura (4), montada sobre el trípode (3), y
     o un soporte (5) conectado al trípode (3) mediante la estructura (4);
   - un conjunto de sensores fotogramétricos (6), montados sobre cada soporte (5) de los módulos conectables (2);
   - un conjunto de módulos de iluminación (7) LED montados sobre cada una de las estructuras (4); y
   - un módulo de control (8) que comprende un conjunto de controladores asociados a los sensores fotogramétricos (6) y los módulos de iluminación (7), conectados en una red controlada de tipo Maestro-Esclavo que controla simultáneamente todos los sensores fotogramétricos (6), y los módulos de iluminación (7).

2. Sistema de caracterización de objetos a partir de su reconstrucción en 360 grados de acuerdo con la reivindicación 1, que además comprende un módulo de calibración (9) que comprende:
   - un brazo robótico (10) que comprende un conjunto de servomotores (11) de 180º y 360º;
   - un soporte de brazo (12) conectado al brazo robótico (10);
   - una placa de calibración (13) montada sobre el soporte de brazo (12); y
   - un controlador de calibración (14) configurado para actuar sobre los servomotores (11) del brazo robótico (10) con el fin de reproducir una rutina automatizada de calibración en la placa de calibración (13).

3. Sistema de generación de imágenes mediante reconstrucción en 360 grados de acuerdo con la reivindicación 1, donde cada soporte (5) del conjunto de módulos conectables (2) es obtenido mediante impresión aditiva en ácido poliláctico (PLA).

4. Sistema de caracterización de objetos a partir de su reconstrucción en 360 grados de acuerdo con la reivindicación 1, donde cada estructura (4) del conjunto de módulos conectables (2) está conformada por perfiles de aluminio.

5. Sistema de caracterización de objetos a partir de su reconstrucción en 360 grados de acuerdo con la reivindicación 1, donde cada trípode (3) del conjunto de módulos conectables (2) está configurado para posicionar cada estructura (4) a diferentes alturas e inclinaciones.

6. Sistema de caracterización de objetos a partir de su reconstrucción en 360 grados de acuerdo con la reivindicación 1, donde los módulos de iluminación (7) se conectan en un circuito en línea.

7. Sistema de caracterización de objetos a partir de su reconstrucción en 360 grados de acuerdo con la reivindicación 1, donde los sensores fotogramétricos (6) son sensores de imagen de la tipología Raspberry Pi HQ Camera con lentes de 16mm.

8. Sistema de caracterización de objetos a partir de su reconstrucción en 360 grados de acuerdo con la reivindicación 1, donde se disponen 12 sensores fotogramétricos (6) separados por un ángulo de 30º uno de otro.

9. Sistema de caracterización de objetos a partir de su reconstrucción en 360 grados de acuerdo con la reivindicación 1, donde la red controlada de tipo Maestro-Esclavo se configura como una red en estrella.

10. Sistema de caracterización de objetos a partir de su reconstrucción en 360 grados de acuerdo con la reivindicación 1, donde el conjunto de controladores del módulo de control (8) asociados a los sensores fotogramétricos (6) y los módulos de iluminación (7) están conectados de forma inalámbrica.

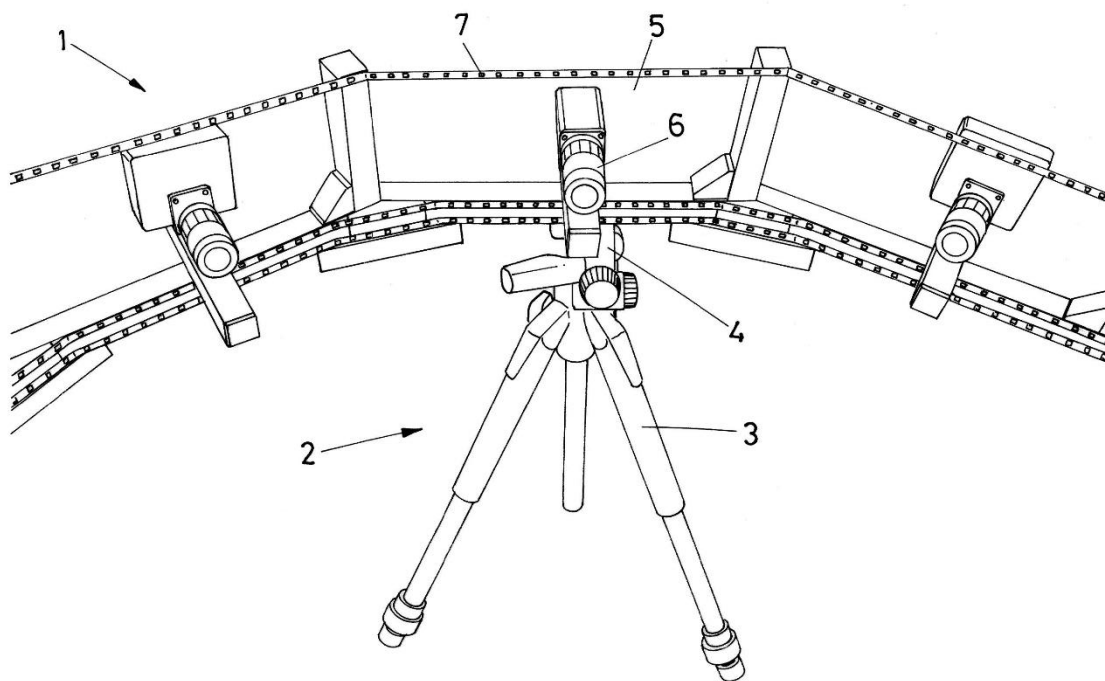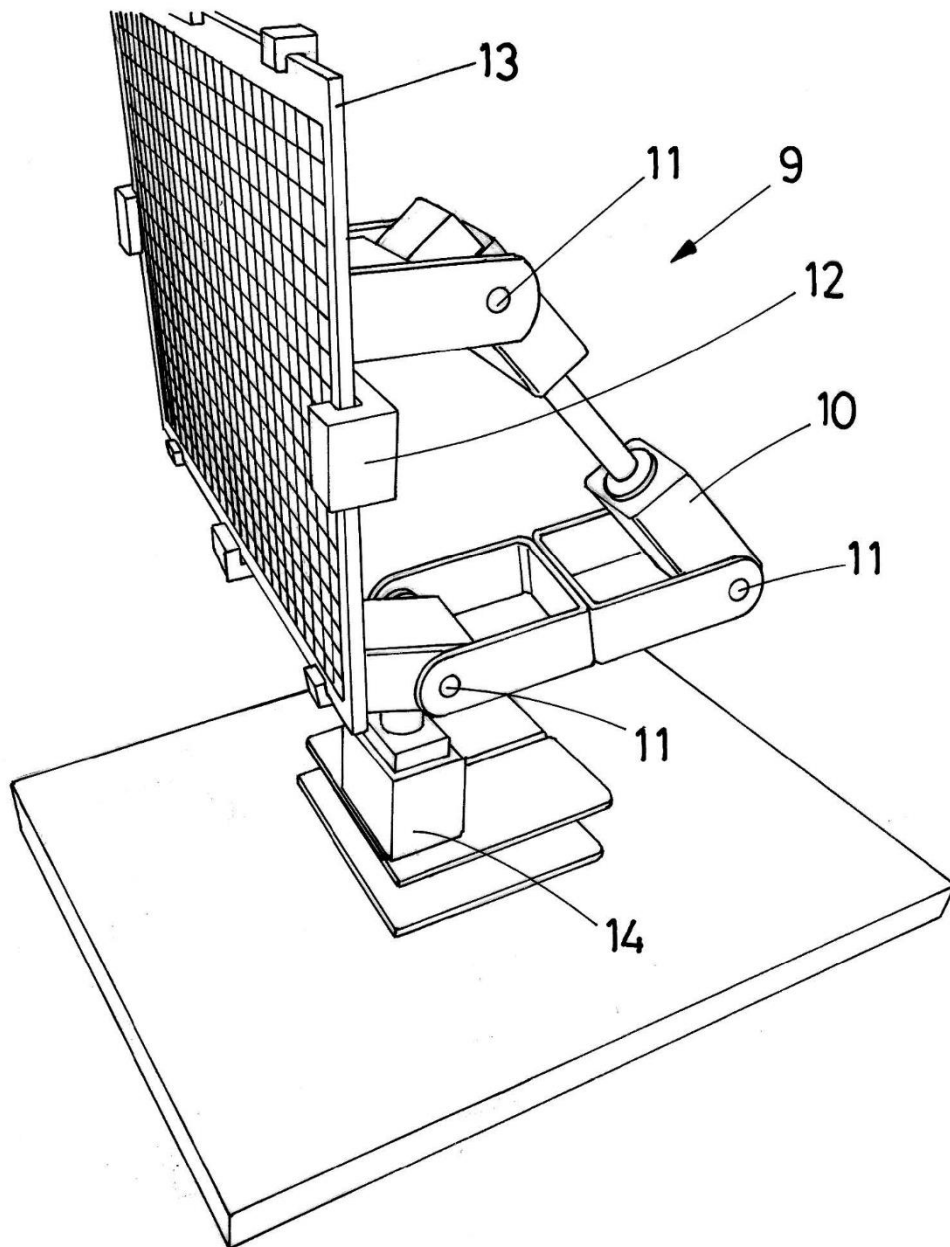# D I B U J O S

FIG.1

FIG.2

FIG.3

FIG.4

R E S U M E N

Sistema de caracterización de objetos a partir de su reconstrucción en 360 grados mediante generación de imágenes que permite hacer uso de una técnica de correlación digital de imágenes, y comprende una plataforma modular, que integra un conjunto de módulos conectables destinados a ser dispuestos en forma circular, los cuales a su vez, comprenden un conjunto de trípodes, un conjunto de estructuras de perfiles de aluminio, montadas sobre los trípodes, y un conjunto de soportes conectados a los trípodes mediante los perfiles de aluminio; un conjunto de sensores fotogramétricos y un conjunto de módulos de iluminación LED montados sobre cada una de las estructuras conectados mediante un módulo de control que comprende un conjunto de controladores asociados a los sensores fotogramétricos y los módulos de iluminación conectados en una red controlada de tipo Maestro-Esclavo.